Stony Brook University

Fate of Nitrogen during Submarine Groundwater Discharge into Long Island North Shore Embayments

A Dissertation Presented

by

Caitlin Young

to

The Graduate School

in Partial Fulfillment of the

Requirements

for the Degree of

Doctor of Philosophy

in

Geosciences

Stony Brook University

December 2013

Stony Brook University

The Graduate School

Caitlin Young

We, the dissertation committee for the above candidate for the

Doctor of Philosophy degree, hereby recommend

acceptance of this dissertation.

Gilbert Hanson

Distinguished Professor, Geosciences

Michael Sperazza

Professor, Geosciences

Henry Bokuniewicz

Professor, School of Marine and Atmospheric Sciences

Robert Aller

Professor, School of Marine and Atmospheric Sciences

Kevin D. Kroeger

Senior Research Scientist

US Geological Survey
Woods Hole Coastal & Marine Science Center

This dissertation is accepted by the Graduate School

Charles Taber

Dean of the Graduate School

Abstract of the Dissertation

Fate of Nitrogen during Submarine Groundwater Discharge into Long Island North Shore Embayments

by

Caitlin Young

Doctor of Philosophy

in

Geosciences

Stony Brook University

2013

Long Island Sound experiences periods of hypoxia attributed to eutrophication, but the magnitude of nitrogen contributed to surface water via submarine groundwater discharge (SGD) entering Long Island's north shore embayments is not well characterized. The coastal aquifer, where fresh groundwater mixes with saline coastal water is termed the subterranean estuary (STE). Advective flow combined with sharp salinity and dissolved oxygen gradients make the STE a zone of intense geochemical cycling. However, the fate of nitrogen during transit through Long island embayment STEs is not well understood, particularly how sediment heterogeneity influences nitrogen attenuation in discharge zones.

Nitrate attenuation mechanisms, principally denitrification, were investigated in three Long Island north shore embayments; Stony Brook Harbor, Setauket Harbor and Port Jefferson Harbor. In Stony Brook Harbor an investigation of freshwater nitrate dynamics over two spring-neap tidal cycles found oscillations in depth stratified nitrate concentrations. Calculation of fresh fraction discharge revealed that water table over-height is responsible for these oscillations, which result from shore perpendicular movement of the coarse sediment freshwater discharge point.

High resolution sampling of STE porewater from Stony Brook Harbor and Setauket Harbor revealed discharge of freshwater continues for tens of meters offshore, which results in two zones of nitrogen removal. When SGD discharges into surface water near low tide through coarse-grain sand

or marsh sediments, denitrification rates are 15 - 50% lower than when SGD passes through into a fine grain sediment layer offshore.

In Port Jefferson Harbor, results from a combined shallow porewater nitrate concentration and geochemical tracer (^{222}Rn) study indicate SGD accounts for similar nitrogen flux to surface water as direct inputs from a local sewage treatment plant. Overall, embayment scale sediment heterogeneity is positively correlated with availability of dissolved organic carbon, which in turn controls the extent of microbially mediated denitrification found in each of the studied embayments.

Dedication Page

To my father, who taught me the value of hard work, dedication and that a person does not need education to be truly intelligent. It was a long journey, and you supported me every step of the way. Even today I hear your voice on the phone, calling me from miles away. Remember the days we traveled together, looking for the 'audubunzoo' and eating alligator on Bourbon Street.

You taught me to reach for the stars

'I'll tell you a story

about Jack a Nory

and now my story's begun

I'll tell you another

about jack and his brother

and now my story's done'

Frontispiece

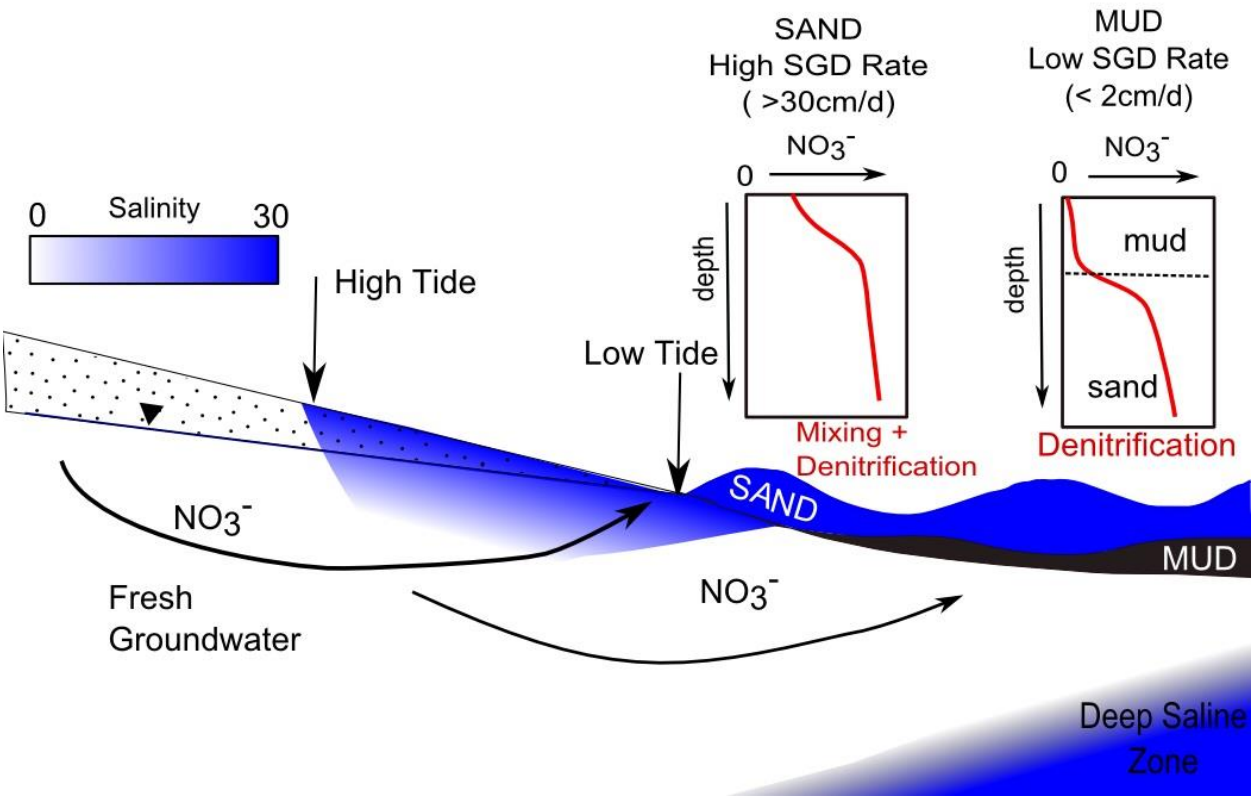

Conceptual model of fate of SGD driven nitrate into Long Island north shore embayments.

Contents

LIST OF FIGURES

CHAPTER I

CHAPTER II

CHAPTER III

CHAPTER IV

CHAPTER V

CHAPTER VI

LIST OF TABLES

CHAPTER II

CHAPTER III

CHAPTER IV

CHPATER V

CHAPTER VI

Acknowledgments

I would like to extend my heartfelt thanks to my advisor Dr. Gil Hanson, for his time patience and wisdom in guiding me through this process. My work would not have been possible without constant input and conversation with Dr. Henry Bokuniewicz and Dr. Teng-Fong Wong. Between the three of them they managed to financially support me through both my Master's and PhD work and provide me with numerous opportunities to attend conferences and explore new avenues of my research.

Financial support for all data collection and scholarly activities contained herein was provided by SeaGrant R/CTP-44-NYCT. In addition, I would like to thank SeaGrant for funding during the writing of this dissertation through their Thesis Completion Award (TCA).

The work herein was supported throughout by the Sufffolk County Department of Health Services (SCDHS). I would like to thank Ron Paulsen for his time and effort in procuring funding for this project as well as his two years of field support to collect data herein. A special thanks to Jonathan Wanlass of the SCDHS for lending equipment, time, energy and bad jokes to every field campaign. Neal Stark was instrumental in field sampling for this project, spending numerous hours in the inclement weather to collect data. Thanks for teaching me so much, particularly the importance of lunch and app time!

I wish to give special thanks to Dr. Bob Aller for his generous use of lab space and assistance in data interpretation. I would also like to thank Dr. Kevin Kroeger for his consistent support over the years and numerous helpful conversations on nitrogen and dissolved gases.

A number of people in the School of Marine and Atmospheric Sciences were always helpful and treated me like their own. I owe a great deal to Christina Heilbrun for her help in sample analysis. Her careful technique has helped me become a better analytical chemist. Her words of wisdom propped me up on long days in the lab. I would also like to thank Dr. Qing Zhu for his careful reading of manuscript drafts during our work together. Finally, thank you to David Hirschberg who taught everything I know about trouble shooting lab equipment.

Big thanks to Alex Smirnov for his practical words of wisdom and consistent mentorship. I am indebted to students I have worked with along the way, including R. Coffey, A.Rajendra, T.Sing and F.Liu. I would like to give special thanks to J. Tamborski and M.Thorpe for their excitement and enthusiasm in SGD projects and their willingness to get their feet wet doing fieldwork with me.

To my dear Millicent, thank you for everything. All the daycare drop offs, middle of the night kiddo wake ups, last minute edits, laundry folding parties and desserts on Dr.Who night. You have brought me joy in times of true hardship and stuck with me through the awkwardness of all the outside world.

Lastly, I owe the underpinnings of these last four years to my beloved Khaled. You supported me through this journey and encouraged me at each step. You kept me sane during so many long days of work and long nights of baby cries. I am eternally grateful his love and sacrifice during this chapter of our life together.

'Take down the clock ticking on the wall, so I can free my mind'

CHAPTER I: INTRODUCTION

Eutrophication of coastal zones resulting from anthropogenic nitrogen

Anthropogenic nutrient additions to coastal waters have substantially increased in the last century with the advent of the industrial revolution and subsequent agricultural revolution. Nutrients in coastal waters are of major concern as the aquatic food web is dependent on stable growth of primary producers, whose biochemistry reflects Redfield release and uptake ratios of nutrients (Redfield, 1963). With the introduction of anthropogenically sourced nutrients, the balance of coastal water concentrations, particularly nitrogen and phosphate, is disrupted which leads to overproduction of phytoplankton. Subsequent plankton die off and bacterial decomposition leads to dissolved oxygen depletion, with negative consequences to the aerobic aquatic food web.

Lacking anthropogenic influence, most coastal zones will be nitrogen limited (Howarth et al., 2011). In mixed salinity zones, typical of coastal estuaries and marshes, phosphate has a high sedimentary recycling capacity. Phosphate is sorbed onto fine- grained material and can undergo desorption and resuspension into the surface water with changing redox conditions or by displacement from competing anions (Froelich, 1988, Spiteri et al., 2008). Additionally, eutrophication can induce geochemical feedbacks in sediments, increasing the bioavailability of phosphate in nutrient rich systems (Conley et al., 2007). The introduction of anthropogenic nitrogen to coastal waters has the capacity to rapidly change a phosphate limited system to a nitrogen limited system (Figure 1) (Conley et al., 2009).

Anthropogenic nitrogen enters coastal systems through three pathways; 1) burning of fossil fuels which increases atmospheric deposition of NO_y, 2) runoff of synthetic fertilizer which is diatomic nitrogen that has been fixed industrially by the Haber-Bosch process and 3) input of septic fluids from dense human and animal centers. When measured at the watershed level Howarth et al (2012) found these net anthropogenic nitrogen inputs are positively correlated with total nitrogen river flux to coastal waters. At the landscape level, studies of long term ecological conditions predict fewer long term sinks of nitrogen (i.e storage, denitrification) as climate change shifts towards wetter conditions (Howarth et al., 2012). Consequently, we expect an increase in anthropogenic nitrogen inputs to coastal waters in the coming decades.

Although net anthropogenic nitrogen inputs to watersheds show good correlation with total nitrogen river flux to the coast, riverine flux only accounts for between 15 and 45% of exports (Howarth, 2008). Data compiled by Howarth et al., (2008) show a strong correlation between net anthropogenic nitrogen inputs to watersheds and riverine nitrogen export, Figure 2. It is clear that watershed inputs of nitrogen reach the coast via other methods besides riverine flux.

Groundwater is normally cited as an environmental sink for nitrogen, as aquifers have a high carrying capacity for nitrate. Yet, in aquifers with direct connection to the coast, Submarine Groundwater Discharge can provide up to 20% of freshwater inputs to the coast. Consequently, groundwater cannot be a true ‘sink’ for anthropogenic nitrogen in coastal aquifers as SGD transports this nitrogen to surface waters.

Submarine Groundwater Discharge (SGD): Physical drivers and measurement techniques

Although SGD has been identified as a process for more than 30 years (Bokuniewicz, 1980, Simmons, 1992), it was only within the last decade that the scientific community settled on a concrete definition (Burnett et al., 2003). The definition "any and all flow of water on continental margins from the seabed to the coastal ocean, regardless of fluid composition or driving force. We thus define SGD without regard to its composition (e.g., salinity), origin, or phenomena driving the flow" given by Burnett et al., (2003) is an important step forward as it recognizes the importance of both fresh and recirculated water. This definition includes both net advection and tidal exchange flow which allows for consideration of pollutant mobilization due to mixing of water masses with distinct redox conditions. With a growing body of literature quantifying SGD in locales worldwide, a need arose for clarification of SGD scale. Bratton (2010) delineated three zones of SGD; a) Shelf scale, which encompasses SGD entering the entire continental shelf, including water from underlying confining layers, b)embayment scale which encompasses the inner continental shelf, to a maximum distance of 10 km offshore and c) near-shore scale where SGD enters coastal water within 10 m of the shore to a maximum depth of the first confining unit (Bratton, 2010). Of these three SGD scales, processes in the near-shore environment are currently the best understood due to numerous investigations of both physical and chemical processes in this zone.

The physical drivers of SGD include hydraulic gradient (Freeze and Cherry, 1979, Cambareri and Eichner, 1998, Bokuniewicz et al., 2004), tidal set up (Taniguchi, 2002, Xin et al., 2011, Santos et al., 2011, Robinson et al., 2007c, Robinson et al., 2007b, Li et al., 1999) including spring-neap cycling (de Sieyes et al., 2008, Robinson et al., 2007a), wave setup (Rotzoll and El-Kadi, 2008, Li et al., 1997, Xin et al., 2010) and bioirrigation which provides structures for conduit of SGD (Martin et al., 2004, Meysman et al., 2006, Emerson et al., 1984). The processes that drive SGD yield varying degrees of salt-freshwater mixing at the discharge point, yet all are important processes with respect to solute transport.

Clearly, SGD is a phenomenon that operates over a wide range of scales due to the diversity of driving forces. In order to tackle the problem of quantifying SGD, researchers in the field have developed a number of direct and indirect measurement techniques. Direct measurement techniques were first adapted from those used in lake settings and involved simple seepage meters that yield point measurements of SGD in the subtidal zone (Lee, 1977). These devices are still widely used today to measure SGD in both sandy and muddy environments. Further development of direct techniques led to autonomous ultrasonic seepage meters that continuously measure SGD rates over a period of days (Paulsen et al., 2001). These devices allow for an averaging of discharge rate over one tidal cycle, which is useful in evaluating total nutrient flux to surface water. Although manual seepage meters can achieve temporal resolution of SGD, and are very useful in the near shore environment, they are less effective at capturing the patchy spatial nature of SGD (Burnett et al., 2006). Geochemical tracer techniques were developed to address this gap in SGD measurement.

Indirect SGD measurement techniques can be broken down into two categories; chemical and remote sensing. Moore (1996) was the first to recognize the potential of the radium as an indirect tracer for SGD after measuring large enrichments of ^{226}Ra in coastal waters of the South Atlantic Bight (Moore, 1996). Measurements of ^{226}Ra concentrations in offshore waters are effective for identifying SGD at the continental shelf and embayment scale (Schmidt et al., 2011,

Smith and Swarzenski, 2012, Stieglitz et al., 2010). Numerous studies have shown the utility of employing the four major radium isotopes (^{226}Ra $t_{1/2=1600y}$; ^{228}Ra $t_{1/2}$=5.8y; ^{223}Ra $t_{1/2}$=11.3d; ^{224}Ra $t_{1/2}$=3.66d) to measure the fresh and salt fractions of SGD (Garcia-Orellana et al., 2010, Beck et al., 2008, Povinec et al., 2008). Radium, produced by the Thorium decay series, is present in aquifer solids which are in equilibrium with fresh groundwater. When fresh groundwater mixes with circulated seawater, ion exchange causes enrichment of radium in porewater, which is subsequently released to surface water (Charette et al., 2001). Radium has been successfully used to determine magnitude (Martin et al., 2007), spatial distribution (Schluter et al., 2004), and seasonal distribution (Charette, 2007) of SGD. In addition to dissolved radium isotopes, Radon (^{222}Rn $t_{1/2}$= 3.83d) a dissolved gas, is currently used to measure SGD in the nearshore environment.

Radon (^{222}Rn) has been shown to be an excellent tracer for SGD as it is highly enriched in groundwater with respect to surface water and can be measured in situ using a continuous monitoring system (Cable et al., 1996, Burnett and Dulaiova, 2003). A box model is employed to calculate ^{222}Rn inventories in surface water, where inputs are the sum of ^{222}Rn from SGD, ^{226}Ra decay and benthic diffusion processes, and outputs are losses to the atmosphere and from mixing offshore with low concentration seawater (Dulaiova et al., 2008, Crusius et al., 2005, Burnett and Dulaiova, 2003). As ^{222}Rn can be measured continuously along a coastline, it can be combined with other data such as nutrient concentrations in either shallow porewater or the water column to estimate SGD contributions of nutrients at the harbor level (Dulaiova et al., 2010).

Remote sensing techniques, particularly thermal infrared imaging (TIR) have been used to identify areas of SGD (Mulligan and Charette, 2006) and more recently to calculate flux of SGD from point source locations such as subterranean springs (Kelly et al., 2013). The ability to calculate SGD flux with TIR is currently limited as diffuse groundwater is significantly more difficult to quantify with this method. The combination of TIR with geochemical tracers such as radon and radium has proven useful in identifying areas of high SGD flux, but have yet to be connected with nutrient flux measurements (Wilson and Rocha, 2012, Varma et al., 2010). As with all SGD measurement techniques, gains in spatial extent are offset by losses in spatial resolution, which results in TIR techniques requiring complementary discharge measurements either by geochemical tracers, such as radium/radon, or by point measurements using seepage meters. Overall, the goal of SGD measurement in many studies is to understand biogeochemical transformations of solutes of interest, in particular nutrients that cause coastal eutrophication.

Nutrient transport through the Subterranean Estuary (STE) during SGD

The nutrient carrying capacity of submarine groundwater discharge is of great interest to coastal ecologists, land managers and research investigators alike. Although researchers long recognized that the intertidal aquifer hosts and moderates biogeochemical reactions, it wasn't until 1999 that the term 'subterranean estuary' was coined to describe this zone (Moore, 1999). The subterranean estuary (STE) was defined by Moore (1999) as 'a coastal aquifer where ground water derived from land drainage measurably dilutes sea water that has invaded the aquifer through a free connection to the sea'. This definition gave rise to work done by Slomp and VanCappellen (2004) who conceptually described four endmember mixing scenarios where rapidly changing redox conditions control the transport of nitrogen and phosphate through the subterranean estuary (Slomp and Van Cappellen, 2004). Although this was the first work to

codify nutrient processing in the STE, concepts of redox controls on groundwater derived nitrogen cycling are clearly older, particularly in studies of marsh settings (Tobias et al., 2001a).

At present, the STE is divided into three zones of freshwater-saltwater mixing; a) upper saline plume, b) freshwater zone and c) deep saline zone (Santos et al., 2012, Santos et al., 2011, Kroeger and Charette, 2008). Although there is wide recognition of all three zones, a majority of studies address solute transport through only one or two of these zones. This is often due to sampling constraints in intertidal sediments. The two most common methods of STE porewater/sediment sampling are done by piezometers and coring, with a wide variety of piezometer systems developed to capture zones or solutes of interest at individual sites (Ibanhez et al., 2011, Charette and Allen, 2006, Beck et al., 2010, Bratton et al., 2009).

The STE is known as a zone with dynamic trace element cycling (Beck et al., 2010) in both the solid and aqueous phases (Charette et al., 2005, Charette and Sholkovitz, 2006, Johannesson et al., 2011). Trace element concentrations, particularly iron and manganese, control removal of phosphate and carbon in the STE. Modeling of seawater intrusion into coastal aquifers indicate pH changes cause desorption of phosphate from iron oxyhydroxides and subsequent release to surface water (Spiteri et al., 2008). Iron is also associated with carbon cycling, particularly in low oxygen and nitrate systems, where iron oxyhydroxide dissolution and downgradient iron sulfide precipitation can sequester carbon in the solid phase in aquifers with small hydraulic gradient (Roy et al., 2011).

From a perspective of nitrogen cycling, carbon dynamics are particularly important in STE systems as they can be the limiting denitrification electron donor in freshwater systems (Green et al., 2008). Although it is not commonly studied in STE settings, initial work on inorganic carbon suggests DIC cycling may contribute to organic carbon remineralization with increased distance offshore, and may influence the microbial assemblage of permeable sediments (Dorsett et al., 2011). In STE's with low hydraulic gradient, such as tidal flats, net DOC export is linked to decomposition of benthic microalgae that is trapped in the nearshore zone (Kim et al., 2012). These findings are expected for tidal flats, where deposition of fine grain sediment is likely to trap phytoplankton and accelerate decomposition during atmospheric exposure at low tide. Recent work has shown that DOC release also occurs from sand sediments in high energy environments (Avery et al., 2012). These carbon releases are calculated to range from 12.4 to 22 mmol C m^{-2} d^{-1} and are an order of magnitude greater than releases from coastal shelf sediments or rainwater which are calculated to be 0.91mmol C m^{-2} d^{-1} and 0.47mmol C m^{-2} d^{-1} respectively(Burdige, 2002). In both high energy sand environments and low energy tidal flats, the freshwater component of SGD is a driver but not in itself a source of DOC. This is due to low DOC concentrations in aquifers with long flowpaths (Pabich et al., 2001, Leenher et al., (1974)).Therefore, although SGD is driven by the freshwater hydraulic gradient, in systems with low groundwater DOC concentrations, the freshwater endmember does not provide the bulk of carbon discharged during SGD.

Clearly chemical loads to coastal waters via SGD can compete with riverine and direct deposition methods (Taniguchi et al., 2002, Hosono et al., 2012, Slomp and Van Cappellen, 2004), and nitrogen is no exception. None of the components of the nitrogen cycle within the STE (nitrification, denitrification, dissimilatory nitrate reduction to ammonium (DNRA), annamox, coupled nitrification-denitrification, microbial assimilation, and anoxic mineralization)

can be classified as 'well understood'. Numerous studies have addressed nitrate exports via SGD to coastal waters but biogeochemical processing in the STE is still poorly quantified. The fact that both SGD and nitrogen cycling are spatially and temporally heterogeneous processes frequently results in investigations with only locally applicable results (Groffman et al., 2009).

Nitrate is of particular interest in most studies, as it is widely recognized that SGD is a new source of nitrate to coastal waters in both agricultural and urban settings (Wakida and Lerner, 2005, Saad, 2008, Knee et al., 2010). Although, recent work indicates even these basic assumptions may be incorrect, as areas with nitrogen limitation can act as net N_2 fixation zones (Rao and Charette, 2012), and dissimillatory nitrate reduction to ammonium (DNRA) is an often overlooked component of nitrogen cycling in the STE (Giblin et al., 2013). Still, at present the majority of nitrogen focused STE studies have sought to quantify total flux to surface waters. This is because understanding denitrification, the microbially mediated reduction of nitrate to nitrogen gas during carbon oxidation, in the STE is critical for evaluating the buffering capacity of coastal zones.

The measurement of denitrification can be approached in a variety of ways, including mass balance modeling, nitrogen isotope measurement (both enrichments and natural occurrence) and by measuring the buildup of dissolved nitrogen gas. Addy et al (2005) used push-pull injections of isotopically heavy nitrate ($^{15}N\text{-}NO_3^-$) to investigate denitrification in a groundwater fed marsh (Addy et al., 2005). This method has subsequently been applied to other settings (Koop-Jakobsen and Giblin, 2010) and is particularly good at determining the ratio of denitrification end products (i.e. N_2 vs N_2O) but has limited use in settings with a deep saline transition zone or long groundwater flow path lengths as long travel times (on the order of months) increase both dilution and degradation of isotopic enrichment . A comprehensive look at nitrogen cycling, including denitrification was done by Kroeger and Charette (2008) using natural isotope signatures of nitrate and ammonium. This work provided the first comprehensive look at nitrogen dynamics in each of the three classically identified and modeled STE zones; upper saline plume (shallow saline transition zone), freshwater zone and deep saline transition zone (Kroeger and Charette, 2008, Robinson et al., 2007c). Although results from one field site must be used cautiously when applied to other regions, Kroeger and Charette (2008) revealed that thermodynamically unstable conditions persist in the STE due to continual mixing between two water masses with contrasting redox conditions. Finally, they revealed a previously unconsidered nitrogen loss mechanism; mixing of nitrate rich freshwater into the deep saline zone, which are zones that store nitrogen reducing capacity in the forms of metals, carbon, sulfide and methane.

Microbially mediated denitrification results in the formation of excess nitrogen gas, which can be measured with high precision using membrane inlet mass spectrometry (MIMS) (Kana et al., 1994). Using dissolved argon to control for solubility changes due to physical factors such as temperature, salinity and pressure, N_2/Ar concentrations are used extensively to measure denitrification in freshwater systems (Bohlke and Denver, 1995, Bernot et al., 2003, Smith et al., 2006, Hopfensperger et al., 2009) sediments (Hopfensperger et al., 2009) and marine systems (Tortell, 2005, Hartnett et al., 2003), but this technique has yet to be applied to the STE. In this work the accumulation of excess dissolved N_2 above atmospheric equilibration and excess air concentrations is entirely attributed to denitrification.

Purpose and outline of the thesis

The purpose of this thesis is twofold; to quantify nitrate flux to surface waters of Long Island north shore embayments and to measure denitrification in the STE using N_2/Ar concentrations. The thesis is broken into six chapters (including this introduction), with chapters 2-6 each written as an article for publication. Chapter six is currently under review in *Applied Geochemistry*. The chapters are organized by embayment, and each uses a combination with SGD measurements and nitrogen flux models to address nitrate transport to surface water (except chapter six).

In chapters two and three I address nitrate discharge to Stony Brook Harbor, and embayment with connection to Long Island Sound via Smithtown Bay. Chapter two addresses the temporal stability of nitrogen and phosphate concentrations in the STE over spring-neap tidal cycling. Data from daily sampling of a multilevel intertidal well is presented in combination with automatic seepage-meter measurements. Results are interpreted using a model of water table over height to explain cycling of nitrate and phosphate concentrations in the STE that are not related to salinity patterns.

Chapter three presents results from a yearlong investigation of nitrate discharge into Stony Brook Harbor through an STE. Both geophysical and geochemical investigations were performed at this site in two locations in the spring and fall of 2011. Results from the geophysical investigation include autonomous seepage meter measurements, resistivity profiling of the STE and offshore locations, and sub-bottom sampling of porewater using a Trident probe. This work is currently in submitted (Durand et al., 2013, Water Resources Research), and will be part of the thesis of Josephine Durand. In this thesis I present results from the geochemical portion of the study. High resolution porewater profiles were taken to measure nitrate flux and denitrification at two sites along the western edge of the harbor at the two time periods described above. Denitrification was measured using N_2/Ar concentrations in conjunction with concentrations of NO_3^+ and a suite of electron donors. Findings indicate fresh groundwater enters the STE with nitrate concentration ranging 200 to 500µmol L^{-1} and undergoes 24%-39% denitrification during discharge through near shore sand sediment zone but undergoes ~55% denitrification during transport into the base of offshore mud sediments. Overall discharge of SGD-sourced nitrate to Stony Brook Harbor is calculated and findings indicate the offshore discharge zone is a sink for nitrate while the near shore discharge zone is a source of nitrate to surface water.

Chapter four is an investigation of nutrient discharge from a tidal flat located in Setauket Harbor, NY. In this study I chose an inlet of the harbor with sand banks and mud interior, which is representative of many Long Island north shore embayments where the quartz sand Upper Glacial aquifer is overlain by fine grain sediments deposited subtidally. A mixture of fresh groundwater and recirculated seawater drains from sand banks into the mud tidal flat at the center of the harbor. Tidal flats are known to be zones of significant biogeochemical cycling, but the influence of SGD on these systems is difficult to measure because traditional seepage meter techniques do not function during the ebb/low tide stage due to exposure. Using standard estuarine model and one dimensional advective-diffusion modeling I determined the harbor inlet acts as net sink for nitrate, phosphate and ammonium but a net source of carbon to surface water. By comparing flux rates of ammonium and nitrate with idealized stoichiometry of nitrogen

cycling I determined that denitrification is the dominant nitrogen loss process in the mud interior of the harbor, but nitrogen processes in the harbor inlet sand banks may be due to DNRA, coupled nitrification-denitrification, ammonium oxidation or a combination of these processes which is dependent on depth beneath the sediment water interface.

Chapter five presents results from a combined geochemical tracer and porewater chemistry study of Port Jefferson Harbor. The purpose of this work is asses total nitrate flux from SGD to the harbor. A shoreline survey of ^{222}Rn was conducted and used to calculate SGD flux from the inter-tidal and subtidal zones every 250m along shore. Data from the ^{222}Rn survey were combined with geochemical results from porewater sampling done using a Trident probe that samples the subtidal zone at a depth of 60cm beneath the sediment water interface. Spatial data from these two surveys were analyzed with GIS to determine harbor-wide discharge of nitrate from the shoreline. These results indicate 11kg $NO_3^-N\ d^{-1}$ is discharged to the harbor via SGD from the intertidal-sub tidal zone. In comparison, the Port Jefferson Sewage Treatment Plant (STP) discharges an average 12.2 kg-N d^{-1} directly into the harbor's southwest corner.

Finally, this thesis concludes with chapter six which presents results from a study done on zero valent iron (ZVI), a remediation tool often used to target nitrate contamination in groundwater. The purpose of this study is to examine the efficiency of nitrogen removal using commercial grade ZVI. Results from this study show that ammonium is produced by bare commercial ZVI when in contact with water. These unexpected findings pose a potential health threat during groundwater remediation as the amount of ammonium produced can exceed the targeted nitrate concentrations.

In sum, the parts of this thesis address how nitrogen behaves during transit through the STE and nitrate receiving loads to surface waters of Long Island north shore embayments. Future work will include two additional manuscripts; one that uses N_2/Ar to determine denitrification rates in two STE's of Port Jefferson Harbor and one that calculates N_2O flux from all three study sites investigated in this thesis.

References

ADDY, K., GOLD, A., NOWICKI, B., MCKENNA, J., STOLT, M. & GROFFMAN, P. 2005. Denitrification capacity in a subterranean estuary below a Rhode Island fringing salt marsh. *Estuaries,* 28**,** 896-908.

AVERY, G. B., KIEBER, R. J., TAYLOR, K. J. & DIXON, J. L. 2012. Dissolved organic carbon release from surface sand of a high energy beach along the Southeastern Coast of North Carolina, USA. *Marine Chemistry,* 132**,** 23-27.

BECK, A. J., COCHRAN, J. K. & SANUDO-WILHELMY, S. A. 2010. The distribution and speciation of dissolved trace metals in a shallow subterranean estuary. *Marine Chemistry,* 121**,** 145-156.

BECK, A. J., RAPAGLIA, J. P., COCHRAN, J. K., BOKUNIEWICZ, H. J. & YANG, S. 2008. Submarine groundwater discharge to Great South Bay, NY, estimated using Ra isotopes. *Marine Chemistry,* 109**,** 279-291.

BERNOT, M. J., DODDS, W. K., GARDNER, W. S., MCCARTHY, M. J., SOBOLEV, D. & TANK, J. L. 2003. Comparing denitrification estimates for a texas estuary by using acetylene inhibition and membrane inlet mass spectrometry. *Applied and Environmental Microbiology,* 69**,** 5950-5956.

BOHLKE, J. K. & DENVER, J. M. 1995. COMBINED USE OF GROUNDWATER DATING, CHEMICAL, AND ISOTOPIC ANALYSES TO RESOLVE THE HISTORY AND FATE OF NITRATE CONTAMINATION IN 2 AGRICULTURAL WATERSHEDS, ATLANTIC COASTAL-PLAIN, MARYLAND. *Water Resources Research,* 31**,** 2319-2339.

BOKUNIEWICZ, H. 1980. Groundwater Seepage Into Great South Bay, New-York. *Estuarine and Coastal Marine Science,* 10**,** 437-444.

BOKUNIEWICZ, H., POLLOCK, M., BLUM, J. & WILSON, R. 2004. Submarine Ground Water Discharge and Salt Penetration Across the Sea Floor. *Ground Water,* 42**,** 983-989.

BRATTON, J. F. 2010. The Three Scales of Submarine Groundwater Flow and Discharge across Passive Continental Margins. *Journal of Geology,* 118**,** 565-575.

BRATTON, J. F., BOHLKE, J. K., KRANTZ, D. E. & TOBIAS, C. R. 2009. Flow and geochemistry of groundwater beneath a back-barrier lagoon: The subterranean estuary at Chincoteague Bay, Maryland, USA. *Marine Chemistry,* 113**,** 78-92.

BURNETT, W. C., AGGARWAL, P. K., AURELI, A., BOKUNIEWICZ, H., CABLE, J. E., CHARETTE, M. A., KONTAR, E., KRUPA, S., KULKARNI, K. M., LOVELESS, A., MOORE, W. S., OBERDORFER, J. A., OLIVEIRA, J., OZYURT, N., POVINEC, P., PRIVITERA, A. M. G., RAJAR, R., RAMASSUR, R. T., SCHOLTEN, J., STIEGLITZ, T., TANIGUCHI, M. & TURNER, J. V. 2006. Quantifying submarine groundwater discharge in the coastal zone via multiple methods. *Science of the Total Environment,* 367**,** 498-543.

BURNETT, W. C., BOKUNIEWICZ, H., HUETTEL, M., MOORE, W. S. & TANIGUCHI, M. 2003. Groundwater and pore water inputs to the coastal zone. *Biogeochemistry,* 66**,** 3-33.

BURNETT, W. C. & DULAIOVA, H. 2003. Estimating the dynamics of groundwater input into the coastal zone via continuous radon-222 measurements. *Journal of Environmental Radioactivity,* 69**,** 21-35.

CABLE, J. E., BURNETT, W. C., CHANTON, J. P. & WEATHERLY, G. 1996. Modeling groundwater flow into the ocean based on ^{222}Rn. *Earth and Planetary Science Letters,* 144**,** 591-604.

CAMBARERI, T. C. & EICHNER, E. M. 1998. Watershed delineation and ground water discharge to a coastal embayment. *Ground Water,* 36**,** 626-634.

CHARETTE, M. A. 2007. Hydrologic forcing of submarine groundwater discharge: Insight from a seasonal study of radium isotopes in a groundwater-dominated salt marsh estuary. *Limnology and Oceanography,* 52**,** 230-239.

CHARETTE, M. A. & ALLEN, M. C. 2006. Precision ground water sampling in coastal aquifers using a direct-push, shielded-screen well-point system. *Ground Water Monitoring and Remediation,* 26**,** 87-93.

CHARETTE, M. A., BUESSELER, K. O. & ANDREWS, J. E. 2001. Utility of radium isotopes for evaluating the input and transport of groundwater-derived nitrogen to a Cape Cod estuary. *Limnology and Oceanography,* 46**,** 465-470.

CHARETTE, M. A. & SHOLKOVITZ, E. R. 2006. Trace element cycling in a subterranean estuary: Part 2. Geochemistry of the pore water. *Geochimica Et Cosmochimica Acta,* 70.

CHARETTE, M. A., SHOLKOVITZ, E. R. & HANSEL, C. M. 2005. Trace element cycling in a subterranean estuary: Part 1. Geochemistry of the permeable sediments. *Geochimica Et Cosmochimica Acta,* 69**,** 2095-2109.

CONLEY, D. J., CARSTENSEN, J., AERTEBJERG, G., CHRISTENSEN, P. B., DALSGAARD, T., HANSEN, J. L. S. & JOSEFSON, A. B. 2007. Long-term changes and impacts of hypoxia in Danish coastal waters. *Ecological Applications,* 17**,** S165-S184.

CONLEY, D. J., PAERL, H. W., HOWARTH, R. W., BOESCH, D. F., SEITZINGER, S. P., HAVENS, K. E., LANCELOT, C. & LIKENS, G. E. 2009. ECOLOGY Controlling Eutrophication: Nitrogen and Phosphorus. *Science,* 323**,** 1014-1015.

CRUSIUS, J., KOOPMANS, D., BRATTON, J. F., CHARETTE, M. A., KROEGER, K., HENDERSON, P., RYCKMAN, L., HALLORAN, K. & COLMAN, J. A. 2005. Submarine groundwater discharge to a small estuary estimated from radon and salinity measurements and a box model. *Biogeosciences,* 2**,** 141-157.

DE SIEYES, N. R., YAMAHARA, K. M., LAYTON, B. A., JOYCE, E. H. & BOEHM, A. B. 2008. Submarine discharge of nutrient-enriched fresh groundwater at Stinson Beach, California is enhanced during neap tides. *Limnology and Oceanography,* 53.

DORSETT, A., CHERRIER, J., MARTIN, J. B. & CABLE, J. E. 2011. Assessing hydrologic and biogeochemical controls on pore-water dissolved inorganic carbon cycling in a subterranean estuary: A C-14 and C-13 mass balance approach. *Marine Chemistry,* 127**,** 76-89.

DULAIOVA, H., CAMILLI, R., HENDERSON, P. B. & CHARETTE, M. A. 2010. Coupled radon, methane and nitrate sensors for large-scale assessment of groundwater discharge and non-point source pollution to coastal waters. *Journal of Environmental Radioactivity,* 101**,** 553-563.

DULAIOVA, H., GONNEEA, M. E., HENDERSON, P. B. & CHARETTE, M. A. 2008. Geochemical and physical sources of radon variation in a subterranean estuary - Implications for groundwater radon activities in submarine groundwater discharge studies. *Marine Chemistry,* 110**,** 120-127.

EMERSON, S., JAHNKE, R. & HEGGIE, D. 1984. SEDIMENT-WATER EXCHANGE IN SHALLOW-WATER ESTUARINE SEDIMENTS. *Journal of Marine Research,* 42**,** 709-730.

FREEZE, R. & CHERRY, J. 1979. *Groundwater,* Englewood Cliffs, NJ, Prentice Hall.

FROELICH, P. N. 1988. KINETIC CONTROL OF DISSOLVED PHOSPHATE IN NATURAL RIVERS AND ESTUARIES - A PRIMER ON THE PHOSPHATE BUFFER MECHANISM. *Limnology and Oceanography,* 33**,** 649-668.

GARCIA-ORELLANA, J., COCHRAN, J. K., BOKUNIEWICZ, H., YANG, S. & BECK, A. J. 2010. Time-series sampling of Ra-223 and Ra-224 at the inlet to Great South Bay (New York): a strategy for characterizing the dominant terms in the Ra budget of the bay. *Journal of Environmental Radioactivity,* 101**,** 582-588.

GIBLIN, A. E., TOBIAS, C. R., SONG, B., WESTON, N., BANTA, G. T. & RIVERA-MONROY, V. H. 2013. The Importance of Dissimilatory Nitrate Reduction to Ammonium (DNRA) in the Nitrogen Cycle of Coastal Ecosystems. *Oceanography,* 26**,** 124-131.

GREEN, C. T., PUCKETT, L. J., BOHLKE, J. K., BEKINS, B. A., PHILLIPS, S. P., KAUFFMAN, L. J., DENVER, J. M. & JOHNSON, H. M. 2008. Limited occurrence of denitrification in four shallow aquifers in agricultural areas of the United States. *Journal of Environmental Quality,* 37**,** 994-1009.

GROFFMAN, P. M., BUTTERBACH-BAHL, K., FULWEILER, R. W., GOLD, A. J., MORSE, J. L., STANDER, E. K., TAGUE, C., TONITTO, C. & VIDON, P. 2009. Challenges to incorporating spatially and temporally explicit phenomena (hotspots and hot moments) in denitrification models. *Biogeochemistry,* 93**,** 49-77.

HARTNETT, H. E., SEITZINGER, S. P. & RZ 2003. High-resolution nitrogen gas profiles in sediment porewaters using a new membrane probe for membrane-inlet mass spectrometry. *Marine Chemistry,* 83**,** 23-30.

HOPFENSPERGER, K. N., KAUSHAL, S. S., FINDLAY, S. E. G. & CORNWELL, J. C. 2009. Influence of Plant Communities on Denitrification in a Tidal Freshwater Marsh of the Potomac River, United States. *Journal of Environmental Quality,* 38**,** 618-626.

HOSONO, T., ONO, M., BURNETT, W. C., TOKUNAGA, T., TANIGUCHI, M. & AKIMICHI, T. 2012. Spatial Distribution of Submarine Groundwater Discharge and Associated Nutrients within a Local Coastal Area. *Environmental Science & Technology,* 46**,** 5319-5326.

HOWARTH, R., CHAN, F., CONLEY, D. J., GARNIER, J., DONEY, S. C., MARINO, R. & BILLEN, G. 2011. Coupled biogeochemical cycles: eutrophication and hypoxia in temperate estuaries and coastal marine ecosystems. *Frontiers in Ecology and the Environment,* 9**,** 18-26.

HOWARTH, R., SWANEY, D., BILLEN, G., GARNIER, J., HONG, B. G., HUMBORG, C., JOHNES, P., MORTH, C. M. & MARINO, R. 2012. Nitrogen fluxes from the landscape are controlled by net anthropogenic nitrogen inputs and by climate. *Frontiers in Ecology and the Environment,* 10**,** 37-43.

IBANHEZ, J. S. P., LEOTE, C. & ROCHA, C. 2011. Porewater nitrate profiles in sandy sediments hosting submarine groundwater discharge described by an advection-dispersion-reaction model. *Biogeochemistry,* 103**,** 159-180.

JOHANNESSON, K. H., CHEVIS, D. A., BURDIGE, D. J., CABLE, J. E., MARTIN, J. B. & ROY, M. 2011. Submarine groundwater discharge is an important net source of light and middle REEs to coastal waters of the Indian River Lagoon, Florida, USA. *Geochimica Et Cosmochimica Acta,* 75**,** 825-843.

KANA, T. M., DARKANGELO, C., HUNT, M. D., OLDHAM, J. B., BENNETT, G. E., CORNWELL, J. C. & PU 1994. Membrane inlet mass-spectrometer for rapid high-

precision determination of N2, O2 and Ar in environmental water samples. *Analytical Chemistry,* 66**,** 4166-4170.

KELLY, J. L., GLENN, C. R. & LUCEY, P. G. 2013. High-resolution aerial infrared mapping of groundwater discharge to the coastal ocean. *Limnology and Oceanography-Methods,* 11**,** 262-277.

KIM, T. H., WASKA, H., KWON, E., SURYAPUTRA, I. G. N. & KIM, G. 2012. Production, degradation, and flux of dissolved organic matter in the subterranean estuary of a large tidal flat. *Marine Chemistry,* 142**,** 1-10.

KINNEY, E. L. & VALIELA, I. 2011. Nitrogen Loading to Great South Bay: Land Use, Sources, Retention, and Transport from Land to Bay. *Journal of Coastal Research,* 27.

KNEE, K. L., STREET, J. H., GROSSMAN, E. E., BOEHM, A. B. & PAYTAN, A. 2010. Nutrient inputs to the coastal ocean from submarine groundwater discharge in a groundwater-dominated system: Relation to land use (Kona coast, Hawaii, USA). *Limnology and Oceanography,* 55**,** 1105-1122.

KOOP-JAKOBSEN, K. & GIBLIN, A. E. 2010. The effect of increased nitrate loading on nitrate reduction via denitrification and DNRA in salt marsh sediments. *Limnology and Oceanography,* 55**,** 789-802.

KROEGER, K. D. & CHARETTE, M. A. 2008. Nitrogen biogeochemistry of submarine groundwater discharge. *Limnology and Oceanography,* 53**,** 1025-1039.

LEE, D. R. 1977. DEVICE FOR MEASURING SEEPAGE FLUX IN LAKES AND ESTUARIES. *Limnology and Oceanography,* 22**,** 140-147.

LEENHER, J., MALCOLM, R., MCKINLEY, P. & ECCLES, L. (1974). Occurrence of dissolved organic carbon in selected ground-water samples in the United States. Journal of Research: U.S Geological Survey.

LI, L., BARRY, D. A., PARLANGE, J. Y. & PATTIARATCHI, C. B. 1997. Beach water table fluctuations due to wave run-up: Capillarity effects. *Water Resources Research,* 33**,** 935-945.

LI, L., BARRY, D. A., STAGNITTI, F. & PARLANGE, J. Y. 1999. Submarine groundwater discharge and associated chemical input to a coastal sea. *Water Resources Research,* 35**,** 3253-3259.

MARTIN, J. B., CABLE, J. E., SMITH, C., ROY, M. & CHERRIER, J. 2007. Magnitudes of submarine groundwater discharge from marine and terrestrial sources: Indian River Lagoon, Florida. *Water Resources Research,* 43.

MARTIN, J. B., CABLE, J. E., SWARZENSKI, P. W. & LINDENBERG, M. K. 2004. Enhanced Submarine Ground Water Discharge from Mixing of Pore Water and Estuarine Water. *Ground Water,* 42**,** 1000-1010.

MEYSMAN, F. J. R., GALAKTIONOV, E. S., GRIBSHOLT, B. & MIDDELBURG, J. J. 2006. Bioirrigation in permeable sediments: Advective pore-water transport induced by burrow ventilation. *Limnology and Oceanography,* 51**,** 142-156.

MOORE, W. S. 1996. Large groundwater inputs to coastal waters revealed by Ra-226 enrichments. *Nature,* 380**,** 612-614.

MOORE, W. S. 1999. The subterranean estuary: a reaction zone of ground water and sea water. *Marine Chemistry,* 65**,** 111-125.

MULLIGAN, A. E. & CHARETTE, M. A. 2006. Intercomparison of submarine groundwater discharge estimates from a sandy unconfined aquifer. *Journal of Hydrology,* 327.

PABICH, W. J., VALIELA, I. & HEMOND, H. F. 2001. Relationship between DOC concentration and vadose zone thickness and depth below water table in groundwater of Cape Cod, USA. *Biogeochemistry,* 55**,** 247-268.

PAULSEN, R. J., SMITH, C. F., O'ROURKE, D. & WONG, T. F. 2001. Development and evaluation of an ultrasonic ground water seepage meter. *Ground Water,* 39**,** 904-911.

POVINEC, P. P., BOKUNIEWICZ, H., BURNETT, W. C., CABLE, J., CHARETTE, M., COMANDUCCI, J. F., KONTAR, E. A., MOORE, W. S., OBERDORFER, J. A., DE OLIVEIRA, J., PETERSON, R., STIEGLITZ, T. & TANIGUCHI, M. 2008. Isotope tracing of submarine groundwater discharge offshore Ubatuba, Brazil: results of the IAEA-UNESCO SGD project. *Journal of Environmental Radioactivity,* 99**,** 1596-1610.

RAO, A. M. F. & CHARETTE, M. A. 2012. Benthic Nitrogen Fixation in an Eutrophic Estuary Affected by Groundwater Discharge. *Journal of Coastal Research,* 28**,** 477-485.

ROBINSON, C., GIBBES, B., CAREY, H. & LI, L. 2007a. Salt-freshwater dynamics in a subterranean estuary over a spring-neap tidal cycle. *Journal of Geophysical Research-Oceans,* 112.

ROBINSON, C., LI, L. & BARRY, D. A. 2007b. Effect of tidal forcing on a subterranean estuary. *Advances in Water Resources,* 30.

ROBINSON, C., LI, L. & PROMMER, H. 2007c. Tide-induced recirculation across the aquifer-ocean interface. *Water Resources Research,* 43.

ROTZOLL, K. & EL-KADI, A. I. 2008. Estimating hydraulic properties of coastal aquifers using wave setup. *Journal of Hydrology,* 353**,** 201-213.

ROY, M., MARTIN, J. B., SMITH, C. G. & CABLE, J. E. 2011. Reactive-transport modeling of iron diagenesis and associated organic carbon remineralization in a Florida (USA) subterranean estuary. *Earth and Planetary Science Letters,* 304.

SAAD, D. A. 2008. Agriculture-related trends in groundwater quality of the glacial deposits aquifer, central Wisconsin. *Journal of Environmental Quality,* 37**,** S209-S225.

SANTOS, I. R., BURNETT, W. C., MISRA, S., SURYAPUTRA, I. G. N. A., CHANTON, J. P., DITTMAR, T., PETERSON, R. N. & SWARZENSKI, P. W. 2011. Uranium and barium cycling in a salt wedge subterranean estuary: The influence of tidal pumping. *Chemical Geology,* 287.

SANTOS, I. R., COOK, P. L. M., ROGERS, L., DE WEYS, J. & EYRE, B. D. 2012. The "salt wedge pump": Convection-driven pore-water exchange as a source of dissolved organic and inorganic carbon and nitrogen to an estuary. *Limnology and Oceanography,* 57**,** 1415-1426.

SCHLUTER, M., SAUTER, E. J., ANDERSEN, C. E., DAHLGAARD, H. & DANDO, P. R. 2004. Spatial distribution and budget for submarine groundwater discharge in Eckernforde Bay (Western Baltic Sea). *Limnology and Oceanography,* 49**,** 157-167.

SCHMIDT, C., HANFLAND, C., REGNIER, P., VAN CAPPELLEN, P., SCHLUTER, M., KNAUTHE, U., STIMAC, I. & GEIBERT, W. 2011. Ra-228, Ra-226, Ra-224 and Ra-223 in potential sources and sinks of land-derived material in the German Bight of the North Sea: implications for the use of radium as a tracer. *Geo-Marine Letters,* 31**,** 259-269.

SIMMONS, G. M. 1992. Importance of Submarine Groundwater Discharge (SGWD) and Seawater cycling to Material Flux Across Sediment Water Interfaces in Marine Environments. *Marine Ecology-Progress Series,* 84**,** 173-184.

SLOMP, C. P. & VAN CAPPELLEN, P. 2004. Nutrient inputs to the coastal ocean through submarine groundwater discharge: controls and potential impact. *Journal of Hydrology,* 295**,** 64-86.

SMITH, C. G. & SWARZENSKI, P. W. 2012. An investigation of submarine groundwater-borne nutrient fluxes to the west Florida shelf and recurrent harmful algal blooms. *Limnology and Oceanography,* 57**,** 471-485.

SMITH, L. K., VOYTEK, M. A., BOHLKE, J. K. & HARVEY, J. W. 2006. Denitrification in nitrate-rich streams: Application of N-2 : Ar and N-15-tracer methods in intact cores. *Ecological Applications,* 16**,** 2191-2207.

SPITERI, C., VAN CAPPELLEN, P. & REGNIER, P. 2008. Surface complexation effects on phosphate adsorption to ferric iron oxyhydroxides along pH and salinity gradients in estuaries and coastal aquifers. *Geochimica Et Cosmochimica Acta,* 72.

STIEGLITZ, T. C., COOK, P. G. & BURNETT, W. C. 2010. Inferring coastal processes from regional-scale mapping of (222)Radon and salinity: examples from the Great Barrier Reef, Australia. *Journal of Environmental Radioactivity,* 101**,** 544-552.

TANIGUCHI, M. 2002. Tidal effects on submarine groundwater discharge into the ocean. *Geophysical Research Letters,* 29.

TANIGUCHI, M., BURNETT, W. C., CABLE, J. E. & TURNER, J. V. 2002. Investigation of submarine groundwater discharge. *Hydrological Processes,* 16**,** 2115-2129.

TOBIAS, C. R., ANDERSON, I. C., CANUEL, E. A. & MACKO, S. A. 2001. Nitrogen cycling through a fringing marsh-aquifer ecotone. *Marine Ecology-Progress Series,* 210**,** 25-39.

TORTELL, P. D. 2005. Dissolved gas measurements in oceanic waters made by membrane inlet mass spectrometry. *Limnology and Oceanography-Methods,* 3**,** 24-37.

VARMA, S., TURNER, J. & UNDERSCHULTZ, J. 2010. Estimation of submarine groundwater discharge into Geographe Bay, Bunbury, Western Australia. *Journal of Geochemical Exploration,* 106**,** 197-210.

WAKIDA, F. T. & LERNER, D. N. 2005. Non-agricultural sources of groundwater nitrate: a review and case study. *Water Research,* 39**,** 3-16.

WILSON, J. & ROCHA, C. 2012. Regional scale assessment of Submarine Groundwater Discharge in Ireland combining medium resolution satellite imagery and geochemical tracing techniques. *Remote Sensing of Environment,* 119**,** 21-34.

XIN, P., ROBINSON, C., LI, L., BARRY, D. A. & BAKHTYAR, R. 2010. Effects of wave forcing on a subterranean estuary. *Water Resources Research,* 46.

XIN, P., YUAN, L. R., LI, L. & BARRY, D. A. 2011. Tidally driven multiscale pore water flow in a creek-marsh system. *Water Resources Research,* 47.

Tables and Figures

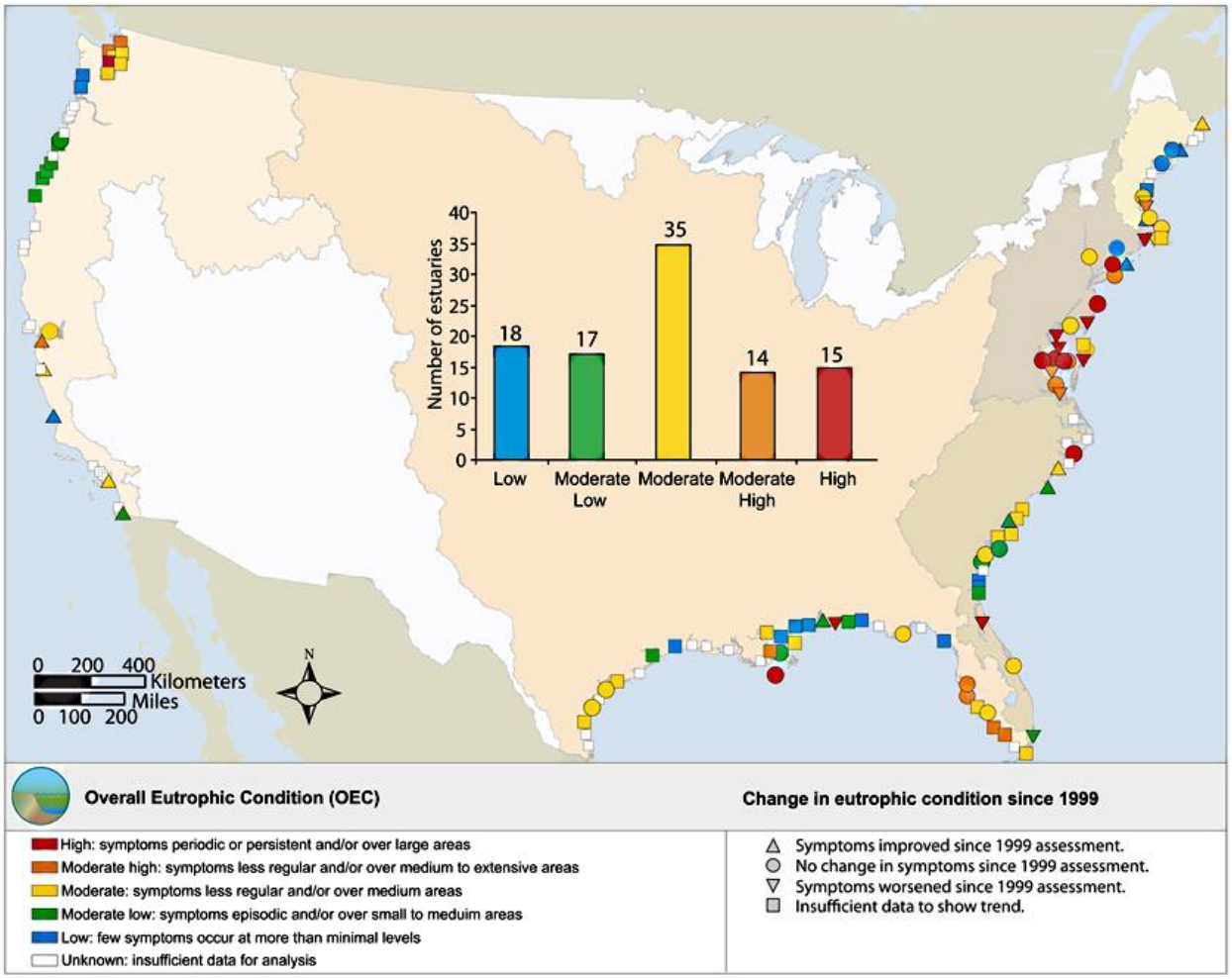

Figure 1 National estuarine eutrophication assessment depicting changes in eutrophic condition since 1999 for major U.S estuaries. Figure adapted from (Bricker et al., 2007)

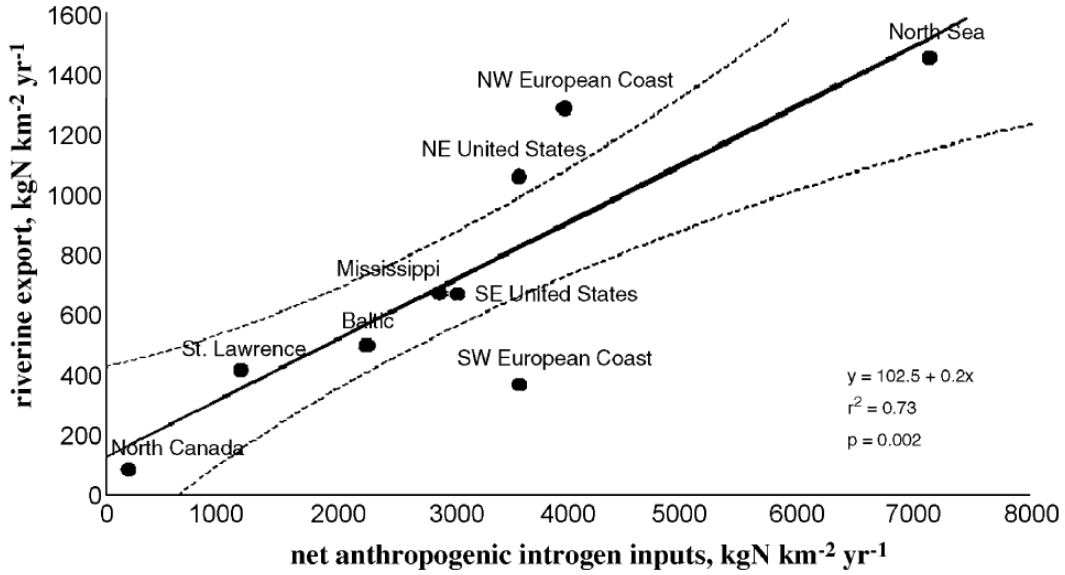

Figure 2 Relationship between anthropogenic nitrogen inputs and riverine export of nitrogen for selected watersheds. An increase in anthropogenic input is positively correlated with riverine export. Figure adapted from (Howarth, 2008).

CHAPTER II: NUTRIENT DYNAMICS IN A SUBTERRANEAN ESTUARY OVER TWO SPRING-NEAP TIDAL CYCLES

Abstract

Variations in nutrient concentrations in a coastal aquifer were investigated over two spring-neap tidal cycles. Porewater samples (n = 262) were collected daily for 30 days from a coastal aquifer at Stony Brook Harbor, Long Island, New York. Porewater was collected from a cluster well installed in an intertidal zone from intervals of 1m to a maximum depth of 9.1m. Results show temporal salinity and dissolved oxygen stability of both the upper saline plume and fresh groundwater zone. A large terrestrial hydraulic gradient results in a stable salinity depth profile despite daily two meter tidal oscillations. Fresh groundwater contains high concentrations of nitrate, averaging 6.3±2.7mgL^{-1} NO_3^--N (450±193µmol L^{-1}) at a depth of 9.1m. Maximum inorganic phosphate concentrations, averaging 0.13mgL^{-1} PO_4^{-3}-P (4.2µmol L^{-1}), are observed at sampling depth 1.8m. Mass balance models were used to estimate fresh and saline fractions of discharge during spring and neap tide periods. Spring tide discharge is estimated at 1.3 L $min^{-1}m^{-1}$ and 48.0 L $min^{-1}m^{-1}$ for freshwater and saltwater respectively. Neap tide discharge is estimated at 6.5 L $min^{-1}m^{-1}$ and 28.0 L $min^{-1}m^{-1}$ for fresh and saltwater respectively. These differences in salt vs fresh water factions of SGD result in water table over height during spring tide. Consequently, water-table over height causes migration of the freshwater discharge point along the beach face resulting in variation of nutrient concentrations.

Introduction

Submarine groundwater discharge (SGD) plays an important role in nutrient loading to coastal embayments (Howarth, 2008). During SGD complex mixing between fresh groundwater and saline surface water in the coastal aquifer, or subterranean estuaries (STE), allows for biogeochemical nutrient transformations at short temporal and spatial scales (Slomp and Van Cappellen, 2004, Kroeger and Charette, 2008). Nutrients originating from household sewage disposal, lawn fertilizers, and agricultural applications mix with meteoric water and recharge the surficial aquifer. During SGD, nutrients in surficial aquifer groundwater traverse the STE and can contribute to surface water eutrophication.. Quantification of nutrient attenuation or remineralization in the STE is required to calculate nutrient budgets for use in land management decisions which protect coastal waterways.

It is important that investigations of nutrient transformation in the STE account for temporal variability in the shallow circulated seawater portion of the system, termed the upper saline plume (USP), and the underlying fresh groundwater cell. The temporal stability of nutrient distribution in a subterranean estuary is affected by both by tidal forcing on the seaward side and meteoric input on the freshwater side (de Sieyes et al., 2008). Typical STE nutrient sampling requires multiple days to complete using and AMS Retract-A-Tip drive point piezometer systems, which are favored for their sampling resolution and minimal perturbation of surrounding sediments (Charette and Allen, 2006).

Tidal variations are known to affect SGD rates by changing groundwater head at the aquifer/sea interface (Thorn and Urish, 2012, Nielsen, 1990, Li et al., 2000). These variations have been observed over both daily and spring-neap tidal cycles. Few studies, however, have documented the significance of spring-neap tidal cycles on total SGD flux (Taniguchi, 2002,

Boehm et al., 2004, Jeng et al., 2005, Robinson et al., 2007a) with only one addressing spring-neap influence on SGD nutrient concentrations (de Sieyes et al., 2008).

In this study I investigate the temporal stability of salinity, dissolved oxygen, nitrate, ammonium and inorganic phosphate within a STE of Stony Brook Harbor, an embayment with direct connection to Long Island Sound. Daily samples were collected from a multi-level intertidal zone cluster well for two spring-neap cycles. Results show a highly stable salinity and dissolved oxygen distribution but variable nitrate and inorganic phosphate concentrations. I find increased inorganic phosphate concentrations during spring tide coincide with increased horizontal width of the intertidal zone and nitrate distribution at the base of the saline transition zone varies with spring-neap cycling. Analytical models of the freshwater budget and tidal forcing were used to estimate fresh and saline discharge during spring and neap tide stages. Although SGD during spring tide is calculated at 49.3 L min^{-1} m^{-1} as compared to discharge during neap tide of 28.0 L min^{-1} m^{-1}, spring tide discharge carries one-fifth of the freshwater fraction when compared to neap discharge. This discrepancy in fresh fraction between the two time periods results in water table over height during spring tides. Variances in both nitrate and inorganic phosphate result from the same physical process of tidal forcing, i.e. water table over height, but with different consequences due to sources of each nutrient.

Materials and Methods

Site Description

Stony Brook Harbor is an embayment located on the southern side of Long Island Sound in New York State (Suffolk County). The shallow harbor covers 4.5 sq. km with direct connection to Long Island Sound via a narrow, northeastern inlet adjacent to the mouth of West Meadow Creek. The deepest point in the inlet is approximately 10 m below mean sea level (msl). Figure 3 shows the location of the cluster well at Stony Brook Harbor.

The adjacent reaches at Stony Brook Harbor are influenced by semi-diurnal tidal variations in water level. The dominant current direction within Stony Brook Harbor is controlled by tidal oscillations rather than a surface stream flow from the land. The average tidal range (measured between mean high and low water levels) have not been measured in Stony Brook Harbor, however in nearby Port Jefferson Harbor, the average tidal range was 2.01m for the period from 1960 to 1978.

The shallow unconfined water table aquifer over most of Long Island is within the Upper Glacial aquifer unit. In general, water north of the regional groundwater divide, which trends east-west across the island, moves northward towards Long Island Sound, and water south of the divide flows southward toward the Atlantic Ocean. Horizontal hydraulic conductivity is estimated at 70.1md^{-1}, with a 10:1 horizontal to vertical anisotropy (Buxton and Modica, 1992).

Nitrogen inputs to the Upper Glacial Aquifer are primarily from atmospheric deposition, septic tank-cesspool systems and turf grass fertilizer. The area around Stony Brook Harbor is classified as low density housing, with 0-1 dwelling units per acre (Koppelman, 1978). Porter (1980) found that on Long Island, turfgrass makes up 33% of land in low density housing, with each dwelling unit containing an on-site wastewater system (Porter, 1980). Munster (2008) used

major cations (Mg^{2+}, Ca^{2+}, Na^{+}, K^{+}) in well samples to estimate nitrogen contributions to Long Island groundwater and determined that in low density housing greater than 50% of groundwater nitrogen originates from rainwater, with septic tank/cesspool systems contributing ≤20% of nitrogen (Munster, 2008b). As the watershed immediately surrounding Stony Brook Harbor is classified as low density housing, nitrogen inputs are primarily from atmospheric deposition and turfgrass leachate, with minor contributions from on-site wastewater systems.

Sample Collection and Analysis

Three monitoring wells were installed as a cluster within 1m of each other to enable easy sample collection; well location shown in Figure 3. Wells were screened at intervals of 0.9m with a screen length of 0.15m. Samples were collected from ten depths: 0.91, 1.8, 2.7, 3.6, 4.6, 5.5, 6.4, 7.3, 8.2, and 9.1 meters below grade. To allow sampling during high tide situation, polyethylene tubing (Grainger, I.D 0.64cm) was extended to a bulkhead, 10m up gradient of the high tide mark. Samples were collected daily between 9:30 am to 10:30am EST, over a 27 day period between 9/26/11 and 10/25/11. Tidal stage during sample collection varied; at times the sample area was completely covered with surface water. Daily tidal stage oscillations are shown in Figure 4 along with high tide envelope for spring-neap tidal amplitude changes.

To prevent cross flow between depth intervals, wells were sampled from alternating depths. Samples were brought to the surface by a peristaltic pump (Coleman Palmer). At each sampling depth, 3 well volumes were pumped prior to sample collection. Field parameters of temperature, conductivity, salinity, dissolved oxygen and pH was measured using a YSI-556 handheld multi-probe meter with flow-through cell. For each parameter, the reported accuracies are: pH 4-10 ± 0.2, temperature ±0.150 ^{o}C, and dissolved oxygen ±0.2 mg/l and conductivity ±0.1% (YSI instruments). To record tidal oscillation during the sampling period a pressure logger (Solinist #3001) was installed in an adjacent well.

Samples for nitrogen and phosphate analysis were filtered through 0.45µM (Whatman GF/B) filter. Samples were field cooled and frozen within 6 hours of collection. Phosphate samples received 50µl of H_2SO_4 upon collection, to prevent HPO_4^{2-} removal from solution due to the formation of iron and manganese oxide precipitation that may occur due to changes in dissolved oxygen concentration of porewater during sampling.

Total NO_3^--N was determined by using Lachat Instruments FIA-6000 flow injection type automated analyzer. Concentrations of NO_3^-+NO_2^-, are expressed in mgL^{-1} of nitrogen. Reactive phosphate was analyzed using the spectrophotometric ascorbic acid method (Johnson and Petty, 1982) and silica was analyzed using the molybdate blue method (Strickland and Parsons, 1978) and are expressed in µmol L^{-1}. For all colorimetric methods, six point calibration curves were used to calibrate sample sets. Precision of NO_3^--N, phosphate and silica are 5%, 5%, and 3% respectively.

Tide Data

To determine if salinity and nutrient variations correlated to tidal fluctuations, a pressure logger was placed in a well adjacent to the sampling well. For some dates, no pressure logger was available to record simultaneous water level variations. For these dates, the tides were extrapolated using the values given by MapTech Chart Navigator Pro software. To validate the

extrapolation, one logger placed at the average low tide in Stony Brook Harbor for 7 days was compared with the software predictions based on the station at Port Jefferson entrance, NY. It was found that the amplitude of tides in Stony Brook Harbor was the same as Port Jefferson but with a lag of 1h 45 minutes. The tidal level in Stony Brook during the sampling of the cluster well was calculated by correcting the Port Jefferson station predictions with the observed time lag. By selecting the high tide value of the water level for each day, meaning by extracting the envelope of the signal, we obtained the spring/neap tidal cycle for this period. All tide level data was corrected to mean low tide for clarity in reporting, Figure 4.

To determine the salinity of seepage water (S_{prism}, equation 2) , a conductivity/ temperature logger was placed inside a ultrasonic seepage meter funnel for six days from 5-18-11 to 5-24-11 (Paulsen et al., 2001), position shown in Figure 3. Real time measurements of temperature and conductivity were used to compute salinity values of the water inside the seepage meters, using the Practical Salinity Scale (PSS78) (Poisson, 1980b, Poisson, 1980a, Lewis and Perkin, 1981). Salinity for S_{prism} was taken as the 24hour average of salinity values inside the ultrasonic seepage meter on spring tide (5-18-11) and neap tide (5-24-11).

Silica Dissolution Experiment

Residence time of porewater in the upper saline plume (τ) was determined using dissolved silica as a tracer to determine kinetics of quartz dissolution in seawater (Anschutz et al., 2009). Sediment samples were collected adjacent to the cluster well location from a depth of 10cm beneath the sediment surface. Overlying water was gathered from a point 12m offshore of mean low tide. Sediment was sieved to remove any grain size larger than 4mm diameter. Homogenized sediment and filtered seawater were placed in 50ml polypropylene vials at a ratio of 1:4. Vials were sealed and placed in a dark temperature bath at 11^0C for the duration of the 38 day experiment. Every 1-3 days, a vial was removed and porewater was collected for silica analysis.

SGD Flux calculations

Flux calculations were used to determine the fractions of fresh and recirculated discharge for spring and neap time periods. Total submarine groundwater discharge (SGD) is defined as $SGD= D_t+ D_m+D_w+D_s$ (de Sieyes et al., 2008, Li et al., 1999). Where D_m is fresh groundwater flux, D_t and D_w are flux due to tidal and wave circulation respectively, and D_s is saline seasonal flux (Michael et al., 2005). Wave action (D_w) is negligible in Stony Brook Harbor due to a narrow inlet with Long Island Sound and small fetch for wind driven waves, therefore we do not include this term in our calculations. As the distance between wave breaker and wave run up is near zero, this term is omitted from our calculation of SGD. Seasonal saline export, D_s, is also omitted from this calculations, as the time period of this study is too short to observe such fulctuations. Therefore in this setting SGD flux is simplified to $SGD= D_t+D_m$.

The height of the water table responds to tidal forcing according to equations detailed in Neilsen (1990), shown in eq. 1 and 2 below. Here we use the solution present by Li et al (1999) to calculate tidally driven seepage rate per alongshore distance (D_t) (Nielsen, 1990, Li et al., 1999). Tidal flux D_t is calculated using a mass balance model applied to the shoreline, as outlined by di Sieyes et al (2008, eq 3). The results obtained from eq. 1 are tidally averaged and therefore imply quasi-steady-state conditions for the spring or neap period.

$$D_t=\frac{neA}{KTt}*\exp(-\propto)*(\cos(\propto)-\sin(\propto))+\frac{\sqrt{2}n_eA^2}{s_bTt}\exp\left(-\sqrt{2\propto}\right)*\cos\left(\sqrt{2\propto}\right)+\frac{n_eA^2}{KTt}$$
(1)

where

$$k=\sqrt{\frac{n_e\omega}{2K_hH}} \qquad \propto=\frac{kA}{s_b} \tag{2}$$

Tidal flux input parameters are as follows:

- n_e effective volumetric porosity is 0.4(Olanrewaju and Wong, 2010)
- A is the tidal amplitude, 2.4m for spring tide and 1.7m for neap tide
- Beach slope, s_b, (0.06) was calculated from beach survey done in October 2011 and assumed horizontally constant for the intertidal zone
- T_t is the tidal period, set to 12.42h
- ω is the tidal frequency of the M_2 harmonic $1.41x10^{-4}$ rad s^{-1}.
- Hydraulic conductivity (K_h=$1.43x10^{-4}$ m s^{-1}) was calculated using Darcy's law using discharge data from ultrasonic seepage meter measurements acquired in May 2011 (see above) and hydraulic head measurements from two inland monitoring wells, locations shown in Figure 3.
- Aquifer thickness (H=40m) was determined from coring data taken in a previous study of Long Island Upper Glacial sediments (Olanrewaju and Wong, 2010).

  Fresh groundwater flux was calculated by employing a mass balance of the discharge zone during spring and neap tides using equation 2 $D_m=\frac{(S_{offshore}-S_{prism})*V_{prism}}{S_{offshore}*L*\tau}$ (3)

- The discharge zone is treated as a prism (V_{prism}) with length of 80m, the distance alongshore with an upgradient retaining wall, height of 40m (aquifer thickness).
- $S_{offshore}$ is the average salinity of surface water in Stony Brook Harbor (Smith et al., 2008),
- S_{prism} is the average salinity during neap and spring tides, taken from ultrasonic seepage meter measurements (see above).
- Residence time of pore water in the prism (τ) was calculated by averaging silica concentrations in seepage meter samples taken during a six hour period on August 14, 2012.

The manual seepage meter (Lee, 1977) was placed below the mean low tide mark. A schematic of the freshwater discharge prism is given in supplemental figure S1.

Results

Samples were analyzed for salinity, dissolved oxygen, nitrate and phosphate. Table 1 summarizes average results for each sampling depth. As shown in table 1, three zones of salinity

are apparent in this STE; upper saline plume from 0.91 to 1.8m beneath sediment surface, a salinity transition zone at 2.7m depth and freshwater zone extending from 3.6m to at least 9.1m depth. Salinity (Figure 5), dissolved oxygen (Figure 6), nitrate (Figure 8) and phosphate (Figure 9) are clearly stratified with depth, as shown in. For clarity salinity, dissolved oxygen and nutrient data are plotted for 5 of the 10 sampling depths (0.91 m, 1.8 m, 2.7 m, 3.6 m, and 9.1 m), which represents the greatest salinity gradient.

Salinity

Salinity of Stony Brook Harbor overlying water averages 26.5 ppt, which is higher than average salinity of 24.3 ppt taken from a depth of 0.91m below the sediment surface. Salinity decreases to an average of 5.27 ppt at a depth of 2.7m, delineating the lower boundary of salt penetration (Figure 7). According to classification by Robinson et al (2007b) this deeper salt penetration may result from tide induced circulation. Although wave set-up is known to affect salinity distribution in the STE (Longuethiggins, 1983) wave set-up in Stony Brook harbor is negligible due to a narrow harbor inlet, shallow depth and limited boat traffic.

Salinity results were compared during precipitation events for September and October 2011. USGS rain gage station at Sag Harbor, NY, located 76.2km from the field site, was used for precipitation data. Cumulative precipitation for September and October were 97.8mm and 103.6mm respectively. No precipitation was recorded on 16 days during the period from September 26 to October 25. One precipitation event, on October 19, recorded 35mm of precipitation. During the following two days a 2.4 ppt decrease in salinity was observed at the 0.91m sampling depth. This decrease corresponds to a 2.1 ppt increase in salinity at the 1.8m sampling depth (Figure 5), which may indicate depression of the upper saline plume in response to freshwater recharge.

Dissolved oxygen

Dissolved oxygen (DO) concentrations exhibit minimal variation in the upper saline plume during the 27 day sampling period (Figure 6). At sampling depth 0.91 m DO averages 1.0 ± 0.3 mgL^{-1} then decreases to 0.9 ± 0.3 mgL^{-1} at a depth of 1.8 m. DO concentrations at the salt-freshwater boundary, located at 2.7m depth, average $1.1\pm0.5mgL^{-1}$. At depths 3.6-9.1m DO concentrations were similar to concentrations observed elsewhere in the Upper Glacial aquifer on the North Shore of Long Island (Young, 2010) with an overall average of $7.6\pm0.8mgL^{-1}$. Maximum variation in DO concentration is observed at a depth of 3.6m and appears to be driven by tidal position. Tide height during sampling is positively correlated with DO concentration at this depth (Figure 6).

In the STE at Stony Brook Harbor DO concentrations deviate from models presented for subterranean estuary chemical interactions (Slomp and Van Cappellen, 2004). Models indicate that in a STE with oxic seawater and oxic groundwater, DO concentrations should remain high. We postulate that in low energy environments the development of *Spartina alterniflora*, a marsh grass (Figure 3), in the intertidal zone sets up an organic rich reducing environment in the top three meters of permeable sediments. A direct connection between depletion of porewater DO and marsh root structures was observed by Xia and Li (2012) who investigated groundwater flow in a tidal marsh and found a mud-sand two layered structure that allowed for a mangrove marsh

to take up oxygen and freshwater via their root penetration into the sand zone(Xia and Li, 2012). Marsh growth in turn enhanced trapping of salt and organic rich silt deposited during high tide. In Stony Brook Harbor, marsh roots trap fine silt and sediments, which increases dissolved organic carbon (DOC) concentrations in the shallow seawater recirculation cell (Young et al, Chapter 3) allowing for biologic consumption of oxygen and observed DO depletion. Increased DOC concentration in a saline recirculation cell was also observed in coastal aquifers of Waquoit Bay, MA, (Charette and Sholkovitz, 2006, Roy et al., 2011).

Dissolved inorganic phosphate

Inorganic phosphate concentrations from Stony Brook Harbor STE are less than $1mgL^{-1}$ for all sampling depths and times. Maximum variability exists in the upper saline plume, where concentrations average $0.08\pm0.04mgL^{-1}$ and $0.13\pm0.05mgL^{-1}$ for sampling depths of 0.91 m and 1.8 m respectively (Figure 10). At sampling depths greater than ranging 2.7-5.5m, inorganic phosphate concentrations average $0.02mgL^{-1}$, and at depths greater than 5.5m concentrations average $0.005mgL^{-1}$, which is at the detection limit for this method.

When inorganic phosphate concentrations are compared with daily tide variations, no pattern is observed (supplemental figure S2). A correlation is observed between spring/neap tidal variations where inorganic phosphate concentrations in samples from depths of 0.91 and 1.8m have maximum values during spring tides on days 9-28-111 and 10-25-11. Spring tides at these dates show range between high and low tide of 2.8-2.7m, as compared to neap tide variation of 1.5-1.7m on 10-5-11 and 10-19-11 (fig 5).

Dissolved inorganic phosphate behaves non-conservatively in the STE due to sorption and desorption onto iron and aluminum (hydro)oxides (Spiteri et al., 2008). Surface charge properties of commonly occurring metals in the STE change depending on freshwater or saltwater conditions(Barrow et al., 1980). Rapid pH changes along a salinity gradient are also known to remove phosphate from solution (Spiteri et al., 2006), particularly when pH varies between 4 and 7. We do not observe significant pH differences between the upper saline plume (pH average 6.2) and fresh groundwater portions (pH average 5.8) of the STE.

Boguslavsky (2000) investigated cation exchange capacity (CEC) from Upper Glacial aquifer sand samples in Long Island and found 80% of CEC in sand is due to grain coatings (Boguslavsky, 2000). Although Fe^{2+} concentrations are not available for this data set, core samples taken from this site do not show an 'iron curtain' as observed in other STE settings (Charette and Sholkovitz, 2002), likely due to the presence of oxygenated groundwater at depth. Therefore reduced, mobile iron is restricted to the upper saline plume at this location, as all other depths contain oxic porewater.

Dissolved inorganic nitrate

Unlike salinity and dissolved oxygen, nitrate concentration in the fresh water zone of the coastal aquifer was not stable during the monitoring period. Nitrate in samples from 0.91 and 1.8m depth are stable and low, averaging 0.7 ± 0.2 mg NO_3^--N L^{-1} throughout the sampling period. Between depths of 2.7 and 3.6 m values rapidly increase, reaching a maximum 27 day average of 8.6 ± 3.8 mg NO_3^--N L^{-1}at 4.6 m below the sediment water interface. Nitrate concentrations then drop to a 27 day average of 5.2 ± 3.7 mgNO_3^--N L^{-1} at 9.1m depth (Figure 9,

Figure 10). Although only one well was used to track nutrient concentrations in this study, it is notable that maximum nitrate concentrations are observed at the top of the fresh groundwater zone located at a depth of 3.6m. Concentrations in excess of 10 mgNO_3^--N L^{-1} and N:P>>16:1 (atomic ratio) indicate the presence of nitrogen inputs in excess of those expected due to atmospheric deposition or seawater circulation. Direct atmospheric deposition at Great South Bay, a water body adjacent to the south shore of Long Island, were estimated at 10kg-N $ha^{-1}yr^{-1}$.

Daily tidal oscillations do not effect nitrate concentrations in any portion of the sampled coastal aquifer, as observed from tidal stage data shown in Figure 4 and supplemental figure S3. As the well was sampled once a day at the same time, tide stage varied throughout the course of the 27 day sampling period. If tidal changes drove nitrate concentrations, we would expect a correlation between nitrate concentrations in some depths with tide stage. In fact, tide stage is not correlated with nitrate concentration in any of the three STE zones; saline circulation, saline transition or fresh groundwater. In all cases linear and polynomial data fits have an r^2 of less than 0.12 (data not shown, refer to figure S3). Variations in spring-neap tidal cycle changes correlate with concentrations in porewater samples from depths 3.6-9.1m. Peak values are observed during falling spring to neap tides, with values of 14.7 mgNO_3^--N L^{-1} and 12.0 mgNO_3^--N L^{-1} at depths 3.6m and 9.1m respectively on 10-3-11, two days prior to neap tide (Figure 9). During neap tide all freshwater depths experience elevated NO_3^- concentrations when compared to spring tide concentrations.

Water table overheight

The influence of spring neap cycling is most apparent in nitrate and phosphate concentrations. In previous studies, water table overheight is noted as a possible explanation for conservative and non-conservative ion changes during spring-neap cycling (Maji and Smith, 2009, Robinson et al., 2007a, Thorn and Urish, 2012, de Sieyes et al., 2008). Water table over height occurs in coastal aquifers when the height of the time average water table differs from mean sea level which results in the formation of a seepage face on the beach. Previous investigators have proposed analytical solutions to the Boussinesq equation and found overheight controls the seaward boundary point of discharging freshwater. Changes in tidal amplitude effect water table overheight and therefore the point of discharge (Song et al., 2006). In systems where spring-neap forces produce change in tidal amplitude, which changes the extent of water table overheight may lead to changes in the position of the seaward boundary. I calculated freshwater (D_m) and saltwater (D_t) discharge rates for the study area to determine if changes in the ratio of D_m/D_t are responsible for observed nitrate and phosphate variance.

Using intertidal-zone mass-balance calculations (eq. 1-3) I found that freshwater discharge (D_m) is 01.3L $min^{-1}m^{-1}$ and 6.5L $min^{-1}m^{-1}$ for spring and neap tide respectively. Using equation 1, I calculated a tidally driven discharge (D_t) of 48.0 L $min^{-1}m^{-1}$ and 21.5 L $min^{-1}m^{-1}$ for spring and neap tide respectively (table 2). The sum of these calculations is 49.3L $min^{-1}m^{-1}$(SGD_{spring}) and 28.0 L $min^{-1}m^{-1}$(SGD_{neap}). Although neap tide D_m flux is five times greater than spring tide D_m, total discharge during spring tide (SGD_{spring}) is twice the flux of neap tide (SGD_{neap}). The difference between spring and neap tide total discharge is higher than those recorded in other studies of unconfined aquifers, but exhibits the same patterns observed elsewhere. The larger freshwater discharge calculated in Stony Brook Harbor during spring tide is possibly due to the absence of waves (D_w) which adds equal amounts of saltwater discharge to spring and neap calculations (de Sieyes et al., 2008, Boehm et al., 2004).

Modeled systems of subterranean estuaries predict increased tidally driven recirculation (TDR) with increased tidal amplitude and small aquifer depth and increased inland hydraulic gradient, defined by Robinson et al., 2007b as:

$$\delta = \frac{A}{H} \quad (4)$$

$$Q_f = \frac{D_{(m\ or\ t)}}{HK} \quad (5)$$

$$TDR = \frac{Q_t}{Q_f} \times 100 \quad (6)$$

Where δ is the dimensionless parameter used to describe the tidal amplitude (A) relative to aquifer thickness (H). Terrestrial groundwater discharge, Q_f, is equal to calculated D_m for spring and neap time periods, and K is hydraulic conductivity. Q_t is taken as the tidally driven component, D_t, which comprises recirculated seawater in the upper saline plume. Tidally driven recirculation percent (TDR) was calculated for spring and neap tidal periods and found to be 3796% and 430% respectively. These values are on the upper end of TDR, but within modeled values for systems with large δ and Q_f* (table 2). Further, these parameters are linked to water table overheight and extreme values of δ can lead to the generation of higher order harmonics (Li et al., 2000, Nielsen, 1990). Modeled values of TDR% with Q_f* of 10^{-3} and $\delta \geq 0.06$ are on the order of 10^3, in line with calculations based on our field measured data.

Increases in both inland hydraulic conductivity and tidal amplitude parameters combine with increased horizontal shoreline excursion during spring tide producing a system where saltwater recirculation exceeds drainage capacity. Therefore vertical movement of freshwater during spring tide will produce dilution effects at the top of the upper saline plume/freshwater boundary.

Comparison with other spring-neap studies

Depth stratified salinity measurements were fairly invariant during the 27 day sampling at Stony Brook Harbor. These results are opposed to observations from other field areas and modeling studies. Robinson et al., (2007b) modeled coastal aquifer salinity distribution during spring-neap tidal variations and found late neap tide corresponds to minimum salt penetration in the STE, due to reduced downward vertical specific discharge. They also found increased horizontal extent of the upper saline plume during spring tide, which increases the fraction of total SGD flux attributable to tidal circulation (D_t). Thorn and Urish (2012) found large salinity changes, ranging from 0.09 – 4.7 ppt, in a coastal aquifer well during a 35 day sampling period. De Sieyes et al., (2008) also found significant salinity variation in near shore monitoring well samples over a spring neap tidal cycle ((de Sieyes et al., 2008). We hypothesize that salinity stability at the cluster well sampling point in Stony Brook Harbor is due to (1) location of the cluster well and (2) the presence of an intertidal marsh. As the cluster well is located on the sea-ward side of an intertidal marsh it is buffered from salinity changes at the high and low tide marks produced by vertical and horizontal expansion of the upper saline plume during spring tide. The intertidal marsh traps suspended sediment and saltwater during high tide stage, stabilizing the underlying upper saline plume. Observations from a larger field campaign at this site indicate sediments in the top meter of the marsh are silty with a high fraction of dissolved organic matter. This is in contrast with the bulk of sediments at the site, which are coarse to medium grain sands. Were the cluster well placed in a beach area not associated with marsh grasses it is plausible that porewater salinity would change in response to variation in tidal amplitude associated with spring-neap forcing.

Dissolved oxygen concentrations indicate invariant biogeochemical zones in the coastal aquifer. Few studies have examined changes in dissolved oxygen concentration over a spring-neap tidal cycle, but results from general coastal aquifer studies indicate dissolved oxygen is rapidly depleted in the upper saline plume due to intense biologic activity. Seawater carries significant dissolved and particulate organic matter concentrations that fuel microbial processes in the upper saline plume (Santos et al., 2011). Dissolved oxygen in Stony Brook Harbor overlying water is high (average 78.2% oxygen saturation) therefore the most likely explanation for hypoxic conditions at depths 0.91-2.7m (Figure 6) is biological consumption of organic matter trapped by marsh roots in the shallowest portion of the aquifer.

Changes in inorganic phosphate concentration during spring/neap tidal changes likely result from horizontal shrinking of the upper salinity plume during neap tide (Robinson et al., 2007a). During spring tide a larger volume of the intertidal aquifer is inundated with harbor water during high tide, as evidenced by the discharge differences shown in table 2. As a result, the marsh grass remains inundated with more iron in silt and sand grain coatings, releasing bound PO_4^{-3}-P into pore water. The onset of neap tides decreases the vertical tidal range by greater than 1m and horizontal tide range by 11.5-12.3m. This variation shortens flow paths in the upper saline plume, allowing oxygen penetration into previously submerged sediments. Increased oxygen promotes development of iron (hydro)oxides which sorb inorganic phosphate, removing it from porewater(Spiteri et al., 2008).

Nitrate concentration changes in the coastal aquifer are linked to changes in freshwater fraction (D_m) of the SGD discharge. The freshwater zone acts as a plume whose discharge point moves landward during spring tide due to water table overheight and large TDR %. Nitrate is stratified with depth in both spring and neap discharge times, indicating incomplete mixing of younger, shallow recently recharged meteoric water with deep, older meteoric water. Groundwater from 3.6m below the surface contains nitrate concentrations 1.2-2.1mgL^{-1} greater than concentrations from 9.1m depth. Further, we see increases of 0.5-0.7mg$L^{-1}$$NO_3^-$-N in the shallowest sampling depth, 0.91m.

The exact physical explanation for changes in nitrate plume pulsing during neap tide is unclear. Previous investigators have modeled coastal aquifers and determined that the point of freshwater discharge migrates seaward and landward depending on tidal amplitude(Robinson et al., 2007b, Taniguchi, 2002), but further investigation revealed no significant change in discharge point over spring-neap tidal period (Robinson et al., 2007a). The extent of this migration, and length of the seepage face at steady state conditions, is particularly sensitive to landward hydraulic gradient, aquifer anisotropy and aquifer storage(Maji and Smith, 2009). Maji and Smith (2009) modeled contaminant loading from an inland source to the nearshore environment and found peak contaminant discharge occurred at falling mid-tide, not low tide as would be expected. Changes in contaminant discharge load coincide with migration of freshwater discharge point within the intertidal zone, as the mid-tide discharge point is ~60m landward of the low tide discharge point. At Stony Brook Harbor, nitrate concentrations occur during falling spring-neap tide, resulting from recession of spring stage water table overheight.

A conceptual model is presented to show how water table overheight during spring tide changes the discharge point of the freshwater tube (Figure 11). During spring tide, water table

overheight moves the discharge point landward, and the cluster well samples only the outer edges of the freshwater tube, therefore nitrate concentrations from all freshwater sampling depths drop. During neap tide, tidal SGD flux (D_t) is reduced by half which moves the freshwater tube exit point seaward. The cluster well then intercepts the entire portion of the nitrate slug (Figure 11). The extent of seaward movement varies, as evidenced by different nitrate maximum concentrations in between neap tide periods (Figure 9).

It is expected that during spring tide, increased tidal amplitude will increase the depth penetration of the upper saline plume (Robinson et al., 2007c). Modeled tracer experiments of conservative contaminant movement indicate that reduction in total mass flux is linked with tidal presence. Further, tides increase the longitudinal spread and total freshwater transit time of a contaminant (Robinson et al., 2007b). In the context of this study, these modeled results provide a possible explanation for the decrease in freshwater nitrate concentrations without increased depth penetration of the upper saline plume. We hypothesize that the presence of an *S.Alternaflora* marsh stabilizes the depth penetration of the upper saline plume on a longer timescale than spring-neap cycling. Despite this stabilization, the freshwater zone may respond to spring-neap forcing by transverse spread of the contaminant, widening of the discharge zone and increased travel time of the nitrate plume, due to water table overheight. Further investigation of lateral extent of the nitrate plume in anisotropic systems is required to confirm transverse contaminant spread. This is particularly important in areas of the shoreline that are not covered by marsh grasses, as these areas should experience increased nitrate concentrations during spring-neap cycling due to spreading of the nitrate plume located in the shallow freshwater zone beneath the *S.Alternaflora* marsh.

Conclusion

Few studies exist of how spring-neap cycling affects nutrient distribution in a subterranean estuary. Here we present results from an investigation of nutrient concentrations in a subterranean estuary over two spring-neap cycles. We find stable salinity and dissolved oxygen structure but variance in both phosphate and nitrate concentrations. Water table overheight calculations indicate freshwater flux during neap tide is five times greater than during spring tide, but total discharge is greater during spring tide due to increased portion of recirculated seawater. A conceptual model is presented to explain how water table overheight moves the point of freshwater discharge during changes in tidal amplitude which results in cycling of nutrient concentrations in the freshwater zone of the subterranean estuary.

References

Anschutz, P. et al., 2009. Tidal sands as biogeochemical reactors. Estuarine Coastal and Shelf Science, 84(1): 84-90.

Barrow, N.J., Bowden, J.W., Posner, A.M., Quirk, J.P., 1980. DESCRIBING THE EFFECTS OF ELECTROLYTE ON ADSORPTION OF PHOSPHATE BY A VARIABLE CHARGE SURFACE. Australian Journal of Soil Research, 18(4).

Boehm, A.B., Shellenbarger, G.G., Paytan, A., 2004. Groundwater discharge: Potential association with fecal indicator bacteria in the surf zone. Environmental Science & Technology, 38(13).

Buxton, H.T., Modica, E., 1992. PATTERNS AND RATES OF GROUNDWATER-FLOW ON LONG-ISLAND, NEW-YORK. Ground Water, 30(6): 857-866.

Charette, M.A., Allen, M.C., 2006. Precision ground water sampling in coastal aquifers using a direct-push, shielded-screen well-point system. Ground Water Monitoring and Remediation, 26(2): 87-93.

Charette, M.A., Sholkovitz, E.R., 2002. Oxidative precipitation of groundwater-derived ferrous iron in the subterranean estuary of a coastal bay. Geophysical Research Letters, 29(10).

Charette, M.A., Sholkovitz, E.R., 2006. Trace element cycling in a subterranean estuary: Part 2. Geochemistry of the pore water. Geochimica Et Cosmochimica Acta, 70(4).

de Sieyes, N.R., Yamahara, K.M., Layton, B.A., Joyce, E.H., Boehm, A.B., 2008. Submarine discharge of nutrient-enriched fresh groundwater at Stinson Beach, California is enhanced during neap tides. Limnology and Oceanography, 53(4).

Howarth, R.W., 2008. Coastal nitrogen pollution: A review of sources and trends globally and regionally. Harmful Algae, 8(1): 14-20.

Jeng, D.S., Mao, X., Enot, P., Barry, D.A., Li, L., 2005. Spring-neap tide-induced beach water table fluctuations in a sloping coastal aquifer. Water Resources Research, 41(7).

Johnson, K.S., Petty, R.L., 1982. Determination of Phosphate in Sea-Water by Flow Injection Analysis with Injection of Reagent. Analytical Chemistry, 54(7): 1185-1187.

Koppelman, L., 1978. The Long Island comprehensive waste treatment management plan: Hauppauge, Long Island Regional Planning Board, pp. 345.

Kroeger, K.D., Charette, M.A., 2008. Nitrogen biogeochemistry of submarine groundwater discharge. Limnology and Oceanography, 53(3): 1025-1039.

Lee, D.R., 1977. DEVICE FOR MEASURING SEEPAGE FLUX IN LAKES AND ESTUARIES. Limnology and Oceanography, 22(1): 140-147.

Lewis, E.L., Perkin, R.G., 1981. THE PRACTICAL SALINITY SCALE 1978 - CONVERSION OF EXISTING DATA. Deep-Sea Research Part a-Oceanographic Research Papers, 28(4).

Li, L., Barry, D.A., Cunningham, C., Stagnitti, F., Parlange, J.Y., 2000. A two-dimensional analytical solution of groundwater responses to tidal loading in an estuary and ocean. Advances in Water Resources, 23(8): 825-833.

Li, L., Barry, D.A., Stagnitti, F., Parlange, J.Y., 1999. Submarine groundwater discharge and associated chemical input to a coastal sea. Water Resources Research, 35(11): 3253-3259.

Longuethiggins, M.S., 1983. WAVE SET-UP, PERCOLATION AND UNDERTOW IN THE SURF ZONE. Proceedings of the Royal Society of London Series a-Mathematical Physical and Engineering Sciences, 390(1799): 283-&.

Maji, R., Smith, L., 2009. Quantitative analysis of seabed mixing and intertidal zone discharge in coastal aquifers. Water Resources Research, 45.

Michael, H.A., Mulligan, A.E., Harvey, C.F., 2005. Seasonal oscillations in water exchange between aquifers and the coastal ocean. Nature, 436(7054): 1145-1148.

Munster, J., 2008. Non-point sources of nitrate and perchlorate in urban land use to groundwater, Suffolk County, NY, http://www.geo.sunysb.edu/reports/.

Nielsen, P., 1990. Tidal Dynamics of the Water-Table in Beaches. Water Resources Research, 26(9): 2127-2134.

Olanrewaju, J., Wong, T.-F., 2010. Hydraulic Conductivity, Porosity and Particle-Size Distribution of Core Samples of the Upper Glacial Aquifer: Laboratory Observations, Stony Brook University, Department of Earth and Space Sciences.

Paulsen, R.J., Smith, C.F., O'Rourke, D., Wong, T.F., 2001. Development and evaluation of an ultrasonic ground water seepage meter. Ground Water, 39(6): 904-911.

Poisson, A., 1980a. CONDUCTIVITY-SALINITY-TEMPERATURE RELATIONSHIP OF DILUTED AND CONCENTRATED STANDARD SEAWATER. Ieee Journal of Oceanic Engineering, 5(1).

Poisson, A., 1980b. Conductivity/salinity/temperature relationship of diluted and concentrated standard seawater. Oceanic Engineering, IEEE Journal of, 5(1): 41-50.

Porter, K.S., 1980. AN EVALUATION OF SOURCES OF NITROGEN AS CAUSES OF GROUNDWATER CONTAMINATION IN NASSAU-COUNTY, LONG-ISLAND. Ground Water, 18(6): 617-625.

Robinson, C., Gibbes, B., Carey, H., Li, L., 2007a. Salt-freshwater dynamics in a subterranean estuary over a spring-neap tidal cycle. Journal of Geophysical Research-Oceans, 112(C9).

Robinson, C., Li, L., Barry, D.A., 2007b. Effect of tidal forcing on a subterranean estuary. Advances in Water Resources, 30(4).

Robinson, C., Li, L., Prommer, H., 2007c. Tide-induced recirculation across the aquifer-ocean interface. Water Resources Research, 43(7).

Roy, M., Martin, J.B., Smith, C.G., Cable, J.E., 2011. Reactive-transport modeling of iron diagenesis and associated organic carbon remineralization in a Florida (USA) subterranean estuary. Earth and Planetary Science Letters, 304(1-2).

Santos, I.R. et al., 2011. Uranium and barium cycling in a salt wedge subterranean estuary: The influence of tidal pumping. Chemical Geology, 287(1-2).

Slomp, C.P., Van Cappellen, P., 2004. Nutrient inputs to the coastal ocean through submarine groundwater discharge: controls and potential impact. Journal of Hydrology, 295(1-4): 64-86.

Smith, J.K., Lonsdale, D.J., Gobler, C.J., Caron, D.A., 2008. Feeding behavior and development of Acartia tonsa nauplii on the brown tide alga Aureococcus anophagefferens. Journal of Plankton Research, 30(8): 937-950.

Spiteri, C., Regnier, P., Slomp, C.P., Charette, M.A., 2006. pH-Dependent iron oxide precipitation in a subterranean estuary. Journal of Geochemical Exploration, 88(1-3): 399-403.

Spiteri, C., Van Cappellen, P., Regnier, P., 2008. Surface complexation effects on phosphate adsorption to ferric iron oxyhydroxides along pH and salinity gradients in estuaries and coastal aquifers. Geochimica Et Cosmochimica Acta, 72(14).

Strickland, J., Parsons, T., 1978. A practical handbook of seawater analysis, 2. Fisheries Research Board of Canada, Ottowa.
Taniguchi, M., 2002. Tidal effects on submarine groundwater discharge into the ocean. Geophysical Research Letters, 29(12).
Thorn, P., Urish, D., 2012. Preliminary Observation of Complex Salt-FreshWater Mixing in a Beach Aquifer. Ground Water.
Xia, Y.Q., Li, H.L., 2012. A combined field and modeling study of groundwater flow in a tidal marsh. Hydrology and Earth System Sciences, 16(3).
Young, C., 2010. Extent of Denitrification in Northport Groundwater, SUNY Stony Brook.

Tables and Figures

Table 1 Average salinity, dissolved oxygen, nitrate and phosphate concentrations for all sampling dates. Standard deviation for each data set is given in parenthesis.

Depth (m)	salinity (27)	dissolved oxygen (27) (mg L^{-1})	NO_3^--N (27) (mg L^{-1})	PO_4^{-3} (23) (mg L^{-1})
0.91	24.2 (0.7)	1.0 (0.3)	0.7 (0.2)	0.08 (0.04)
1.8	17.9 (1.3)	0.9 (0.3)	0.7 (0.3)	0.1 (0.05)
2.7	5.3 (0.9)	1.3 (1.1)	1.6 (0.7)	0.02 (0.02)
3.6	1.3 (0.5)	7.1 (0.9)	8.2 (2.6)	0.02 (0.02)
4.6	1.4 (0.6)	7.5 (0.5)	8.5 (3.8)	0.02 (0.03)
5.5	0.9 (0.4)	7.5 (0.5)	7.9 (3.3)	0.02 (0.02)
6.4	0.8 (0.7)	7.8 (0.7)	6.1 (3.2)	0.01 (0.01)
7.3	0.6 (0.3)	7.9 (0.5)	6.3 (2.3)	0.01 (0.01)
8.2	0.5 (0.5)	7.7 (0.8)	6.2 (2.5)	0.01 (0.01)
9.1	0.8 (1.1)	7.7 (1.5)	6.2 (2.7)	0.01 (0.01)

Table 2 Spring and neap calculations of fresh groundwater flux (D_m), tidal flux (D_t), ratio of aquifer thickness to tidal amplitude (δ), normalized terrestrial groundwater discharge (Q_f) and percent of tidally driven recirculation (TDR).

Parameter	Spring	Neap
D_m(L $min^{-1}m^{-1}$)	1.3	6.5
D_t(L $min^{-1}m^{-1}$)	48	21.5
δ	0.06	0.04
Qf	3.84E-03	1.92E-02
TDR (%)	3796	430.4

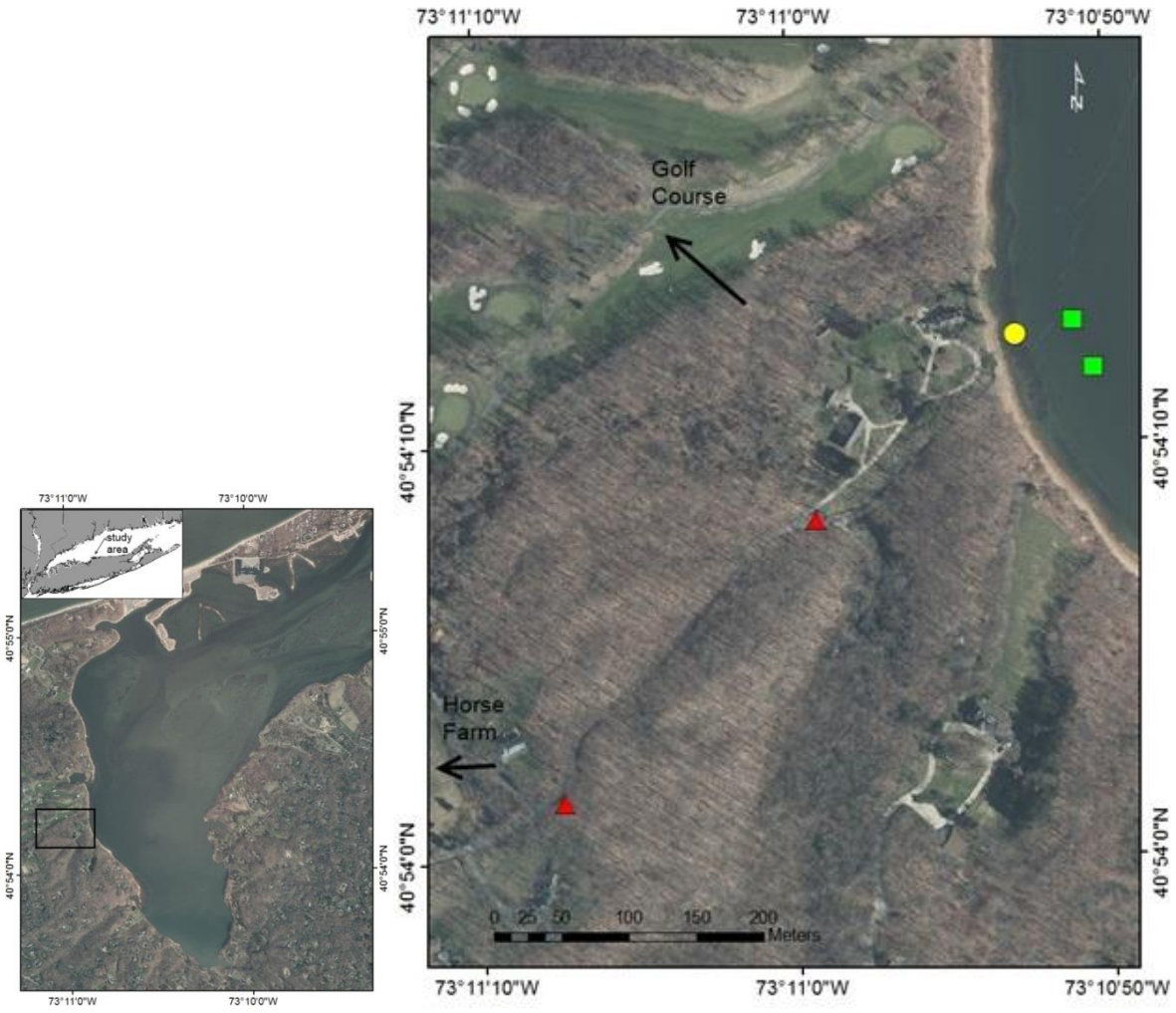

Figure 3 Site map showing Stony Brook Harbor (left) and detailed sample location (right). Map of study site (right) showing location of cluster well (●), seepage meters (□) and inland monitoring wells (Δ). 'Golf Course' and 'Horse Farm' indicate locations of Nissequogue Golf Course and horse farms on Moriches road, St.James, NY.

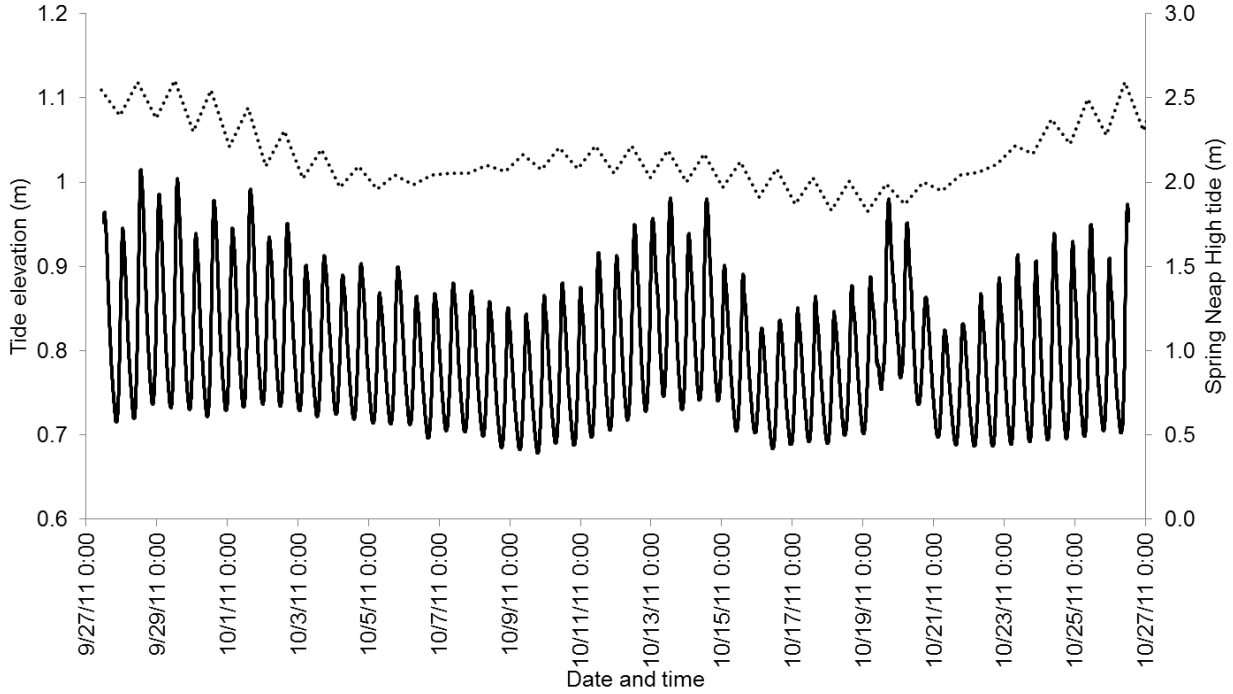

Figure 4 Tidal elevation data at Stony Brook Harbor during cluster well sampling period.

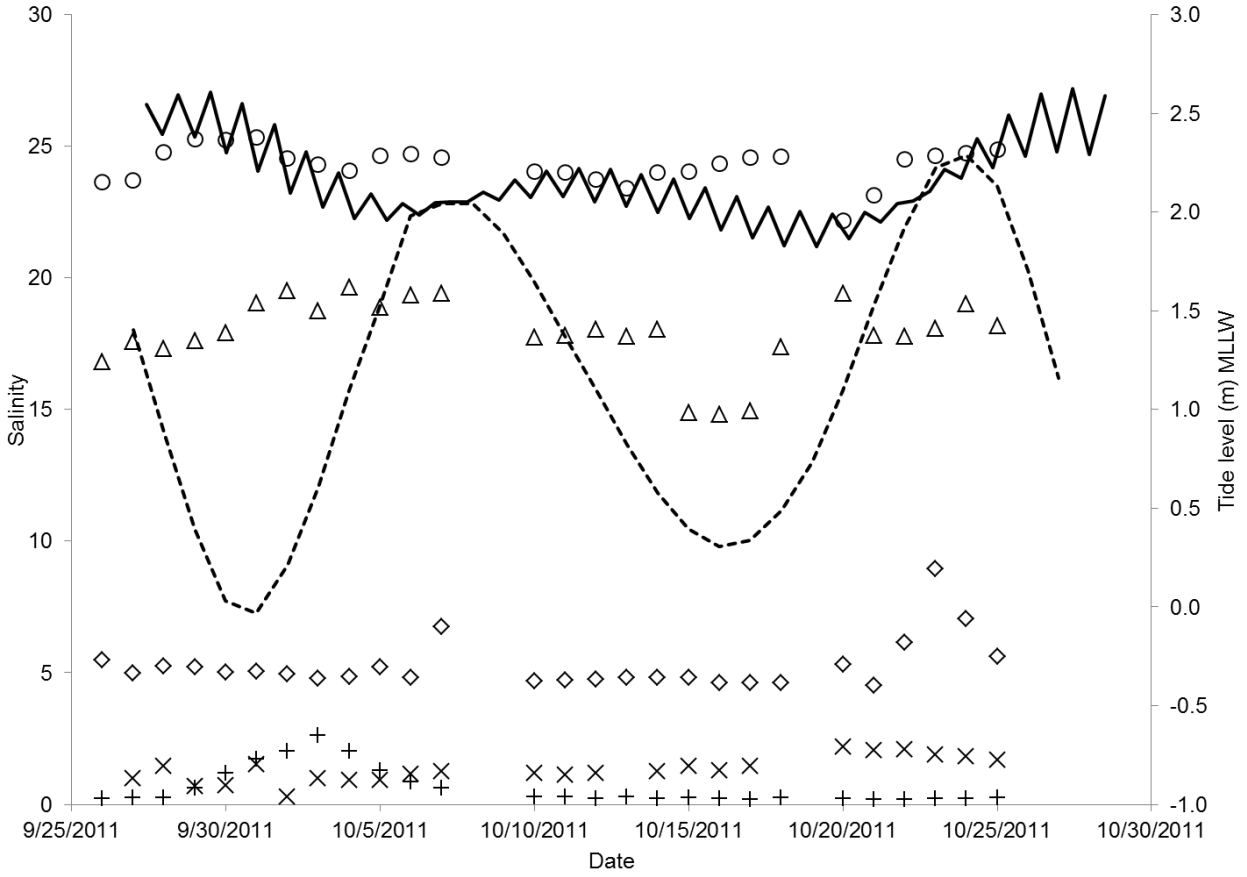

Figure 5 Salinity plot for 5 well sampling depths. Sampling depths of 0.91m (○), 1.8m (Δ), 2.7m(◊), 3.6m(X) and 9.1m(+). High tide envelope (—) and tide station during sample time (9:30am) (--) shown for reference.

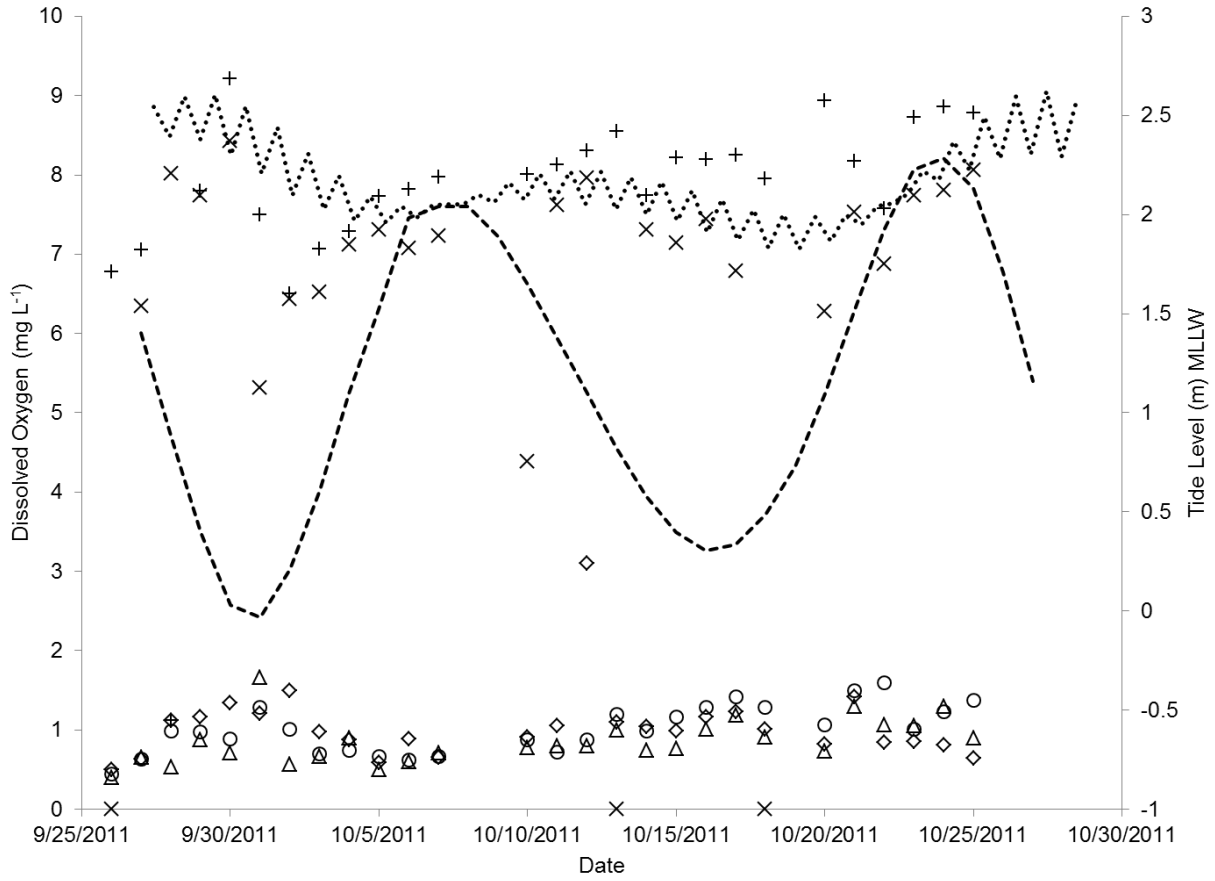

Figure 6 Dissolved Oxygen plot for 5 well sampling depths. Sampling depths of 0.91m (○), 1.8m (Δ), 2.7m(◊), 3.6m(X) and 9.1m(+). High tide envelope (—) and tide station during sample time (9:30am) (--) shown for reference.

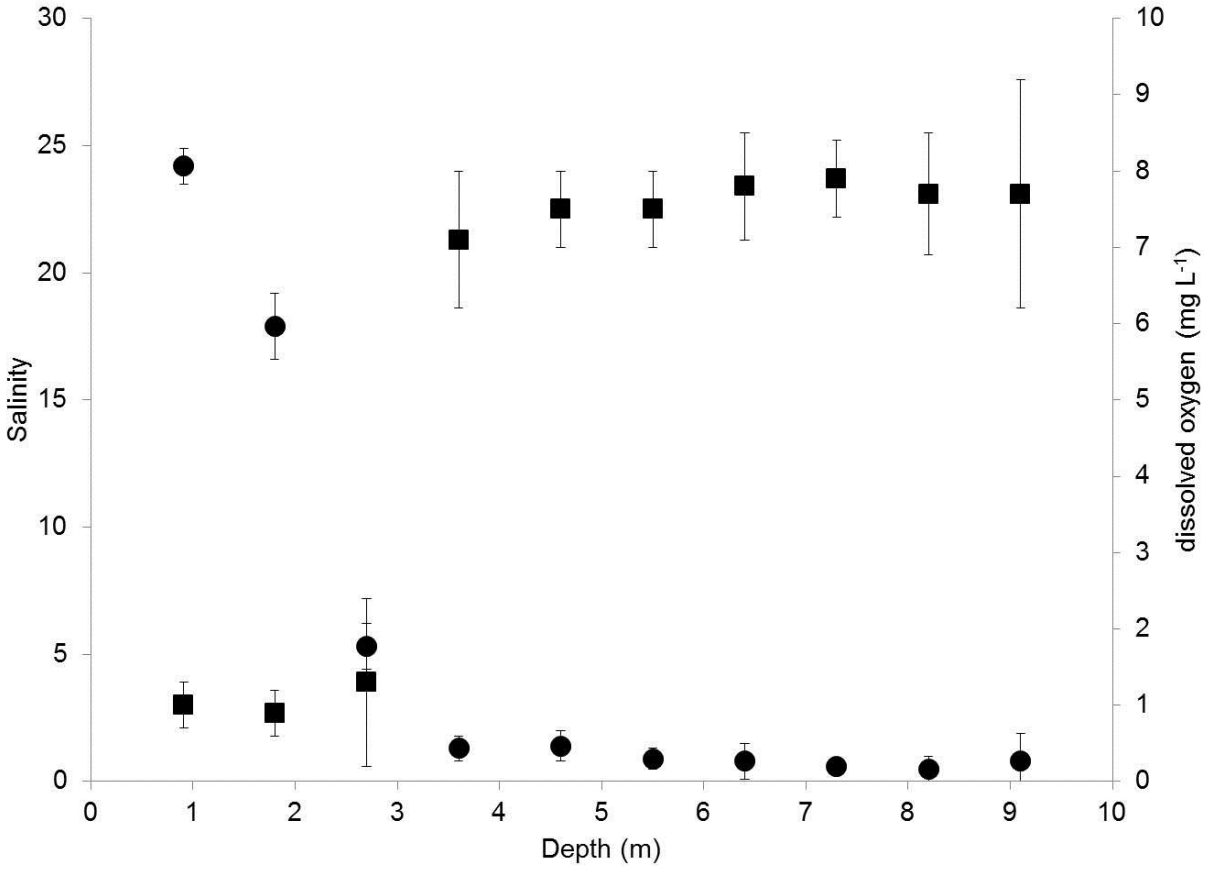

Figure 7 Average salinity (●) and dissolved oxygen (■) concentration for each well depth for the two spring-neap sampling period.

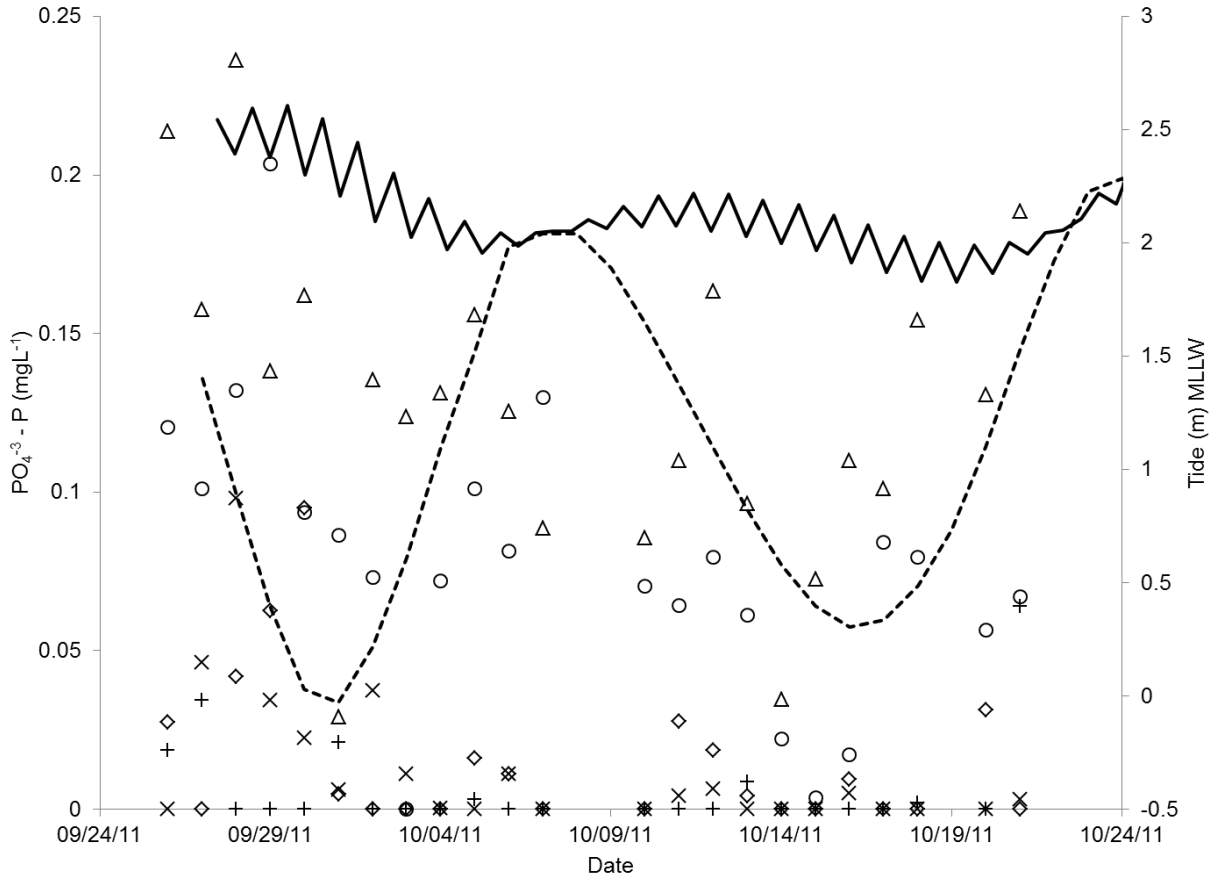

Figure 8 Inorganic phosphate concentrations for 5 well sampling depths. Sampling depths of 0.91m (○), 1.8m (Δ), 2.7m(◊), 3.6m(X) and 9.1m(+). High tide envelope (—) and tide station during sample time (9:30am) (--) shown.

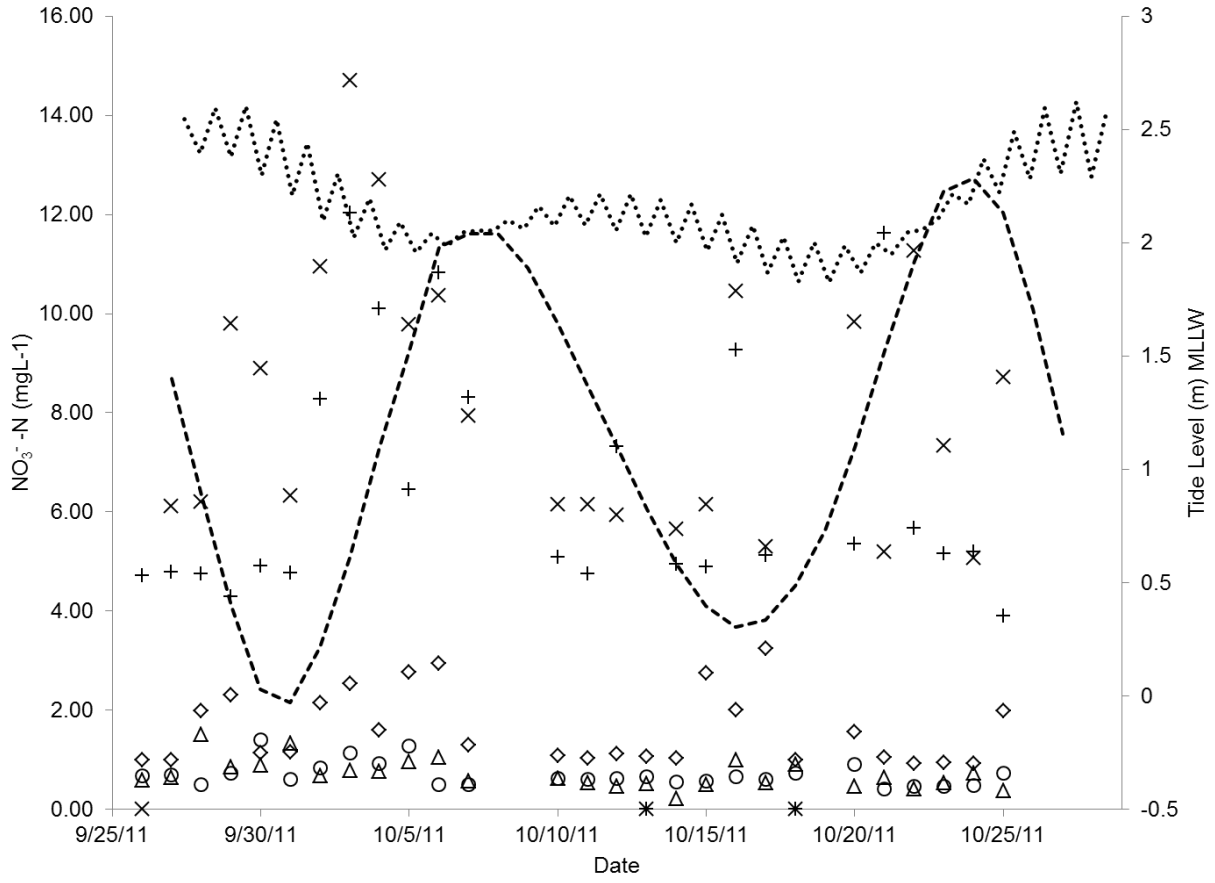

Figure 9 Nitrate concentrations for 5 well sampling depths. Sampling depths of 0.91m (○), 1.8m (Δ), 2.7m(◊), 3.6m(X) and 9.1m(+). High tide envelope (—) and tide station during sample time (9:30am) (--) is shown.

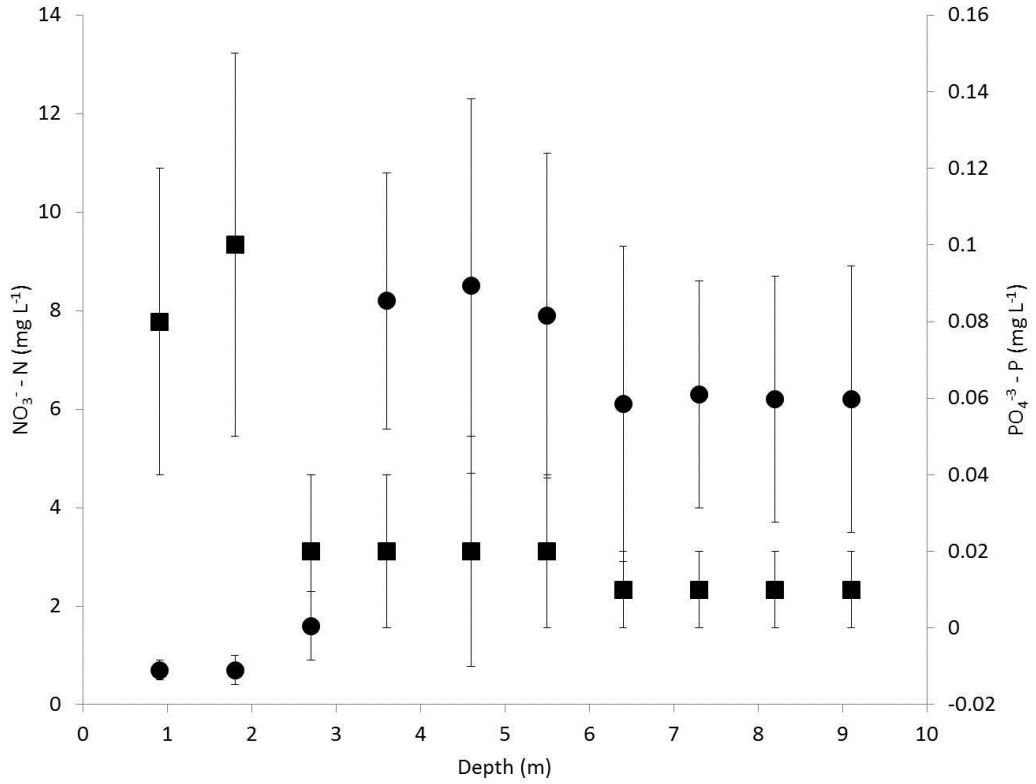

Figure 10 Average nitrate (●) and phosphate (■) concentration for each well depth for the two spring-neap sampling period.

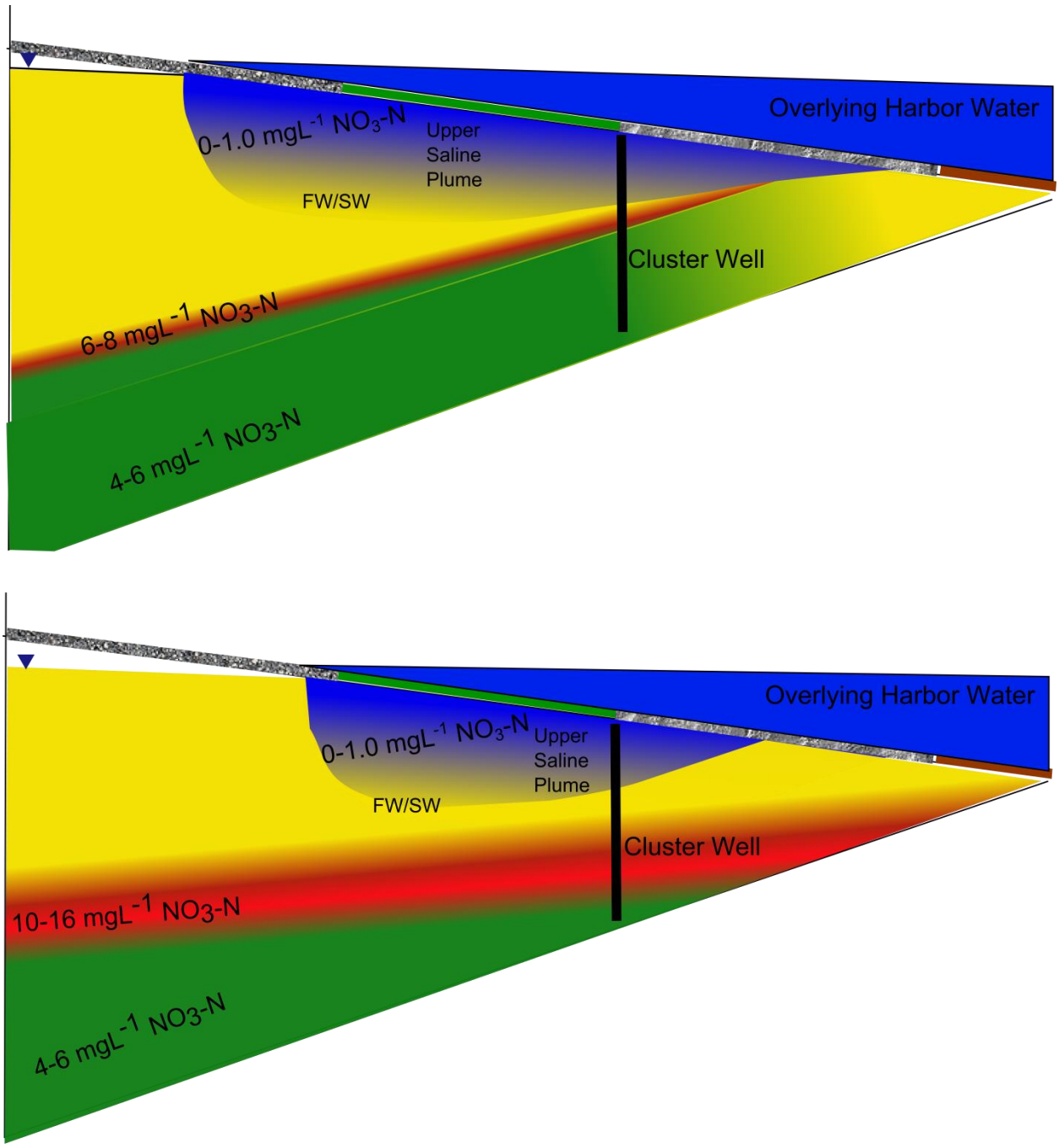

Figure 11 Conceptual model of nitrogen concentration changes due to movement of freshwater tube exit point. Spring tide (top) causes water table overheight, moving freshwater tube discharge point landward. Neap tide (bottom) lessens water table overheight, moving freshwater tube discharge seaward so cluster well intercepts the entire nitrogen plume.

Supplemental data

$$D_m = \frac{(S_{offshore} - S_{prism}) * V_{prism}}{S_{offshore} * L * \tau}$$

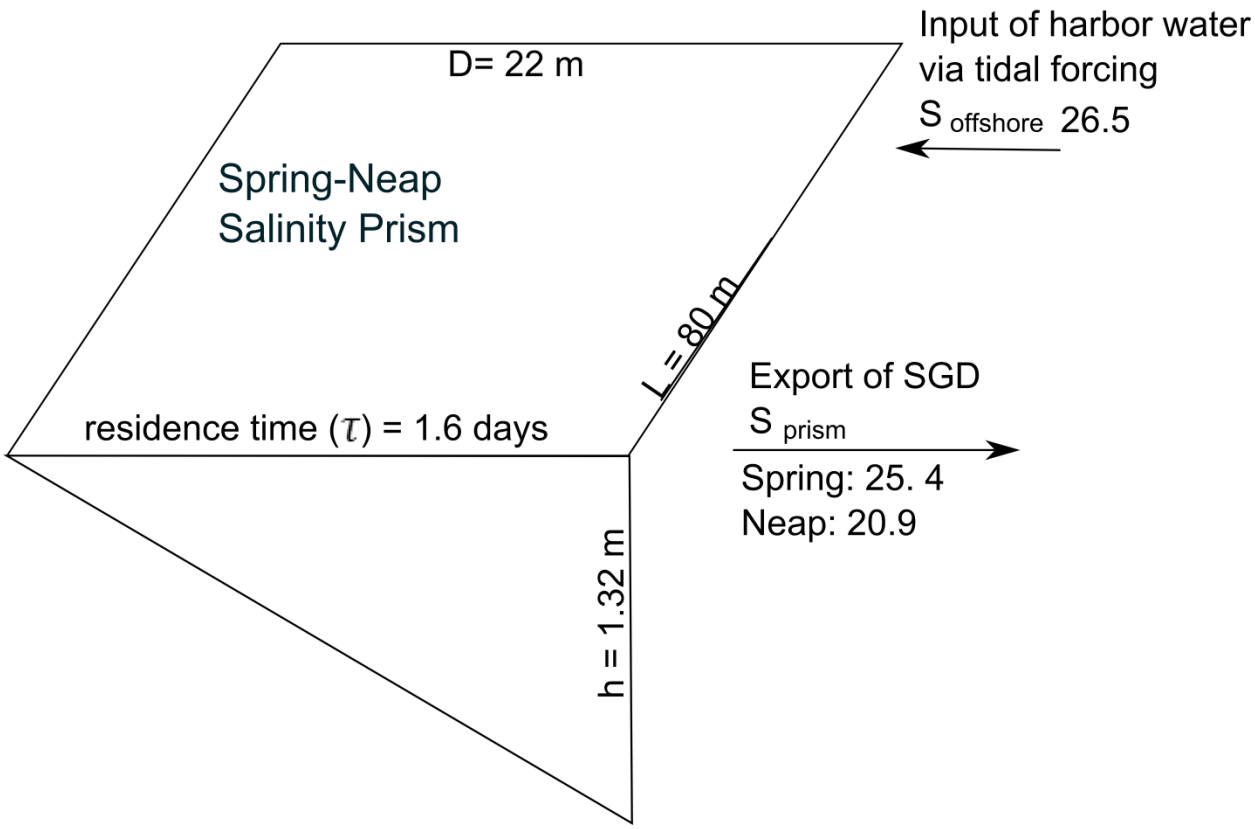

Figure S1. Spring neap freshwater prism used to calculate D_m. See text for explanation of variables.

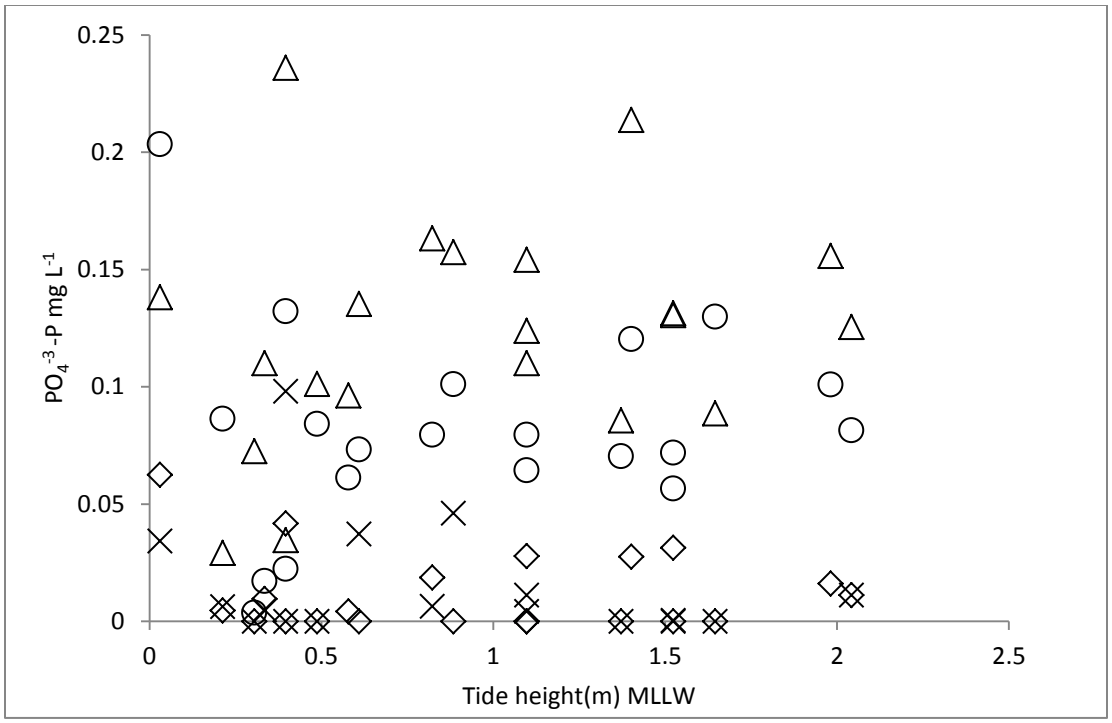

Figure S2 Inorganic phosphate concentrations for 4 well sampling depths vs tide height during sampling. Sampling depths of 0.91m (○), 1.8m (Δ), 2.7m(◊), 3.6m(X). Tide height during sampling is not correlated with PO_4^{-3}-P concentrations in the upper saline plume and saline transition zone.

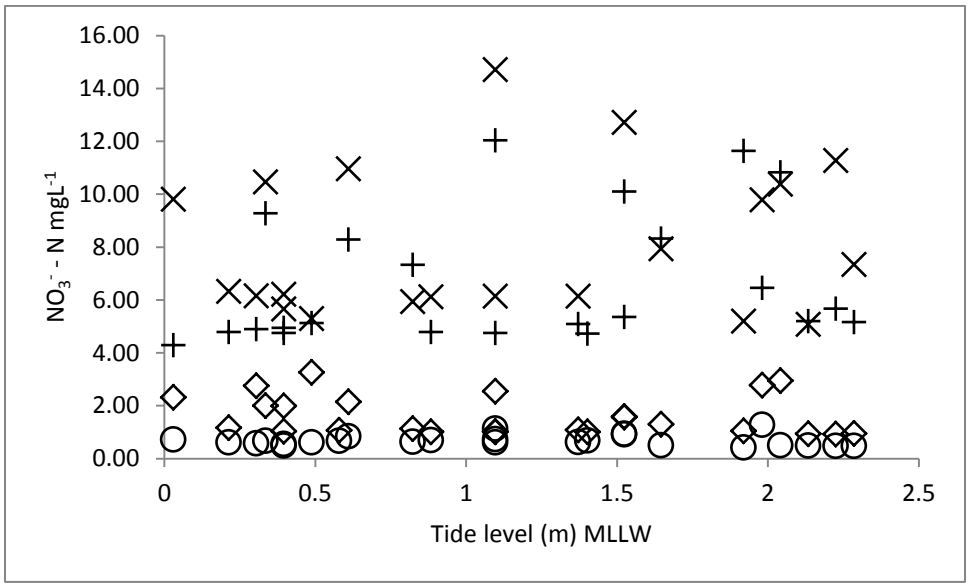

Figure S3 Nitrate as nitrogen concentrations for 4 well sampling depths vs tide height during sampling. Sampling depths of 0.91m (○), 2.7m(◊), 3.6m(X) and 9.1m (+). Tide height during sampling is not correlated with NO_3-N concentrations in the upper saline plume, saline transition zone or deep freshwater zone.

Table S1: Porewater pH for all sampling days. Average pH for each depth is shown at bottom. ND indicates

	Depth (m)									
Date	0.91	1.8	2.7	3.6	4.6	5.5	6.4	7.3	8.2	9.1
09/26/2011	6.19	6.35	6.34	ND	6.24	5.78	ND	6.01	6.06	5.97
09/27/2011	6.15	6.27	6.25	6.21	6.22	5.97	6.19	6.03	6.13	5.87
09/28/2011	6.1	6.27	6.35	6.31	6.24	5.9	6.1	6.16	6.23	6.35
09/29/2011	6.14	6.32	6.29	6.18	6.39	6.01	6.05	5.98	6.31	5.69
09/30/2011	5.94	6.11	5.95	5.94	6.01	5.72	6.04	5.83	6.06	5.48
10/1/2011	6.01	6.16	6.19	6.2	5.96	6.11	5.93	6.2	5.19	5.58
10/2/2011	6.11	6.2	6.04	6.01	5.83	6.06	6.1	6.2	5.94	5.56
10/3/2011	6.09	6.24	6.21	6.12	5.89	6.26	6.18	5.87	5.76	5.6
10/4/2011	6.12	6.14	6.27	6.02	5.85	6.18	6.04	6.07	5.6	5.66
10/5/2011	6.16	6.28	6.24	6.07	5.77	6.06	6.08	5.89	5.74	5.79
10/6/2011	6.11	6.28	6.21	6.1	5.88	5.87	5.66	6.97	5.5	5.74
10/7/2011	6.06	6.22	6.15	6.02	5.68	5.85	5.6	5.79	5.49	5.71
10/10/2011	6.03	6.14	6.02	5.76	5.56	5.32	5.48	5.4	5.62	5.78
10/11/2011	6.08	6.14	6.13	5.86	5.78	5.6	5.74	5.54	5.61	5.99
10/12/2011	6.09	6.14	6.22	5.79	5.64	5.35	5.75	5.58	5.58	5.98
10/13/2011	6.02	6.14	6.09	ND	5.64	5.56	5.84	ND	ND	5.96
10/14/2011	6.01	6.15	6.09	5.83	5.71	5.57	5.81	5.59	5.58	5.92
10/15/2011	6.01	6.2	6.13	5.88	5.65	5.56	5.68	5.53	5.6	5.89
10/16/2011	6.07	6.27	6.12	5.79	5.58	5.55	5.78	5.8	5.74	5.91
10/17/2011	6.02	6.24	6.08	5.69	5.54	5.36	5.91	5.55	5.72	5.93
10/18/2011	6.15	6.35	6.25	ND	5.67	5.52	6.01	5.47	ND	6.21
10/20/2011	6.15	6.29	6.36	5.93	5.75	5.46	6.43	5.54	5.91	6.06
10/21/2011	5.99	6.14	6.12	5.68	5.68	5.64	6.03	5.38	5.91	5.91
10/22/2011	6.07	6.19	6.11	5.67	5.68	5.52	6.02	5.43	5.93	5.86
10/23/2011	5.95	6.02	5.98	5.69	5.92	5.67	6.1	5.45	6.01	5.94
10/24/2011	6.17	6.17	6.15	5.75	6.03	5.67	5.98	5.53	5.83	5.95
10/25/2011	5.94	6.09	6.1	5.71	5.8	5.45	5.9	5.61	5.8	5.8
Average	6.07	6.20	6.16	5.93	5.84	5.72	5.94	5.78	5.79	5.86

CHAPTER III: DENITRIFICATION AND NITRATE BIOGEOCHEMISTRY IN A SUBTERRANEAN ESTUARY OF STONY BROOK HARBOR

Abstract

Nitrate loading via submarine groundwater discharge (SGD) was investigated in Stony Brook Harbor, NY, an embayment of Long Island Sound. Intertidal porewater profiles were sampled at two locations and analyzed for dissolved N_2/Ar and nitrogen compounds to examine the amount of nitrate lost due to denitrification during SGD. Previous work on nitrogen cycling in the coastal aquifer identified three zones of redox activity; the upper saline plume, fresh groundwater zone and deep saline zone. At this site, we find denitrification in the coastal aquifer is additionally controlled by sediment heterogeneity between discharge through sand at low tide and a mud cap that convers the sand offshore. Nitrate flux into the harbor was calculated through these two different sediment regimes; a near shore zone where SGD discharges through sand sediments at rates ranging 26-100cm d^{-1} and an offshore zone where SGD discharges through mud sediments at rates ranging 0-3cm d^{-1}. Findings indicate more nitrate is denitrified during SGD to the base of mud cap sediments (47%) than during SGD through sand sediments (<35%). Calculations of nitrate discharge to surface water through sand along the embayment shoreline nitrate indicate inputs ranged $1.3x10^4$mol d^{-1} to $4.8x10^4$mol d^{-1}. Although both fresh groundwater and overlying surface water are well oxygenated, the formation of an upper saline plume generates reducing conditions and porewater denitrification occurs during tidal pumping.

Introduction

In the last two decades submarine groundwater discharge (SGD) has gained recognition as an important freshwater source to coastal surface water bodies (Johannes, 1980, Hosono et al., 2012). SGD, defined as the total fresh and saline ground waters discharging at the land sea interface (Burnett et al., 2006), is known to contribute anthropogenic pollutants and nutrients via both direct freshwater discharge (Knee et al., 2010, Hosono et al., 2012, Taniguchi et al., 2002) and remineralization during seawater infiltration (Santos et al., 2009, Dorsett et al., 2011). Depending on local aquifer characteristics SGD may enter surface water as plumes (Peterson et al., 2009)or as diffuse underflow (Bowen et al., 2007). In unconsolidated surficial aquifers of the U.S North eastern Atlantic coast diffuse SGD is known to contribute up to 20% of total inputs (Bokuniewicz, 1980). Quantifying diffuse inputs to embayments and harbors is a critical, but often overlooked, component of water budgets in urban coastal zones. Although numerous studies have documented the presence of SGD in embayments (Loveless and Oldham, 2010, Bratton, 2010, Burnett et al., 2006) , spatial heterogeneity of both SGD freshwater fraction and coastal aquifer dynamics limit our ability to populate coastal zone models with one universal SGD rate.

Eutrophication resulting from non-point source nitrogen loading is known to affect coastal waters worldwide (Howarth, 2008). Nitrogen loading to surface water via SGD is documented in a number of studies (Knee et al., 2010, Weinstein et al., 2011, Slomp and Van Cappellen, 2004) but nitrogen biogeochemical transformations within the coastal aquifer are less well understood (Kroeger and Charette, 2008). Denitrification, the reduction of NO_3^- to N_2 gas, is an important pathway for nitrate reduction but is particularly difficult to quantify in mixed waters

of coastal aquifers. The terminal product of denitrification, dissolved N_2 gas is difficult to measure due to high atmospheric background concentrations (Groffman et al., 2006). Despite these challenges a number of researchers have successfully determined denitrification rates in riparian zones (Blicher-Mathiesen and Hoffmann, 1999) and deep groundwater (Bohlke et al., 2002) by using dissolved Argon to correct for physical effects such as pressure, temperature and excess air incorporation (Heaton and Vogel, 1981). The use of membrane inlet mass spectrometry (MIMS) to determine dissolved N_2:Ar concentrations has provided a rapid low-cost technique for determining net denitrification flux along groundwater flow paths (Kana et al., 1994).

Recent efforts to model coastal aquifer dynamics have provided insight on the physical controls of SGD rates. Tidal pumping (Robinson et al., 2007c), wave set up (Li et al., 1997) and seasonal aquifer recharge cycles (Michael et al., 2005) influence the timing and magnitude of SGD rates. These studies demonstrate large variance in the coastal aquifer salinity transition zone, termed the subterranean estuary (STE) (Moore, 1999), with respect to conservative ion movement (i.e chloride) but do not elucidate how these variations affect nitrogen biogeochemistry. The primary limitation in modeling studies is the assumed isotopic and homogeneous aquifer conditions, which are rarely found in the natural environment. Field studies demonstrate the importance of fringing marshes (Tobias et al., 2001b) and sediment stratification(Kumar et al., 2013) on chemical composition of SGD. Further, anthropogenic plumes of nitrate can create geochemical gradients at the spatial scale of tens of meters in coastal aquifers (Dillon et al., 2007, Kroeger and Charette, 2008). Consequently, we must quantify denitrification as discharging water moves from through the freshwater and the salt water portion of the subterranean estuary to determine how aquifer heterogeneity affects nitrogen attenuation during SGD.

The subterranean estuary is typically depicted in three zones; the upper saline plume (USP), the fresh groundwater zone and the deep saline zone (Kroeger and Charette, 2008). Biogeochemical reactions, such as denitrification, are thought to occur rapidly during porewater movement between zones. In this study we measured denitrification in the three zones of a subterranean estuary of Stony Brook Harbor, an embayment with direct connection to Long Island Sound. We sampled high-resolution depth profiles across a salinity gradient for dissolved inorganic nitrogen, dissolved N_2/Ar gas and a suite of solutes known to contribute to nitrogen cycling. This study was done in parallel with an investigation of physical properties of SGD using manual and automatic seepage meters and resistivity transects (Durand et al., submitted). Physical studies at this site find a thick freshwater plume extending tens of meters offshore beneath harbor sediments. I present data for three porewater profile transects that show spatial and temporal heterogeneity in both freshwater nitrate concentration and net denitrification in this subterranean estuary. I examined which drivers of denitrification (DOC, Fe, Mn) were statistically correlated with $N_{2\ \text{denitrification}}$ production in the different biogeochemical zones of the subterranean estuary. Finally, porewater profiles were used to calculate net nitrate flux to overlying water through differing sediment regimes in the intertidal and sub-tidal zones.

Methods

Site Description

Stony Brook Harbor is a shallow bay on Long Island's north shore with direct connection to Smithtown bay and Long Island Sound (figure 1). The harbor covers 4.5km^2 and is bound on the north edge by the Long Beach and West meadow sand spits. The Harbor is subjected to tidal forcing from Long Island Sound via a single narrow inlet, with a minimum width of 75m. A two channel system produces uneven tidal effects within the Harbor, with approximately 30% of the tidal prism propagated into the southeastern portion of the main harbor affecting the study area (Georgas, 2001). The tidal range averages 2 meters, with approximately 65% of the harbor shallower than 1m below mean sea level (Cademartori, 2000). Two main channels are maintained by sporadic dredging to a maximum depth of 2.7m below the mean water level. Espisodic (3-10 year intervals) dredging maintains navigable channel to the southern tip of the harbor. The northern section of the harbor is characterized by shallow tidal flats containing stands of *Spartina Alternaflora* and associated marsh grasses (Georgas, 2001).

Stony Brook Harbor rests on Long Island's shallow unconfined aquifer, the Upper Glacial aquifer. The Upper Glacial is comprised of medium-to coarse-grain sanded overlain by a layer of glacial till. The regional groundwater divide trends east-west along the horizontal axis of Long Island, therefore groundwater north of the divide moves northward towards Long Island Sound, and water south of the divide flows southward toward the Atlantic Ocean. Horizontal hydraulic conductivity is estimated at 70.1md^{-1}, with 10:1 horizontal to vertical anisotropy (Buxton and Modica, 1992). Previous work indicates nitrogen inputs to the Upper Glacial Aquifer are from atmospheric deposition, septic tank-cesspool systems and turf grass fertilizer (Scorca and Monti, 2001). Zhao et al., (2011) sampled groundwater from two subterranean estuary sites on Long Island's north shore, Northport Harbor and Manhassett Bay. Using pharmaceuticals and pesticides as tracers, they determined that nutrient contributions in Northport Harbor, where primary watershed land use is high density housing without municipal sewering, originate from wastewater and atmospheric input (Zhao et al., 2011). The area around Stony Brook Harbor is classified as low density housing, with 0-1 dwelling unit per acre (Koppelman, 1978). Porter (1980) found that tufrgrass makes up 33% of land cover in low density housing, with each dwelling unit containing an on-site wastewater system (Porter, 1980). Munster (2008a) used major cations in well samples to estimate source contributions to Long Island groundwater and determined that in low density housing greater than 50% of groundwater nitrogen originates from rainwater, with turf-grass leachate contributing 30-50% and on-site wastewater systems contributing $\leq$20% of nitrogen (Munster, 2008a). As the watershed immediately surrounding Stony Brook Harbor is classified as low density housing, nitrogen inputs to the shallow coastal aquifer are most likely from atmospheric deposition and turf-grass leachate, with minor contributions from on-site wastewater systems.

SGD rate measurements were taken simultaneously with porewater profiles using Ultrasonic Seepage meters in 2011 (Paulsen et al., 2001). SGD rates were also measured by manual seepage meter in August 2012 (Lee, 1977). Results from these sampling periods are presented along with conductivity surveys of the field site by Durand et al (submitted). Although seepage measurements were taken on different dates (May 2011, July 2011 and August 2012), seepage rates were temporally consistent in each of the different sediment zones.

Discharge rates are spatially dependent, with highest rates ranging 26-102cm d^{-1} observed at the low-tide shoreline while low rates of 0-3cm d^{-1} were found offshore, where a mud layer caps the fresh groundwater zone. Terrestrial hydraulic gradient data was acquired from two inland monitoring wells installed prior to porewater sampling. Inland wells were sampled during seepage meter deployment; resulting data was combined to determine average hydraulic gradient during piezometer sampling periods. Average hydraulic conductivity for the study site was calculated using Darcy's law and found to average 4.3 x 10^{-3}cm s^{-1} for the three seepage meter measurement periods (Durand et al., submitted).

Sediment Sampling and analysis

Sediment samples were taken from the intertidal and offshore areas to examine sediment controls on SGD rates and denitrification rates. Sediment samples were taken from the intertidal and subtidal areas of each field site. Cores were collected in acid rinsed (10% HCl) 12.7mm I.D pre-cut PVC pipe. Sediment samples were analyzed for grain-size distribution using a Malvern Mastersizer 2000 laser diffractometer, with a precision of 5% at 2 standard deviations. Separate sediment samples were weighed, dried and re-weighed to determine effective porosity of sediments in the intertidal zone.

Porewater sampling and analysis

Porewater samples were collected using an AMS Retract-A-Tip sampling system (Charette and Allen, 2006). LDPE tubing was rinsed with deionized water (18.2mΩ) and connected to peristaltic pump (Cole-Parmer) using low gas permeability Viton tubing (Masterflex). Samples were collected at depths ranging from 0.5m to 10m beneath the sediment surface. Sampling interval ranged from 0.5 to 1m, as determined in the field from salinity and dissolved oxygen parameters. Measurements of temperature, pH, dissolved oxygen, and conductivity were measured in the field using YSI 556 handheld multi-probe meter connected to a flow through cell. Samples for MIMS analysis of dissolved N_2/Ar were collected in 12ml vials with no headspace (Labco Exetainer®). Dissolved organic carbon samples (DOC) and total dissolved nitrogen (TDN) samples were filtered (0.45µM), collected in acid rinsed combusted bottles, acidified with HCl (Fisher Scientific) to pH 2 and at 4^{o}C and analyzed within 2 weeks of collection. Samples for Fe and Mn were filtered through 0.2 µM capsule filters, acidified with Trace Metal Grade HCl (Fisher) to a pH<2 and frozen. Samples for NO_3^-, NO_2^- and NH_4^+ were filtered through 0.45µM filters (Whatman GF/B) and frozen within 8 hours of collection. Samples for dissolved inorganic phosphate (DIP) were collected separately by filtering and acidification with 50µl 8M H_2SO_4 to prevent precipitation of PO_4^{-2} due to changing oxygen conditions. All nutrient samples were field cooled and frozen within 8 hours of collection.

Samples were analyzed for NH_4^+, HPO_4^{-2}, Fe and Mn using colorimetric methods (Stookey, 1970, Strickland and Parsons, 1978, Solorzano, 1969). Concentrations are average of three replicate analyses, with precision of ±5% for NH_4^+, HPO_4^{-2} and ±9% for Fe and Mn. Nitrate (NO_3^- + NO_2^-) analysis was performed by cadmium reduction in a flow injection automated analyzer (Lachat Instruments FIA-6000). Nitrate sample concentrations are reported as the average of three replicate injections, inclusive of nitrate and nitrite. One standard deviation precision is ±2% of sample concentration. DOC was analyzed on a Shimadzu TOC;

precision is the standard deviation of three replicate injections of an intermediate standard, with a percent coefficient of the mean of ± 5% for any run.

Dissolved N_2/Ar was analyzed by Membrane Inlet Mass Spectrometry (MIMS) at the University of California Stable Isotope Facility (Kana et al., 1994). MIMS has been used to obtain high precision gas concentrations for N_2 and Ar in both saline and freshwater samples (Eyre et al., 2002). A water bath with deionized water was held at constant temperature and several readings were made between sets of 15 to 20 samples to test for instrument drift. Standard deviation calculated as deviation from theoretical values (Weiss, 1970) for reference water held at 15^0C, equal to 0.05 for N_2/Ar and ±0.96µmol L^{-1} for N_2 alone. $N_{2\ denitrification}$ concentrations were calculated following the method of Weymann et al.,(2008) with modifications as described below.

Calculation of $N_{2\ denitrification}$ and excess air incorporation

Three sources of gas contribute to the total concentration N_2 in coastal pore water; N_2 from atmospheric equilibration during recharge, N_2 from excess air (EA) that is air entrapped at the top of the water table, and N_2 due to denitrification, as shown in equation 1.

$$N_{2\ sample}/Ar_{\ sample} = [(N_{2\ atmosphere} + N_{2\ EA} + N_{2\ denitrification}) / (Ar_{\ atmosphere} + Ar_{\ EA})] \quad (1)$$

Where $N_{2\ sample}$ and $Ar_{\ sample}$ are concentrations of dissolved nitrogen and argon in the porewater sample, respectively. $N_{2\ atmosphere}$ and $Ar_{atmosphere}$ are the concentrations of nitrogen and argon in air saturated water in equilibrium with the atmosphere at a given temperature, salinity and, pressure. $N_{2\ EA}$ and $Ar_{\ EA}$ are additional amounts of these gases found in the sample attributable to dissolution of air bubbles trapped at the top of the water table (Aeschbach-Hertig et al., 1999). The remaining N_2 in the sample is due to the presence of denitrification, $N_{2\ denitrification}$.

To determine the amount of nitrogen in the sample due to atmospheric equilibration, $N_{2atmosphere}$, solubility N_2 concentrations were calculated for representative recharge temperatures at each sampling site and period, inclusive of the recorded salinity of each sample (Weiss, 1970). The selection of a recharge temperature is critical in calculating the final amount of $N_{2\ denitrification}$ in each sample. Up to 90% of groundwater recharge to Long Island aquifers occurs between October 15-May 15 (Steenhuis et al., 1985), during which time mean air temperature is 9.6C (NOAA, 2011). During porewater sampling at Stony Brook Harbor the recorded average porewater temperature was 25.3^0C in May and 16.9^0C in October at site 1 and 19.9^0C in May at site 2. These temperatures likely reflect two factors; mixing of cool fresh groundwater with warm overlying water and /or solar heating of water during sampling. Overlying harbor water temperatures ranged from 21.3-25.5 in May and 14.4 to 19.8 in October during porewater sampling. Heating during water sampling cannot be ruled out, as shown by figure 2, dissolved N_2 vs Ar in samples with salinity less than 1ppt are positively correlated with temperature and fall along a temperature solubility line. Figure 2 also reveals differences in freshwater temperature between sites and time periods. Freshwater samples from site 1 taken in May cluster near a higher recharge temperature of 18^oC, while temperatures from site 1 in October and site 2 in May cluster between 12-14^oC.

Samples with salinity between 16ppt and 18ppt were selected to examine the initial temperature of saline porewater, as shown in figure 3. This salinity range was selected as all three sampling periods contained samples in this range, and these salinity values represent only a slight mixing with fresh groundwater. Samples from site 1 in October and site 2 in May cluster near 10-12^{0}C but samples from site 1 in May are closer to 14^{0}C. Taken together, figures 2 and 3 were used to select a representative recharge temperature for each sampling period. A lower recharge temperature of 12^{0}C was selected for site 1 in October and site 2 in May. A slightly higher recharge temperature of 14^{0}C was selected for site 1 in May. It must be stated that despite efforts to limit exposure of piezometer tubing from sunlight, data from figures 2 and 3 suggest porewater samples taken at site 1 in May experienced 5-8^{0}C warming during collection. A plot of N_2/Ar vs salinity for all porewater samples, figure 4, shows data lies slightly above the solubility values for12°C and 14 $^{\circ}$C, indicating these two recharge temperatures are a reasonable interpretation.

Two additional physical processes are known to affect dissolved N_2/Ar concentrations; degassing and excess air (Mookherji et al., 2003, Heaton and Vogel, 1981). Degassing occurs when the partial pressure of dissolved gases exceed the hydrostatic pressure of the water. Degassing has been observed as a significant N_2 loss mechanism in reducing aquifers and riparian wetlands (Blicher-Mathiesen et al., 1998, Mookherji et al., 2003). Evidence of degassing can be implied from either production of CH_4 or increasing Ar concentrations with increasing depth. Coastal aquifers typically contain a tidally induced upper saline plume overlying fresh groundwater zone, causing a salinity gradient which affects gas solubility and mimics degassing due to salinity solubility decreases in Ar concentrations. Due to this, we checked for degassing using only concentrations within the freshwater zone at the high tide piezometer and found that degassing was not present in this system, as evidenced by decreasing Ar concentrations with depth (Table 3).

Excess air, the process of air entrapment at the water table interface, is found to effect dissolved N_2 concentrations by mimicking denitrification produced excess N_2 (Heaton and Vogel, 1981). In a tidal system where aquifer void spaces are rapidly filled and drained diurnally, formation of excess air in shallow samples is possible, therefore we use the method outlined by Weymann et al., (2008) to calculate excess air in samples with Ar concentrations more than 0.5µmol L^{-1} difference from theoretical solubility concentrations (Weiss, 1970). We find excess air in 58% of N_2/Ar samples (Table 3), as calculated from recharge temperatures of 12°C to 14°C, as described above.

Maximum and minimum excess air incorporation are calculated according to equations 2 and 3

$$N_{2\ EA\ max} = (Ar_{total} - Ar_{atmosphere}) * (N_{2\ atm\ fraction} / Ar_{atm\ fraction}) \quad (2)$$

$$N_{2\ EA\ min} = (Ar_{total} - Ar_{atmosphere}) * (N_{2\ EQ} / Ar_{EQ}) \quad (3)$$

Ar_{total} is the total amount of Argon in the sample, $Ar_{atmosphere}$ is the concentration of argon in the sample due to atmospheric equilibration at 12 ^{o}C or 14^{o}C, $N_{2\ EQ}$ and $Ar_{\ EQ}$ are the equilibrium mole fractions of N_2 and Ar, respectively and $Ar_{atm\ fraction}$ and $N_{2\ atm\ fraction}$ are the fractional

amounts of atmospheric gas contained in excess air. Maximum excess air, $N_{2\ EA\ max}$, accounts for excess air incorporation during complete capillary bubble dissolution and reflecting full dissolved atmospheric concentrations of both N_2 and Ar. Minimum excess air, $N_{2\ EA\ min}$, is defined as minimal excess air incorporation which is due to capillary bubble fractionation at the recharge temperatures of 12 ^{o}C and 14^{o}C. Excess air is the most difficult portion of total $N_{2\ sample}$ to constrain, as dissolved argon is the only gas available to correct for physical effects. A full suite of noble gasses is required to best constrain excess air content and temperature disequilibrium due to the mixing of cool groundwater with warm coastal water (Wilson and McNeill, 1997). Maximum error for excess air estimates is taken as half the difference between maximum and minimum excess air N_2 for a given recharge temperature.

Using equations 2 and 3 to obtain $N_{2\ EA\ max}$ and $N_{2\ EA\ min}$, we then calculate the residual amount of dissolved N_2 in the sample, which is attributed to denitrification, $N_{2\ denitrification}$.

$$N_{2\ denitrification} = N_{2\ sample} - N_{2\ atmosphere} - N_{2\ EA\ (min/max)} \quad (4)$$

Using equation 4 the average value of $N_{2\ denitrification}$ was calculated for both 12^{o}C and 14^{o}C, with results shown in Table 3. The remaining calculations in this report are completed using average $N_{2\ denitrification}$ for each porewater sample as calculated from a recharge temperature of 12^{0} for site 2 in May and Site 1 in October and a recharge temperature of 14^{o}C for site 1 in May.

Results

A total of three transects were sampled during this study; P1 was sampled at site 1 during May 2011, P2 was sampled at site 2 during May 2011 and P3 was sampled at site 1 during October 2011. Each sampling period lasted between 5-7 days and with an entire porewater profile taken over the course of 1-2 days, depending on tidal stage respective to profile location. Sites 1 and 2 were chosen to observe spatial heterogeneity in nitrogen biogeochemistry while sampling during May and October at P1 was done to observe temporal heterogeneity in nitrogen biogeochemistry. Three porewater zones are defined in the results section, based on salinity measurements: the upper saline plume, fresh water zone, deep saline zone. Not all zones were captured during all sampling periods. For instance the deep saline zone was not observed during May 2011 sampling at site 1. Finally, we describe how SGD traverses two different sediment regimes at site 1, one consisting of sandy material located at low tide and the other consisting of organic rich mud located offshore. Nitrate carried to the harbor via SGD are interpreted using these two sediment regimes, with a discussion of how much nitrate is denitrified during transport to the overlying water through sand material and nitrate denitrified during transport to the base of the mud sediment offshore.

Sediment distribution

Sediment samples taken from low tide at site 1 (P1-19, figure 1) at depths of 0-120 cm contain coarse silt, average grain size d_{50} of 0.058mm. An intertidal marsh extends from P-7 to P-19 an area which corresponds to observed high silt content and porewater DOC in porewater samples taken at shallow depths. Observed high silt content is possibly due to marsh grass roots trapping fine grained sediments. This feature of the STE provides a stable horizontal extent of the upper saline plume, as observed from temporal profiles of salinity and DOC concentrations

reported in Table 5 and shown in Figure 16c, Figure 17c, Figure 18c. As this area undergoes rapid inundation and exposure during each tidal cycle, we do not have SGD rate measurements for the upper saline plume. Sediment cores taken from a depth 120-365cm beneath the sediment surface at P1-1, P1-19 and P1-25 all contain medium to coarse grain sand, with an average grain size d_{50} of 0.57mm. These results combined with DOC data (described below) from the same locations indicate that sediments in the freshwater zone are comprised of well sorted glacial sands with low organic matter content. Water discharging through these sediments reaches the surface between P1-19 and P1-25, at the base of an intertidal marsh, with discharge rates ranging 23cm d^{-1} to 109cm d^{-1} (Durand et al.,submitted).

Below the low tide line fresh groundwater extends beneath a mud cap that exists for at least 60m offshore, as determined from resistivity transects taken at this site during porewater sampling (Durand et al., submitted). Sediment samples were taken from this zone in October 2011, corresponding to the location of porewater profile P3-35 (figure 1) from depths 0-100cm contain medium to coarse silt, d_{50} of 0.03mm. The maximum thickness of this layer is 85cm, containing average porewater DOC concentration (n=4) of 2200µmolL^{-1}. This mud layer caps permeable sands observed elsewhere at the site, causing a decrease in SGD rates to rates of 0cm d^{-1} to 3cm d^{-1}. At depths greater than 85cm betenath the sediment water interface, sediments consist of medium to coarse grain sand, as observed in the low tide portion of the STE. Porewater profiles from P3-35 indicate freshwater salinities from depths 122cm to 740cm below the sediment water interface and then increasing salinity at depths greater than 740cm, indicating the presences of a deep saline zone, typically observed in STE systems (Kroeger et al., 2008).

Spatial distribution: Shore normal 2D transects

Significant spatial variations of salinity, dissolved oxygen, DOC, nitrate and $N_{2\ \text{denitrification}}$ were observed between the porewater 2D sections of site 1 and 2, sampled in May 2011 (figures 4 and 5)and site 1 in October 2011 (figure 6). The two sites were separated by approximately 40m along shore (figure 1). At site 1 a shallow upper saline plume was evident from 0 -220cm below the sediment surface in three of four piezometer locations. Maximum infiltration of seawater was observed to a depth of 406cm in a piezometer located 7m below mean high tide line, resulting in a wedge shaped upper saline plume that narrowed towards the mean low tide mark (figure 2A). At site 2, located 40m south of site 1, the upper saline plume extended from 0-380cm in all piezometers seaward of the high tide mark. The maximum depth of the upper saline plume was located 15m below mean high tide, where salinity reached a minimum of 12.6 at a depth of 412cm and then increased to 21.5 at a depth of 730cm. A fresh water zone, with salinities of 5 or less, was observed at in samples taken from the mean high tide mark and in samples 30m below the high tide mark. These features indicated the upper saline plume and the deep saline zone periodically mix, creating a low salinity mid-point in place of a fresh groundwater zone which is typically observed in the subterranean estuary (figure 5a).

Dissolved oxygen concentrations were high in fresh porewater (6-8 mg L^{-1}) and hypoxic (>2mgL^{-1}) in saline porewater. At site 1, dissolved oxygen ranged from 0.13-1.88mgL^{-1} in the upper saline plume then increased with increasing depth, to maximum observed value of 6.88 mgL^{-1} in the fresh groundwater zone (figure 4b). At site 2, distribution of dissolved oxygen concentrations was more complicated. Hypoxic conditions were observed in the upper saline

plume at locations 15m or more seaward of mean high tide (figure 5b). Samples taken from 0-5.5m beneath the sediment surface in piezometers P2-23 and P2-30 contain salinities of ~5; this indicates mixing of overlying water into fresh porewater. In the fresh groundwater zone at site 1 we observed high dissolved oxygen concentrations, which are consistent with groundwater oxygenation observed elsewhere in the Upper Glacial aquifer (Young et al., 2013). At site 2 mixing of saline overlying water into fresh porewater resulted in decreased dissolved oxygen levels, which ranged 2.7-4.5mgL^{-1}. Decreased dissolved oxygen concentrations were possibly due to increased microbial activity in shallow porewater near mean low tide, but if this is the case seawater derived DOC was rapidly used, as dissolved organic carbon concentrations in this zone measured less than 50µmol L^{-1} (Figure 17c and Table 5).

Spatial distribution of nitrate closely followed salinity distribution. At site 1, nitrate concentrations averaged 63µmol L^{-1} in all upper saline plume piezometer samples from depths 0m-2m. Maximum nitrate values of 378µmol L^{-1} to 545µmol L^{-1} recorded in samples from P1-0 in the fresh water zone at depths ranging 4.3-7.1m (Figure 16c). Nitrate concentrations in the fresh water zone decreased towards the low tide point, with samples from P1-25 containing 173µmol L^{-1} to 24µmol L^{-1} at depths 4.5-7.5m beneath sediment surface. Similar results are observed at site 2, where nitrate in the upper saline plume averaged 80µmol L^{-1}(Figure 17d). Similar to site 1 nitrate distribution, at site 2 maximum nitrate concentrations were observed in fresh porewater from high tide point and decrease towards low tide, where porewater nitrate concentration averaged 125µmolL^{-1} in the fresh water zone at P2-30. Nitrate distribution at both sites implies groundwater is the dominant nitrogen source in the subterranean estuary. Salinity-nitrate scatter plots indicate nitrate is sourced from low salinity water (i.e. upgradient groundwater) rather than being introduced during seawater infiltration of the upper saline plume. Conservative mixing of salinity and groundwater cannot account for nitrate losses across the subterranean estuary (Figure 19), suggesting partial denitrification despite high dissolved oxygen concentrations. All samples were also analyzed for NH_4^- but levels were below detection limit of 0.01µML^{-1}. This indicates either surface water derived NH_4^+ undergoes either rapid microbial utilization or oxidation. Absence of NH_4^+ in porewater indicated nitrate loss is not due to dissimilatory nitrate reduction to ammonium (DNRA).

Distribution of DOC at site 1 closely followed areas of high salinity (Figure 20, Table 5) ranging 61µmolL^{-1} to 320µmolL^{-1} for salinities ranging 8.8 – 26.4 for samples collected in May. Linear regression for these two data sets yields an r^2 of 0.61 for samples taken in May and 0.58 for samples collected in October, as shown in Figure 20. At site 2, DOC concentrations do not exhibit as strong a pattern. For example, a DOC concentration of 240µM L^{-1} was observed at a depth of 160cm at P2-8, in the upper saline plume, while other DOC maxima points were observed at depths greater than 600cm in P2-15 and P2-30, corresponding to the top of the deep salinity zone (Figure 17 and Figure 20).

Temporal Distribution: Shore normal 2D transects

To investigate temporal variations of nitrate in this subterranean estuary samples from site 1 were collected in May 2011 and October 2011. The October transect (P3) samples the same locations as transect 1 taken in May, with the addition of two porewater profiles; one at the base of the intertidal marsh (P3-13) and one offshore porewater profile (P3-35). The additional

offshore piezometer allowed us to locate and sample the deep saline zone at site 1, as well as providing information on nutrient dynamics beneath the harbor bottom mud cap, where SGD rates are ~8 times slower than rates found at or near low tide (Durand et al, submitted). During both site 1 sampling periods we observed freshwater discharge in the near shore environment through medium to fine quartz sand sediments and discharge at distances up to 60m beyond low tide through mud layer at the harbor bottom.

A comparison of salinity, dissolved oxygen and nitrate concentrations between from site 1 taken in May (P1) and October (P3) showed similar horizontal distribution of solutes (Figure 16 and Figure 18). One feature to note was the narrowing of the upper saline plume during October sampling, as shown in Figure 18a. Previous investigators have modeled expansion and contraction due to tidal forcing, spring-neap variations and seasonal discharge patterns (Robinson et al., 2007b, Robinson et al., 2007a, Michael et al., 2005). It is unlikely that the compression of the upper saline plume observed in October is due to spring-neap cycling as a month long time series at this site showed minimal variation in USP distribution (see Chapter 2). Therefore the compression of the USP is possibly due to seasonal discharge patterns, that favor increased freshwater discharge in the fall and increased infiltration of saltwater in the spring (Michael et al., 2005), leading to greater depth penetration of the USP in the spring, as seen by comparing Figure 16a with Figure 18a.

Sampling periods at site 1 both in May and October occurred during falling spring to rising neap tide, therefore any variances that occurred in nitrate concentration in the freshwater zone should not be reflected in the average concentrations (Figure 16d, Figure 18d). Nitrate concentrations data sets from May and October were analyzed by t-test to determine if a significant seasonal difference exists. October concentrations were found to be significantly higher ($p=0.007$), with an average concentration of 310µmol L^{-1}, as compared to 200µmol L^{-1} during May. During May maximum nitrate values are observed in P1-0, at the high tide point (Figure 16d) but in October maximum nitrate values are observed in piezometers P3-7 and P3-13, in the fresh water zone at the base of the intertidal marsh (Figure 18d).

$N_{2\ denitrification}$ profiles

$N_{2\ denitrification}$ was calculated as described by Weymann et al., (2008) using 12^0C for site 1 in October and site 2 in May and 14^0C for site 1 in May as a theoretical solubility concentration (Table 1 and Figure 15). For each sample, solubility concentrations of N_2 and Ar were additionally corrected for salinity concentration according to equations described by (Weiss, 1970). Values below the solubility line indicate degassing of samples, as both nitrogen and argon are depleted with respect to temperature and salinity equilibrium. For all three data sets, only three samples from site 2 and one sample from site 1 show evidence of degassing and therefore these samples were omitted from denitrification mass balance calculations. The remaining samples lie on or above the solubility line, indicating porewater was either in equilibrium or contains $N_{2\ denitrification}$.

Comparison of dissolved $N_{2\ denitrification}$ concentrations at site 1 in May (P1) and October (P3) show spatially consistent areas of denitrification in the STE but higher values in October. In May $N_{2\ denitrification}$ was absent from the high tide position (P1-0) at all depths. At P1-7 and P1-

19 maximum $N_{2\ denitrification}$ was found at in samples from 100-200cm beneath the sediment surface, with 33µmolL^{-1} and 130µmol L^{-1} respectively. In P1-25 $N_{2\ denitrification}$ was less than 10µmol L^{-1} at all sample depths (Figure 16, Table 4).

In October (P3) $N_{2\ denitrification}$ concentrations were higher, particularly in zones where piezometers intercept the upper saline plume. Porewater samples from mean high tide, P3-0, contained a maximum $N_{2\ denitrification}$ of 48µmol L^{-1} at 197cm beneath the sediment surface. $N_{2\ denitrification}$ then decreased with depth to values less than 10µmol L^{-1} at a depth of 365cm, consistent with patterns of $N_{2\ denitrification}$ observed in other porewater profiles. Porewater from the top of the intertidal marsh and in low tide sand sediments, P3-7 and P3-25, exhibit similar $N_{2\ denitrification}$ patterns, with maximum concentrations observed at depths 120-300cm and decreasing $N_{2\ denitrification}$ concentrations in the fresh water zone (Figure 18e). The lack of $N_{2\ denitrification}$ in P3-25 at the shallowest sample is likely due to heating during sampling, as evidenced by Argon under-saturation in this sample. The highest porewater $N_{2\ denitrification}$ concentration, 346µmolL^{-1}, was recorded at P3-35 at a depth of 120cm. This sample was collected the base of the mud cap, where sediments rapidly transition from organic rich mud to medium grain sand. This transition coincided with a decrease in $N_{2\ denitrification}$, from 346µmolL^{-1} at to 24µmolL^{-1} from depths 120cm to 370cm beneath the sediment-water interface.

Discussion

Mass balance estimates of denitrification

In the coastal aquifer in Stony Brook Harbor porewater movement in the vertical and horizontal directions are examined for nitrate loss due to denitrification and dilution. Nitrate loss and corresponding $N_{2\ denitrification}$ formation were calculated for vertical porewater flux in 11 porewater profiles. This calculation was performed as follows; the vertical change in NO_3^- concentration and $N_{2\ denitrification}$ between the fresh water zone and the top of the upper saline plume was calculated for each porewater profile. The lower boundary for NO_3^- loss was chosen as the maximum concentration observed in the freshwater portion of the coastal aquifer. The upper boundary was taken as the shallowest sample, which contained the maximum salinity and therefore contained the largest fraction of recirculated seawater. The calculation interval was the same for both NO_3^- and $N_{2\ denitrification}$. Then seepage rates were multiplied with vertical changes in NO_3^- and $N_{2\ denitrification}$. Seepage data was collected at the same time as porewater sampling using both electronic seepage meters and Lee style meters (Lee, 1977). For denitrification estimates a seepage rates of 2.6 m^3 (m shoreline)$^{-1}d^{-1}$ was applied to previously described nitrate loss and $N_{2\ denitrification}$ calculations. This rate was the lowest recorded seepage rate in low tide sand zone, and was applied to all porewater profiles except P3-35. At P3-35 the fresh water layer is capped by mud, therefore denitrification during transport to the base of this mud cap was calculated using a seepage rates of 0.03m^3 (m shoreline)$^{-1}d^{-1}$, which was measured in this zone during the same period as the sand zone discharge rate. These nitrate and $N_{2\ denitrification}$ flux rates were used to calculate the percentage nitrate loss due to denitrification, with results given in Table 4. A number of assumptions are made in these calculations. We assumed loss of NO_3^- in each porewater profile was due to (1) dilution with recirculated seawater and (2) microbially mediated denitrification. We are unable to account for other processes such as DNRA or anammox in this study, but it is noted that no NH_4^+ was measured in any samples. Therefore, we hypothesize that any NH_4^+entering the coastal aquifer is microbially utilized,

undergoes nitrification, or undergoes coupled nitrification-denitrification. The application of 2.6(m shoreline)$^{-1}$d^{-1} to all intertidal porewater profiles assumes constant discharge at all intertidal zones, but it is unlikely that significant seepage occurs from the high tide zone. Instead, the bulk of porewater in this zone moves likely moves horizontally.

A summary of denitrification rates and total NO_3^- flux are shown in Table 4. At site 2 denitrification flux, mmol N_2 (m shoreline)$^{-1}$d^{-1}, did not vary significantly from high to low tide porewater profiles, ranging from 110mmol N_2 (m shoreline)$^{-1}$d^{-1} at the high tide point (P2-0) to 170mmol N_2 (m shoreline)$^{-1}$d^{-1} at P2-30, located 2m below low tide (Figure 17e). We note that lower initial NO_3^- concentrations in the fresh groundwater zone at site 2 give rise to a larger percentage of total nitrogen denitrified, 35%, at the low tide mark when compared to low tide denitrification at site 1, which ranged from 1% to 20% (Table 4). Piezometers P2-15, P2-23 and P3-30 exhibit high salinity at all depths, indicating freshwater dilution to a depth of 5m in all cases. Previous work modeling tidal forcing on the USP and deep saline zone in coastal aquifers demonstrates that systems with tidal amplitudes in excess of 2m experience USP penetration to depths in excess of 5 meters (Robinson et al., 2007b). Modeled studies separate the USP from the deep saline zone by integrating two distinct domains, resulting in a prominent freshwater 'tube' that separates the two salt masses. Results in Stony Brook Harbor at P2 indicate these two domains do not act independently. Instead, the high tidal amplitude of 1.7m-2.2m forced mixing of the USP with the freshwater discharge zone and the deep saline zone that produced a mid-salinity (8.4-18.2ppt) 'tube' that exited the sediment near mean low tide. Therefore, at site 2 nitrate in the shallow low tide USP underwent ~65% dilution with saline water prior to discharge.

Denitrification at site 1 showed temporal variance, with higher $N_{2\ \text{denitrification}}$ concentrations in October (P3) than in May (P1). In May, $N_{2\ \text{denitrification}}$ was absent from high tide porewater profiles but was present in low tide porewater profiles, reaching a maximum rate of 330mmol (m shoreline)$^{-1}$ d^{-1} in P1-19, located at the base of the intertidal marsh. Denitrification rate then decreased precipitously to 3mmol (m shoreline)$^{-1}$ d^{-1} at P1-27, located sub-tidal sand sediments. In October (P3) denitrification rates were 106, 107 and 174mmol (m shoreline)$^{-1}$ d^{-1} in profiles P3-0, P3-7 and P3-25 respectively. Denitrification accounted for 11-20% nitrate attenuation in October. At the offshore piezometer, where SGD entered the base of the mud cap, 47% nitrate is denitrified with approximately 7mmol (m shore)$^{-1}$d^{-1} of $N_{2\ \text{denitrification}}$ produced over a vertical distance of 150cm. Despite a lack of data for denitrification in the mud cap itself, it is evident that the presence of the mud increased porewater DOC concentrations in the underlying sand sediments which facilitated microbial denitrification, resulting in the highest denitrification rates observed throughout the study period.

Total NO_3^- flux was calculated by applying the shallow saline NO_3^- concentration (table S2) to respective SGD rate for piezometers located in the low tide discharge zone (2.6 m^3 (m shoreline)$^{-1}$d^{-1}) and beneath the mud zone (0.03m^3 (m shoreline)$^{-1}$d^{-1}) for the four piezometers located in these positions, results shown in table 2. Results show nitrate loading rates ranged from 70 mmol (m shoreline^{-1} d^{-1}) to 265mmol (m shoreline^{-1} d^{-1}) with lowest rates occurring during the fall sampling period, shown in Table 4. As the concentrations used to calculated nitrate flux were derived from the sum of denitrification and mixing processes that occurred during transport through the biogeochemically active shallow saline zone, they represent the

loading concentration most likely to affect surface water, particularly for the sandy low tide discharge zone. It is important to note that nitrate flux from the offshore piezometer reflects a nitrate concentration of 2µmol L^{-1} in porewater from the mud-sand interface at a depth of 1.2m beneath the sediment-water interface. It is likely that the remaining nitrate is denitrified during discharge through the mud zone. Due to sampling constraints we do not have data to support this hypothesis, but previous workers have observed near complete consumption of nitrate during porewater movement through mud sediments (Hulth et al., 2005, Deutsch et al., 2010, Cabrita and Brotas, 2000).

Geochemical mechanisms of nitrate loss

Aquifers are traditionally thought to contain groundwater in equilibrium with sediment and therefore groundwater nutrient concentrations do not typically display large gradients over short spatial distances (Rivett et al., 2007). In coastal aquifers, mixing of groundwater with seawater in both the upper saline plume and deep saline zone produces redox gradients along porewater flow paths that result in large nitrogen variations over spatial distances less than ten meters. Microbially mediated reduction of nitrogen is driven by electron donors, so the concentration of electron donors is thought to play a major role in both O_2 reduction and NO_3^- reduction in aquatic environments (Tesoriero and Puckett, 2011). Dissolved organic carbon (DOC) is known to drive microbial denitrification (Korom, 1992) but iron and manganese can also drive denitrification in coastal aquifer sediments (Charette et al., 2005, Kroeger and Charette, 2008) as dissolved and solid phase concentrations of reduced iron are enriched in some porewater samples. Table 5 gives electron donor (DOC, Fe, Mn) concentrations for all sampling periods, along with pH and salinity which were used to determine how $N_{2\ denitrification}$ concentrations correlate with various electron donors (Table 6).

Groundwater DOC concentrations in Long Island's Upper Glacial aquifer are low, typically less than 30µML^{-1} (Young et al., 2013). Inland of this STE site, a combination of low DOC and high dissolved oxygen prevents extensive denitrification in the Upper Glacial aquifer. When Upper Glacial groundwater enters the coastal aquifer, it is mixed with DOC enriched seawater which averaged 180µML^{-1} during the study period. In the upper saline plume, this provides electron donors that can contribute to microbial denitrification. Microbial denitrification consumes labile carbon according to equation 5:

$$1.25\ CH_2O + NO_3^- + H^+ \rightarrow 0.5N_2 + 1.25CO_2 + 1.75H_2O \quad (5)$$

Pearson correlation coefficients were used to determine if $N_{2\ denitrification}$ was significantly correlated with salinity, DOC, Fe_{total}, pH and Mn (P1 and P2 only), with significance of $p<0.05$ (Table 6). Salinity is correlated to DOC in all three piezometer transects, indicating that seawater is a source of DOC to porewater in both the upper saline plume and the lower saline zone. At site 1, during May sampling (P1) $N_{2\ denitrification}$ was significantly correlated with Fe_{total}, ($p=0.0005$) but not with DOC or Mn^{2+} concentrations. Nitrate reduction via Fe^{2+} occurs according to equation 6.

$$NO_3^- + Fe^{2+} + 12H_2O \rightarrow 5Fe(OH)_3 + 0.5N_2 + 9H^+ \quad (6)$$

The mixing of reduced and oxidized porewater allows for the precipitation of iron-(oxy)hydroxides, which provide a surface for nitrate reduction (Postma et al., 1991). Tests for Fe^{2+} were below detection limit in porewater samples from this STE, indicating that either Fe^{2+} was removed from solution during sampling and/or Fe^{2+} is rapidly precipitated during mixing of saline porewater with fresh groundwater. The origin of iron in this system is not clear; as shown in Figure 21 salinity was not correlated with Fe_{total} in any of the porewater data sets. Elevated Fe_{total} concentrations were found in some porewater profiles, such as P1-0 and P1-27, at the interface between the upper saline plume and the fresh groundwater zone, but this trend does not hold for all porewater profiles. At site 2 maximum Fe_{total} concentrations are observed at the fresh groundwater- deep saline zone transition. In both cases the mixing of two water masses with distinct dissolved oxygen concentrations is linked with the maximum porewater concentrations of Fe_{total}.

At site 1, October sampling (P3), $N_{2\ denitrification}$ is significantly correlated with only pH ($p=0.03$) but not with DOC or Fe_{total} concentrations, even though pH was correlated with salinity, DOC and $Fe_{total.}$ While seawater controls the distribution of pH and electron donors during the October sampling period, no direct correlations existed between primary drivers of denitrification and production of $N_{2\ denitrification}$. Previous investigators have observed thermodynamically unstable settings in the subterranean estuary; for instance Kroeger and Charette (2008) found the nitrate and ammonium coexisted in some porewater samples, therefore it is possible that seasonal changes in groundwater residence time produce disequilibrium between distribution of electron donors and accumulation of $N_{2\ denitrification}$ (Kroeger and Charette, 2008).

Controls on DOC concentration are not limited to surface water concentrations of DOC. At site 1, in samples from depths less than 200cm taken from P1-19, P1-25, P3-7 and P3-25 DOC values exceeded those found in surface water samples, particularly in P3-25 at a depth of 45cm, where DOC concentration was $1251.5 \mu ML^{-1}$. DOC concentration in these shallow samples was likely controlled by remineralization of nutrients in marsh sediments. As described previously, the intertidal zone at this site is characterized by a *Spartina Alterniflora*, a salt marsh grass that reproduces by a subterranean rhizome system. This rhizome system traps sediment and fine particles, producing a substrate that can export carbon to underlying groundwater (Yelverton and Hackney, 1986). Horizontal movement of porewater during receding tide allows DOC derived from marsh sediments to infiltrate the upper portion of the underlying sand. Previous studies have examined the influence of nutrient loading to Long Island Sound marsh grasses and found nutrient additions, specifically combined nitrogen and phosphate loading, lead to both increased rates of marsh accretion and marsh elevation (Anisfeld and Hill, 2012). Despite different nutrient loading methodology (i.e above ground vs. below ground), results from this study are in agreement with Anisfeld and Hill (2012). At site 2, the absence of an intertidal marsh led to lower DOC concentrations in the upper saline plume, with concentrations of 100-240$\mu mol\ L^{-1}$in shallow high tide piezometers. Enrichment in this zone was due possibly to the breakdown of marine macrophyte wrack that accumulates on surface sediments (Dugan et al., 2011) in this low energy tidally dominated environment.

A comparison of site 1 and 2 show the importance of marsh formation on a number of factors in the coastal aquifer. First, the formation of a marsh leads to the stabilization of the

USP, trapping salt water in the upper 2m at site 1, which prevents mixing of the USP with deep saline zone observed at site 2. Although salinity was statistically correlated to DOC at both sites, denitrification rates were higher in the intertidal zone at site 1, whereas at site 2 denitrification rates were highest in the sub-tidal zone. This indicated that mixing of overlying water does not, by itself, produce conditions favorable for denitrification. In fact, the highest denitrification rates observed during the study were at the base of the intertidal marsh in May (P1-19)(Table 4).

As described by Durand et al.,2013 (submitted) groundwater at site 1 extended tens of meters offshore and discharged through a mud layer that covers the harbor bottom. Results from porewater samples taken from the base of this mud layer (P3-35) indicated near complete consumption of nitrate in the transition zone between sand and mud sediments. As this area was only sampled once during this study it is difficult to draw conclusions regarding denitrification mechanisms of this zone, but we note a DOC concentration of 2070µmol L^{-1} at the base of mud layer, which is sufficient to support denitrification of all fresh groundwater derived nitrate as it enters the mud cap (equation 5). The base of the mud layer acted as a sink of fresh groundwater nitrate, consuming 8mmol (m shoreline)$^{-1}d^{-1}$, which was expected given the high DOC concentration in these samples. Rates of reduction were similar to those observed for benthic muds, as found in this study of Stony Brook Harbor and by other investigators (LaMontagne et al., 2002).

Large differences in porewater nitrate concentrations between site 1 and site 2 indicate that site 1 experiences 2-3 times greater nitrate inputs than site 2. Moreover these inputs did not move uniformly through the coastal aquifer, but existed as a plume with maximum concentrations centered between 4 and 5m beneath the sediment surface. Porewater samples taken in May (P1) contain maximum nitrate concentrations in the fresh water zone at high tide position, but samples taken in October contain maximum nitrate concentration seaward most position (i.e base) of the intertidal marsh. This is possibly a result of seasonal increases in SGD fresh fraction, which has been observed in a STE at Waquoit Bay, MA (Michael et al., 2005). The presence of marsh at site 1 may, in fact, be supported by high nitrate concentrations in discharging porewater at this location. If effects from nutrient loading to the base of the marsh are similar to effects from surficial loading then it is possible that marsh grasses concentrate in areas where nitrate plumes exit the shallow portion of the coastal aquifer.

Calculated nitrate exports through the intertidal marsh are higher than those previously reported in Waquoit Bay, MA (Kroeger and Charette, 2008), but this is likely due to two things; elevated groundwater dissolved oxygen in the freshwater portion of the subterranean estuary and well documented high nitrate concentrations in Long Island's north shore aquifer (Porter, 1980, Young, 2010, Young et al., 2013). Further, this study does not account for nitrate uptake and utilization by marsh grasses as porewater within the root zone was not sampled due to rapid drainage of this zone during ebb tide. It is possible that denitrification further decreases any SGD driven nitrate entering the harbor water after passing through this zone.

Nitrate flux to Stony Brook Harbor

To calculate SGD nitrate flux to Stony Brook Harbor, porewater nitrate flux from the sand sediment zone is applied to the low tide area of the harbor perimeter. Nitrate flux was also

estimated from freshwater moving further offshore and approaching the base of the mud cap. The mud cap was observed to extend 60m offshore at 6 locations during electrical resistivity surveys completed during April-October of 2011, time periods coinciding with porewater sampling completed in this study (Durand et al., 2013). As described above, the highest denitrification rate was found at the base of the intertidal marsh at site 1 but this value is not used to calculate export to the harbor for two reasons. First, there are no measured SGD rates from the intertidal zone. Second, due to difficulty sampling porewater from low density marsh grass roots, no porewater samples were taken from the shallowest (and likely most biogeochemically active) zone of the intertidal marsh. Therefore, only piezometers located in the low-tide zone, profiles P1-27, P2-25 and P3-25 for the sandy zone and piezometer P3-35 for porewater intercepting the mud cap were used to estimate nitrate inputs into harbor surface water.

Discharge from sub-tidal sand comprises the bulk of nitrate flux to Stony Brook Harbor. Shoreline length of the southern lobe of the harbor was measured from aerial photos, and estimated to be 18,000m. I assume an average intertidal zone width of 10m, comprising 7m of intertidal zone from the base of the marsh at site 1 to the low tide mark and extending 3m offshore. Using nitrate flux of 231mmol (m shore)$^{-1}$ d^{-1}from P1-27 (May) and a discharge of 26cm d^{-1} nitrate flux to the harbor from sand is estimated at 4.2 x 10^{4}mol d^{-1}. Similar results are found using a nitrate flux of 265mmol (m shore)$^{-1}$ d^{-1} from P2-30 of 4.8 x 10^{4}mol d^{-1}. In October, shallow porewater concentration at P3-25 was 71mmol (m shoreline)$^{-1}$d^{-1}, which yields a flux of 1.3x10^{4}mol d^{-1}. As our study is limited to these two sites and time periods, I am unable to determine how much of the coastline is represented by site 1 as compared to site 2, and therefore the range of harbor flux is 1.3x 10^{4}mol d^{-1} to 4.8 x 10^{4}mol d^{-1}. It is important to note that all three flux calculations are based on the lowest recorded SGD rate at this site, 26cm d^{-1}, and therefore this nitrate flux range represents the a conservative estimate.

As shown in Table 4, nitrate in the freshwater zone undergoes 47% denitrification as it enters the base of the mud layer. In this layer porewater nitrate concentration was 2µmol L^{-1}, and discharge rates ranged 0 to 3cmd^{-1}. The mud layer with underlying freshwater zone was observed to extend for 60m offshore in all 6 resistivity surveys, therefore we assume this discharge area is consistent along the 18,000m perimeter of the harbor. The area of this mud cap is 1.08x10^{6}m^{2}, and the nitrate flux from the freshwater zone to the base of the mud is 1.1x10^{2}mol d^{-1}. Assuming no further denitrification of porewater and maximum discharge rate, this is the maximum amount of nitrate entering surface water through the mud cap, significantly less than nitrate entering the harbor through the sand sediments.

As observed from $N_{2\ \text{denitrification}}$ profiles, nitrate undergoes significant denitrification during discharge into the base of the mud layer. Our calculations of nitrate consumption through this portion of the harbor floor are dependent on a number of assumptions. First, we assume the observed freshwater plume extends beneath the harbor floor for 60m offshore along the entire perimeter. Electrical resistivity surveys completed at this site indicate freshwater extends at least 60m off the western and eastern shoreline. Additional resistivity surveys find freshwater extends at least 30m offshore beyond the mean low tide mark on the southeast and northwest portions of the harbor's main lobe. Second, as we have limited data for nitrate and $N_{2\ \text{denitrification}}$ values in the mud (i.e P3-35) we assume consistent nitrate concentrations exiting the freshwater zone throughout the base of the mud cap. We note higher $N_{2\ \text{denitrification}}$ values in samples collected in

October from other porewater profiles, likely due to lower dissolved oxygen content and increased DOC concentrations at the base of the mud cap. Given this, the calculated nitrate flux values to the base of the mud cap may be an overestimate of nitrate flux in this zone, and further data is needed to understand the extent of denitrification that occurs as fresh groundwater sourced nitrate exiting mud caps affects surface water. Finally, we note spatial variability in nitrate concentration between site 1 and site 2; therefore it is likely that nitrate concentrations in the freshwater zone offshore are also highly variable.

Conclusion

Microbially mediated nitrate reduction is known to occur in aquatic environments and within to the subterranean estuary (Kroeger and Charette, 2008). Exact amounts of subterranean estuary nitrate loss are frequently speculative, given difficulty in measuring denitrification end products. $N_{2\ \text{denitrification}}$ data in this study shows up to 35% of nitrate is denitrified during discharge through the sand low tide sediments. During freshwater transport to the base of the offshore mud cap, up to 47% of nitrate is denitrified. Despite reducing conditions in the upper saline plume, concentrations of ammonium are undetectable during all sampling periods at both site 1 and 2. Lack of ammonium in porewater samples may be due to ammonium utilization during anammox or coupled nitrification-denitrification reactions. At site 2, $N_{2\ \text{denitrification}}$ is significantly correlated with DOC ($p=0.01$), and therefore shows the clearest evidence of microbially mediated denitrification linked to mineralization of organic matter. Finally, this study highlights the importance of sediment composition on controlling both discharge rates and percent of nitrate denitrified at the embayment scale.

References

AESCHBACH-HERTIG, W., PEETERS, F., BEYERLE, U. & KIPFER, R. 1999. Interpretation of dissolved atmospheric noble gases in natural waters. *Water Resources Research,* 35**,** 2779-2792.

ANISFELD, S. C. & HILL, T. D. 2012. Fertilization Effects on Elevation Change and Belowground Carbon Balance in a Long Island Sound Tidal Marsh. *Estuaries and Coasts,* 35**,** 201-211.

BLICHER-MATHIESEN, G. & HOFFMANN, C. C. 1999. Denitrification as a sink for dissolved nitrous oxide in a freshwater riparian fen. *Journal of Environmental Quality,* 28**,** 257-262.

BOHLKE, J. K., WANTY, R., TUTTLE, M., DELIN, G. & LANDON, M. 2002. Denitrification in the recharge area and discharge area of a transient agricultural nitrate plume in a glacial outwash sand aquifer, Minnesota. *Water Resources Research,* 38**,** 26.

BOKUNIEWICZ, H. 1980. Groundwater Seepage Into Great South Bay, New-York. *Estuarine and Coastal Marine Science,* 10**,** 437-444.

BOWEN, J. L., KROEGER, K. D., TOMASKY, G., PABICH, W. J., COLE, M. L., CARMICHAEL, R. H. & VALIELA, I. 2007. A review of land-sea coupling by groundwater discharge of nitrogen to New England estuaries: Mechanisms and effects. *Applied Geochemistry,* 22**,** 175-191.

BRATTON, J. F. 2010. The Three Scales of Submarine Groundwater Flow and Discharge across Passive Continental Margins. *Journal of Geology,* 118**,** 565-575.

BURNETT, W. C., AGGARWAL, P. K., AURELI, A., BOKUNIEWICZ, H., CABLE, J. E., CHARETTE, M. A., KONTAR, E., KRUPA, S., KULKARNI, K. M., LOVELESS, A., MOORE, W. S., OBERDORFER, J. A., OLIVEIRA, J., OZYURT, N., POVINEC, P., PRIVITERA, A. M. G., RAJAR, R., RAMASSUR, R. T., SCHOLTEN, J., STIEGLITZ, T., TANIGUCHI, M. & TURNER, J. V. 2006. Quantifying submarine groundwater discharge in the coastal zone via multiple methods. *Science of the Total Environment,* 367**,** 498-543.

BUXTON, H. T. & MODICA, E. 1992. PATTERNS AND RATES OF GROUNDWATER-FLOW ON LONG-ISLAND, NEW-YORK. *Ground Water,* 30**,** 857-866.

CHARETTE, M. A. & ALLEN, M. C. 2006. Precision ground water sampling in coastal aquifers using a direct-push, shielded-screen well-point system. *Ground Water Monitoring and Remediation,* 26**,** 87-93.

CHARETTE, M. A., SHOLKOVITZ, E. R. & HANSEL, C. M. 2005. Trace element cycling in a subterranean estuary: Part 1. Geochemistry of the permeable sediments. *Geochimica Et Cosmochimica Acta,* 69**,** 2095-2109.

DE SIEYES, N. R., YAMAHARA, K. M., LAYTON, B. A., JOYCE, E. H. & BOEHM, A. B. 2008. Submarine discharge of nutrient-enriched fresh groundwater at Stinson Beach, California is enhanced during neap tides. *Limnology and Oceanography,* 53.

DILLON, K. S., CHANTON, J. P. & SMITH, L. K. 2007. Nitrogen sources and sinks in a wastewater impacted saline aquifer beneath the Florida Keys, USA. *Estuarine Coastal and Shelf Science,* 73**,** 148-164.

DORSETT, A., CHERRIER, J., MARTIN, J. B. & CABLE, J. E. 2011. Assessing hydrologic and biogeochemical controls on pore-water dissolved inorganic carbon cycling in a subterranean estuary: A C-14 and C-13 mass balance approach. *Marine Chemistry,* 127**,** 76-89.

DUGAN, J. E., HUBBARD, D. M., PAGE, H. M. & SCHIMEL, J. P. 2011. Marine Macrophyte Wrack Inputs and Dissolved Nutrients in Beach Sands. *Estuaries and Coasts,* 34**,** 839-850.

EYRE, B. D., RYSGAARD, S., DALSGAARD, T. & CHRISTENSEN, P. B. 2002. Comparison of isotope pairing and N-2 : Ar methods for measuring sediment-denitrification-assumptions, modifications, and implications. *Estuaries,* 25**,** 1077-1087.

GEORGAS, N. 2001. *Tidal Hydrodynamics and Bedload Transport in a Shallow, Vegetated Harbor (Stony Brook Harbor, Long Island, New York): A Modeling Approach with Management Implications* Masters of Science, State University of New York at Stony Brook.

GROFFMAN, P. M., ALTABET, M. A., BOHLKE, J. K., BUTTERBACH-BAHL, K., DAVID, M. B., FIRESTONE, M. K., GIBLIN, A. E., KANA, T. M., NIELSEN, L. P., VOYTEK, M. A. & CC 2006. Methods for measuring denitrification: Diverse approaches to a difficult problem. *Ecological Applications,* 16**,** 2091-2122.

HEATON, T. H. E. & VOGEL, J. C. 1981. EXCESS AIR IN GROUNDWATER. *Journal of Hydrology,* 50**,** 201-216.

HOSONO, T., ONO, M., BURNETT, W. C., TOKUNAGA, T., TANIGUCHI, M. & AKIMICHI, T. 2012. Spatial Distribution of Submarine Groundwater Discharge and Associated Nutrients within a Local Coastal Area. *Environmental Science & Technology,* 46**,** 5319-5326.

HOWARTH, R. W. 2008. Coastal nitrogen pollution: A review of sources and trends globally and regionally. *Harmful Algae,* 8**,** 14-20.

JOHANNES, R. E. 1980. THE ECOLOGICAL SIGNIFICANCE OF THE SUBMARINE DISCHARGE OF GROUNDWATER. *Marine Ecology Progress Series,* 3**,** 365-373.

KANA, T. M., DARKANGELO, C., HUNT, M. D., OLDHAM, J. B., BENNETT, G. E., CORNWELL, J. C. & PU 1994. Membrane inlet mass-spectrometer for rapid high-precision determination of N2, O2 and Ar in environmental water samples. *Analytical Chemistry,* 66**,** 4166-4170.

KNEE, K. L., STREET, J. H., GROSSMAN, E. E., BOEHM, A. B. & PAYTAN, A. 2010. Nutrient inputs to the coastal ocean from submarine groundwater discharge in a groundwater-dominated system: Relation to land use (Kona coast, Hawaii, USA). *Limnology and Oceanography,* 55**,** 1105-1122.

KOPPELMAN, L. 1978. The Long Island comprehensive waste treatment management plan: Hauppauge, Long Island Regional Planning Board.

KOROM, S. F. & HX 1992. NATURAL DENITRIFICATION IN THE SATURATED ZONE - A REVIEW. *Water Resources Research,* 28**,** 1657-1668.

KROEGER, K. D. & CHARETTE, M. A. 2008. Nitrogen biogeochemistry of submarine groundwater discharge. *Limnology and Oceanography,* 53**,** 1025-1039.

KUMAR, P., TSUJIMURA, M., NAKANO, T. & MINORU, T. 2013. Time series analysis for the estimation of tidal fluctuation effect on different aquifers in a small coastal area of Saijo plain, Ehime prefecture, Japan. *Environmental geochemistry and health,* 35**,** 239-50.

LAMONTAGNE, M., ASTORGA, V., GIBLIN, A. E. & VALIELA, I. 2002. Denitrification and the stoichiometry of nutrient regeneration in Waquoit Bay, Massachusetts. *Estuaries,* 25**,** 272-281.

LEE, D. R. 1977. DEVICE FOR MEASURING SEEPAGE FLUX IN LAKES AND ESTUARIES. *Limnology and Oceanography,* 22**,** 140-147.

LI, L., BARRY, D. A., PARLANGE, J. Y. & PATTIARATCHI, C. B. 1997. Beach water table fluctuations due to wave run-up: Capillarity effects. *Water Resources Research,* 33**,** 935-945.

LOVELESS, A. M. & OLDHAM, C. E. 2010. Natural attenuation of nitrogen in groundwater discharging through a sandy beach. *Biogeochemistry,* 98**,** 75-87.

MICHAEL, H. A., MULLIGAN, A. E. & HARVEY, C. F. 2005. Seasonal oscillations in water exchange between aquifers and the coastal ocean. *Nature,* 436**,** 1145-1148.

MOOKHERJI, S., MCCARTY, G. W., ANGIER, J. T. & BR 2003. Dissolved gas analysis for assessing the fate of nitrate in wetlands. *Journal of the American Water Resources Association,* 39**,** 381-387.

MOORE, W. S. 1999. The subterranean estuary: a reaction zone of ground water and sea water. *Marine Chemistry,* 65**,** 111-125.

MUNSTER, J. 2008a. *Non-point sources of nitrate and perchlorate in urban land use to groundwater, Suffolk County, NY.* Ph.D, Stony Brook University, Stony Brook, NY.

MUNSTER, J. 2008b. Non-point sources of nitrate and perchlorate in urban land use to groundwater, Suffolk County, NY. http://www.geo.sunysb.edu/reports/.

NOAA. 2011. *Climatological Report (Annual)* [Online]. http://www.crh.noaa.gov/product.php?site=NWS&issuedby=ISP&product=CLA&format=CI&version=1&glossary=1&highlight=off. [Accessed 4-10-2012 2012].

PAULSEN, R. J., SMITH, C. F., O'ROURKE, D. & WONG, T. F. 2001. Development and evaluation of an ultrasonic ground water seepage meter. *Ground Water,* 39**,** 904-911.

PETERSON, R. N., BURNETT, W. C., GLENN, C. R. & JOHNSON, A. G. 2009. Quantification of point-source groundwater discharges to the ocean from the shoreline of the Big Island, Hawaii. *Limnology and Oceanography,* 54**,** 890-904.

PORTER, K. S. 1980. AN EVALUATION OF SOURCES OF NITROGEN AS CAUSES OF GROUNDWATER CONTAMINATION IN NASSAU-COUNTY, LONG-ISLAND. *Ground Water,* 18**,** 617-625.

POSTMA, D., BOESEN, C., KRISTIANSEN, H. & LARSEN, F. 1991. NITRATE REDUCTION IN AN UNCONFINED SANDY AQUIFER - WATER CHEMISTRY, REDUCTION PROCESSES, AND GEOCHEMICAL MODELING. *Water Resources Research,* 27**,** 2027-2045.

RIVETT, M. O., SMITH, J. W. N., BUSS, S. R. & MORGAN, P. 2007. Nitrate occurrence and attenuation in the major aquifers of England and Wales. *Quarterly Journal of Engineering Geology and Hydrogeology,* 40**,** 335-352.

ROBINSON, C., GIBBES, B., CAREY, H. & LI, L. 2007a. Salt-freshwater dynamics in a subterranean estuary over a spring-neap tidal cycle. *Journal of Geophysical Research-Oceans,* 112.

ROBINSON, C., LI, L. & BARRY, D. A. 2007b. Effect of tidal forcing on a subterranean estuary. *Advances in Water Resources,* 30.

ROBINSON, C., LI, L. & PROMMER, H. 2007c. Tide-induced recirculation across the aquifer-ocean interface. *Water Resources Research,* 43.

SANTOS, I. R., BURNETT, W. C., DITTMAR, T., SURYAPUTRA, I. & CHANTON, J. 2009. Tidal pumping drives nutrient and dissolved organic matter dynamics in a Gulf of Mexico subterranean estuary. *Geochimica Et Cosmochimica Acta,* 73**,** 1325-1339.

SANTOS, I. R., EYRE, B. D. & HUETTEL, M. 2012. The driving forces of porewater and groundwater flow in permeable coastal sediments: A review. *Estuarine Coastal and Shelf Science,* 98**,** 1-15.

SCORCA, M. & MONTI, J. 2001. Estimates of Nitrogen Loads Entering Long Island Sound from Ground Water and Streams on Long Island, New York, 1985-96. *In:* INVESTIGATION, W. R. (ed.). Troy, NY: U.S Geological Survey.

SLOMP, C. P. & VAN CAPPELLEN, P. 2004. Nutrient inputs to the coastal ocean through submarine groundwater discharge: controls and potential impact. *Journal of Hydrology,* 295**,** 64-86.

SOLORZANO, L. 1969. Determination of Ammonia in Natural Waters by Phenolhypochlorite Method. *Limnology and Oceanography,* 14**,** 799-&.

STEENHUIS, T. S., JACKSON, C. D., KUNG, S. K. J. & BRUTSAERT, W. 1985. MEASUREMENT OF GROUNDWATER RECHARGE ON EASTERN LONG-ISLAND, NEW-YORK, USA. *Journal of Hydrology,* 79**,** 145-169.

STOOKEY, L. L. 1970. Ferrozine- A New Spectrophotometric Reagent for Iron. *Analytical Chemistry,* 42**,** 779-&.

STRICKLAND, J. & PARSONS, T. 1978. *A practical handbook of seawater analysis,* Ottowa, Fisheries Research Board of Canada.

TANIGUCHI, M., BURNETT, W. C., CABLE, J. E. & TURNER, J. V. 2002. Investigation of submarine groundwater discharge. *Hydrological Processes,* 16**,** 2115-2129.

TESORIERO, A. J. & PUCKETT, L. J. 2011. O-2 reduction and denitrification rates in shallow aquifers. *Water Resources Research,* 47.

TOBIAS, C. R., MACKO, S. A., ANDERSON, I. C., CANUEL, E. A. & HARVEY, J. W. 2001. Tracking the fate of a high concentration groundwater nitrate plume through a fringing marsh: A combined groundwater tracer and in situ isotope enrichment study. *Limnology and Oceanography,* 46**,** 1977-1989.

WEINSTEIN, Y., YECHIELI, Y., SHALEM, Y., BURNETT, W. C., SWARZENSKI, P. W. & HERUT, B. 2011. What Is the Role of Fresh Groundwater and Recirculated Seawater in Conveying Nutrients to the Coastal Ocean? *Environmental Science & Technology,* 45**,** 5195-5200.

WEISS, R. F. 1970. SOLUBILITY OF NITROGEN, OXYGEN AND ARGON IN WATER AND SEAWATER. *Deep-Sea Research,* 17**,** 721-&.

WEYMANN, D., WELL, R., FLESSA, H., VON DER HEIDE, C., DEURER, M., MEYER, K., KONRAD, C. & WALTHER, W. 2008. Groundwater N2O emission factors of nitrate-contaminated aquifers as derived from denitrification progress and N2O accumulation. *Biogeosciences,* 5**,** 1215-1226.

WILSON, G. B. & MCNEILL, G. W. 1997. Noble gas recharge temperatures and the excess air component. *Applied Geochemistry,* 12**,** 747-762.

YELVERTON, G. F. & HACKNEY, C. T. 1986. FLUX OF DISSOLVED ORGANIC-CARBON AND PORE WATER THROUGH THE SUBSTRATE OF A SPARTINA-ALTERNIFLORA MARSH IN NORTH-CAROLINA. *Estuarine Coastal and Shelf Science,* 22**,** 255-267.

YOUNG, C. 2010. *Extent of Denitrification in Northport Groundwater.* M.S. Geosciences, SUNY Stony Brook.

YOUNG, C., KROEGER, K. & HANSON, G. 2013. Limited denitrification in glacial deposit aquifers having thick unsaturated zones (Long Island, USA). *Hydrogeology Journal*.

Tables and Figures

Table 3 Raw N_2 and Ar, calculated excess air at 14 °C and average $N_{2denitrification}$ at 12°C and 14°C for STE porewater samples in Stony Brook Harbor.

				Excess Air N_2 µmol L^{-1}		$N_{2\ denitrification}$ (µmol L^{-1})	
Sample	Depth (cm)	N_2 (µmol L^{-1})	Ar (µmolL^{-1})	Max 14^0C	Min 14^0C	Average at 14^0C	Average at 12^0C
Site 1 May							
P1-0	101.6	539.5	14.2	N/A	N/A	BDL	BDL
P1-0	167.64	516.3	13.7	N/A	N/A	BDL	BDL
P1-0	220.98	510.4	13.6	N/A	N/A	BDL	BDL
P1-0	280.67	547.3	14.4	N/A	N/A	BDL	BDL
P1-0	347.98	534.6	14.2	N/A	N/A	BDL	BDL
P1-0	434.34	497.7	13.4	N/A	N/A	BDL	BDL
P1-0	525.78	529.9	14.0	N/A	N/A	BDL	BDL
P1-0	617.22	537.4	14.2	N/A	N/A	BDL	BDL
P1-0	708.66	538.2	14.2	N/A	N/A	BDL	BDL
P1-7	182.88	602.5	15.2	107.7	48.2	33.2	38.2
P1-7	243.84	581.8	15.2	51.5	23.1	8.9	20.1
P1-7	304.8	571.1	15.0	56.9	25.5	6.7	12.2
P1-7	365.76	566.6	14.8	N/A	N/A	3.9	BDL
P1-7	523.24	539.2	14.2	N/A	N/A	BDL	BDL
P1-7	591.82	543.1	14.2	N/A	N/A	BDL	BDL
P1-19	401.32	637.7	16.6	83.3	37.6	12.3	14.5
P1-19	431.8	547.9	14.3	N/A	N/A	BDL	BDL
P1-19	525.78	612.8	16.2	45.0	20.3	0.8	BDL
P1-19	594.36	611.2	16.0	21.5	9.7	5.8	BDL
P1-19	640.08	594.1	15.8	1.6	0.7	BDL	BDL
P1-19	708.66	593.6	15.9	16.3	7.4	BDL	BDL
P1-19	238.76	660.3	15.6	27.1	12.2	128.9	124.5
P1-19	355.6	581.6	15.2	N/A	N/A	BDL	BDL
P1-19	137.16	324.4	9.7	N/A	N/A	BDL	BDL
P1-27	53.34	547.2	14.5	15.9	7.1	4.7	BDL
P1-27	248.92	576.5	14.5	N/A	N/A	BDL	BDL
P1-27	299.72	559.7	14.5	N/A	N/A	BDL	BDL
P1-27	360.68	544.5	14.4	N/A	N/A	BDL	BDL
P1-27	452.12	613.5	16.1	42.9	19.3	6.3	0.3
P1-27	538.48	645.1	17.0	118.7	53.6	3.7	5.8
P1-27	657.86	519.1	13.6	N/A	N/A	BDL	BDL
P1-27	756.92	539.9	14.2	N/A	N/A	BDL	BDL
Site 2 May							

P2-0	99.06	658.3	16.7	85.2	38.5	27.8	45.4
P2-0	203.2	670.9	17.1	117.8	53.2	25.7	27.8
P2-0	256.54	653.9	16.8	93.3	42.1	19.8	25.1
P2-0	320.04	627.7	16.6	69.6	31.4	1.9	3.9
P2-0	472.44	621.4	16.5	62.4	28.2	BDL	0.0
P2-0	612.14	632.1	16.6	70.1	31.6	5.2	8.8
P2-0	698.5	668.6	17.2	122.4	55.2	18.0	20.2
P2-8	480.06	592.8	15.9	16.8	7.6	BDL	BDL
P2-8	558.8	602.9	16.0	37.6	16.9	BDL	BDL
P2-15	589.28	586.1	15.3	91.1	40.8	12.5	14.4
P2-23	121.92	627.3	16.3	146.6	65.8	13.7	15.8
P2-23	182.88	572.9	15.1	N/A	N/A	3.5	BDL
P2-23	243.84	597.4	15.6	56.4	25.3	8.3	20.1
P2-23	297.18	603.2	15.8	63.7	28.7	6.6	13.0
P2-23	471.17	376.5	10.9	N/A	N/A	BDL	BDL
P2-23	518.16	460.9	12.4	N/A	N/A	BDL	BDL
P2-23	567.69	570.0	14.9	21.7	9.7	7.9	BDL
P2-23	609.6	583.9	15.3	71.3	32.0	9.6	13.1
P2-23	656.59	587.2	15.3	93.8	42.0	14.7	16.6
P2-23	767.08	532.8	14.0	27.2	12.1	10.7	5.5
P2-30	45.72	628.6	15.2	31.2	14.0	93.3	92.8
P2-30	121.92	544.2	14.5	N/A	N/A	BDL	BDL
P2-30	300.99	463.3	12.9	N/A	N/A	BDL	BDL
P2-30	532.13	589.6	15.4	53.7	24.1	9.6	22.2
P2-30	619.76	584.0	15.3	60.0	26.9	8.0	16.5
P2-30	693.42	549.7	14.3	4.6	2.1	23.2	BDL
Site 1 October							
P3-0	196.9	615.2	15.7	59.4	26.7	23.7	48.3
P3-0	243.8	622.7	16.1	93.8	42.2	15.8	17.7
P3-0	298.5	596.6	15.5	38.3	17.2	14.7	20.3
P3-0	365.8	617.5	16.2	76.7	34.6	6.8	10.1
P3-0	403.9	598.9	15.6	28.9	13.0	9.7	4.6
P3-0	491.5	642.2	16.8	90.5	40.9	5.6	7.7
P3-0	701.0	585.5	15.5	N/A	N/A	10.1	0.0
P3-0	838.2	587.5	15.5	N/A	N/A	0.0	0.0
P3-7	195.6	636.1	15.6	128.6	57.6	50.3	61.9
P3-7	254.0	618.2	15.7	56.4	25.4	28.1	57.2
P3-7	294.6	630.5	16.1	89.1	40.1	25.8	42.7
P3-7	365.8	610.1	16.0	17.7	8.0	6.4	0.0
P3-7	454.7	593.9	15.6	N/A	N/A	11.0	0.0
P3-7	548.6	613.0	16.2	33.2	15.0	2.3	0.0
P3-7	640.1	591.9	15.6	NA	-6.8	14.2	0.0
P3-7	731.5	615.6	16.3	44.0	19.9	BDL	0.0

P3-7	924.6	590.1	15.7	N/A	N/A	BDL	BDL
P3-13	121.9	615.5	15.7	68.2	30.4	28.2	28.3
P3-13	243.8	633.7	16.5	75.7	34.1	11.8	16.4
P3-13	365.8	643.5	17.0	105.5	47.6	0.2	2.4
P3-13	487.7	634.9	16.7	84.6	38.2	5.0	7.0
P3-25	223.5	556.8	13.7	N/A	N/A	BDL	BDL
P3-25	307.3	671.7	16.8	123.5	55.6	39.9	51.8
P3-25	365.8	621.1	16.1	33.0	14.9	14.5	16.2
P3-25	424.2	601.0	15.6	N/A	N/A	18.5	BDL
P3-25	467.4	620.6	16.4	65.0	29.3	BDL	BDL
P3-25	579.1	648.2	16.8	99.9	45.1	15.3	17.6
P3-25	688.3	630.9	16.5	66.3	29.9	5.3	10.3
P3-25	772.2	629.3	16.3	41.9	18.9	14.7	18.2
P3-25	883.9	673.1	17.0	116.8	52.7	32.6	38.1
P3-35	121.9	804.8	17.5	154.2	69.6	202.2	236.7
P3-35	365.8	627.9	16.6	68.0	30.7	1.5	3.7
P3-35	530.9	630.6	16.4	65.4	29.5	9.3	19.3
P3-35	739.1	647.7	16.8	83.4	37.7	14.3	16.6
P3-35	853.4	660.5	16.6	113.6	51.2	33.2	44.2
P3-35	1005.8	637.5	16.2	47.0	21.0	31.2	30.1

Table 4 Calculations of nitrate loss, accumulation of $N_{2\ denitrification}$ and NO_3^- export to surface waters (see table S2) based on vertical porewater nitrogen.

Piezometer	Time	NO_3^- Loss mmol (m shore)$^{-1}$ d^{-1}	N2 denitrification mmol (m shore)$^{-1}$ d^{-1}	% denitrified	NO_3^- release to surface mmol (m shore)$^{-1}$ d^{-1}
P1-0	May	1154	0	0	264
P1-7	May	446	86	16	88
P1-19	May	552	333	38	44
P1-27	May	400	3	1	231
P3-0	October	866	106	11	80
P3-7	October	773	107	12	64
P3-25	October	681	174	20	71
P3-35	October	8	7	47	0
P2-0	May	172	118	41	465
P2-23	May	106	7	6	319
P2-30	May	338	184	35	265

Table 5 List of electron donors used to calculate correlation coefficients. ND indicates no data available; BDL indicates concentration is below detection limit.

				Electron Donors (μmol L^{-1})		
piezometer	depth (cm)	salinity	pH	DOC	Fe_{total}	Mn
Site 1- May						
P1-0	101.6	12.8	6.4	157.8	1.5	0.0
P1-0	167.6	13.1	6.7	ND	21.3	1.0
P1-0	221.0	2.3	5.7	78.2	14.1	
P1-0	280.7	0.1	5.9	79.8	2.3	1.7
P1-0	348.0	0.1	5.6	ND	3.1	3.7
P1-0	434.3	0.2	5.8	86.2	3.0	3.3
P1-0	525.8	0.1	5.7	ND	2.8	1.0
P1-0	617.2	0.1	5.7	ND	3.3	0.0
P1-0	708.7	0.1	5.7	87.4	3.3	0.0
P1-7	182.9	20.1	6.5	ND	0.8	0.0
P1-7	243.8	12.8	6.7	219.1	3.5	0.5
P1-7	304.8	15.7	6.5	ND	2.3	0.3
P1-7	365.8	8.8	5.6	60.8	15.6	2.9
P1-7	406.4	14.5	5.2	ND	3.1	0.9
P1-7	475.0	5.8	5.4	123.2	2.0	0.0
P1-7	523.2	3.0	5.4	208.8	3.3	2.1
P1-7	591.8	0.2	5.6	133.2	0.2	2.8
P1-19	137.2	26.4	6.7	320.3	BDL	13.5
P1-19	238.8	5.5	6.4	107.2	22.7	4.6
P1-19	297.2	4.6	6.4	135.4	2.8	1.7
P1-19	355.6	2.7	6.2	28.1	0.7	0.0
P1-19	401.3	2.2	6.1	31.1	5.6	3.4
P1-19	431.8	4.7	6.5	111.0	4.1	0.0
P1-19	525.8	1.4	6.0	39.8	3.9	2.3
P1-19	594.4	0.9	5.5	73.6	0.6	2.1
P1-19	640.1	0.9	5.2	ND	0.8	0.7
P1-19	708.7	1.3	5.3	ND	2.3	3.7
P1-27	53.3	16.5	6.2	171.8	0.2	4.0
P1-27	248.9	2.8	6.2	84.6	7.0	2.6
P1-27	299.7	2.5	6.1	ND	3.2	0.1
P1-27	360.7	1.2	6.5	84.1	1.1	0.0
P1-27	452.1	1.8	6.2	ND	4.7	2.1
P1-27	538.5	1.9	6.0	32.5	3.6	4.1
P1-27	657.9	1.5	5.7	ND	0.8	1.7
P1-27	756.9	0.2	5.7	36.5	0.4	0.0
Site 2- May						

P2-0	99.1	12.0	6.8	203.5	4.4	1.0
P2-0	203.2	0.9	5.9	106.2	16.9	0.2
P2-0	256.5	1.0	5.6	85.2	4.0	0.0
P2-0	320.0	0.3	5.8	60.0	3.0	0.1
P2-0	472.4	0.1	6.0	34.5	46.7	8.9
P2-0	612.1	0.1	5.8	32.6	15.3	3.7
P2-0	698.5	0.1	5.6	27.3	0.3	2.4
P2-8	63.5	28.5	7.3	88.7	BDL	0.4
P2-8	161.3	27.3	7.5	239.5	2.7	8.9
P2-8	299.7	3.4	6.7	103.2	2.8	45.2
P2-8	375.9	7.1	5.8	58.6	0.6	2.6
P2-8	408.9	4.1	5.9	ND	0.5	0.0
P2-8	457.2	4.2	5.6	41.7	0.4	2.8
P2-8	480.1	0.6	5.8	51.5	1.1	2.1
P2-8	558.8	2.1	5.4	45.3	3.6	0.3
P2-8	594.4	0.3	5.8	44.7	2.8	1.1
P2-15	66.0	25.1	6.3	81.9	22.8	3.6
P2-15	124.5	27.4	6.6	59.8	3.4	0.0
P2-15	191.8	24.1	6.3	ND	7.5	0.0
P2-15	248.9	23.9	6.4	98.6	7.7	
P2-15	284.5	24.0	6.5	ND	11.4	4.2
P2-15	365.8	18.3	5.4	80.1	2.5	3.3
P2-15	411.5	12.6	7.2	62.1	16.6	2.6
P2-15	412.8	16.5	6.8	60.9	BDL	0.0
P2-15	548.6	13.0	6.5	ND	5.7	
P2-15	589.3	16.7	6.5	125.2	5.6	0.0
P2-15	640.1	20.2	6.3	97.6	8.3	4.7
P2-15	669.3	21.2	6.1	ND	4.3	4.5
P2-15	731.5	21.6	6.0	86.9	2.9	4.5
P2-23	121.9	12.6	6.8	73.7	0.9	0.7
P2-23	182.9	6.3	6.9	46.1	1.8	2.5
P2-23	243.8	8.2	6.7	48.5	0.5	0.0
P2-23	297.2	7.1	6.7	ND	15.4	0.0
P2-23	396.2	7.9	6.9	47.7	2.2	2.5
P2-23	471.2	10.7	6.8	ND	5.8	0.0
P2-23	518.2	9.9	7.0	71.5	5.5	0.9
P2-23	567.7	11.3	6.9	65.3	2.0	
P2-23	609.6	14.1	6.9	ND	25.0	2.2
P2-23	656.6	17.3	6.7	66.3	8.5	
P2-23	767.1	23.3	6.3	86.6	71.6	18.4
P2-30	45.7	9.4	6.0	130.4	7.4	0.0
P2-30	121.9	8.3	6.1	35.8	2.9	0.0
P2-30	160.0	7.6	6.4	34.7	1.8	0.0

P2-30	229.9	8.0	6.7	ND	1.0	0.0
P2-30	301.0	9.1	6.7	46.2	0.2	1.4
P2-30	358.1	9.2	6.5	ND	2.0	0.7
P2-30	435.6	8.4	6.6	54.7	2.9	0.3
P2-30	532.1	10.4	6.4	ND	4.3	1.4
P2-30	619.8	12.2	6.3	67.1	2.3	0.0
P2-30	693.4	16.2	6.5	130.2	17.5	9.0
Site 1- October						
P3-0	196.9	8.3	6.1	114.1	BDL	
P3-0	243.8	7.8	6.1	118.8	BDL	
P3-0	298.5	8.4	6.0	140.1	BDL	
P3-0	365.8	4.2	6.4	128.4	BDL	
P3-0	403.9	5.8	5.4	102.3	5.0	
P3-0	491.5	0.1	6.0	76.9	2.9	
P3-0	594.4	0.1	5.9	77.0	0.3	
P3-0	701.0	0.1	5.6	ND	1.6	
P3-0	838.2	0.1	5.6	94.1	1.6	
P3-7	195.6	17.9	6.4	182.4	0.4	
P3-7	254.0	7.6	6.9	138.3	0.5	
P3-7	294.6	6.6	6.4	158.7	1.0	
P3-7	365.8	1.0	5.9	106.0	2.3	
P3-7	454.7	0.6	6.0	ND	4.3	
P3-7	548.6	0.6	5.6	ND	1.7	
P3-7	640.1	0.4	5.6	100.9	0.1	
P3-7	731.5	0.5	5.7	ND	BDL	
P3-7	924.6	0.2	6.0	ND	BDL	
P3-7	1041.4	0.1	5.9	ND	BDL	
P3-7	1193.8	1.6	5.4	ND	BDL	
P3-25	45.7	24.9		1251.5	ND	
P3-25	109.2	21.2		210.4	31.8	
P3-25	223.5	1.8	6.1	120.9	ND	
P3-25	307.3	3.9	6.2	128.8	18.5	
P3-25	365.8	1.8	6.2	93.8	ND	
P3-25	424.2	1.3	6.3	91.4	34.4	
P3-25	467.4	1.1	6.3	56.2	ND	
P3-25	579.1	2.7	5.6	56.4	8.6	
P3-25	688.3	0.2	6.2	44.3	ND	
P3-25	772.2	0.1	5.8	ND	ND	
P3-25	883.9	1.9	6.2	54.1	19.7	
P3-35	121.9	1.5	6.3	113.1	BDL	
P3-35	365.8	0.6	6.3	60.9	BDL	
P3-35	530.9	1.0	5.7	35.8	BDL	
P3-35	739.1	1.0	6.1	ND	16.1	

P3-35	853.4	3.8	5.9	43.9	ND
P3-35	1005.8	8.3	6.0	64.0	ND

Table 6 Pearson correlation coefficients for geochemical indicators of denitrification. Coefficients with a $p<0.05$ shown in bold.

	pH	DOC	Fe_{total}	$N_{2\ denitrification}$	Mn^{2+}
site 1, May 2011 (P1) (n=35)					
salinity	0.52	**0.79**	0.04	0.13	0.35
pH		0.36	0.20	**0.79**	0.14
DOC			-0.20	0.00	**0.52**
Fe_{total}				**0.54**	0.08
$N_{2\ denitrification}$					0.14
site 2, May 2011 (P2) (n=50)					
salinity	0.44	**0.46**	0.14	0.12	0.02
pH		0.36	-0.04	-0.14	0.09
DOC			0.03	**0.57**	0.20
Fe_{total}				-0.02	0.31
$N_{2\ denitrification}$					-0.07
site 1, October 2011 (P3) (n=38)					
salinity	0.43	**0.65**	-0.23	0.24	
pH		0.38	**0.47**	0.35	
DOC			-0.33	0.26	
Fe_{total}				0.31	

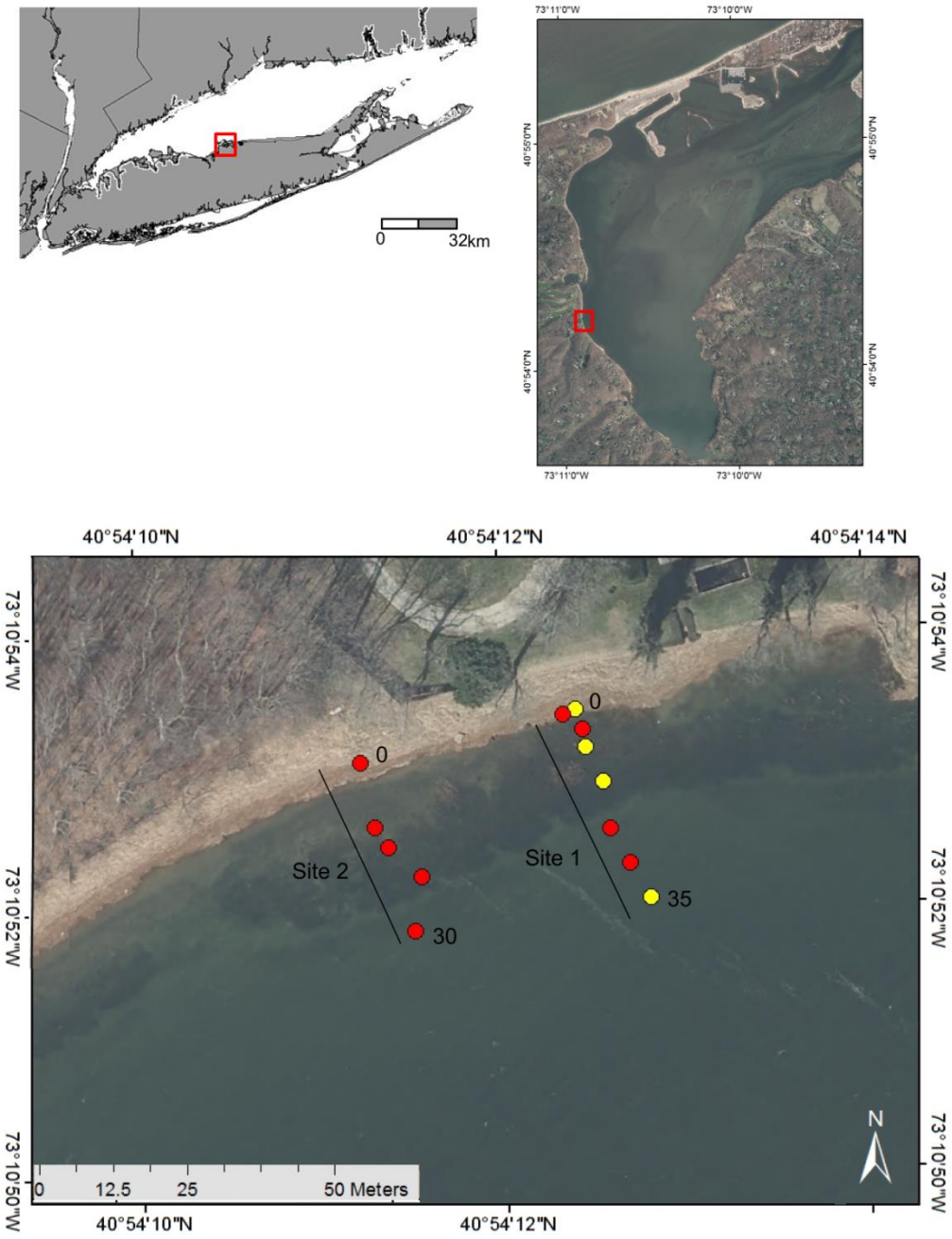

Figure 12 Map of study sites in Long Island, NY, USA (top left). Stony Brook Harbor (top right) is located on the south shore of Long Island Sound, with the sampling area outlined. Site 1 and site 2 porewater profiles (red circles, bottom) were sampled in the spring of 2011, site 1 was sampled again in fall of 2011 (yellow circles, bottom). Numbers adjacent to porewater profile location indicate shore perpendicular distance, shown as x-axis in figures 4, 5 and 6.

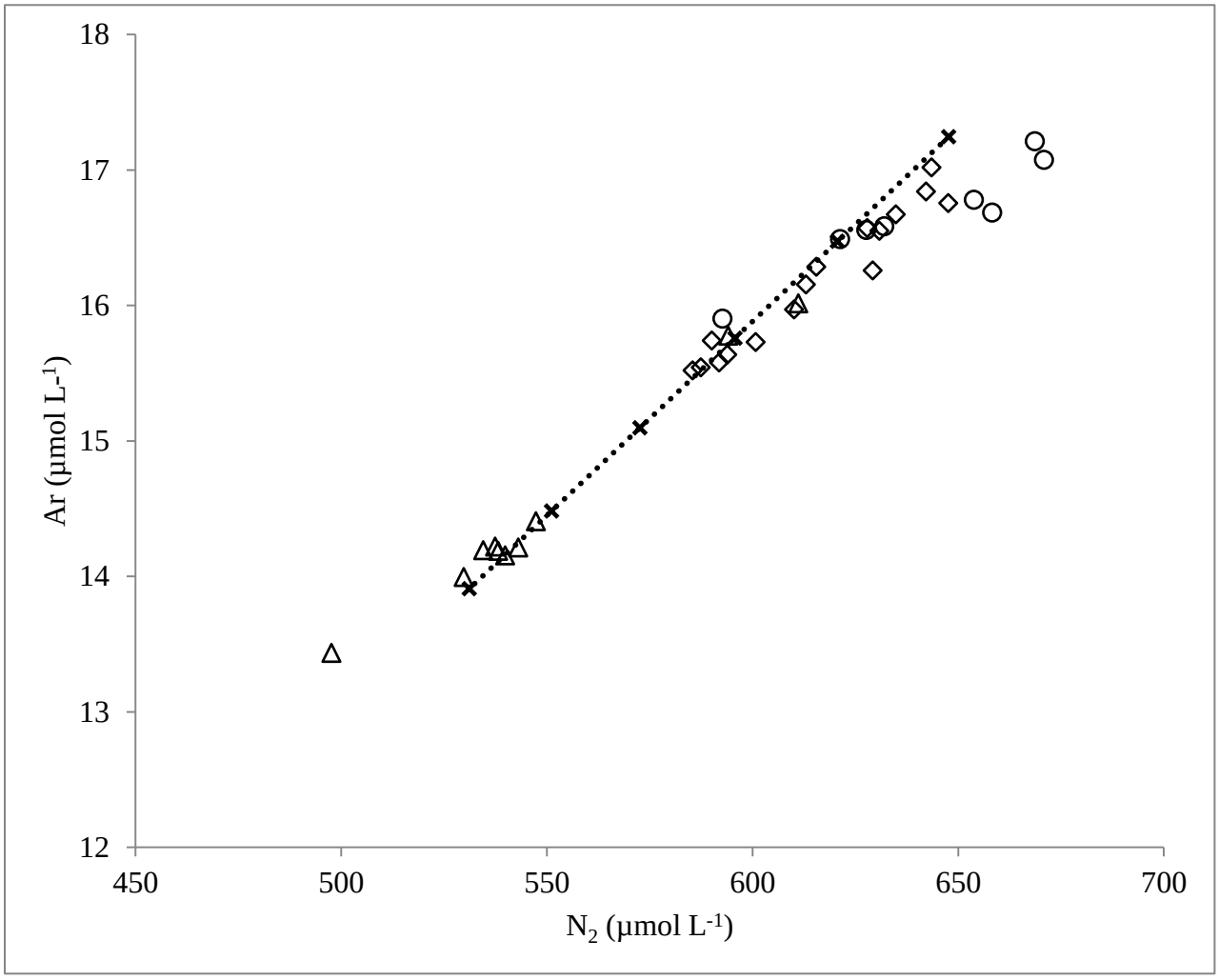

Figure 13 N_2 vs Ar for porewater samples with salinity less than 1ppt. Samples from site 1 in May (Δ) and October (◊) and site 2 in May (○).

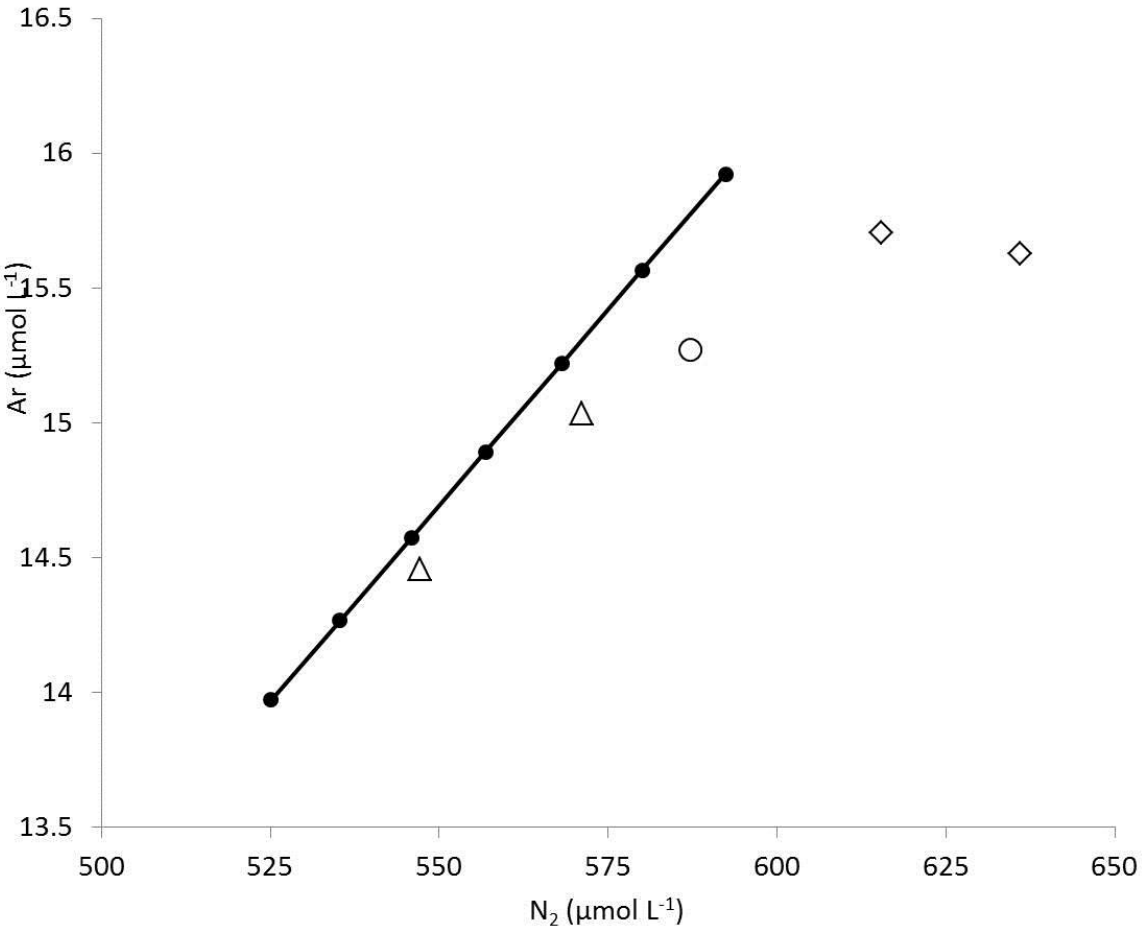

Figure 14 N_2 vs Ar for porewater samples with salinity range 16-18ppt. Samples from site 1 in May (Δ) and October (◊) and site 2 in May (○).

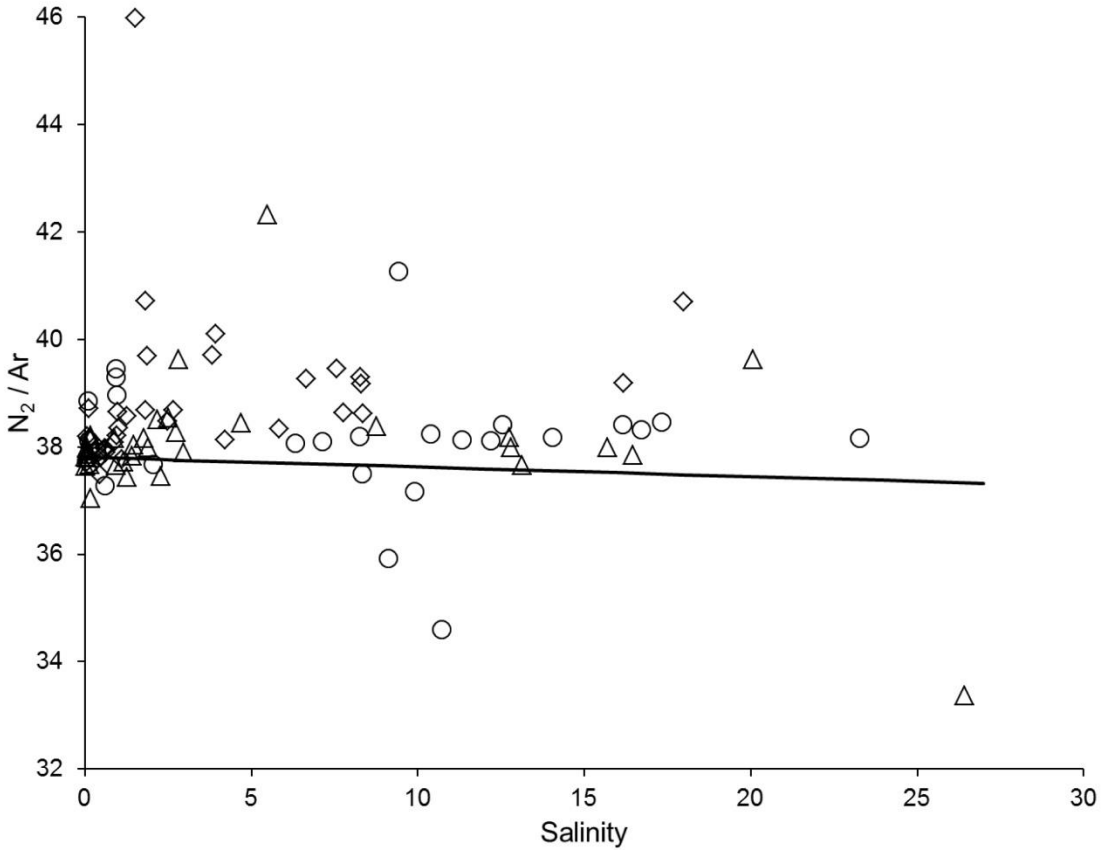

Figure 15 Dissolved nitrogen to argon (N_2/Ar) concentrations vs salinity. Samples from site 1 in May (Δ) and October (◊) and site 2 in May (○). Solid line (─) indicates air saturated water N_2/Ar ratio at 14^0C for the range of porewater salinities found at this site.

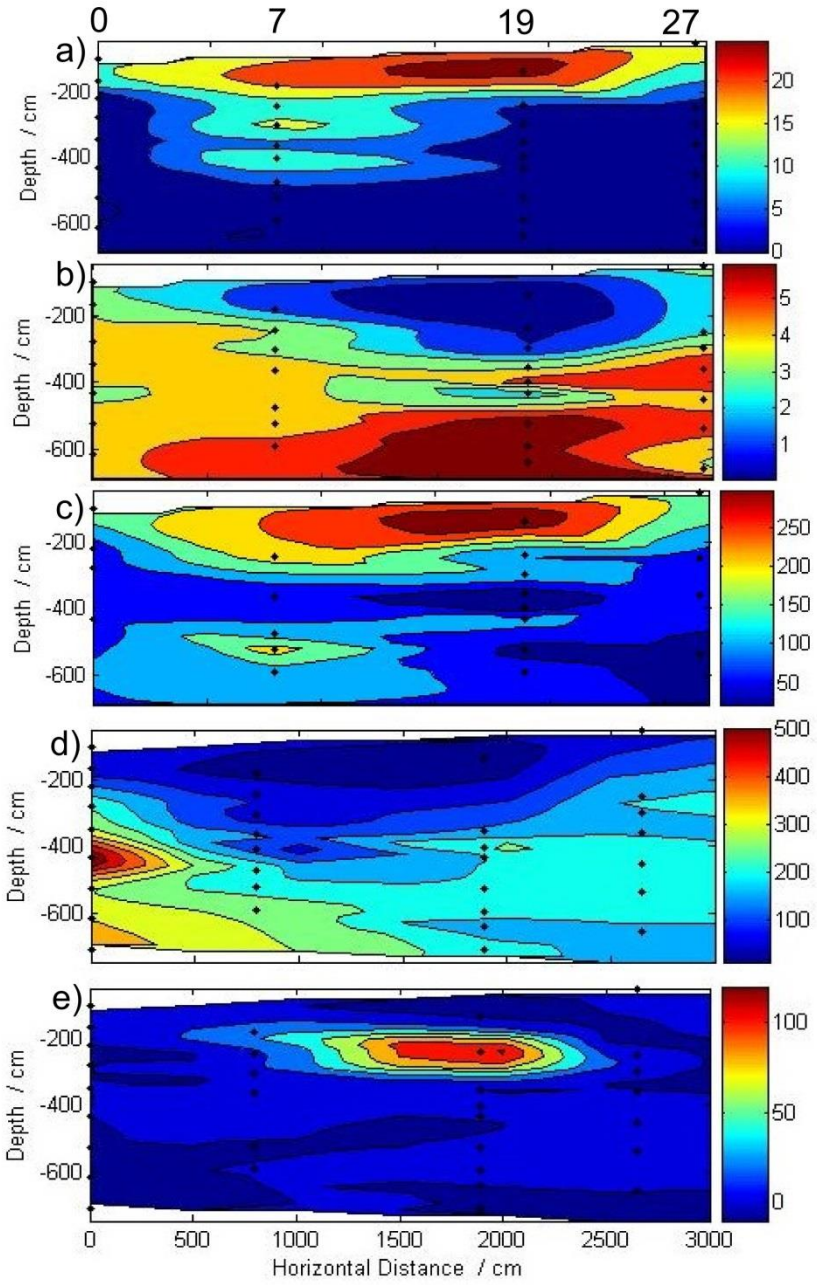

Figure 16 Porewater profiles of selected solutes for site 1- May. Five analyte profiles are shown; a) salinity (ppt), b) dissolved oxygen (mg L^{-1}), c) DOC (µmol L^{-1}), d) nitrate (µmol L^{-1}), e) $N_{2\ denitrification}$ (µmol L^{-1}). Scale bar shown for each individual analyte profile. Top numbers denote piezometer number and cross shore position, as calculated from mean high tide, in meters. Individual sample points (●) are shown for each piezometer well.

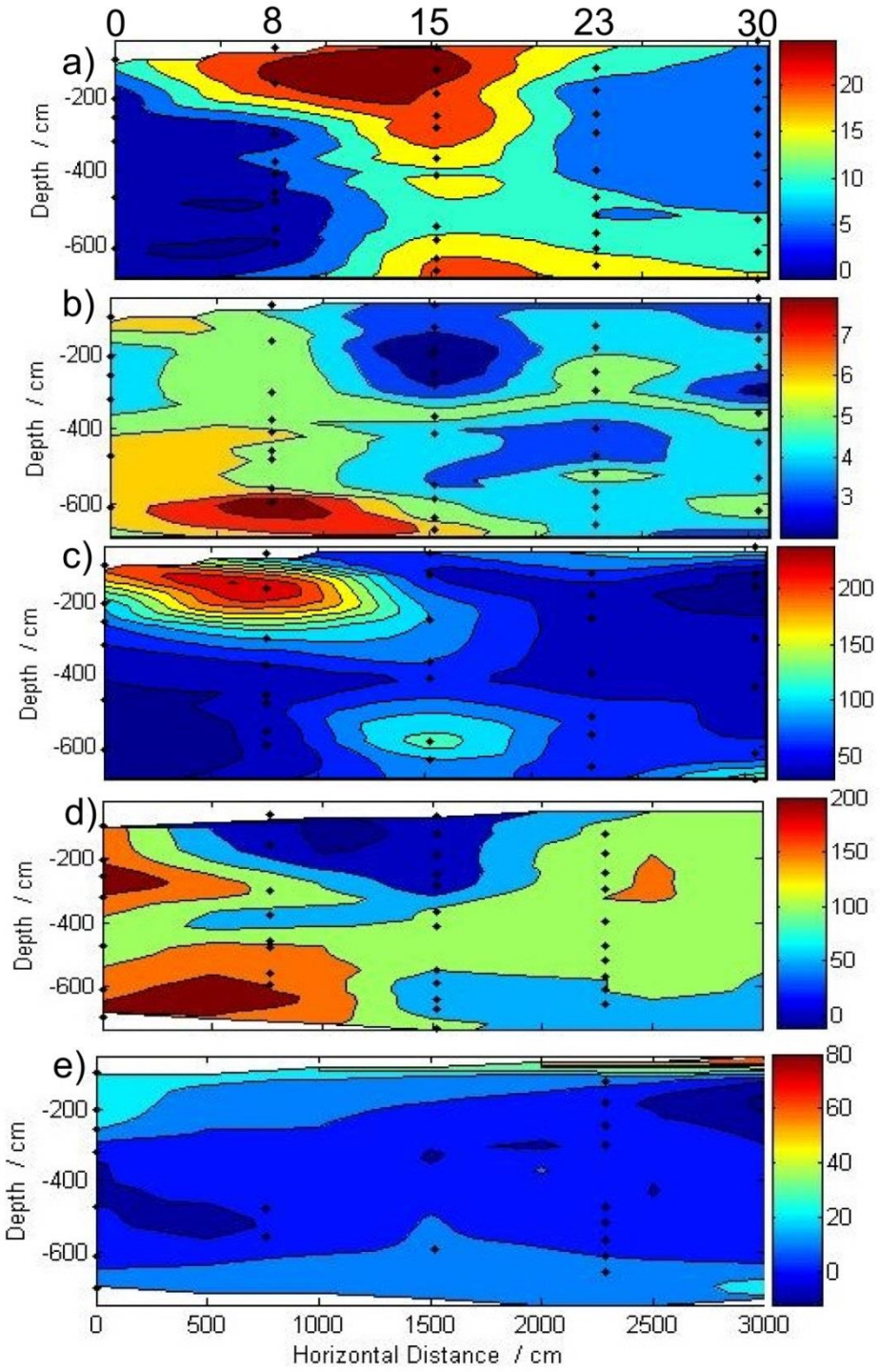

Figure 17 Porewater profiles of selected solutes for site 2- May. Five analyte profiles are shown; a) salinity (ppt), b) dissolved oxygen (mg L^{-1}), c) DOC (µmol L^{-1}), d) nitrate (µmol L^{-1}), e) N_2 $_{denitrification}$ (µmol L^{-1}). Scale bar shown for each individual analyte profile. Top numbers denote piezometer number and cross shore position, as calculated from mean high tide, in meters. Individual sample points (●) are shown for each piezometer well.

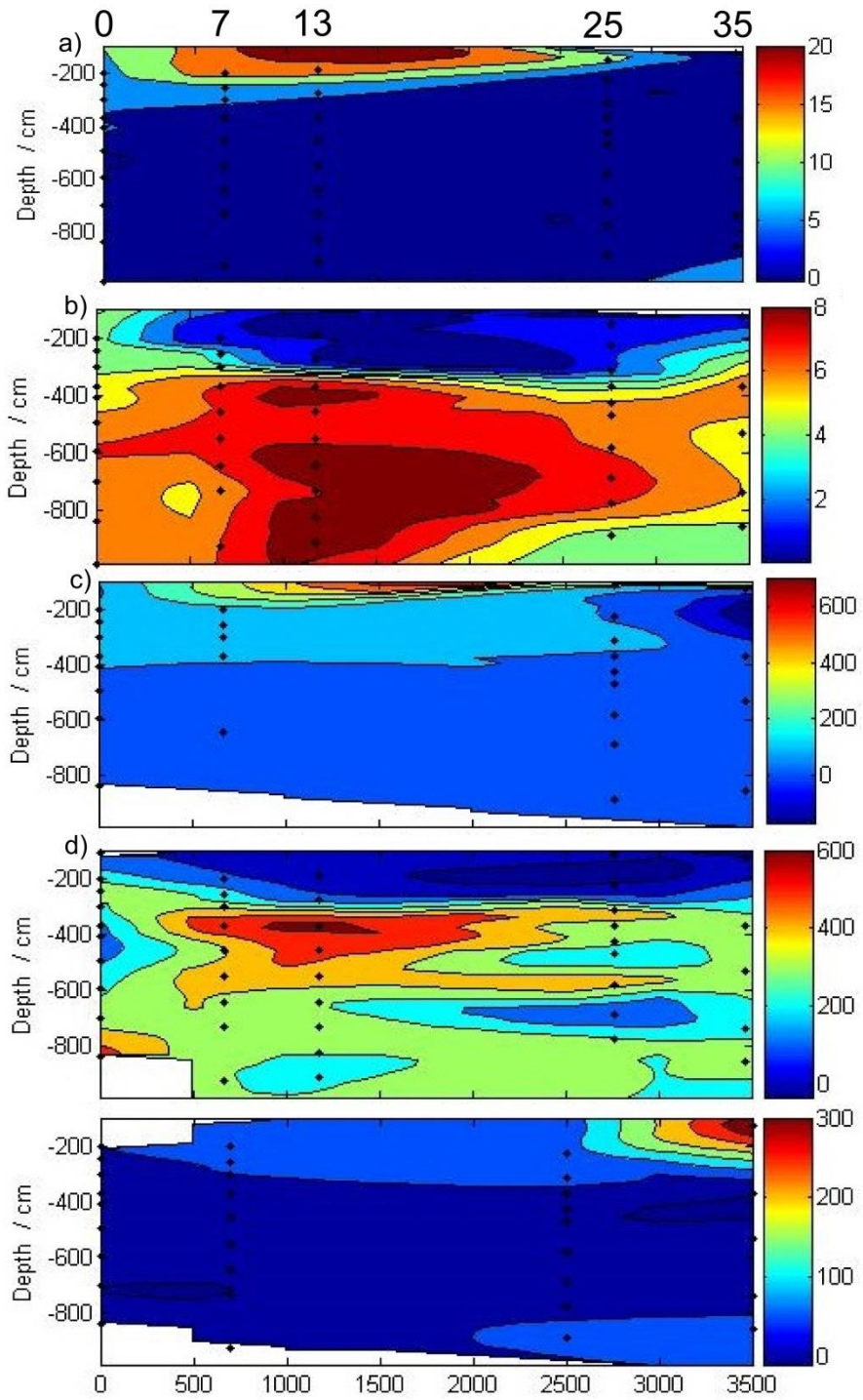

Figure 18 Porewater profiles of selected solutes for site 1- October. Five analyte profiles are shown; a) salinity (ppt), b) dissolved oxygen (mg L^{-1}), c) DOC (µmol L^{-1}), d) nitrate (µmol L^{-1}), e) $N_{2\ denitrification}$ (µmol L^{-1}). Scale bar shown for each individual analyte profile. Top numbers denote piezometer number and cross shore position, as calculated from mean high tide, in meters. Individual sample points (●) are shown for each piezometer well.

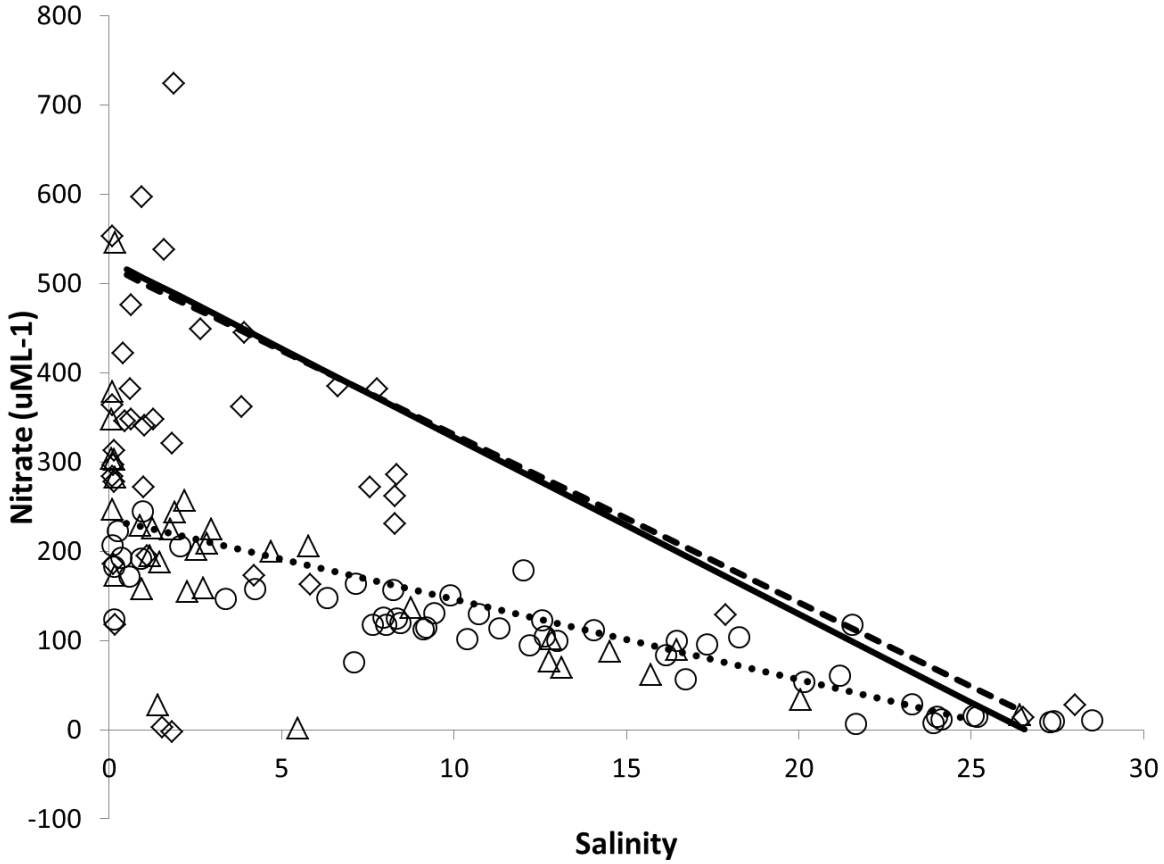

Figure 19 –Salinity vs nitrate mixing plot for three porewater sample transects. Samples from site 1 (P1 Δ and P3 ◊) and site 2 (P2 ○) are shown with theoretical mixing lines for each transect. Theoretical mixing lines for site 1 (─, --) and for site 2 (⋯) show that nitrate loss with increased salinity is not due solely to mixing with nitrate depleted seawater.

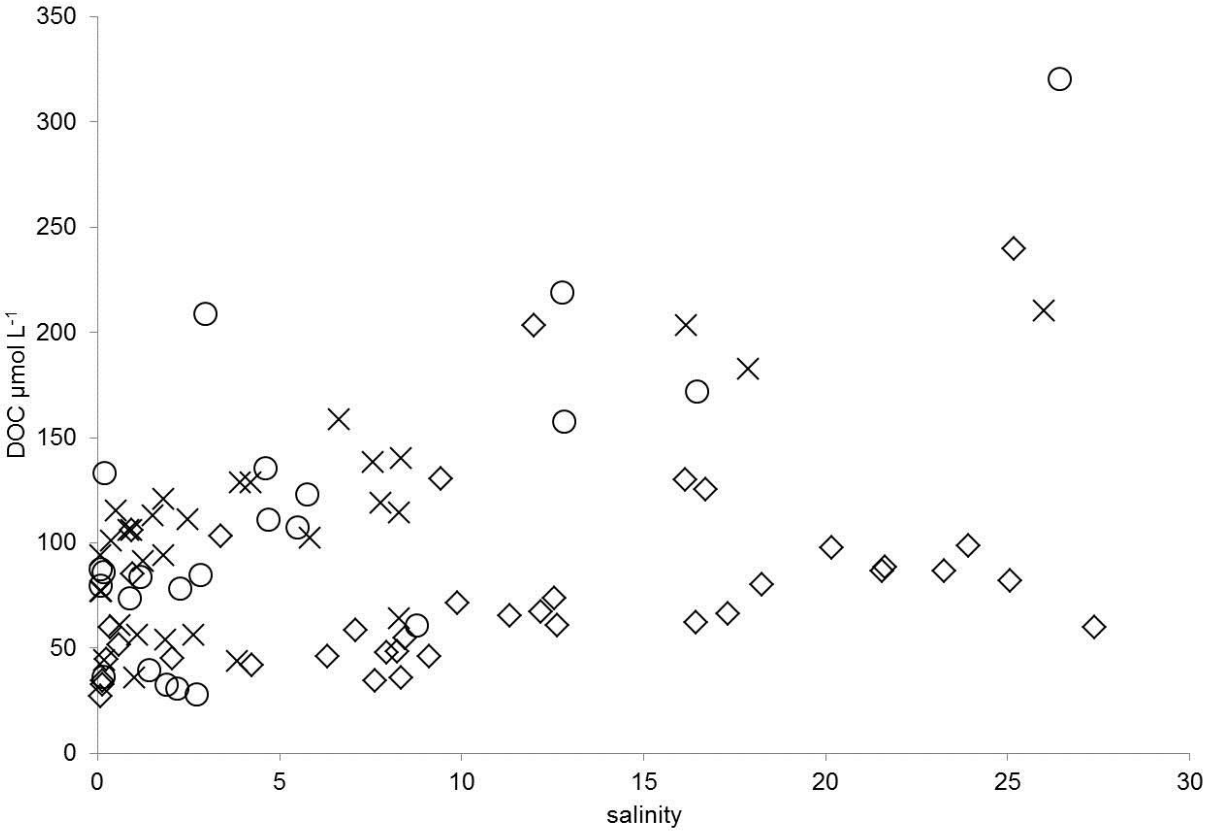

Figure 20 Salinity correlation with dissolved organic carbon (DOC) for all porewater samples. Samples from site 1 in May (○) and October (X) have linear correlations r^2 values of 0.61 and 0.58 respectively. Samples from site 2 taken in May (◊) have a lower linear correlation r^2 value of 0.21.

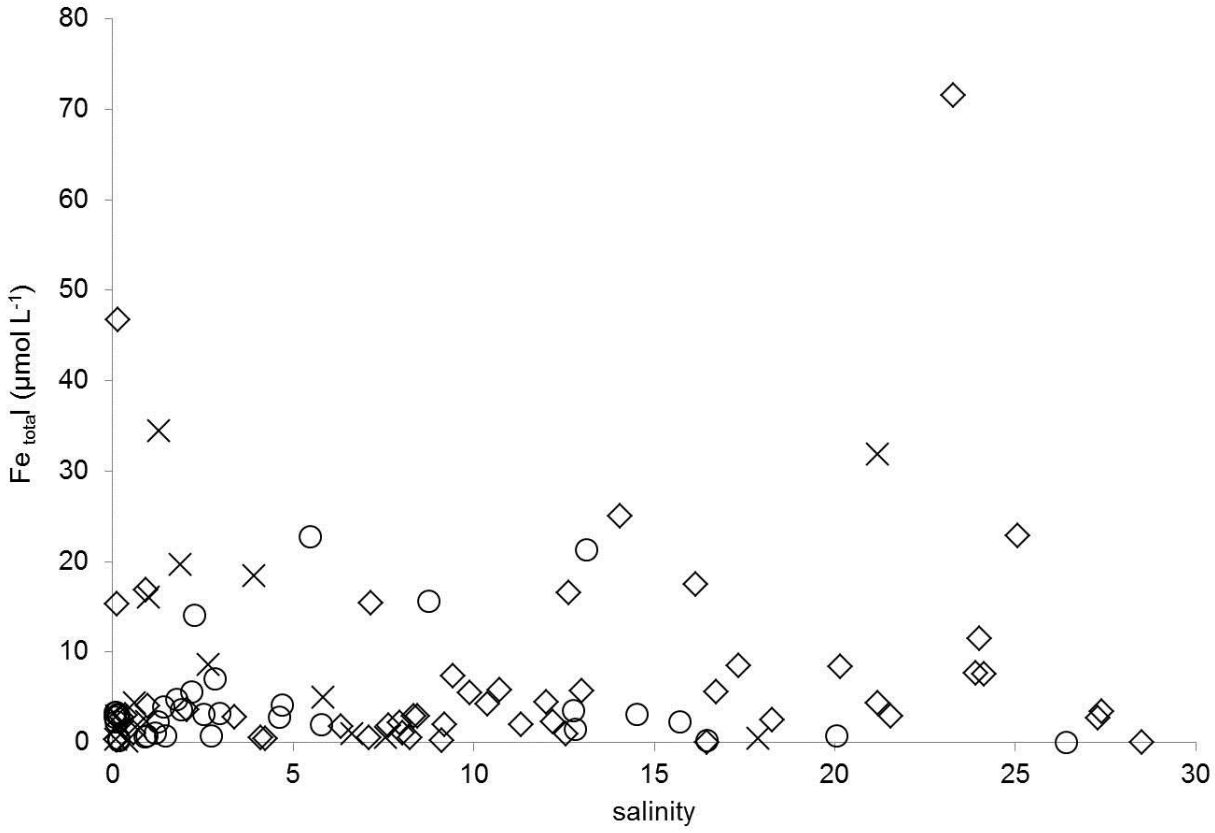

Figure 21 Salinity and Fe_{total} for all porewater samples. Samples from site 1 in May (○) and October (X) and site 2 in May (◊) do not show a correlation with salinity. Linear correlation r^2 values are below 0.1 for each of the three data sets.

Supplemental Data

Table S2 Depth, nitrate and $N_{2\ denitrification}$ concentrations for each piezometer porewater profile used to calculate denitrification flux shown in Table 4.

	Fresh Groundwater			Shallow Saline Zone		
Piezometer	depth (cm)	NO_3^- (µmol L^{-1})	$N_{2\ denitrification}$ (µmol L^{-1})	depth (cm)	NO_3^- (µmol L^{-1})	$N_{2\ denitrification}$ (µmol L^{-1})
P1-0	525	545	0	102	101	0
P1-7	474.98	206	0	183	34	33
P1-19	525.78	229	1	137	17	129
P1-27	538.48	243	4	53	89	5
P3-0	701.04	364	8	197	31	49
P3-7	548.64	322	21	196	25	62
P3-25	424.18	289	0	224	27	67
P3-35	365.76	263	4	122	3	237
P2-0	256.54	245	0	99	179	45
P2-23	297.18	163	13	122	123	16
P2-30	532.13	130	22	46	102	93

CHAPTER IV: NUTRIENT RELEASE FROM A GROUNDWATER FED TIDAL FLAT IN SETAUKET HARBOR, LONG ISLAND NY

Abstract

In this study we investigated geochemical transformations of nutrients during submarine groundwater discharge into an inlet of Setauket Harbor, NY. Porewater nutrient concentrations were used in two models; a standard estuarine model and a one-dimensional advection diffusion model to calculate nutrient flux to surface waters. Results from a standard estuarine model analysis show net consumption of nitrate (-40mmol m^{-2} d^{-1}) and ammonium (-2mmol m^{-2} d^{-1}) but a net production of dissolved organic carbon (60mmol m^{-2} d^{-1}). Individual porewater profiles were modeled using a one-dimensional advection diffusion model and show submarine groundwater discharge rates vary range from 1.7cm d^{-1} at harbor inlet banks to 7x 10^{-5}cm d^{-1} at the inlet center. Large differences in discharge rates are attributed to sediment heterogeneity between medium grain sand inlet banks and silty mud inlet center. These sediment differences affect both porewater flow rates and nutrient reaction rates during SGD transport from the fresh groundwater zone into the saline transition zone.

During SGD fresh groundwater mixes with saline water brought into sediments during tidal pumping which creates a biogeochemically active saline transition zone. One dimensional advection diffusion modeling was used to investigate mass transfer of nitrate and ammonium as fresh SGD enters the saline transition zone. Results indicate a net neutral flux of nitrate and ammonium in the harbor center, where discharge rates through silty mud are slow. Results of nitrate and ammonium discharge into the STZ at harbor banks is more dynamic, with uptake of nitrate and production of ammonium on the eastern shore, but uptake of ammonium and production of nitrate on the western shore. Possible nitrogen reaction mechanisms during SGD through sandy harbor banks include DNRA and ammonium remineralization.

Introduction

Submarine groundwater discharge (SGD) is recognized as a significant source of freshwater and dissolved solutes to the coastal zone(Burnett et al., 2003). In the nearshore area, fresh groundwater mixes with tidally pumped saline water and discharges to the surface through a variety of environments including sand beaches (Santos et al., 2009), tidal sand flats (Billerbeck et al., 2006), tidal mud flats (Hyun et al., 2009) and coastal marshes (Wang et al., 2011, Addy et al., 2005). The biogeochemical pathways regulating nutrient transport through each environment varies significantly, with sediment composition playing a dominant role in regulating whether nutrients are produced and released into overlying water or retained in the subsurface by sorption or microbial uptake (Deborde et al., 2008).

Investigations into the release of nutrients to surface water via SGD show that in coarse grain sediment dominated settings, such as beaches and tidal sand flats, nutrients behave non-conservatively. An investigation of SGD through a sand aquifer in northern Denmark found that nitrate rich groundwater travels through sand filled channels and discharges to coastal water, yet high nitrate surface water concentrations are observed only at high tide discharge points, and not found in low tide discharge zones (Andersen et al., 2007). In Cockburn Australia, a seasonal study of nitrate rich SGD traveling through a sand beach found nitrate reduction and phosphate release rates in excess of those expected from conservative mixing with seawater (Loveless and

Oldham, 2010). In both cases, nitrate reduction occurred despite low DOC concentrations, which are typically thought to drive microbially mediated denitrification (Groffman et al., 2006).

In fine grain sediments typical of shallow marine settings zones molecular diffusion and bioturbation control linear velocity flux of porewater to surface water. Electron donors in shallow sediments originate from a combination of microphytobenthos decomposition and infiltration of particulate organic matter. Top down inputs of electron donors creates a predictable pattern of redox conditions, where peak concentrations of sequentially lower energy yield electron acceptors produced at increasing depth beneath sediment water interface (Jørgensen, 2006). Fresh groundwater inputs to these mud sediments perturb typical redox patterns by altering dissolved oxygen and pH gradients. In addition, tidally dominated systems experience increased porewater linear velocity as tide ebb sets up hydraulic head gradient which generates a surficial drainage network of solute rich porewater (Billerbeck et al., 2006). A study of muddy tidal flats of the Yellow Sea, Hampyeong Bay, found that SGD contributed 50-70% of nutrient fluxes to the bay, with carbon exports fueling benthic and water column primary productivity. Further, a study of nutrient dynamics in a tidal marsh of the Yangtze estuary found tidal driven flux between nitrate rich overlying water and ammonium rich resulted in a net reduction of nitrogen to receiving coastal waters (Wang et al., 2011). The wide variance of nutrient uptake and release rates are further complicated by the presence of tidal marshes, which are dominated by macrophyte plants that can increase sediment permeability (Davis et al., 2004, Hyun et al., 2009). Increased permeability around macrophyte plant root zones traps fine, nutrient rich sediments and increases depth of oxygen penetration in mud. These effects alter biogeochemical cycling by altering the release rates of organic carbon and early diagenesis products (Riedel et al., 2011).

Even at small spatial scales, many tidal coastal environments are comprised of a mixture of both sand and mud sediments. In tidal flats and marshes mud layers overly permeable sand aquifers, which leads to a mixture of flow regimes(Xin et al., 2012). It has been shown that during tidal flood surface water infiltrates both sand and mud sediments and mixes with fresh groundwater generating a solute matrix that is highly variable, with rapid nutrient exchange occurring in sandy or marsh dominated sediments and slow exchange in mud sediments. During tidal ebb, receding water carries a mixture of nutrients sourced from fresh groundwater, recycled seawater and diagenesis. Modeling studies have shown pore water flow associated with different types of sediment/marsh settings can vary over orders of magnitude (Xin et al., 2012). How this effects porewater nutrient fluxes in each sediment setting is not well understood.

In recent studies of Long Island Sound embayments we investigated nutrient flux to surface water during SGD. We found 23% of nitrogen loss was due to denitrification as water discharges through sand at low tide, but 56% denitrification of groundwater sourced nitrate as water discharges through a mud cap in the sub-tidal zone. Due to this large variance in nitrogen loss rates we hypothesized that embayments comprised of two or more sediment regimes will exhibit differences in nitrogen attenuation modes over short spatial scales. In these embayments freshwater layer extends horizontally tens of kilometers below mean low tide. Despite being capped by mud layers that decrease SGD rates an order of magnitude, the aerial size of mud capped discharge zones is large, when compared to the aerial extent of the sand discharge zone, leading to a higher than expected overall denitrification.

In this study we investigate how groundwater sourced nitrate is processed as it enters an inlet of Setauket Harbor, NY, an embayment of Long Island Sound. Setauket Harbor experiences 2m tidal variation; therefore the inlet study site is flushed twice daily as it is completely drained during low tide. Our objective was to determine how nitrogen, phosphate and carbon flux rates vary in a system comprised of both sand and mud sediments. We employ two modeling techniques; the standard estuarine model and a one dimensional advective diffusion model to calculate flow in a system with large tidal variation. Our work demonstrates that nitrogen attenuation rates and processes exhibit substantial variation between both sand and mud sediments. Calculated nitrogen flux from inlet banks suggests a combination of DNRA and ammonium assimilation controls the amount of nitrogen discharged in advective regimes. Unexpectedly, we find large difference in carbon flux to the surface between permanently submerged tidal drainage channel and exposed margins of the channel, despite similar sediment composition between these two locations.

Methods

Study Site

Setauket harbor, along with Conscience Bay and Little Bay, are located on the northwest portion of Port Jefferson Harbor, with direct connection to Long Island Sound. Setauket Harbor is connected to Port Jefferson Harbor via a 0.22km opening, which is in turn connected to Long Island Sound by a 0.4km embayment mouth. Setauket Harbor is a tidally dominated environment, with average daily tidal range of 2.1meters. Average water depth is less than one meter and harbor inlets are completely drained at low tide. Harbor bottom sediments are poorly sorted, with the percentage of fine particles increasing away from shore. Modal particle size in the main channel is 125-250μm, with 2% silt-clay (Forbes and Lopez, 1990).

Setauket Harbor rests on the Upper Glacial aquifer, which is comprised of poorly sorted medium to fine grained sand. Groundwater is typically >50% oxygen saturation with solid phase carbon less than 5% (Bohlke et al., 2009). Bohlke et al., (2009) used CFCs, SF_6 and ^3H-^3He to determine groundwater age on the North Fork of Long Island and found groundwater ages ranging 1-39 years, with a trend of increased age with increasing depth. This same study also determined a mean recharge rate of 0.5±0.5m $year^{-1}$ corresponding to ~44% of annual precipitation for this coastal setting (Bohlke et al., 2009).

No rivers or streams discharge to Setauket Harbor, therefore the primary sources of freshwater to the harbor are rainfall and SGD. Mean annual precipitation on Long Island is 1268mm (years 1981-2010, NOAA), with consistent input through both warm and cold seasons (Zhou, 2008). Average surface water salinity during the time of sampling was 24.7(n=7), slightly lower than salinity of 25.1-26.9 recorded during May in Smithtown Bay, located on the adjacent south shore of Long Island Sound (Bauer, 2012).

Together, Setauket Harbor, Conscience Bay and Little Bay comprise one of the largest tidal mudflats on the north shore of Long Island. Collectively these harbors span ~560acres of mud flats, sand flats, salt marshes and shallow open water. Of the three areas, Setauket Harbor has undergone the most human impact via residential building and mooring for recreational boats, despite low density (<1 dwelling/ac) housing in the harbor vicinity. Limited documentation exists for this area, but a coastal fish and wildlife habitat assessment form completed by the NYS Department of State Habitat Unit finds these tidal mud flats contain

northern gamma grass (Trypsacum dactyloides),which is threatened in New York State. In addition, Setauket Harbor and environs host a variety of shellfish species, is a feeding area for gulls, terns, and black ducks as well as providing critical habitat for juvenile Atlantic Ridley sea turtles in the late summer and fall (Riexinger, 2005).

Porewater Sampling and analysis

Sampling took place in early to mid-April 2012, during falling to low tide. The area selected for sampling is on the south east shore of Setauket Harbor, along a lobe of the harbor, hereafter referred to as the inlet. Porewater was collected using AMS Retract-A-Tip piezometer system (Charette and Allen, 2006). The piezometer system consists of a drive point well with a 5.6cm screen connected to a length of acid cleaned fluoropolymer tubing that is driven to discreet sampling depths. We allowed porewater redox conditions to dictate the frequency of sampling, therefore distance between sampling depths ranges 50-150cm in sand sediments. The AMS system is suitable for sandy sediments but is incapable of sampling in silt-mud sediments. For well locations B, C and D (Figure 22) we employed a porewater sampling system that consists of a PVC pipe with a fiberglass tip that is manually pushed into the muddy sediments. Porous plastic cylinders act as ports along the PVC pipe, placed at ~2-4cm intervals in the top 30cm of the pipe and at ~5-10cm in the lower 30cm of the pipe (Beck, 2007). Each port is internally attached to an acid cleaned polymer tube that exits the PVC pipe at the top of the apparatus. Samples are collected by attaching a acid cleaned 60ml syringe to the end of the port, creating a vacuum that is filled by porewater from the desired depth. Samplers were emplaced in the sediment and allowed to equilibrate for 2 hours before purging. The initial syringe volume is discarded and the sampler was allowed a further 2 hours for equilibration prior to sample collection.

Temperature, pH, salinity, ORP and dissolved oxygen data were collected for each sampling depth using a hand held YSI 556 probe with a flow through cell for samples collected using the AMS Retract-a-Tip system. For samples collected using the PVC sampling device, sample volume was insufficient for flow through cell usage, therefore a subsample was collected for dissolved oxygen analysis by Winkler titration, and the remaining parameters were analyzed by YSI 556. Dissolved organic carbon samples (DOC) and total dissolved nitrogen (TDN) samples were filtered (0.45µM), collected in acid rinsed combusted bottles, acidified with HCl (Fisher Scientific) to pH 2 and at 4^{0}C and analyzed within 2 weeks of collection. Samples for Fe and Mn were filtered through 0.2 µM capsule filters, acidified with Trace Metal Grade HCl (Fisher) to a pH<2 and frozen. Samples for NO_3^-, NO_2^- and NH_4^+ were filtered through 0.45µM filters (Whatman GF/B) and frozen within 8 hours of collection. Samples for dissolved inorganic phosphate (DIP) were collected separately by filtering and acidification with 50µl 8M H_2SO_4 to prevent precipitation of PO_4^{-2} due to changing oxygen conditions. All nutrient samples were field cooled and frozen within 8 hours of collection.

Sediment samples were collected from the inlet margins and center using acid rinsed 15cm PVC pipes. PVC pipes were inserted into the sediment at low tide, the surrounding material was removed with a trowel and the filled core was collected. Core ends were sealed with parafilm then the core was placed on ice and frozen upon return to the lab. Porosity was determined using the volumetric method. Grain size distribution was measured by laser diffractometer (Malvern Mastersizer 2000).

Nitrate ($NO_3^-+NO_2^-$) was analyzed on a Lachat Instruments FIA-6000, ammonium (NH_4^+), phosphate (PO_4^{-3}), iron (Fe_{total}), manganese (Mn^{2+}) were analyzed spectrophotometrically (Solorzano, 1969, Johnson and Petty, 1982, Stookey, 1970). Relative uncertainty of repeated sample runs (n=3) is 5% or less. Dissolved organic carbon was analyzed by Shimadzu TOC analyzer (TOC-V CPH/CPN); precision is the standard deviation of three replicate injections of an intermediate standard, with a percent coefficient of the mean of ± 5% for any run.

Results

Three areas of the harbor are described below, each representing a different sediment and/or tidal inundation regime. Inlet banks refer to porewater profiles A and E (Figure 22), which are on the shoreline edges of Setauket Harbor. Inlet banks are tidally submerged only during high tide stage, typically for 1.5-2.0 hours per tidal cycle. Porewater profiles taken from inlet banks are located 1.2m and 1.4m above the main harbor floor, respectively, and are covered with stands of *S.Alternaflora* sea grass. Inlet margins refer to porewater profiles B and D, located on the harbor floor. Inlet margins are submerged during rising, high and ebb tide but are exposed for approximately 3-4 hours per tidal cycle, during low tide. These areas are characterized by highly bioturbated silty-mud sediments overlying medium to fine grained sand. Finally, the inlet center refers to porewater profile C, which is continuously submerged throughout the tidal cycle. This area is characterized by mud sediments overlying medium to fine grained sand.

Chloride, dissolved oxygen and nutrient distribution patterns

Porewater chloride concentrations ranged from 0.8mmol L^{-1} to 380mmol L^{-1} during the survey. Maximum chloride concentrations were recorded in the shallow porewater sampled from wells located at the inlet banks (A and C, Figure 22). In contrast porewater taken from the inlet margin (B and D, Figure 22) and center (C, Figure 22) contains a high fraction of freshwater in the entire sediment column, as evidenced by transitional chloride values ranging of 81mmol L^{-1} to 183mmol L^{-1} at depths less than 50cm beneath sediment floor (bsf). Porewater from the inlet margin and center is entirely fresh starting at depth of 50cmbsf, with the exception of a single point located 600cmbsf. This is possibly due to sediment heterogeneity at this depth, as the upper glacial aquifer is known to contain localized clay/silt lenses and this layer is not observed in the other four piezometer wells taken during this survey.

Dissolved oxygen concentrations range from 6 to 342µmol L^{-1} (1.6 to 75.3% oxygen saturation). In each porewater profile oxygen minimums are observed in the upper 300cmbsf (Figure 24) with highest values observed at depths greater than 300cmbsf. At inlet banks porewater from depths 0 to 30cm are hypoxic and oxygen concentration decreases to anoxic levels (<12% saturation) from 100-250cmbsf before slowly increasing with depth in the underlying aquifer. In the inlet margin and center dissolved oxygen concentrations are less than 130µmol L^{-1} (34% saturation) at depths less than 50cmbsf and rise to 220µmol L^{-1} (57% saturation) or greater at a depth of 100cm-bsf.

Nitrate concentrations range from below detection limit (<0.01 µmol L^{-1}) to 640µmol L^{-1} with highest concentrations usually observed at the base of the transition zone from salt to freshwater (Figure 25). In all porewater profiles nitrate concentration minima is found in the top 60cm-bsf. Average nitrate concentration in porewater in the freshwater zone is 260±90µmol L^{-1}.

Ammonium concentrations range from below detection limit (<0.1 µmol L^{-1}) to 230µmol L^{-1} with highest concentrations observed in shallow porewater samples at depths less than 100cmbsf (Figure 26). While ammonium concentrations generally decrease with increasing depth below sea floor, zones of ammonium ranging 30-65µmol L^{-1} are observed centered 400-500cmbsf in the inlet margin and center porewater profiles. Co-occurrence of ammonium and nitrate is found in 54% of samples, particularly in porewater from inlet banks, where we observe areas that contain near equal amounts of both ammonium (34µmol L^{-1}) and nitrate (35µmol L^{-1}). Phosphate concentrations range from below detection limit to 25µmol L^{-1} and display patterns similar to ammonium concentrations. In all profiles phosphate maxima is observed in the top 50cmbsf, with the exception of the inlet center which contains maximum phosphate at a depth of 500cmbsf (Figure 27).

Iron (Fe^{2+}) concentrations are low throughout the study area, ranging 3to 23µmol L^{-1}, but are not clearly correlated with depth or salinity (Figure 28). Iron concentrations are greatest at depths less than 60cmbsf,but zones of higher iron concentrations are observed at depths of 400-500cmbsf in eastern shore piezometers, coinciding with areas of high ammonia, yet not with areas of significant dissolved oxygen depletion (D.O average 5mg L^{-1}). Dissolved organic carbon (DOC) concentrations range from 9 to 640µmol L^{-1} for the study period (Figure 29). In porewater with salinity <5 DOC ranges 9µmol L^{-1} to 110µmol L^{-1}, indicating that fresh porewater is not the source of DOC in the Harbor. Maximum DOC concentrations are recorded in the salinity values greater than 15, particularly in porewater in the eastern inlet bank. A comparison of porewater DOC and iron concentrations did not find any correlation between these two electron donors (Figure 30)

Standard estuarine model

Tidal mud flats are similar to subterranean estuary systems as they can control the flux of nutrients to overlying water during SGD (Kim et al., 2012). Nutrients that originate in fresh groundwater may be removed by biological consumption or particle adsorption, and conversely nutrients in the tidally influenced shallow zone may be remineralized or released from particles. In studies of surface and subterranean estuaries, salinity was used to determine if there is a net gain or loss of nutrients during mixing of saltwater and groundwater (Santos et al., 2009, Kaul and Froelich, 1984). This analysis assumes constant endmember salinity and nutrient concentrations. At the Setauket Harbor site we take the average freshwater (salinity < 1ppt) concentration as the groundwater end member and the average saltwater (salinity> 21ppt) as the saline end member. Using salinity-nutrient mixing plots (Figure 31) we model the overall biogeochemical reaction rates (*R*) by:

$$R = \frac{1}{t}\int_{S=0}^{S=26}(N_r - N_c)dS \qquad (1)$$

Where t is the residence time of the mixing zone, S is salinity, N_r is the equation that best describes the salinity-nutrient mixing relationship, and N_c is the equation for conservative mixing between salinity and the given nutrient. N_r was determined using salinity nutrient mixing plots (Figure 31), and N_c was calculated using standard mixing curve methods (Langmuir et al., 1978) Positive R indicates production of the nutrient during SGD (i.e. release of nutrient to overlying water) while negative R indicates consumption or sorption of the nutrient during SGD. We cannot determine mechanisms of nutrient production or consumption using this method. Further

we cannot discriminate between reactions that occur in the inlet banks or the inlet center using this analysis, as salinity-nutrient data is lumped together in order to have sufficient data for entire salinity spectrum. Residence time, t, is 14 days, representing an integration of data over one spring-neap tidal cycle. As shown in Chapter 2, we do not observe significant variation in porewater chloride (salinity) profiles over a spring-neap period in Stony Brook Harbor. We do not use the shorter porewater residence time calculated for Stony Brook Harbor as in Setauket Harbor SGD rates in the center of the harbor are orders of magnitude lower than those along the banks. Finally, the choice of 14 days is on par with residence time estimates from subterranean estuary studies in Florida, which range from 18-20 days. (Santos et al., 2008a)

Standard estuarine model results are summarized in Table 7. The tidal mud flat was a net consumer of nitrate, ammonium, and phosphate. Nitrate consumption rates were highest of all nutrient fluxes, with an average consumption rate of -40mmol m^{-2} d^{-1}, followed by ammonium consumption of -2mmol m^{-2} d^{-1}. Phosphate behavior is unclear due to large uncertainty in model standard error (Table 7). DOC is the only nutrient that is consistently released during SGD, with an average rate of 60mmol m^{-2} d^{-1}.

It is known that coastal marshes import nutrients and export organic carbon (Dacey and Howes, 1984). Numerical simulations of pore water flow in tidal marshes demonstrate an order of magnitude difference in porewater velocity between marsh edges and receiving tidal creeks (Xin et al., 2011). This is attributed to heterogeneity in hydraulic conductivity between sandy loam sediments found at marsh banks and slit loam (mud) found in tidal creeks (Xin et al., 2012). Use of the standard estuarine model, shown above, does not allow for calculation of nutrient fluxes from different porewater velocity regimes. Using the standard estuarine model, we determined that Setauket Harbor acts as a coastal marsh, indicating porewater velocity varies between inlet banks and inlet center. Therefore we employ a one dimensional advection-diffusion model to elucidate the connection between porewater velocity and nutrient flux in Setauket Harbor.

One dimensional advection-diffusion model

To determine nutrient fluxes into Setauket Harbor, porewater velocities are calculated at each of the five piezometer sampling locations. Due to entire tidal flushing at this site we are unable to use traditional methods of porewater sampling such as manual or automatic seepage meters, which require the seepage meter to remain completely submerged throughout the measurement period (Lee, 1977, Paulsen et al., 2001). Each piezometer well location was sampled from shallow to deep, starting at high tide and ending within 2 hours of low tide, ensuring that each well was sampled during the same tidal window. Cl^- concentration profiles were used to determine porewater velocity using a modification of the method outlined by Martin et al., 2007. Porewater velocity (v) from each piezometer well was then used to calculate nutrient flux during fresh groundwater transport to the saline transition zone for each of the five piezometer locations.

The velocity of porewater movement is governed by upward movement of freshwater at the lower boundary and downward diffusion/advection of saltwater on the upper boundary. The stead state advection-diffusion reaction model of the form

$$0 = \frac{\partial}{\partial z}\left(D_s \frac{\partial^2 C}{\partial z^2}\right) - v\frac{\partial C}{\partial z} + \sum R \qquad (2)$$

Where C is the concentration of the analyte in porewater, t is time, z is depth beneath the sediment water interface, v is freshwater velocity and D_s is the sediment dispersion coefficient, and ∑R is the sum of all reactions that can change the analyte concentration.

An analytical solution to the equation was determined by choosing constant concentration boundary conditions for each piezometer well. The upper boundary (C_u) for Cl^- profiles was chosen as the sediment water interface. For nutrient profiles the C_u was taken as top of the upward curve of the profile, which ranged from 0-20cm beneath the sediment water interface. The lower boundary (C_L) was chosen as the depth where the profile asymptotically reached a constant concentration or at the lower boundary of the saltwater transition zone (Martin, et al., 2007). Using these boundary conditions the analytical solution is

$$C(z) = \frac{1}{1-exp\left(\frac{v}{D_s}L\right)}\left\{C_L\left[1 - exp\left(\frac{v}{D_s}z\right)\right] + C_U\left[exp\left(\frac{v}{D_s}z\right) - exp\left(\frac{v}{D_s}L\right)\right]\right\} \qquad (3)$$

Where C_L is the lower boundary, C_u is the upper boundary, C_z is the porewater concentration at depth z, z is the depth beneath sediment water interface, D_s is the diffusion coefficient and v is the linear velocity. For Cl^- profiles ∑R=0, as chloride is conservative. The $\frac{D_s}{v}$ value for each of the five porewater profiles was calculated by fitting the solute concentration profiles and best fit determined by minimizing the squared residuals between measured and modeled concentrations. The resulting $\frac{D_s}{v}$ was then used to determine v by applying dispersion coefficients appropriate for the two different sediment types that comprise the harbor.

In the center of the harbor sediments are comprised of medium to fine grained sand sediments of the Upper Glacial Aquifer with a capping layer of mud (silt loam) that ranges from 0.6 to 1.2m thick. Core samples of the top 10cm of sediment below the sediment-water interface were collected to determine porosity of sediments at inlet center (n=3) and inlet margin (n=6) profile locations. Results from this analysis yield a porosity ranging 0.57 for center and margin porewater profiles. In addition, porosity was assumed to be constant over C_U to C_L interval. Assuming infinite dilution and 25^0C, molecular diffusion coefficient (D_m) is estimated at $20.3x10^{-6}cm^2/s$ (Li and Gregory, 1974). Using a porosity of 0.57 in the center of the harbor inlet, the bulk diffusion coefficient is calculated using the method outlined by (Boudreau, 1996);

$$\theta^2 = 1 - \ln(\varphi^2) \qquad (4)$$

$$D_s = \frac{D_m}{\theta} \qquad (5)$$

where θ is tortuosity, ϕ is porosity and D_m is molecular diffusion as described above . For the central portion of the harbor D_s is calculated at $9.56x10^{-6}cm^2\ s^{-1}$.

Rapaglia and Bokuniewicz (2009) used a salt balance model to determine dispersion coefficients for sand sediments on Long Island and found values range $0.4m^2d^{-1}$ to $0.8m^2d^{-1}$

((Rapaglia and Bokuniewicz, 2009). In Setauket Harbor the dispersion coefficient for sand sediments located in porewater profiles A and E was taken as the minimum value of this range for Long Island SGD through sands, $0.4 m^2 d^{-1}$. Velocity was determined by combining the modeled $\frac{D_s}{v}$ and the $D_s$values for the two respective sediment settings, results of this analysis shown in Table 8

The calculated SGD rates, i.e porewater velocity *v*, ranges 0.1 to 2cm d^{-1} from sand banks and 8.0×10^{-4} to 8.0×10^{-7} cm d^{-1} from the center of the harbor. The large range in SGD rate at this site can be attributed to two factors; 1) differences in composition of the permeable sediments between the banks and center of the harbor and 2) negligible hydraulic head in the center of the harbor, even at low tide. These results imply an unaccounted for residual horizontal advection component in these sediments. Horizontal advection rates are usually much higher than vertical advection rates, and are estimated to be 40:1 in sand sediments of Long Island's Upper Glacial aquifer. Therefore it is possible that SGD rates from harbor banks, porewater profile locations A and E, underestimates. In fact, during sampling at this site we observed draining of porewater from these zones during ebb and low tide.

Velocity results obtained from equations 2-3 were used in conjunction with nutrient profiles to determine the nutrient flux during porewater movement from the fresh groundwater zone into the saline transition zone. In this analysis, equations were fit to nitrate, ammonium and DOC porewater profile concentrations with the lower boundary set to the minimum chloride concentration (C_L from above) and the upper boundary equal to the sediment water interface (C_U from above). By rearranging equation 3, the solution a depth dependent reaction rate is;

$$R = v\frac{\partial C}{\partial z} - \left(D_s \frac{\partial^2 C}{\partial z^2}\right) \qquad (6)$$

The porewater profiles were described by a second order polynomial in the form $c = Az^2 + Bz + D$ (Table 9). Then uing equation 6 we obtain a solution for R that describes the flux of nutrients during transport into the saline transition zone of the harbor as a function of depth.

$$R(z) = v(2Az + B) - D_s(2A) \qquad (7)$$

Results from this analysis are shown in Table 10.

One dimensional advection-diffusion modeled nutrient production

A modeled sum of the reactions ($\sum$R) determines if the nutrient is consumed (-R) or produced (+R) during porewater movement. Results from nitrate modeling indicate the highest area of nitrate consumption is on the western shore of the harbor, with a consumption rate of -11mmol $m^{-1}d^{-1}$. Nitrate is released to the overlying water in the center and eastern edge of the harbor at rates ranging 0.01mmol $m^{-1}d^{-1}$to 0.4mmol $m^{-1}d^{-1}$, respectively.

Ammonium forms during SGD at the western inlet bank, 3.4mmol $m^{-2}d^{-1}$ but is consumed on the eastern bank, at a rate of -1.2mmol $m^{-2}d^{-1}$. Ammonium is also consumed in the center of the harbor at the base of the STZ, although very slow SGD rates in mud produce low ammonium consumption rates ranging -1.6×10^{-2}mmol $m^{-2}d^{-1}$ to -8×10^{-5}mmol $m^{-2}d^{-1}$. DOC was produced in porewater in harbor banks during SGD, with values ranging 3.2mmol $m^{-1}d^{-1}$ to

13.4mmol $m^{-1}d^{-1}$. As with nitrate and ammonium concentrations, the center of the harbor exhibits reaction rates near zero, ranging $-4.3x10^{-3}$mmol $m^{-2}d^{-1}$ to 0.9mmol $m^{-2}d^{-1}$.

Discussion

Previous work modeling nutrient behavior during SGD into a tidal sand flat in the Yellow Sea indicates net production of silicate, phosphate and ammonium (Waska and Kim, 2011). Other work in subterranean estuaries in Cape Cod, MA and Indian River Lagoon, FL consistently find that nutrient processing in subterranean estuaries results in a net positive flux of nitrate and dissolved organic nitrogen to surface waters (Santos et al., 2009, Kroeger and Charette, 2008). In Setauket Harbor, DOC is the only nutrient whose production rates are similar to those calculated for subterranean estuary settings, as it is comparable to summer DOC discharge rates in the Indian River Lagoon, FL (Roy et al., 2013). The standard estuarine model and one dimensional advection-diffusion modeling indicate that nitrate is primarily consumed in the saline transition zone of the STE. The STE at Setauket harbor acts less like a traditional subterranean estuary and displays nutrient uptake patterns similar to coastal marshes or tidal flats.

Mechanism for variation in nitrogen fluxes

Application of the standard estuarine model at the harbor inlet level indicates that nitrate is consumed during discharge at this site with a net consumption of -40mmol $m^{-2}d^{-1}$. Nitrate concentration increases with depth in all five porewater profiles, indicating that nitrate is sourced from fresh groundwater upwelling, as typically seen in subterranean estuary settings (Kroeger and Charette, 2008, Santos et al., 2008a, Howarth, 2008, Knee et al., 2010). Despite this, distinct local patterns of nitrate consumption and production are visible when applying a one-dimensional advective diffusion model. This model shows active nitrate loss occurs during porewater movement in western inlet bank of the harbor while on the eastern edge and center nitrate forms at the base of the saline transition zone.

In the harbor inlet banks, where the upper sediments consist of unconsolidated sands covered with marsh vegetation, three dissolved oxygen zones exist that drive nitrogen cycling. At depths greater than 400cmbsf dissolved oxygen is greater than 90µmol L^{-1} and nitrate concentrations are greater than 120µmol L^{-1}. In this zone nitrogen is sourced fresh groundwater, as evidenced by lack of ammonium in samples at depth. In the saline transition zone (STZ), which exists from 90 to 230cmbsf, upwelling groundwater mixes with saline overlying water which produces an area of rapidly changing redox conditions. Nitrogen in the STZ exists as both ammonium and nitrate, with a pattern of increasing nitrate and decreasing ammonium with increased depth beneath the sediment water interface. Given these conditions either dissimilatory nitrate reduction to ammonium (DNRA) or anaerobic denitrification are the most likely microbially mediated nitrate reduction processes. Fermentative DNRA is driven by DOC in low nitrate concentration systems (Burgin and Hamilton, 2007), while denitrification can occur under low carbon conditions (Kelso et al., 1997). In harbor inlet banks, DOC concentrations decrease with increasing depth beneath the sediment water interface, and exceed 200µmol L^{-1}, in the shallowest porewater samples. Denitrification may be responsible for initial loss of nitrate at the base of the STZ, where ammonium levels are low, but denitrification coupled with ammonium release from sediment is a possible mechanism for nitrate loss and

ammonium production in the shallow portion of the STZ. Without excess N_2 information it is not possible to determine which process controls nitrate transformations. Finally, the saline zone exists from 0 to 90cmbsf, an area that is well oxygenated due to rapid draining during ebb tide. Assuming upward advection of groundwater, approximately 60% of the nitrate in the shallowest samples can be directly attributed to nitrification of ammonium. The increase in nitrate concentration could also be due to transport of nitrate from overlying water. If ammonium forms in the STZ due to release from sediments and is then transported to the saline zone where it is nitrified, it is possible that groundwater nitrate is a 'new', albeit extensively recycled, source of nitrogen to the harbor water.

Results from the standard estuarine model using salinity and ammonium concentrations indicate net consumption of ammonium in harbor sediments, with a rate of -2mmol m^{-2} d^{-1}. A breakdown of rates based on one dimensional advection-diffusion modeling shows the shallow saline portion of inlet banks can both consume and produce ammonium, with rates ranging -1.2mmol $m^{-2}d^{-1}$ to -3.4mmol $m^{-2}d^{-1}$. As described above, ammonium consumption in the western inlet bank is most likely due to nitrification of ammonium during advective transport of porewater in the saline transition zone. It is clear that at depths greater than 100cmbsf in the STZ, ammonium is produced during nitrate reduction. In the inlet center ammonium concentrations are below detection limit at depths 58 to 370cmbsf, in areas where dissolved oxygen concentrations range 160µmol L^{-1} to 230µmol L^{-1}. Ammonium is present in small amounts, 2.1µmol L^{-1} at a depth of 378cmbsf, which yields a modeled consumption rate of $-8x10^{-5}$ mmol m^{-2} d^{-1}. At inlet margins ammonium flux ranges $-2.0x10^{-2}$mmol $m^{-2}d^{-1}$ to $-4x10^{-3}$mmol $m^{-2}d^{-1}$. The Inlet margins of Setauket Harbor have properties analogous to tidal mud flats, where mud capped sands undergo complete draining during a tidal cycle and secondary porosity is due to bioturbation (Forbes and Lopez, 1990, Volkenborn et al., 2007). Previous work in mud flats show remineralized NH_4^+ is constantly added to porewater and diffused to surface water, which can offset biological uptake in the shallowest sediments (Waska and Kim, 2011). In the case of Setauket Harbor a slight negative reaction rate indicate biological uptake can exceed sediment release of ammonium.

As shown by Hays and Ullman (2007) the relationship between the flux of nitrate and ammonium in a discharge zone can be described by plotting the two fluxes and viewing how the two fluxes relate to idealized stoichiometry for each of the modes of nitrogen cycling (Hays and Ullman, 2007). This analysis provides insight into the mechanisms of nitrogen cycling and if mechanisms are spatially related to sediment differences. In Setauket Harbor, three possible modes of nitrogen behavior are observed (Figure 32); ammonium assimilation, DNRA and denitrification. The stoichiometry of DNRA is (Stumm and Morgan, 1996)

$$2CH_2O + NO_3^- + 2H^+ \rightarrow 2CO_2 + NH_4^+ + H_2O \quad (4)$$

As shown by equation 4, the production of ammonium combined with nitrate consumption at the western harbor bank is linked to the elevated DOC concentrations and likely due to DNRA that occurs as porewater enters the saline transition zone. These results indicate that complex biogeochemical processes likely operate simultaneously to regulate nitrogen in Setauket Harbor. Ammonium assimilation is the dominant nitrogen transformation mechanism in the eastern inlet bank as well as the inlet center, as evidenced by the negative ammonium flux and slightly positive nitrate flux Figure 32.

In the STZ of the inlet margins either nitrate consumption or net neutral reactions occur (Figure 32). Microbial denitrification resulting in the production of N_2O/ N_2 gas is the most likely cause for nitrate consumption in these locations. The stoichiometry for denitrification is (Stumm and Morgan, 1996):

$$5CH_2O + 4H^+ + 4NO_3^- \rightarrow 5CO_2 + 2N_2 + 7H_2O \quad (8)$$

Inlet margins contain an excess of DOC, as evidenced by modeled carbon flux, therefore microbial denitrification supported by either solid phase carbon or DOC drives the loss of groundwater sourced nitrate in this zone, as shown by equation 5. Microbial assimilation of nitrate is also possible at in these portions of the harbor but we note that NH_4^+ is known to inhibit assimilation (Zehr and Paerl, 2008, An and Gardner, 2002) and given the coexistence of NH_4^+ and NO_3^- in shallow samples, it is unlikely that assimilation is a significant nitrate attenuation mechanism. Ammonium production rates less than 1mmol m^{-2} d^{-1} indicate that DNRA is not a likely attenuation mechanism but we cannot rule out the possibility of DNRA coupled to NH_4^+ assimilation (Ullman et al., 2003) minor source of nitrogen loss.

Mechanism of carbon flux

DOC is consistently produced at this site, with and overall production rate of 60mmol $m^{-2}d^{-1}$ calculated from standard estuarine model and individual porewater profile rates ranging $4.3x10^{-3}$ mmol $m^{-2}d^{-1}$ to13.4mmol $m^{-2}d^{-1}$ as calculated from one-dimensional advection-diffusion model. Highest rates are observed at the inlet banks with the lowest rates in the inlet center. Billerbeck et al (2006a) showed that organic matter decomposition in a sandy tidal flat can produce seepage water nutrient concentrations 10 to 15 times higher than concentrations in porewater. DOC flux to surface water at inlet margins is enhanced by sediment heterogeneity that causes preferential draining of the highly permeable sand layer during low tide. Drainage channels were observed during ebb and low tide during porewater sampling. Although velocity of draining fluid exceeds molecular diffusion rates by orders of magnitude the surface area of drainage channels represent a small fraction of the total harbor inlet surface area. Draining of inlet banks porewater contributes to enhanced sediment organic mineralization as atmospheric oxygen likely interacts with decomposing organic matter in the top of the mud layer. Upon flood tide DOC generated during mud flat exposure is mobilized and can be released during subsequent tidal draining. The center of the harbor is continually submerged, and receives discharged porewater from draining inlet banks, yet has a low DOC production rate, $1.3x10^{-4}$ mmol $m^{-2}d^{-1}$. Sakamaki et al (2006) observed a strong correlation between nutrient concentration in overlying water and porewater nutrient concentration. When surface water nutrient concentrations are high, release of nutrients from sediments is suppressed during ebb and low tide (Sakamaki et al., 2006). In Setauket Harbor average DOC concentration in surface water from the inlet center during low tide is 220µmol L^{-1}, which is significantly higher than porewater values from this location that range 18µmol L^{-1} to 29µmol L^{-1}. Therefore overlying water concentrations of DOC are the most likely control on DOC flux at the inlet center.

Range in nutrient flux variation

While there are numerous studies of nutrient flux to overlying water in tidal flats and harbors, few studies have investigated sites comprised of both sand and mud settings. Sakamaki et al., (2006) investigated a sand and mud tidal flat and found greater consumption of oxygen,

PO_4^{-3}, NO_3^- and NH_4^+ in sand flats than in mud flats. Our results show clear patterns of nitrogen consumption vs production between sand and mud zones of Setauket Harbor. The process governing nitrate loss in sand sediments on the eastern bank is likely DNRA, which is linked to high DOC and reducing conditions in the saline transition zone. On the western bank ammonium assimilation regulates nitrogen processes as porewater moves from the freshwater zone to the saline transition zone.

When compared to other studies (**Error! Reference source not found.**) nitrate flux during SGD in Setauket Harbor varies more than previously reported for differences between mud and sand settings(Sakamaki et al., 2006). In the sand setting, groundwater advection brings nitrate rich freshwater to the STZ, with resulting nitrate loss in both shoreline cases, but subsequent secondary nitrification of ammonium is observed in the eastern shore. Previous work on microbial community assemblages in a sandy coastal aquifer identified distinct microbial clades for low nitrate/high salinity vs high nitrate/low salinity environments (Santoro et al., 2006, Mosier and Francis, 2010), indicating microbial populations of denitrifiying bacteria exist at small spatial scales. Although this study does not directly address microbial populations, we hypothesize that steep microbial community shifts accompany steep gradients in nutrients that lead to the large range in nitrate fluxes found at this site. Highly variable nitrate concentrations in the freshwater zone do not allow for determination of an exact freshwater endmember Figure 31c. Despite this, it is clear that groundwater is a significant source of nitrate to the saline transition zone in the sand edges of the harbor, as evidenced by maximum nitrate concentrations for inlet bank porewater located in the freshwater zone. In contrast, maximum nitrate concentrations in the mud portion of the harbor are found at the base of the saline transition zone, suggesting nitrification of either dissolved organic nitrogen or ammonium.

Ammonium flux rates observed in the sandy portion of the harbor are driven by tidal pumping, as high concentrations in the saline zone decrease at depth. In the mud portions of the harbor, ammonium flux values are similar to those observed in other tidal settings (**Error! Reference source not found.**). Although porewater profiles through mud sediments show elevated levels in the saline transition zone, due to either molecular diffusion or bioturbation enhanced transport of ammonium rich surface water. When compared to other tidally dominated sand settings, Setauket Harbor is unusual as one inlet bank produces ammonium while the opposite bank consumes ammonium in the shallowest saline zone. Ammonium flux is significantly lower than reported values from other sites (**Error! Reference source not found.**), but this is due to the lack of ammonium in the deep groundwater. At depth beneath the STZ, the majority of fresh groundwater samples contain less than 5 μmol L^{-1} of ammonium, which is expected given oxygen saturation of 33% to 75% in these samples. This should generate negative ammonium flux numbers, but model results do not bear this out. One possible explanation for this is downward flux of ammonium released from sediments during flood tide which may mix with groundwater during ebb tide.

Conclusion

Previous work in sandy tidal flats demonstrates that infiltration during flood tide supplies nutrients to sediments which in turn enhances organic matter mineralization and promotes nutrient release via mixed surface water-groundwater discharge during ebb tide. In this study two estuarine models were utilized to determine the fate of nutrients during movement from

fresh groundwater into the saline transition zone in a tidally dominated harbor inlet. Both models agree that the inlet acts as an overall sink for groundwater sourced nitrate. In Setauket Harbor inlet banks, infiltrating surface water interacts with upwelling groundwater in permeable sand sediments to create an active zone of nitrate loss at the base of the STZ. Taken together, these results show that groundwater fed harbor inlets act to bio-geochemically remove nitrate prior to porewater discharge to surface water. Ammonium and inputs are largely autochthonous in mud capped portions of the inlet, but likely allochthonous in sand portions where nitrate reduction and ammonium production coincide.

References

ADDY, K., GOLD, A., NOWICKI, B., MCKENNA, J., STOLT, M. & GROFFMAN, P. 2005. Denitrification capacity in a subterranean estuary below a Rhode Island fringing salt marsh. *Estuaries,* 28**,** 896-908.

AN, S. M. & GARDNER, W. S. 2002. Dissimilatory nitrate reduction to ammonium (DNRA) as a nitrogen link, versus denitrification as a sink in a shallow estuary (Laguna Madre/Baffin Bay, Texas). *Marine Ecology-Progress Series,* 237**,** 41-50.

ANDERSEN, M. S., BARON, L., GUDBJERG, J., GREGERSEN, J., CHAPELLIER, D., JAKOBSEN, R. & POSTMA, D. 2007. Discharge of nitrate-containing groundwater into a coastal marine environment. *Journal of Hydrology,* 336**,** 98-114.

BAUER, C. 2012. ***Physical Processes Contributing to Localized, Seasonal Hypoxic Conditions in the Bottom Waters of Smithtown Bay, Long Island Sound, New York****.* MS, Stony Brook University.

BECK, A. 2007. *SUBMARINE GROUNDWATER DISCHARGE (SGD) AND DISSOLVED TRACE METAL CYCLING IN THE SUBTERRANEAN ESTUARY AND COASTAL OCEAN.* Ph.D, Stony Brook University.

BECK, A. J., COCHRAN, J. K. & SANUDO-WILHELMY, S. A. 2010. The distribution and speciation of dissolved trace metals in a shallow subterranean estuary. *Marine Chemistry,* 121**,** 145-156.

BILLERBECK, M., WERNER, U., BOSSELMANN, K., WALPERSDORF, E. & HUETTEL, M. 2006. Nutrient release from an exposed intertidal sand flat. *Marine Ecology Progress Series,* 316**,** 35-51.

BOHLKE, J. K., HATZINGER, P. B., STURCHIO, N. C., GU, B. H., ABBENE, I. & MROCZKOWSKI, S. J. 2009. Atacama Perchlorate as an Agricultural Contaminant in Groundwater: Isotopic and Chronologic Evidence from Long Island, New York. *Environmental Science & Technology,* 43**,** 5619-5625.

BOUDREAU, B. P. 1996. The diffusive tortuosity of fine-grained unlithified sediments. *Geochimica Et Cosmochimica Acta,* 60**,** 3139-3142.

BURGIN, A. J. & HAMILTON, S. K. 2007. Have we overemphasized the role of denitrification in aquatic ecosystems? A review of nitrate removal pathways. *Frontiers in Ecology and the Environment,* 5**,** 89-96.

BURNETT, W. C., BOKUNIEWICZ, H., HUETTEL, M., MOORE, W. S. & TANIGUCHI, M. 2003. Groundwater and pore water inputs to the coastal zone. *Biogeochemistry,* 66**,** 3-33.

CHARETTE, M. A. & ALLEN, M. C. 2006. Precision ground water sampling in coastal aquifers using a direct-push, shielded-screen well-point system. *Ground Water Monitoring and Remediation,* 26**,** 87-93.

DACEY, J. W. H. & HOWES, B. L. 1984. WATER-UPTAKE BY ROOTS CONTROLS WATER-TABLE MOVEMENT AND SEDIMENT OXIDATION IN SHORT SPARTINA MARSH. *Science,* 224**,** 487-489.

DAVIS, J. L., NOWICKI, B. & WIGAND, C. 2004. Denitrification in fringing salt marshes of Narragansett Bay, Rhode Island, USA. *Wetlands,* 24**,** 870-878.

DEBORDE, J., ANSCHUTZ, P., AUBY, I., GLE, C., COMMARIEU, M. V., MAURER, D., LECROART, P. & ABRIL, G. 2008. Role of tidal pumping on nutrient cycling in a temperate lagoon (Arcachon Bay, France). *Marine Chemistry,* 109**,** 98-114.

FETTER, C. W. 2001. *Applied Hydrogeology*, Prentice Hall.

FORBES, V. E. & LOPEZ, G. R. 1990. THE ROLE OF SEDIMENT TYPE IN GROWTH AND FECUNDITY OF MUD SNAILS (HYDROBIIDAE). *Oecologia,* 83**,** 53-61.

GROFFMAN, P. M., ALTABET, M. A., BOHLKE, J. K., BUTTERBACH-BAHL, K., DAVID, M. B., FIRESTONE, M. K., GIBLIN, A. E., KANA, T. M., NIELSEN, L. P., VOYTEK, M. A. & CC 2006. Methods for measuring denitrification: Diverse approaches to a difficult problem. *Ecological Applications,* 16**,** 2091-2122.

HAYS, R. L. & ULLMAN, W. J. 2007. Dissolved nutrient fluxes through a sandy estuarine beachface (Cape Henlopen, Delaware, USA): Contributions from fresh groundwater discharge, Seawater recycling, and diagenesis. *Estuaries and Coasts,* 30**,** 710-724.

HOFFMANN, C. C., HEIBERG, L., AUDET, J., SCHONFELDT, B., FUGLSANG, A., KRONVANG, B., OVESEN, N. B., KJAERGAARD, C., HANSEN, H. C. B. & JENSEN, H. S. 2012. Low phosphorus release but high nitrogen removal in two restored riparian wetlands inundated with agricultural drainage water. *Ecological Engineering,* 46**,** 75-87.

HOWARTH, R. W. 2008. Coastal nitrogen pollution: A review of sources and trends globally and regionally. *Harmful Algae,* 8**,** 14-20.

HYUN, J. H., MOK, J. S., CHO, H. Y., KIM, S. H., LEE, K. S. & KOSTKA, J. E. 2009. Rapid organic matter mineralization coupled to iron cycling in intertidal mud flats of the Han River estuary, Yellow Sea. *Biogeochemistry,* 92**,** 231-245.

JOHNSON, K. S. & PETTY, R. L. 1982. Determination of Phosphate in Sea-Water by Flow Injection Analysis with Injection of Reagent. *Analytical Chemistry,* 54**,** 1185-1187.

JØRGENSEN, B. 2006. Bacteria and Marine Biogeochemistry. *Marine Geochemistry.* Berlin: Springer.

KAUL, L. W. & FROELICH, P. N. 1984. MODELING ESTUARINE NUTRIENT GEOCHEMISTRY IN A SIMPLE SYSTEM. *Geochimica Et Cosmochimica Acta,* 48**,** 1417-1433.

KELSO, B. H. L., SMITH, R. V., LAUGHLIN, R. J. & LENNOX, S. D. 1997. Dissimilatory nitrate reduction in anaerobic sediments leading to river nitrite accumulation. *Applied and Environmental Microbiology,* 63**,** 4679-4685.

KIM, T. H., WASKA, H., KWON, E., SURYAPUTRA, I. G. N. & KIM, G. 2012. Production, degradation, and flux of dissolved organic matter in the subterranean estuary of a large tidal flat. *Marine Chemistry,* 142**,** 1-10.

KNEE, K. L., STREET, J. H., GROSSMAN, E. E., BOEHM, A. B. & PAYTAN, A. 2010. Nutrient inputs to the coastal ocean from submarine groundwater discharge in a groundwater-dominated system: Relation to land use (Kona coast, Hawaii, USA). *Limnology and Oceanography,* 55**,** 1105-1122.

KROEGER, K. D. & CHARETTE, M. A. 2008. Nitrogen biogeochemistry of submarine groundwater discharge. *Limnology and Oceanography,* 53**,** 1025-1039.

KROM, M. D. & BERNER, R. A. 1980. ADSORPTION OF PHOSPHATE IN ANOXIC MARINE-SEDIMENTS. *Limnology and Oceanography,* 25**,** 797-806.

LANGMUIR, C. H., VOCKE, R. D., HANSON, G. N. & HART, S. R. 1978. General Mixing Equation with Applications to Icelandic Basalts. *Earth and Planetary Science Letters,* 37**,** 380-392.

LEE, D. R. 1977. DEVICE FOR MEASURING SEEPAGE FLUX IN LAKES AND ESTUARIES. *Limnology and Oceanography,* 22**,** 140-147.

LOVELESS, A. M. & OLDHAM, C. E. 2010. Natural attenuation of nitrogen in groundwater discharging through a sandy beach. *Biogeochemistry,* 98**,** 75-87.

MAGALHAES, C. M., BORDALO, A. A. & WIEBE, W. J. 2002. Temporal and spatial patterns of intertidal sediment-water nutrient and oxygen fluxes in the Douro River estuary, Portugal. *Marine Ecology Progress Series,* 233**,** 55-71.

MARTIN, J. B., CABLE, J. E., SMITH, C., ROY, M. & CHERRIER, J. 2007. Magnitudes of submarine groundwater discharge from marine and terrestrial sources: Indian River Lagoon, Florida. *Water Resources Research,* 43.

MOSIER, A. C. & FRANCIS, C. A. 2010. Denitrifier abundance and activity across the San Francisco Bay estuary. *Environmental Microbiology Reports,* 2**,** 667-676.

PAULSEN, R. J., SMITH, C. F., O'ROURKE, D. & WONG, T. F. 2001. Development and evaluation of an ultrasonic ground water seepage meter. *Ground Water,* 39**,** 904-911.

RICHARDS, F., CLINE, J., BROENKOW, W. & ATKINSON, L. 1966. Some consequences of the decomposition of organic matter in Lake Nitinat, an anoxic fjord. *American Society of Limnology and Oceanography,* 10**,** R185-R199.

RIEDEL, T., LETTMANN, K., SCHNETGER, B., BECK, M. & BRUMSACK, H. J. 2011. Rates of trace metal and nutrient diagenesis in an intertidal creek bank. *Geochimica Et Cosmochimica Acta,* 75**,** 134-147.

RIEXINGER, P. 2005. *COASTAL FISH & WILDLIFE HABITAT ASSESSMENT FORM* [Online]. New York: NYS Department of State. [Accessed July 18 2013].

ROY, M., MARTIN, J. B., CABLE, J. E. & SMITH, C. G. 2013. Variations of iron flux and organic carbon remineralization in a subterranean estuary caused by inter-annual variations in recharge. *Geochimica Et Cosmochimica Acta,* 103**,** 301-315.

SAKAMAKI, T., NISHIMURA, O. & SUDO, R. 2006. Tidal time-scale variation in nutrient flux across the sediment-water interface of an estuarine tidal flat. *Estuarine Coastal and Shelf Science,* 67**,** 653-663.

SANTORO, A. E., BOEHM, A. B. & FRANCIS, C. A. 2006. Denitrifier community composition along a nitrate and salinity gradient in a coastal aquifer. *Applied and Environmental Microbiology,* 72**,** 2102-2109.

SANTOS, I. R., BURNETT, W. C., CHANTON, J., MWASHOTE, B., SURYAPUTRA, I. G. N. A. & DITTMAR, T. 2008. Nutrient biogeochemistry in a Gulf of Mexico subterranean estuary and groundwater-derived fluxes to the coastal ocean. *Limnology and Oceanography,* 53.

SANTOS, I. R., BURNETT, W. C., DITTMAR, T., SURYAPUTRA, I. & CHANTON, J. 2009. Tidal pumping drives nutrient and dissolved organic matter dynamics in a Gulf of Mexico subterranean estuary. *Geochimica Et Cosmochimica Acta,* 73**,** 1325-1339.

SOLORZANO, L. 1969. Determination of Ammonia in Natural Waters by Phenolhypochlorite Method. *Limnology and Oceanography,* 14**,** 799-&.

SPITERI, C., VAN CAPPELLEN, P. & REGNIER, P. 2008. Surface complexation effects on phosphate adsorption to ferric iron oxyhydroxides along pH and salinity gradients in estuaries and coastal aquifers. *Geochimica Et Cosmochimica Acta,* 72.

STOOKEY, L. L. 1970. Ferrozine- A New Spectrophotometric Reagent for Iron. *Analytical Chemistry,* 42**,** 779-&.

STUMM, W. & MORGAN, J. 1996. *Aquatic Chemistry: Chemical Equilibria and Rates in Natural Waters,* New York, Wiley.

TEIXEIRA, C., MAGALHAES, C., JOYE, S. B. & BORDALO, A. A. 2013. The role of salinity in shaping dissolved inorganic nitrogen and N2O dynamics in estuarine sediment-water interface. *Marine Pollution Bulletin,* 66**,** 225-229.

ULLMAN, W. J., CHANG, B., MILLER, D. C. & MADSEN, J. A. 2003. Groundwater mixing, nutrient diagenesis, and discharges across a sandy beachface, Cape Henlopen, Delaware (USA). *Estuarine Coastal and Shelf Science,* 57**,** 539-552.

VOLKENBORN, N., HEDTKAMP, S. I. C., VAN BEUSEKOM, J. E. E. & REISE, K. 2007. Effects of bioturbation and bioirrigation by lugworms (Arenicola marina) on physical and chemical sediment properties and implications for intertidal habitat succession. *Estuarine Coastal and Shelf Science,* 74**,** 331-343.

WANG, W. W., LI, D. J., ZHOU, J. L. & GAO, L. 2011. Nutrient dynamics in pore water of tidal marshes near the Yangtze Estuary and Hangzhou Bay, China. *Environmental Earth Sciences,* 63**,** 1067-1077.

WASKA, H. & KIM, G. 2011. Submarine groundwater discharge (SGD) as a main nutrient source for benthic and water-column primary production in a large intertidal environment of the Yellow Sea. *Journal of Sea Research,* 65**,** 103-113.

XIN, P., KONG, J., LI, L. & BARRY, D. A. 2012. Effects of soil stratigraphy on pore-water flow in a creek-marsh system. *Journal of Hydrology,* 475**,** 175-187.

XIN, P., YUAN, L. R., LI, L. & BARRY, D. A. 2011. Tidally driven multiscale pore water flow in a creek-marsh system. *Water Resources Research,* 47.

ZEHR, J. & PAERL, H. 2008. *Microbial Ecology of the Oceans,* New York, Wiley.

ZHOU, L. 2008. *Annual precipitation pattern over Long Island Based on Radar Data* M.S, Stony Brook University.

Tables and Figures

Table 7 Standard estuarine model equations and coefficient standard deviations. Average R is integrated over 0 to 1m beneath sediment water interface.

Analyte	R^2	a	±	b	±	c	±	Average R mmol m^{-2} d^{-1}
NO_3^-	0.4	0.2	0.7	-19.4	15.6	3532	48.6	-41
NH_4^+	0.5	0.1	0.1	1.5	2.7	0.9	8.72	-2
DOC	0.8	-1.2	0.4	44.1	8.3	16.6	27.3	60
PO_4^{-3}	0.7	-0.02	0.02	1.0	0.4	-0.23	1.15	-4

Table 8 Summary of modeled porewater chloride results (D_s v^{-1}), dispersion coefficients (D_s) and derived porewater velocity (v) for each porewater profile.

Porewater Profile	modeled D_s v^{-1}	Ds cm^2 s^{-1}	v cm d^{-1}
A (bank, sand)	5.0E-04	4.6E-03	2.0E-01
B (margin, mud)	1.0E-04	9.6E-06	8.3E-05
C (margin, mud	1.0E-06	9.6E-06	8.3E-07
D (margin, mud	1.0E-04	9.6E-06	8.3E-05
E (bank, sand)	3.0E-04	4.6E-03	1.2E-01

Table 9 Equations fit to nutrient concentration profiles. Associated r^2 value is given for each equation fit

	Nitrate	r^2	Ammonium	r^2	Dissolved organic carbon	r2
A	$0.0143x^2 - 3.3355x + 179.11$	1.00	$-0.0043x^2 + 1.0857x - 26.5$	1.00	$-0.0165x^2 + 4.0739x + 49.696$	0.99
B	$0.0286x^2 - 0.1886x + 0.1028$	1.00	$0.0022x^2 - 0.8888x + 72.253$	0.58	$854.53x^{-0.6}$	0.79
C	$-0.0032x^2 + 1.2109x + 267.2$	0.72	$5E\text{-}05x^2 - 0.0153x + 0.9382$	0.88	$-8E\text{-}05x^2 - 0.0177x + 30.379$	1.00
D	$-0.0409x^2 + 11.985x - 175.52$	0.88	$0.0097x^2 - 1.3129x + 40.938$	0.95	$48633x^{-1.415}$	0.95
E	$-0.0002x^2 + 1.9853x - 29.854$	1.00	$0.0014x^2 - 1.0152x + 183.19$	0.82	$-0.0041x^2 + 0.0185x + 539.12$	0.80

Table 10 Modeled nutrient fluxes during fresh groundwater transport into saline transition zone. Values calculated using equation 6 and concentration profile fits shown in Table 9. All values in mmol $m^{-2}d^{-1}$.

Porewater Profile	Nitrate flux	Ammonium flux	DOC flux
A	-11.0	3.4	13.4
B	$-4.7x10^{-2}$	$-3.7x10^{-3}$	$-4.3x10^{-3}$
C	$5.3x10^{-3}$	$-8.3x10^{-5}$	$1.3x10^{-4}$
D	$6.8x10^{-2}$	$-1.6x10^{-2}$	0.9
E	0.4	-1.2	3.2

Table 11 Nutrient flux reported in previous studies of tidal flats and estuaries. Significant site characteristics described in site column.

Site	Nitrate flux	Ammonium flux	Study
Sand flat, northeast japan	-565µmol m^{-2} h^{-1}	-850µmol m^{-2} h^{-1}	(Sakamaki et al., 2006)
Mud flat, northeast japan	-452µmol m^{-2} h^{-1}	-49 µmol m^{-2} h^{-1}	(Sakamaki et al., 2006)
Ave River estuary, NW Portugal	-7 to -50 nmol cm^{-3} h^{-1}	40 to 120nmol $cm^{-3}h^{-1}$	(Teixeira et al., 2013)
Fenun-xiang tidal flat, Hangzhou Bay, China, unvegetated	-60 to -10µmol $m^{-2}h^{-1}$	-3 to 52µmol $m^{-2}h^{-1}$	(Wang et al., 2011)
Fengxiang tidal flat, Hangzhou Bay, China, vegetated	-16 to -63µmol $m^{-2}h^{-1}$	-2 to 48µmol $m^{-2}h^{-1}$	(Wang et al., 2011)
Arcachon Bay, French Atlantic Coast	1.44 to 21.4 mmol m^{-3} d^{-1}	132.7 to 691.4 mmol m^{-3} d^{-1}	(Deborde et al., 2008)
Douro Estuary (Portugal)- mud site	-512 to -129µmol $m^{-2}h^{-1}$	-109 to 106µmol $m^{-2}h^{-1}$	(Magalhaes et al., 2002)
Douro Estuary (Portugal)-sand site	-608 to -115µmol $m^{-2}h^{-1}$	-104 to 0 µmol$m^{-2}h^{-1}$	(Magalhaes et al., 2002)
Setauket Harbor- mud capped sediments	-4.7x10^{-2} to 6.8x10^{-2} mmol m^{-2} d^{-1}	-3.7x10^{-3} to -1.6x10^{-2} mmol m^{-2} d^{-1}	this study
Setauket Harbor- sand sediments	-26.3 to 2.mmol m^{-2} d^{-1}	-1.1 to 3.4mmol m^{-2} d^{-1}	this study

Figure 22 Study location in Setauket Harbor, located adjacent to Port Jefferson Harbor and Long Island Sound (inset). Porewater profiles span a lobe of the harbor from southwest to northeast, shown in figures below as A-E.

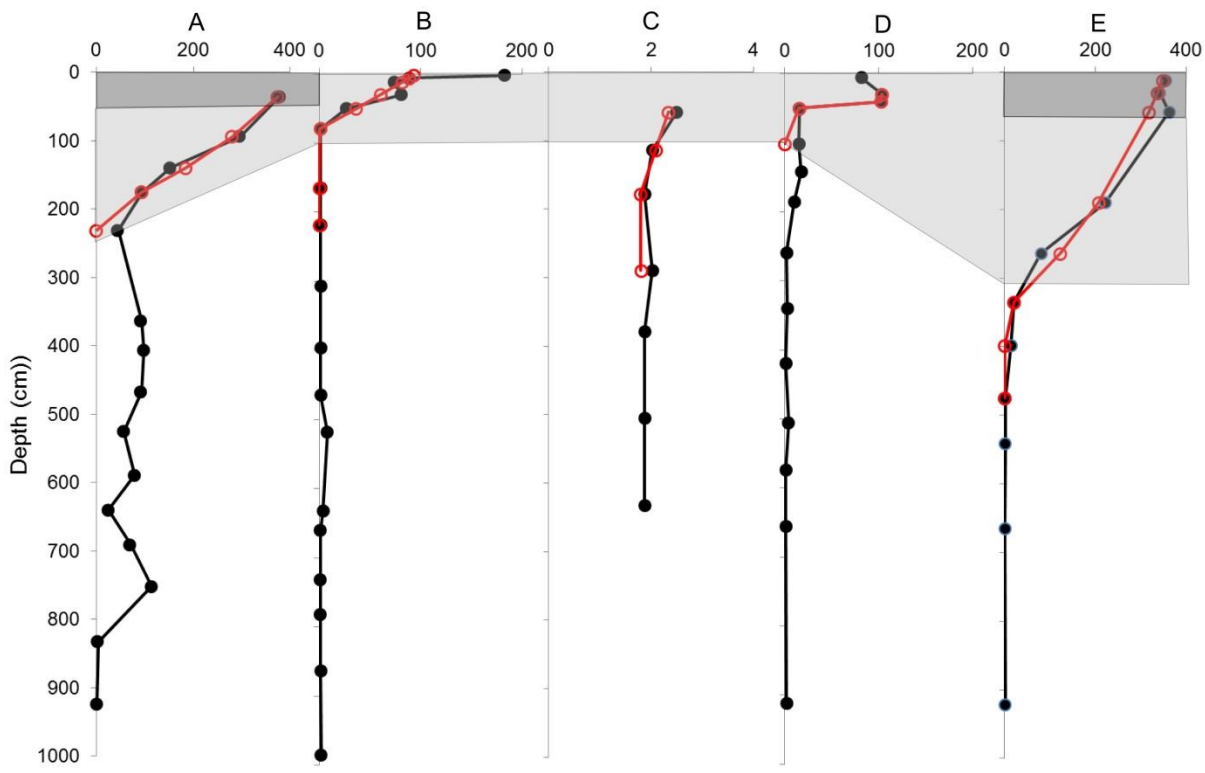

Figure 23 Porewater chloride profiles. Sample (●) and one-dimensional advection-diffusion model modeled concentration (○, red) shown in mmol L-1. Dark shading represents shallow saline zone, only observed in inlet bank profiles; light shading represents the saline transition zone (STZ).

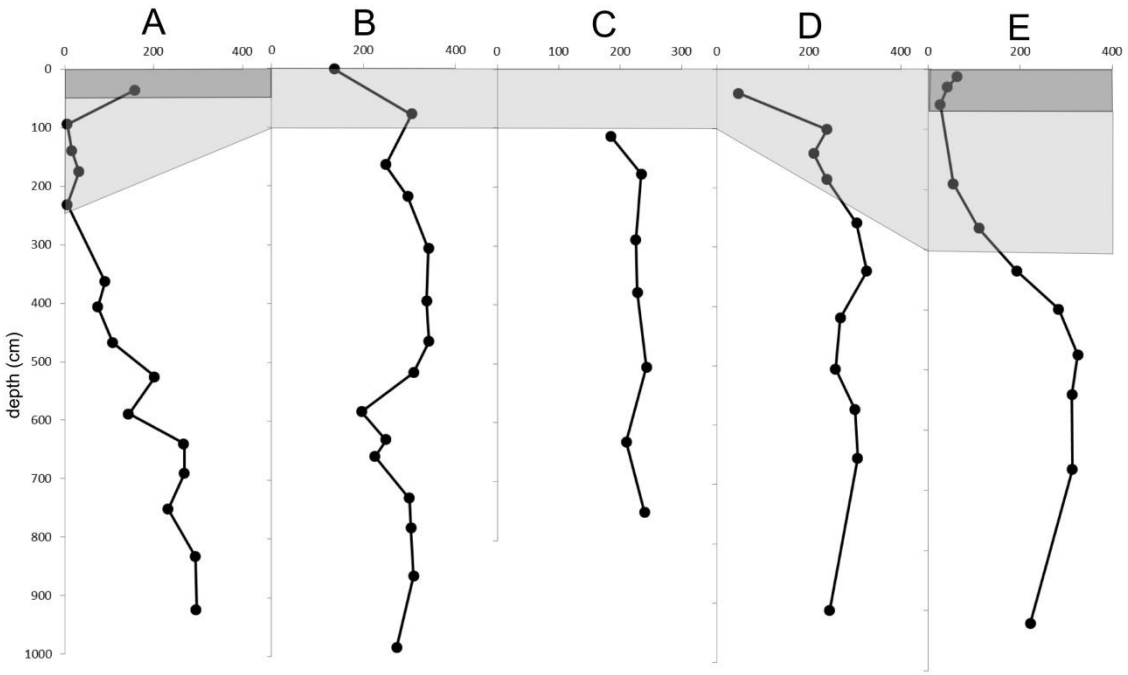

Figure 24 Dissolved oxygen porewater concentrations (µmol L-1). Dark shading represents shallow saline zone, only observed in inlet bank profiles; light shading represents the saline transition zone (STZ).

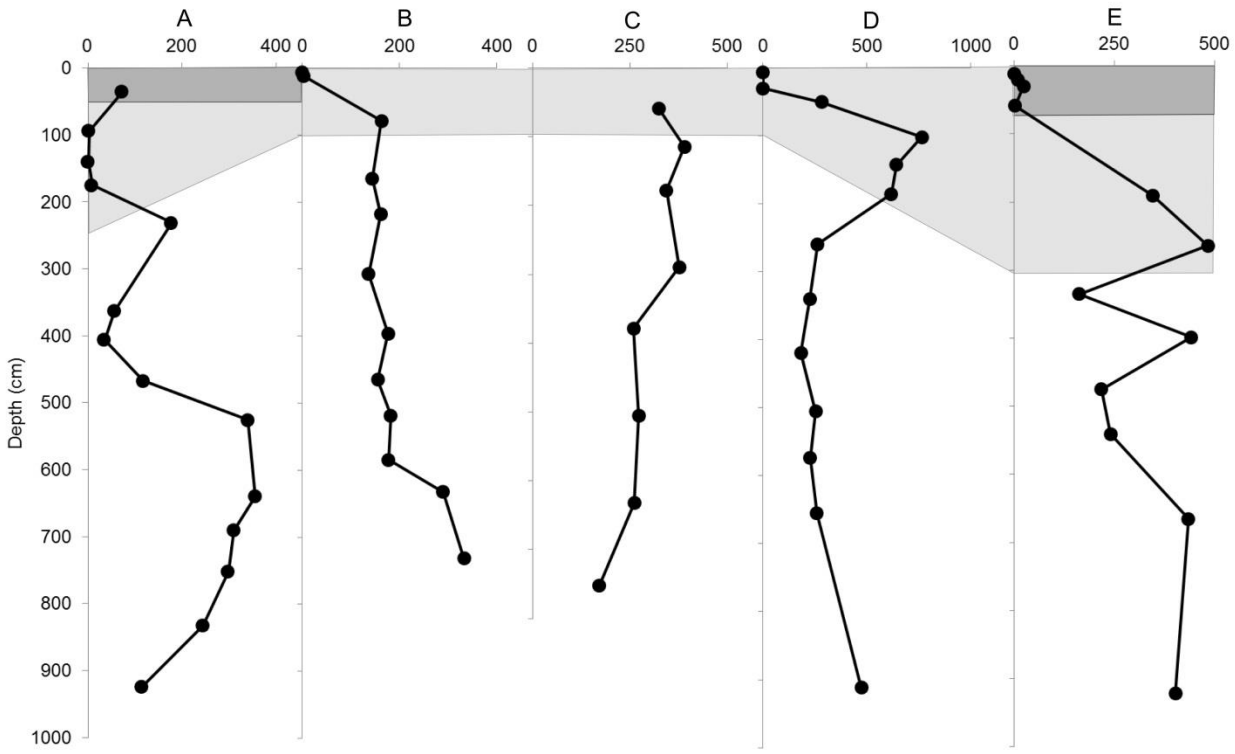

Figure 25 Porewater nitrate concentrations ($\mu molL^{-1}$). Dark shading represents shallow saline zone, only observed in inlet bank profiles; light shading represents the saline transition zone (STZ).

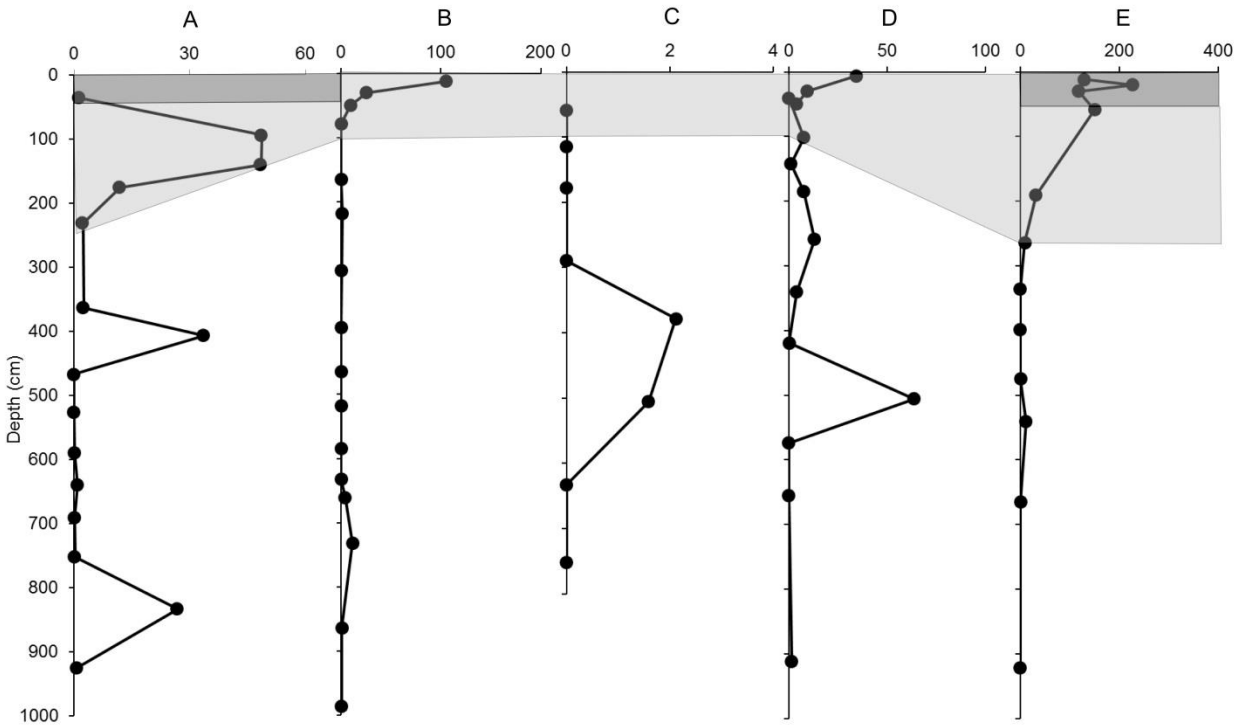

Figure 26 Porewater ammonium concentrations (µmol L^{-1}). Dark shading represents shallow saline zone, only observed in inlet bank profiles; light shading represents the saline transition zone (STZ).

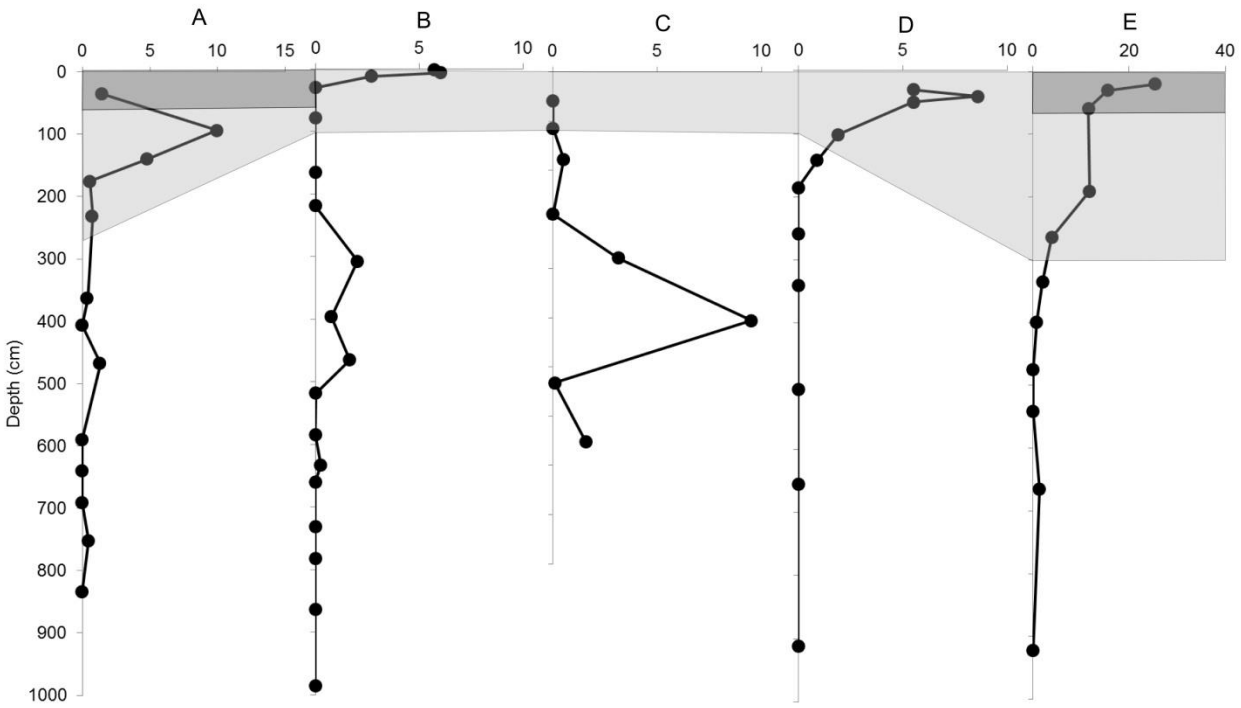

Figure 27 Porewater phosphate concentrations (µmol L^{-1}). Dark shading represents shallow saline zone, only observed in inlet bank profiles; light shading represents the saline transition zone (STZ).

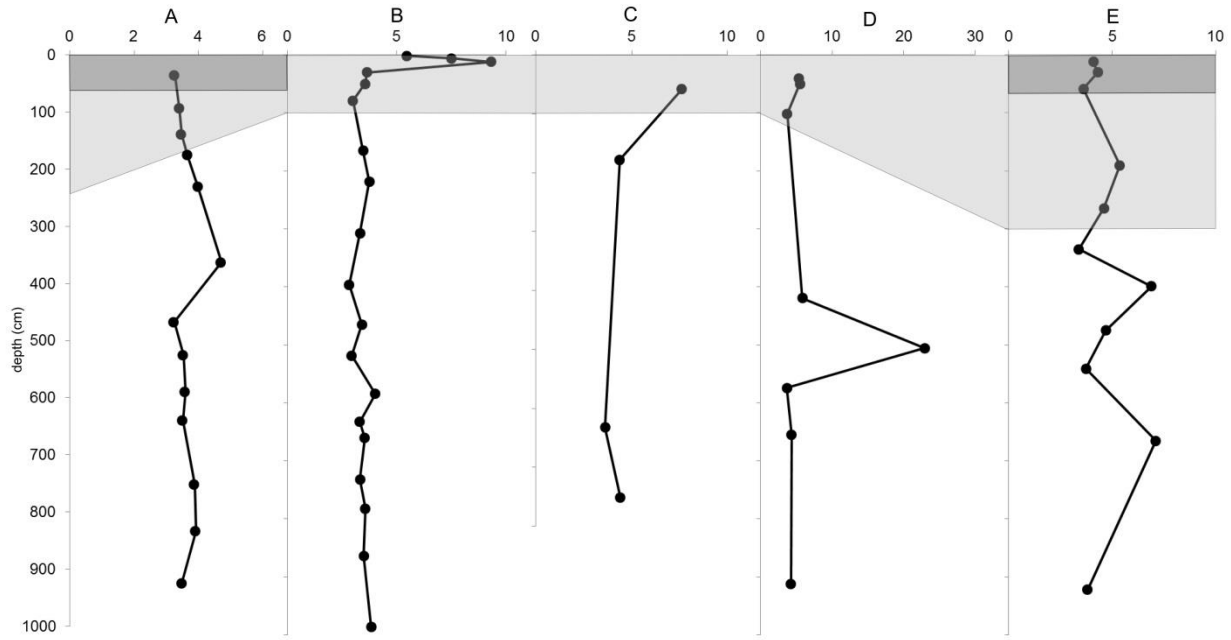

Figure 28 Porewater iron concentrations (µmol L^{-1}). Dark shading represents shallow saline zone, only observed in inlet bank profiles; light shading represents the saline transition zone (STZ).

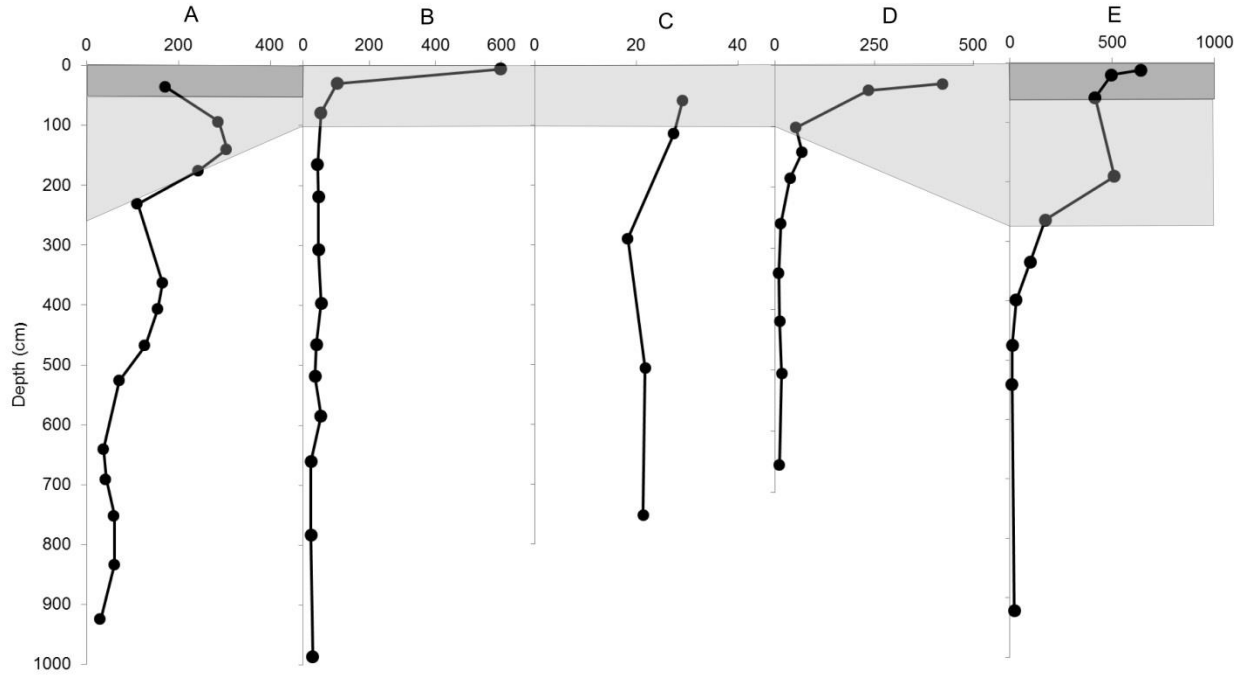

Figure 29 Porewater DOC concentrations (µmol L^{-1}). Dark shading represents shallow saline zone, only observed in inlet bank profiles; light shading represents the saline transition zone (STZ).

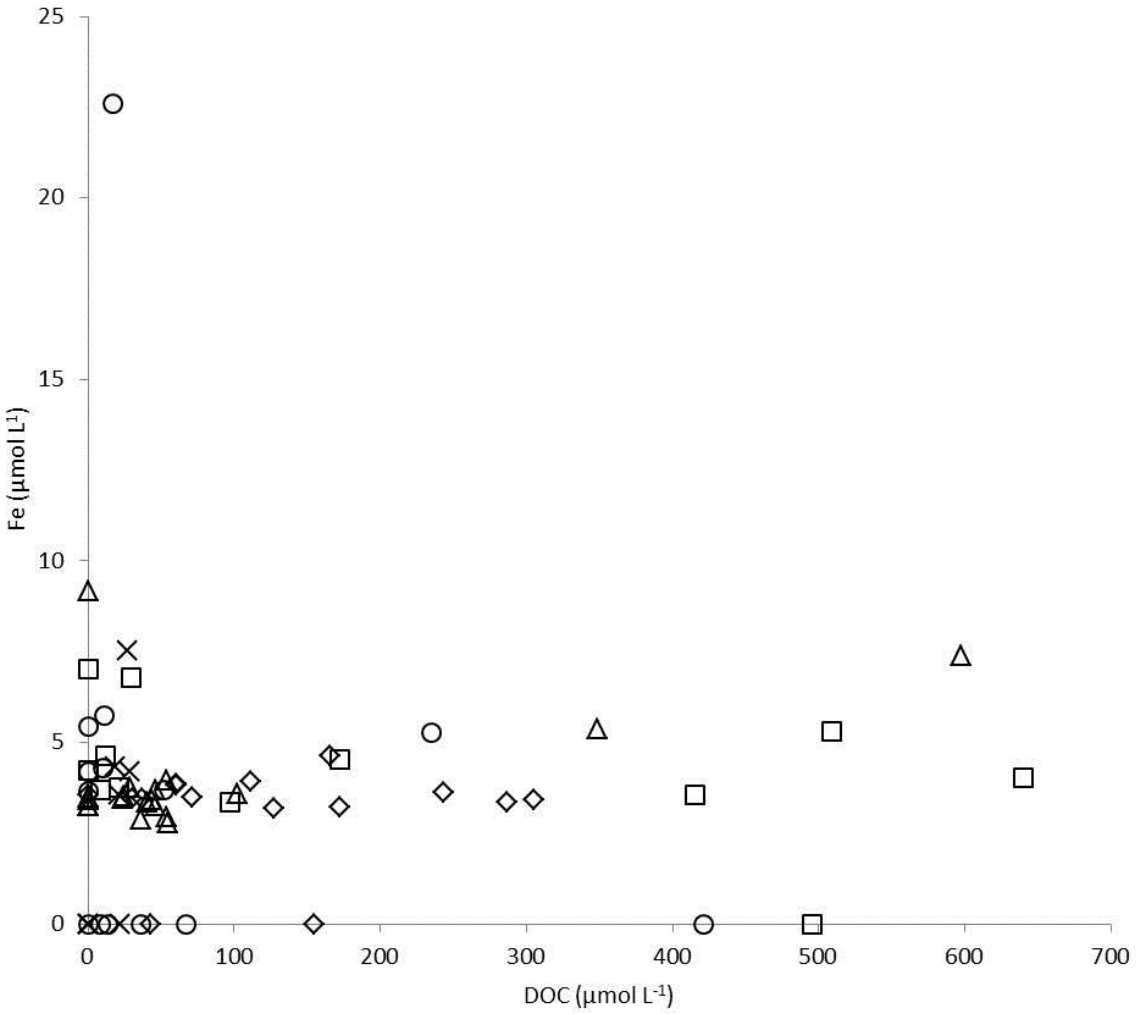

Figure 30 Comparison between dissolved organic carbon (DOC) and iron (Fe^{2+}) concentrations for porewater profiles located on harbor banks A (◊) ,E(□) ; harbor margins B(Δ), D(○) and harbor center C(X).

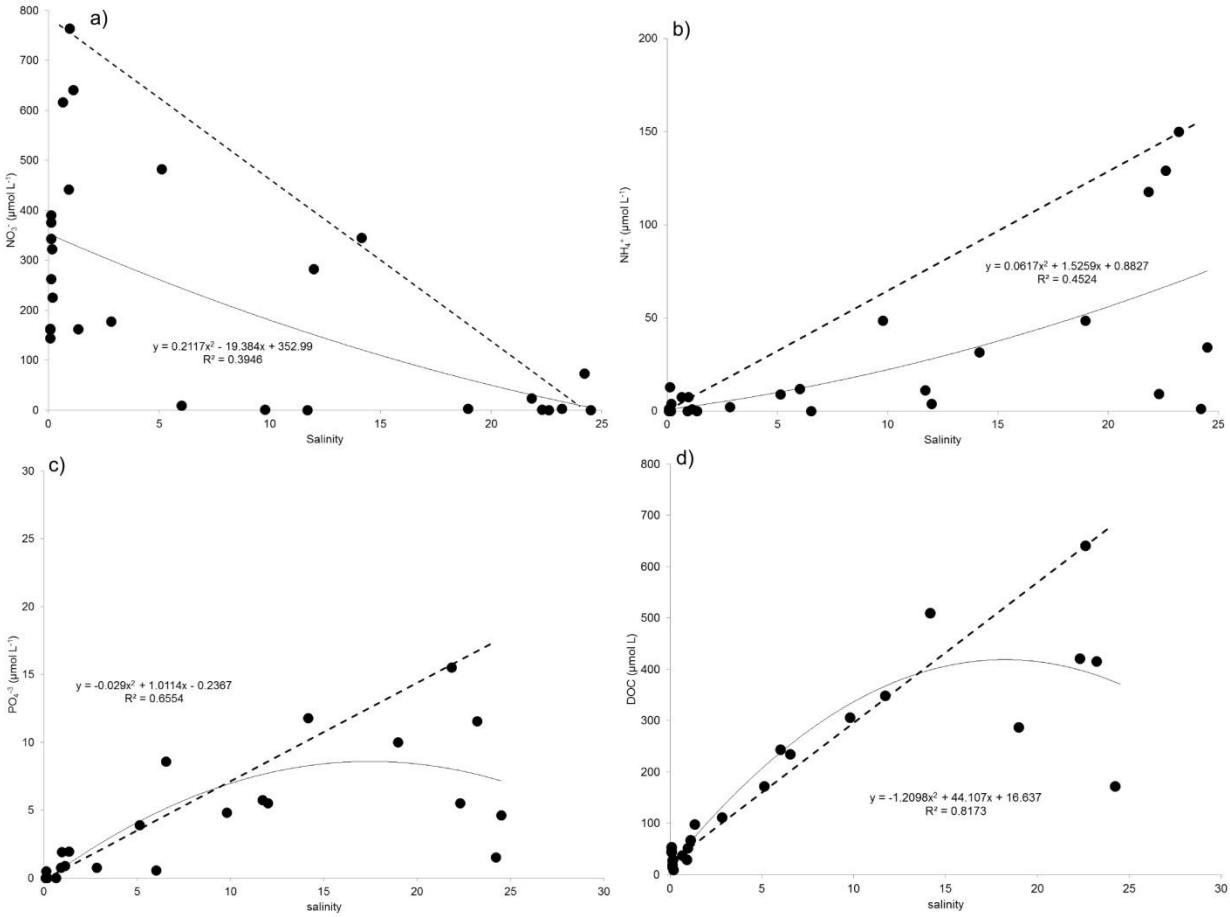

Figure 31 Salinity nutrient mixing plots for nitrate (a), ammonium (b), phosphate (c), and DOC (d). Comparison of polynomial trend line (solid) and conservative mixing lines (dashed) indicate removal of nitrate, ammonium and phosphate but net production of DOC.

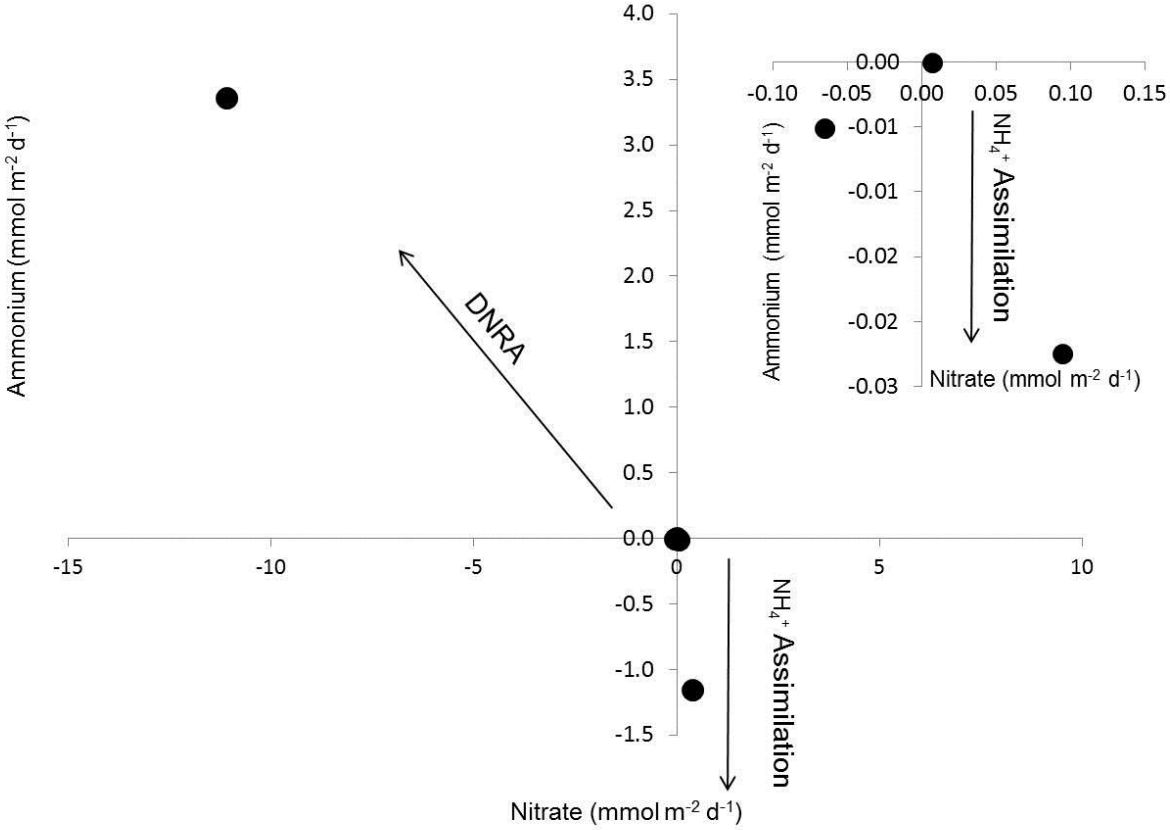

Figure 32 Relationship between ammonium and nitrate diagenetic reactions. Arrows indicate idealized stoichiometry for nitrogen cycling mechanisms. Inset graph is enlarged to show harbor center and margin points, which are porewater profiles B, C and D. Two mechanisms of nitrogen cycling are identified in Setauket Harbor; DNRA and ammonium assimilation.

Chapter V: EMBAYMENT SCALE ASSESSMENT OF SUBMARINE GROUNDWATER DISCHARGE NUTRIENT LOADING TO PORT JEFFERSON HARBOR, LONG ISLAND NY

Abstract

A shoreline survey of porewater nutrient concentrations and ^{222}Rn surface water activities was performed in Port Jefferson Harbor, NY, an embayment of Long Island Sound. Submarine groundwater discharge (SGD) rates were calculated for individual shoreline segments with nutrient concentrations applied to calculated groundwater flux values in order to spatially depict the nutrient flux to overlying harbor water. Nitrate inputs range from 0.5 to 217.2 mol d^{-1} per shoreline segment. Analysis of nitrate to phosphate ratios (N:P) identified three distinct modes of nutrient transport or recirculation into the harbor, with the southernmost portion of the harbor having the highest fresh SGD fraction. Total nitrate inputs to the harbor from SGD alone are 780mol d^{-1} (11kg d^{-1}), similar to average daily direct nitrogen inputs of 870mol d^{-1}(12 kg-N d^{-1}) from a nearby sewage treatment plant.

Introduction

Submarine groundwater discharge (SGD) is the discharge of groundwater across the sea floor, composed of both meteoric water from the inland, freshwater aquifers and recirculated seawater (Burnett et al., 2006, Slomp and Van Cappellen, 2004). Although freshwater contributions from SGD to the coastal ocean is estimated at only a few percent of total inputs (Burnett et al., 2006, Beck et al., 2008), SGD can carry significantly more nutrients than surface water loads (Santos et al., 2008b, Taniguchi et al., 2002).

Nitrogen flux to coastal waters in known to be a function of anthropogenic inputs (Howarth et al., 2002), with an estimated 15-45% of anthropogenic nitrogen inputs flowing towards the coast (Howarth, 2008). Groundwater is a primary sink of nitrogen entering the hydrosphere, with most models assuming denitrification along groundwater flowpaths to surface waters (Van Breemen et al., 2002, Valiela et al., 2000). Despite this, many studies have identified nitrogen loading to surface waters via SGD at single point locations within a coastal zone. Embayment and continental shelf estimates of SGD derived nitrogen loads are more difficult to obtain.

Nutrient loading to surface water via SGD have been estimated by multiplying average inland groundwater nutrient concentrations by freshwater underflow (Scorca and Monti, 2001, Gross et al., 1972), which neglects significant biogeochemical processing of nutrients in the coastal aquifer. These transformations, however, are known to be both a source and sink for nitrogen and phosphate (Kroeger and Charette, 2008, Charette et al., 2010, Santos et al., 2012). The use of nutrient concentrations in porewater of the stubterranean estuary (Moore, 1999), in conjunction with geochemical tracers of SGD, provide a better estimate of the total flux of nutrients from coastal aquifers to overlying surface waters (Santos et al., 2009). For example, increases in the fresh SGD fraction during rain events causes a substantial increase in N:P ratios which shifts surface waters towards P limitation in Trukean Swamp, Australia (Santos et al. 2009). Similar results are observed in Jamaica, where fresh groundwater inputs *via* SGD shift microalgae communities towards P limitation in a coral reef lined embayment (Lapointe, 1997). In Waquoit Bay, MA, representative groundwater DIN concentrations of fresh and circulated

porewater were used to characterize groundwater-derived nitrogen fluxes to be between 9.5-13 kg N d^{-1} during the summer months (Dulaiova et al. 2010). Beck et al. (2007) use shallow intertidal wells for calculating chemical fluxes of non-conservative elements at a similar study site in West Neck Bay, Long Island, NY, where nitrate flux was estimated to be $3.3x10^6$µmol d^{-1}.

The heterogeneous nature of SGD, even in systems with diffuse flow, makes direct measurements at the scale of individual embayments difficult. However, geochemical tracers have been used to provide estimates of average SGD. Radon (^{222}Rn), in particular, has been used as a geochemical tracer of total SGD in numerous settings. ^{222}Rn is highly enriched by three to four orders of magnitude in groundwater with respect to surface water; it has a short half-life of 3.8 days and it is non-reactive. Radon enters groundwater by recoil from the solid aquifer material, and as a result, it is present in both fresh groundwater and saline groundwater circulated through the coastal aquifer (Dulaiova et al., 2008). In systems lacking significant stream or river input, SGD is the only significant source of radon in surface waters. Continuous measurement of ^{222}Rn has been used successfully to qualitatively map the distribution of SGD along coastlines (Burnett et al., 2006). Recent investigations in two harbors in the Massachusetts, have demonstrated the ability of spatial surveys to provide quantitative information on the shoreline variation in SGD rates (Dulaiova et al., 2010).

Harbors and embayments comprise 30% of the total shoreline distance of Long Island Sound (LIS) and are particularly sensitive to nutrient loading as they experience concentrated human activity along their shorelines. Harbors may have longer flushing times because of restricted tidal exchange with the main body of the Sound through narrow inlets. Along the LIS's south shore, groundwater enters LIS harbors via surface water inputs and SGD (Scorca and Monti, 2001). Aquifers on Long Island are a thick sequence of unconsolidated sands and gravels; therefore SGD is a diffuse process that occurs along the entire southern shoreline. Within Port Jefferson Harbor, an embayment of Long Island Sound, diffuse SGD is often the only freshwater source, which, combined with long flushing times, acts to retain nonpoint-source, groundwater-derived nutrients within the embayment and may lead to surface water eutrophication. Studies of Northport Harbor, a LIS embayment, indicate that SGD carries nutrients from atmospheric inputs, agriculture and turf grass fertilizers and septic tank systems (Zhao et al., 2011).

In this study, measurements of the ^{222}Rn surface-water activity and of porewater nutrient concentrations were used to calculate the flux of nitrogen and phosphate from SGD into surface water of Port Jefferson Harbor. The goal of this study was 1) calculate the amount of SGD derived nitrogen entering the harbor and compare it with point source inputs and 2) use N:P ratios to quantify the relative contribution of freshwater SGD from various locations along the harbor shoreline. Previous investigations have combined radon and nitrogen surveys, providing a framework for interpreting the surface water distribution of these two solutes (Dulaiova et al., 2010, Null et al., 2011, Mwashote et al., 2013). Here, N:P ratios were used to advance the understanding of how SGD carries fractions of circulated seawater vs. fresh nutrients along harbor coastlines. I will show that areas of high SGD do not necessarily correspond to inputs of fresh-fractions of groundwater; nitrogen discharged under these conditions is largely recirculated. In these recirculation zones, which characterize a large portion of the shoreline, SGD is not a net source of nitrogen to the harbor.

Methods

Site Description

Port Jefferson Harbor is located on the North Shore of Long Island, NY, with direct connection to Long Island Sound through a 0.2km wide inlet (Figure 33). The harbor is 3.4km long and 1.3km wide. It is adjoined on its west shore to two small shallow bays; Setauket Harbor and Conscience Bay (Breslin and Sanudo-Wilhelmy, 1999). Port Jefferson Harbor has an average depth of 4.4m but contains a 7-9m deep dredged navigation channel oriented along the north-south harbor axis (Gross et al., 1972).

Port Jefferson Harbor rests on the Upper Glacial aquifer which is composed of glacially deposited, medium to coarse grained sand. Hydraulic conductivities in the Upper Glacial aquifer range 27 x 10^{-3} to 84 x 10^{-3} cm/s, with a 10:1 horizontal to vertical anisotropy (Buxton and Modica, 1992). Sediments in the northern half of the harbor are fine- to coarse -grain sanded with increasing proportion of fine grain sediments (<62μm) in the southern portion of the harbor. The exception is the western edge of the harbor, which is characterized by coarse sand, pebbles and cobbles (Bittner, 1997).

Previous investigations of Port Jefferson geomorphology indicate that the sediments were deposited during glacial retreat, forming the easternmost portion of the Harbor Hill Moraine (Bennington, 2003). Tunnel valleys, formed by subglacial melt water, trend north south along the north shore of Long Island, incising Harbor Hill moraine deposits. Tunnel valleys create steep topography in the watershed along the southeastern portion of Port Jefferson Harbor. In unconfined aquifers comprised of unconsolidated glacial sediments and the absence of clay lenses, water table elevation follows surface topography (Desbarats et al., 2002).

There is no existing data for direct deposition of nitrogen on water bodies on Long Island's north shore which includes Port Jefferson Harbor, however direct atmospheric deposition accounts for 26% of new nitrogen inputs to Great South Bay, located on Long Island's southern shore (Kinney and Valiela, 2011). Bowen and Valiela (2001) reported an atmospheric nitrogen deposition average of 10kg-N ha^{-1} y^{-1} for New England/Cape Cod area (Bowen and Valiela, 2001). Applying the area of Port Jefferson Harbor to this figure atmospheric nitrogen deposition is estimated to be 0.12kg-N d^{-1}. The Port Jefferson Sewage Treatment Plant is limited to 36.3kg-N d^{-1} and currently discharges an average of 12.2kg-N d^{-1}. In 2014 the total maximum daily load is intended to be lowered to 17.7kg-N d^{-1}. Previous estimates of SGD derived nitrogen inputs to Port Jefferson Harbor are 384kg-N d^{-1}(Koppelman, 1976), which was calculated using a hydrologic mass balance model which assigned inland groundwater nitrogen concentrations from inland wells to the fresh component of SGD entering the harbor.

Geochemical measurements and analysis

Two geochemical surveys were used to capture spatial distribution of SGD and porewater nutrient concentrations throughout the harbor. A porewater nutrient sampling survey was completed in June, 2012. The spatial survey of porewater nutrient concentrations was performed in order to calculate nutrient flux *via* SGD from the intertidal and sub-tidal zone. A Trident probe (Paulsen et al., 2001) was used to collect porewater from 60cm beneath the sediment-water interface. The Trident probe provides bulk conductivity and temperature measurements in addition to porewater samples. Bulk conductivity is directly related to porewater conductivity by

Archie's Law and was used to calculate salinity of porewater samples. Samples were analyzed in triplicate for dissolved nitrate ($NO_3^-+NO_2^-$) using a Lachat Quickchem 6000 series with a precision of ±5% for each sample (Strickland and Parsons, 1978). Ammonium (NH_4^+) and phosphate (PO_4^{-3}) were analyzed using standard colorimetric methods, with analytical precision of ±5% for NH_4^+ and ±3% for PO_4^{-3} (Johnson and Petty, 1982, Solorzano, 1969).

Continuous ^{222}Rn measurements were taken to determine the spatial distribution of SGD throughout the harbor during August 2012. Two RAD-7 (Durridge Co., Inc.) radon-in-air monitors equipped with a RAD-AQUA water- air exchanger attachment (Durridge Co., Inc) were used to measure ^{222}Rn activity *in-situ* (Dulaiova et al., 2005). Peristaltic pumps continuously pumped harbor water from a depth of 1m below the water surface from a slow moving vessel which remained within 5m of the shoreline, when its path was not obstructed by docks. Dissolved radon was de-gassed into a closed air loop, passed through two dessicant chambers (Drierite, W.A Hammond Co.) and fed into the RAD7 detection chamber. Alpha decay of ^{222}Rn to $^{218}Po^+$ was counted every 10 minutes. Temperature was monitored to determine ^{222}Rn activity in water, according to the Fitz-Weigel equation (Weigel, 1978):

$$^{222}Rn_{water} = {}^{222}Rn_{air} \text{ x } (0.105 + 0.405e^{-0.0502T}) \quad (1)$$

Where $^{222}Rn_{water}$ and $^{222}Rn_{air}$ are the activities of radon in water and air respectively and T is the temperature (^0C) recorded in the water-air exchanger. A Garmin GPS continuously recorded vessel position in order to determine the location of each reading. The two RAD7 machines were offset by 10 minutes to allow for a measurement every 5 minutes, which corresponded to an integrated measurement of near shore surface water every 200 to 250m of shoreline.

To determine ^{222}Rn activity of the groundwater endmember, porewater was collected from a shallow monitoring well located in the southeast corner of the harbor (Figure 33). The well is located at mean low-tide and screened at a depth of 1m beneath the sediment surface with a 5cm screen length. Previous sampling of this well indicated the presence of fresh groundwater with an average salinity of 0.14ppt. A peristaltic pump was used to draw a continuous flow of groundwater into a RAD7 machine as described above and ^{222}Rn measurements were collected for 2 hours during ebb-low tide. Analytical precision for these measurements is ±10%.

Results and Discussion

Calculation of SGD Rates

Each point in the ^{222}Rn spatial survey was treated as a discrete SGD rate according to equation 2 with total SGD respectively calculated from equation 3;

$$SGD_{discrete} = \frac{Rn_{cw}}{Rn_{gw}} \quad (2)$$

$$SGD_{total} = \frac{Rn_{cw}}{Rn_{gw}} * A \quad (3)$$

Where SGD_{total} is the volume of discharge for each segment of coastline, Rn_{cw} is the activity of radon in the coastal water (dpm m^{-2} d^{-1}) Rn_{gw} is the activity of radon in the groundwater end

member (dpm m^{-3}) and A is the area of the coastline representative of the integrated ^{222}Rn measurement (m^2).

The area, A, was the product of a shoreline length times the width of the intertidal zone. The length (long-shore) distance of each discharge polygon is the half-way point between ^{222}Rn measurements. In this case, lengths varied between 200-250m, depending on the shoreline typology. The width (intertidal) distance of the discharge polygon is equal to 19m, half of the mean intertidal zone (22m) plus 8m of sub tidal sediments. This distance was chosen because SGD is known to primarily occur at or near low tide (Robinson et al., 2007b) and additional work at two sites along the south and eastern coasts of the harbor indicate freshwater discharge from sand starting at the mid-tide point (Young et al., in prep). Results from a harbor wide Trident survey (Table 12) indicated that sand extended no further than 8m beyond mean low tide. Offshore, the harbor bottom consists of silt/mud size sediments, characteristic of other harbor bottoms adjacent to Long Island Sound (Gregorcyk and Hill, 2013).

The terms within equation 2 were calculated using the methods outlined by Dulaiova et al (2010) and Burnett and Dulaiova (2003). Each individual Rn_{cw} measurement was representative of a coastline segment and corrected for non-SGD components according to the following method.

- Excess ^{222}Rn is the difference between ^{222}Rn measured and the dissolved parent ^{226}Ra produced in the water column. Measurements of ^{226}Ra in Smithtown Bay and Port Jefferson Harbor that were taken in summer (2010) averaged 1000dpm m^{-3}. This value was used to calculate excess ^{222}Rn for each measurement in the spatial survey (Kirk Cochran, Stony Brook University 2013, unpublished data).

$$Excess\ ^{222}Rn = Rn_{\ total}(dpm\,L^{-1}) - ^{226}Ra\ (dpm\,L^{-1}) \qquad (4)$$

  Where Rn_{total} was each measurement taken during the survey and ^{226}Ra was the concentration of Radium measured in Smithtown Bay water column samples.

- Diffusive radon flux from the sediments has been shown to be low in sediments from Long Island Sound. Indeed, previous authors found this component accounted for less than 3% of the total radon flux to overlying water in harbor settings of Massachusetts (Dulaiova et al., 2010, Gonneea et al., 2008)). As we have no experimental data of sediment ^{222}Rn from Port Jefferson Harbor, this term was neglected.
- Losses of Radon due to water column radioactive decay to daughter products were corrected for by first multiplying the excess ^{222}Rn concentration by the water column depth during survey, and then multiplying this factor by the decay constant according to (5),

$$Rn_{cw}\ (dpm\,m^{-2}\ d^{-1}) = Excess\ ^{222}Rn\ (dpm\,m^{-3}) * wc\ depth\ (m) * \lambda \qquad (5)$$

  Where "wc depth" is the depth of the water column during sampling, taken as 2.5m which was estimated to be the average water column depth during the shoreline portion of the survey and λ is the decay constant of ^{222}Rn (0.18 d^{-1}).

- Atmospheric losses were calculated from wind speed measurements made during the survey, which was measured to be 2.2m s^{-1} using a handheld anemometer. Losses of ^{222}Rn are calculated *via* an empirical relationship (Burnett and Dulaiova, 2003) described by (6).

$$Atmospheric\ Rn = k * (Excess\ ^{222}Rn\ (dpm\ m^{-3}) - (\alpha * Rn_{air}\ \ (dpm\ m^{-3}))) \qquad (6)$$

Where k is the gas transfer coefficient, dependent on kinematic viscosity, molecular diffusion, turbulence and wind speed (Macintyre et al., 1995) and α is Oswald's solubility coefficient, calculated at 22^0C for this survey. Atmospheric ^{222}Rn (Rn_{air}) was measured before and after the spatial survey.

Groundwater radon activities in the coastal aquifer can vary significantly due to radioactive disequilibrium between the sediments and rapidly moving porewater. In the coastal aquifer surrounding Port Jefferson Harbor, radon concentrations in porewater were measured at a depth of 3.2m to be about four times higher than activities at 0.5m depth. At depths of both 0.5 and 3.2m, salinity was less than 2ppt; therefore radon depletion in shallow porewater was not due to saltwater recirculation, but likely due instead to a short porewater residence time. Shallow porewater, at 0.5m depth, represented the water nearest to discharge into the harbor. Therefore, the groundwater end member, Rn_{gw}, concentration was measured at 0.5m beneath the sediment surface, sampled at low tide, with six readings averaged to an endmember Rn_{gw} activity of 92,000 dpm m^{-3}.

Total Harbor SGD

Along the shoreline, excess radon, as calculated from equation 4, ranges 0.7 to 26.8 $dpmL^{-1}$ for the entire harbor survey (Figure 34a). Calculated $SGD_{discrete}$ for the harbor shoreline range 2.5 to 13.2 cmd^{-1}, (Figure 34b). SGD rates taken more than 1000m from the nearest shoreline ranged 1.2 to 2.4cmd^{-1}. These offshore values reflect the relatively long residence time of water within the harbor (Rose, 2011). As Port Jefferson Harbor is connected to Long Island Sound via Smithtown Bay through a narrow channel, residence time with in the harbor is estimated to be 20 days (Rose, 2011). Further, harbor geometry prevents calculation of decreased discharge from shore, as the SGD from all shorelines mix during counter-clockwise water circulation. The highest values of calculated SGD rate, from 10cmd^{-1} to 13cmd^{-1}, were found in the southeastern shoreline, with a pattern of decreasing SGD rate calculated for northeast and northwest shoreline segments (Figure 34).

Calculations of $SGD_{discrete}$ were used to determine SGD_{total} for each ^{222}Rn measurement, according to equation 3. SGD total ranged from 50 to 1400m^3d^{-1} with maximum discharge in the southern and southeastern portion of the harbor (Figure 35). The SGD_{total} for the entire shoreline area was estimated to be 9300 m^3d^{-1}. This value is only 25% of earlier estimates where total SGD was calculated using a mass balance method applied to the entire harbor (Gross et al., 1972), which found 38,356m^3d^{-1} SGD to Port Jefferson Harbor. The earlier estimate was calculated using a mass balance for the entire basin, including discharge through the mud sediment layer that covers the offshore portion of the harbor As the focus of this study was to understand how nitrate enters the harbor via SGD, discharge through the mud sediment zone was not included in calculations here.

During offshore SGD, the mud layer acted as an aquitard and decreased flow rates by at least an order of magnitude, as recorded using a series of manual seepage meters at this site in 2011. In addition, nitrate is expected to undergo denitrification of about 60% during transit from underlying sand sediments to the overlying mud layer, ((Nowicki et al., 1997). As a result of these uncertainties, our estimate of total SGD is a conservative one but it accounted for the majority of nutrient-bearing fresh groundwater inputs to the harbor.

Salinity, Nitrate and Phosphate distribution

The survey of salinity, nitrate and phosphate distribution along the harbor shoreline indicated freshwater inputs were concentrated in the southeastern and southern shore of the harbor. Porewater salinity ranged from 31 to 35 in the northern portion of the harbor with values decreasing to a minimum of 0.15 in the southeast corner of the harbor (Figure 32a).

Nitrate concentrations did not show a distinct correlation with salinity, as shown in Figure 36. At the sample depth (60cm) fresh groundwater from deeper in the coastal aquifer had apparently undergone mixing with overlying water in highly permeable sediments. Therefore, concentrations recorded at this depth are representative of nitrate concentrations discharging into the open water. Porewater nitrate concentrations ranged from 2.9µmol L^{-1} to 265.8µmol L^{-1}. The lower concentrations (0-24.3µmol L^{-1}) were found in the northern and western portion of the harbor (Figure 37b). Nitrate concentrations were consistently higher in samples from the inner harbor. In the southeast corner of the harbor, maximum concentrations of 270µmol L^{-1} were recorded. Porewater nitrate concentrations along the east shore varied by as much as 152µmol L^{-1} over a 500-m shore segment. Shoreline structures prevented sampling in the southwest corner of the harbor. As a result, the analysis of nitrate inputs from the coastal aquifer did not include this zone of the inner harbor.

Phosphate concentrations were substantially lower than nitrate concentrations for the entire survey, ranging 0.01-36.2µmol L^{-1} (Figure 37c). When compared to salinity and nitrate, porewater phosphate concentrations did not show a recognizable pattern. Low concentrations tended to be found along the eastern and northwestern shore. Slightly higher (~3µmol L^{-1}) concentrations were observed in the northeastern corner of the harbor. The highest recorded value was 36µmol L^{-1}, on the eastern shore adjacent to porewater concentrations ~0.01 µmol L^{-1} suggesting a local, isolated source.

SGD derived nutrient flux

SGD derived nutrient inputs *via* SGD to the harbor were estimated by multiplying the nearest nutrient concentration to the radon-derived groundwater discharge (SGD_{total}) for each shoreline segment. Calculated nitrate discharge ranged from 0.5 to 220mol d^{-1} per segment (Figure 38a). This corresponded to a total nitrate discharge for the entire harbor of 800mol d^{-1}(11kg NO_3^--N d^{-1}). The calculation accounted only for nitrate discharged from the shore, and not nitrogen inputs of NH_4^+ or DON. Previously, Gross et al. (1972) had estimated that 26,300mol d^{-1} (369kg-N d^{-1}) of SGD driven nitrogen enters Port Jefferson Harbor, which is significantly higher than the estimate made here using a combination of surface water radon and porewater nitrate concentrations. This difference may be due to three factors. First, Gross et al. (1972) used average nitrogen concentration from inland wells, where nitrate concentrations were several times higher than those recorded in the near shore environment (Young et al., 2013). Second, total discharge estimated by hydrologic mass balance (Gross et al. 1972) was four-times greater than SGD estimated here from the radon measurements. Finally, although groundwater

studies of Long Island's north shore Upper Glacial Aquifer indicate nitrogen exists as nitrate, due to high dissolved oxygen in the system (Scorca and Monti, 2001, Munster, 2004, Zhao et al., 2011, Young et al., 2013), Gross et al., (1972) presents a calculation for all nitrogen species, whereas our study only addresses inputs of nitrate.

Phosphate discharge ranged up to 22mol d^{-1} for individual shoreline segments, with a total estimated phosphate discharge of 55.4mol d^{-1} for the entire shoreline (Figure 38b). Phosphate did not have a direct relationship with excess ^{222}Rn concentration (Figure 38d). Given this, nitrogen to phosphate ratios were used to determine if areas of freshwater input, as indicated by low salinity, coincide with N:P ratios in excess of the Redfield ratio (Slomp and Van Cappellen, 2004).

In this way, SGD was linked to nutrient ratios in shallow porewaters (Figure 39). Radon was significantly correlated with nitrogen to phosphate ratios ($p = 0.03$), which range .004 to 11,992 for the entire survey. Plots of radon with nitrate (Figure 38c), phosphate (Figure 38d) and N:P (Figure 39) ratios imply there were three mechanisms that affected porewater nutrient concentrations: (1) in-mixing of groundwater rich SGD, (2) addition of recirculated seawater SGD, and (3) consumption and/or degradation of overlying water nutrients.

(1) Fresh groundwater-rich SGD is characterized by elevated NO_3^- concentrations and excess ^{222}Rn, porewater nitrate is weakly correlated to excess ^{222}Rn activity (R^2=0.44, Figure 38c), and to a lesser extent salinity (R^2= 0.28, Figure 36). N:P ratios in the southern portion of the harbor ranged from 30 to 11,992, N: P ratios were significantly higher in the southern portion than those in the northeast and northwest portions. Porewater salinity ranged from 4.4 to 7.8, indicating that SGD was comprised of primarily fresh groundwater, with a flux zone centered at the head of the harbor where inland topography coupled with high-density housing drive freshwater nitrate inputs to the harbor (Figure 37a). In this geological setting, increased freshwater inputs to Port Jefferson Harbor were likely the result of tunnel-valley structures that produce large hydraulic gradients in the southern watershed of the harbor (Bennington, 2003, Mulch and Hanson, 2010). Fresh groundwater in the south and eastern shore of Port Jefferson Harbor comes from areas with a population density ranging 4-7 people km^{-2}, as compared to a population density of 0-3 people per $4x10^{-3}km^2$ on the western shore according to the Suffolk County Comprehensive Plan 2035(Levy, 2011). Lower porewater nitrate concentrations on this shoreline were likely caused by the lower population density in this region. In Suffolk County, about 70% of homes contain onsite wastewater systems (i.e septic tank/cesspools) which create multiple, point-source nitrogen plumes in shallow groundwater (Koppelman, 1978). Previous investigators have found that on site wastewater system density, functionality and distance from shore controls nitrogen loading to adjacent coastal water bodies (Meile et al., 2010, Lu et al., 2008). In the case of Port Jefferson Harbor, porewater nitrate spatial patterns and population density suggest anthropogenic nitrogen sources for SGD nitrate loading in the southern portion of the harbor.

(2) Circulated seawater SGD contains elevated levels of excess ^{222}Rn but low nitrate. Previous investigators have observed a correlation between high excess ^{222}Rn and low nitrate and salinity in marshes and enclosed bays (Stieglitz et al., 2010). In cases of

enclosed bays with permeable sands, circulated seawater tidally pumped through the beach is enriched in excess ^{222}Rn when compared to open coastal systems. The northeastern portion of Port Jefferson Harbor is comprised of a small enclosed bay, which contains elevated excess ^{222}Rn, porewater salinity ~30-33 and low porewater nitrate concentrations lending support to the hypothesis that fresh SGD is limited in these instances (Figure 37a,b). Further, in this area N:P ratios ranged 3.6-8.5 indicating phosphate inputs increased in this portion of the harbor, while nitrate inputs decreased. Phosphate remineralization during seawater recirculation occurs in tidally dominated sands (Billerbeck et al., 2006) due to organic carbon breakdown during tidal exposure. Due to high salinity in the northeastern shoreline of the harbor, nitrate was most likely derived from seawater and atmospheric deposition, with possible consumption of nitrogen from the recirculated seawater.

(3) Finally, areas of low excess ^{222}Rn were found in conjunction with low nitrate concentrations and low N:P ratios. Porewater from the north and northwestern shore of Port Jefferson Harbor contained N:P ratios ranging 1.8 to 13.2, below the expected Redfield ratio. Salinity in these samples ranged 30 to 34, therefore it is likely that nutrients are derived from overlying water. The low N:P ratios, combined with limited excess ^{222}Rn indicated that nutrients derived from either infiltrating seawater or sediment remineralization are consumed *in situ.* Restricted flow through sediments in similar settings is known to cause hypoxia in porewater which can lead to oxygen depletion of tidally pumped overlying water and reducing conditions in the upper 60cm of sediment (Santos et al., 2009, Slomp and Van Cappellen, 2004).

Ammonium was present at low concentrations (<15µmol L^{-1}) in most samples, but it was not positively correlated with salinity or excess ^{222}Rn. The fact that ~90% of samples (Figure 40) contained both nitrate and ammonium indicated chemical disequilibrium of discharging SGD, a nitrogen cycling behavior that was observed in coastal aquifers of Cape Cod (Kroeger and Charette, 2008). In Long Island groundwater, ammonium concentrations are typically less than detection limits, due to highly oxidizing conditions in the vadose zone and Upper Glacial Aquifer. As a result, ammonium in porewater samples may have been derived either from production in overlying water or from nutrient remineralization of muddy offshore sediments, and would not have contributed new nitrogen load to the overlying water.

Conclusion

In Port Jefferson Harbor nitrate inputs from SGD_{total} were estimated to be 800mol d^{-1} (11kg d^{-1}). Although this estimate is restricted to shoreline discharges of nitrate and does not account for input entering the harbor through offshore mud sediments, it is similar to the nitrogen input to the harbor from the Port Jefferson Sewage Treatment Plant (STP). Estimates of nitrate input to Port Jefferson Harbor (this study) are ~1.2% of total SGD nitrogen inputs to Long Island Sound from all of Suffolk County (Scorca and Monti, 2001). Three modes of nutrient additions were observed in the correlation between N:P ratios and excess ^{222}Rn which indicate the bulk of new nitrogen enters the harbor in the southernmost end, which contains the highest watershed housing density. Findings from this study indicate that coupling of shallow porewater nutrient concentrations with surface water ^{222}Rn concentrations is a rapid and effective way to identify areas of SGD nutrient loading. Although more labor intensive than coupled nutrient and ^{222}Rn surface water surveys, the method developed in here is favorable in systems that undergo surface water inputs, such as those from sewage treatment plants. The use of porewater nutrient

concentrations instead of surface water concentrations avoids issues mixing and harbor circulation patterns and yields useful spatial maps of SGD derived nutrients.

References

BECK, A. J., RAPAGLIA, J. P., COCHRAN, J. K., BOKUNIEWICZ, H. J. & YANG, S. 2008. Submarine groundwater discharge to Great South Bay, NY, estimated using Ra isotopes. *Marine Chemistry,* 109**,** 279-291.

BECK, A. J., TSUKAMOTO, Y., TOVAR-SANCHEZ, A., HUERTA-DIAZ, M., BOKUNIEWICZ, H. J. & SANUDO-WILHELMY, S. A. 2007. Importance of geochemical transformations in determining submarine groundwater discharge-derived trace metal and nutrient fluxes. *Applied Geochemistry,* 22**,** 477-490.

BENNINGTON, B. 2003. NEW OBSERVATIONS ON THE GLACIAL GEOMORPHOLOGY OF LONG ISLANDFROM A DIGITAL ELEVATION MODEL (DEM). *Long Island Geologists Conference.* Stony Brook, NY.

BILLERBECK, M., WERNER, U., BOSSELMANN, K., WALPERSDORF, E. & HUETTEL, M. 2006. Nutrient release from an exposed intertidal sand flat. *Marine Ecology Progress Series,* 316**,** 35-51.

BITTNER, H. 1997. *Characterization of Port Jefferson Harbor Sediments using a recoverable bottom penetrometer.* Ph.D, Stony Brook University, School of Atmospheric and Marine Sciences.

BOWEN, J. L. & VALIELA, I. 2001. Historical changes in atmospheric nitrogen deposition to Cape Cod, Massachusetts, USA. *Atmospheric Environment,* 35**,** 1039-1051.

BRESLIN, V. T. & SANUDO-WILHELMY, S. A. 1999. High spatial resolution sampling of metals in the sediment and water column in Port Jefferson Harbor, New York. *Estuaries,* 22**,** 669-680.

BURNETT, W. C., AGGARWAL, P. K., AURELI, A., BOKUNIEWICZ, H., CABLE, J. E., CHARETTE, M. A., KONTAR, E., KRUPA, S., KULKARNI, K. M., LOVELESS, A., MOORE, W. S., OBERDORFER, J. A., OLIVEIRA, J., OZYURT, N., POVINEC, P., PRIVITERA, A. M. G., RAJAR, R., RAMASSUR, R. T., SCHOLTEN, J., STIEGLITZ, T., TANIGUCHI, M. & TURNER, J. V. 2006. Quantifying submarine groundwater discharge in the coastal zone via multiple methods. *Science of the Total Environment,* 367**,** 498-543.

BURNETT, W. C. & DULAIOVA, H. 2003. Estimating the dynamics of groundwater input into the coastal zone via continuous radon-222 measurements. *Journal of Environmental Radioactivity,* 69**,** 21-35.

BUXTON, H. T. & MODICA, E. 1992. PATTERNS AND RATES OF GROUNDWATER-FLOW ON LONG-ISLAND, NEW-YORK. *Ground Water,* 30**,** 857-866.

CHARETTE, M., BREIER, C., DULAIOVA, H., GONNEEA, M., HENDERSON, P., KROEGER, K., MULLIGAN, A., RAO, A. & SLOMP, C. 2010. Nutrient biogeochemistry in permeable sediments impacted by submarine groundwater discharge. *Geochimica Et Cosmochimica Acta,* 74.

DESBARATS, A. J., LOGAN, C. E., HINTON, M. J. & SHARPE, D. R. 2002. On the kriging of water table elevations using collateral information from a digital elevation model. *Journal of Hydrology,* 255**,** 25-38.

DULAIOVA, H., CAMILLI, R., HENDERSON, P. B. & CHARETTE, M. A. 2010. Coupled radon, methane and nitrate sensors for large-scale assessment of groundwater discharge and non-point source pollution to coastal waters. *Journal of Environmental Radioactivity,* 101**,** 553-563.

DULAIOVA, H., GONNEEA, M. E., HENDERSON, P. B. & CHARETTE, M. A. 2008. Geochemical and physical sources of radon variation in a subterranean estuary - Implications for groundwater radon activities in submarine groundwater discharge studies. *Marine Chemistry,* 110**,** 120-127.

DULAIOVA, H., PETERSON, R., BURNETT, W. C. & LANE-SMITH, D. 2005. A multi-detector continuous monitor for assessment of Rn-222 in the coastal ocean. *Journal of Radioanalytical and Nuclear Chemistry,* 263**,** 361-365.

GONNEEA, M. E., MORRIS, P. J., DULAIOVA, H. & CHARETTE, M. A. 2008. New perspectives on radium behavior within a subterranean estuary. *Marine Chemistry,* 109**,** 250-267.

GROSS, W., GRANT, M., DAVIES, D. & LIN, P. 1972. Characteristics and Environmental Quality of Six North Shore Bays, Nassau and Suffolk Counties, Long Island, New York. *In:* CENTER, M. S. R. (ed.) *Technical Report.* Stony Brook, NY: State University of New York.

JOHNSON, K. S. & PETTY, R. L. 1982. Determination of Phosphate in Sea-Water by Flow Injection Analysis with Injection of Reagent. *Analytical Chemistry,* 54**,** 1185-1187.

KINNEY, E. L. & VALIELA, I. 2011. Nitrogen Loading to Great South Bay: Land Use, Sources, Retention, and Transport from Land to Bay. *Journal of Coastal Research,* 27.

KOPPELMAN, L. 1976. ***The Urban sea: Long Island Sound****,* New York, Praeger.

KOPPELMAN, L. 1978. The Long Island comprehensive waste treatment management plan: Hauppauge, Long Island Regional Planning Board.

KROEGER, K. D. & CHARETTE, M. A. 2008. Nitrogen biogeochemistry of submarine groundwater discharge. *Limnology and Oceanography,* 53**,** 1025-1039.

LAPOINTE, B. E. 1997. Nutrient thresholds for bottom-up control of macroalgal blooms on coral reefs in Jamaica and southeast Florida. *Limnology and Oceanography,* 42**,** 1119-1131.

LU, Y., TANG, C., CHEN, J. & SAKURA, Y. 2008. Impact of septic tank systems on local groundwater quality and water supply in the Pearl River Delta, China: case study. *Hydrological Processes,* 22**,** 443-450.

MACINTYRE, S., WANNINKHOF, R. & J.P, C. 1995. **Trace gas exchange across the air-sea interface in freshwater and coastal marine environments**. *In:* MATSON, P. A. & R.C, H. (eds.) *Biogenic Trace Gases: Measuring Emissions from Soil and Water.* Blackwell Science Ltd.

MEILE, C., PORUBSKY, W. P., WALKER, R. L. & PAYNE, K. 2010. Natural attenuation of nitrogen loading from septic effluents: Spatial and environmental controls. *Water Research,* 44**,** 1399-1408.

MICHAEL, H. A., MULLIGAN, A. E. & HARVEY, C. F. 2005. Seasonal oscillations in water exchange between aquifers and the coastal ocean. *Nature,* 436**,** 1145-1148.

MULCH, D. & HANSON, G. 2010. Port Jefferson Geomorphology *Geology of Long Island and Metropolitan New York.* Stony Brook University.

MUNSTER, J. 2004. *Evaluating Nitrate Sources in Suffolk County groundwater, Long Island, New York.* M.S., SUNY Stony Brook.

MWASHOTE, B. M., MURRAY, M., BURNETT, W. C., CHANTON, J., KRUSE, S. & FORDE, A. 2013. Submarine groundwater discharge in the Sarasota Bay system: Its assessment and implications for the nearshore coastal environment. *Continental Shelf Research,* 53**,** 63-76.

NOWICKI, B. L., REQUINTINA, E., VANKEUREN, D. & KELLY, J. R. 1997. Nitrogen losses through sediment denitrification in Boston Harbor and Massachusetts Bay. *Estuaries,* 20**,** 626-639.

NULL, K. A., CORBETT, D. R., DEMASTER, D. J., BURKHOLDER, J. M., THOMAS, C. J. & REED, R. E. 2011. Porewater advection of ammonium into the Neuse River Estuary, North Carolina, USA. *Estuarine Coastal and Shelf Science,* 95**,** 314-325.

PAULSEN, R. J., SMITH, C. F., O'ROURKE, D. & WONG, T. F. 2001. Development and evaluation of an ultrasonic ground water seepage meter. *Ground Water,* 39**,** 904-911.

ROBINSON, C., LI, L. & BARRY, D. A. 2007. Effect of tidal forcing on a subterranean estuary. *Advances in Water Resources,* 30.

ROSE, P. 2011. *Medically-derived ^{131}I as a tracer in aquatic environments.* Ph.D, Stony Brook University.

SANTOS, I. R., BURNETT, W. C., DITTMAR, T., SURYAPUTRA, I. & CHANTON, J. 2009. Tidal pumping drives nutrient and dissolved organic matter dynamics in a Gulf of Mexico subterranean estuary. *Geochimica Et Cosmochimica Acta,* 73**,** 1325-1339.

SANTOS, I. R., COOK, P. L. M., ROGERS, L., DE WEYS, J. & EYRE, B. D. 2012. The "salt wedge pump": Convection-driven pore-water exchange as a source of dissolved organic and inorganic carbon and nitrogen to an estuary. *Limnology and Oceanography,* 57**,** 1415-1426.

SANTOS, I. R., MACHADO, M. I., NIENCHESKI, L. F., BURNETT, W., MILANI, I. B., ANDRADE, C. F. F., PETERSON, R. N., CHANTON, J. & BAISCH, P. 2008. Major ion chemistry in a freshwater coastal lagoon from southern Brazil (Mangueira Lagoon): Influence of groundwater inputs. *Aquatic Geochemistry,* 14**,** 133-146.

SCORCA, M. & MONTI, J. 2001. Estimates of Nitrogen Loads Entering Long Island Sound from Ground Water and Streams on Long Island, New York, 1985-96. *In:* INVESTIGATION, W. R. (ed.). Troy, NY: U.S Geological Survey.

SLOMP, C. P. & VAN CAPPELLEN, P. 2004. Nutrient inputs to the coastal ocean through submarine groundwater discharge: controls and potential impact. *Journal of Hydrology,* 295**,** 64-86.

SOLORZANO, L. 1969. Determination of Ammonia in Natural Waters by Phenolhypochlorite Method. *Limnology and Oceanography,* 14**,** 799-&.

STIEGLITZ, T. C., COOK, P. G. & BURNETT, W. C. 2010. Inferring coastal processes from regional-scale mapping of (222)Radon and salinity: examples from the Great Barrier Reef, Australia. *Journal of Environmental Radioactivity,* 101**,** 544-552.

STRICKLAND, J. & PARSONS, T. 1978. *A practical handbook of seawater analysis,* Ottowa, Fisheries Research Board of Canada.

TANIGUCHI, M., BURNETT, W. C., CABLE, J. E. & TURNER, J. V. 2002. Investigation of submarine groundwater discharge. *Hydrological Processes,* 16**,** 2115-2129.

WEIGEL, V. F. 1978. Radon. *Chemiker Zeitung,* 102**,** 287-299.

WILSON, J. & ROCHA, C. 2012. Regional scale assessment of Submarine Groundwater Discharge in Ireland combining medium resolution satellite imagery and geochemical tracing techniques. *Remote Sensing of Environment,* 119**,** 21-34.

YOUNG, C., KROEGER, K. & HANSON, G. 2013. Limited denitrification in glacial deposit aquifers having thick unsaturated zones (Long Island, USA). *Hydrogeology Journal*.

ZHAO, S., ZHANG, P., CRUSIUS, J., KROEGER, K. D. & BRATTON, J. F. 2011. Use of pharmaceuticals and pesticides to constrain nutrient sources in coastal groundwater of northwestern Long Island, New York, USA. *Journal of Environmental Monitoring,* 13.

Tables and Figures

Table 12 Salinity, pH and nutrient concentrations of porewater taken from 60cm beneath the sediment water interface using a Trident probe. Data collected in March 2012. ND indicates no data available.

Trident Point	Latitude	Longitude	salinity	pH	PO_4^{-3} (µmol L^{-1})	NH_4^{+} (µmol L^{-1})	NO_3^{-} (µmol L^{-1})
47	40.95169	-73.096	6.1	6.8	1.2	0.8	0.0
49	40.95106	-73.0964	2.9	6.9	2.2	4.0	0.0
53	40.95686	-73.0916	35.6	6.5	1.0	1.6	12.8
55	40.95422	-73.0858	33.7	6.8	4.8	0.5	9.0
65	40.95322	-73.0819	29.2	6.9	2.1	1.1	24.3
71	40.95225	-73.0679	26.7	6.0	2.9	0.9	50.3
79	40.96164	-73.0751	18	7.0	2.4	0.8	14.4
81	40.96536	-73.0779	34.4	7.3	1.6	1.9	2.9
83	40.96861	-73.0738	34.9	7.3	1.7	1.0	7.1
85	40.96097	-73.0748	33	7.0	5.2	0.5	8.2
87	40.96094	-73.0749	34.7	7.4	1.0	0.2	8.5
89	40.95075	73.06733	32.8	6.8	1.8	3.3	14.2
91	40.95075	-73.0673	7.8	7.0	4.0	1.0	265.6
93	40.95081	-73.0674	4.4	7.1	5.2	0.0	156.6
53B	40.95789	-73.0727	35.9	6.8	36.2	15.0	0.0
79B	40.96158	-73.0752	26.6	6.6	0.7	3.9	8.0
81B	40.96531	-73.078	32.3	7.3	1.7	9.4	10.9
83B	40.96997	-73.0746	32.5	6.8	2.1	0.0	8.0
85B	40.96861	-73.0739	34	6.8	2.5	0.7	21.0
77	40.95828	-73.0728	24.5	6.6	0.0	0.0	119.9
53C	40.95667	-73.091	33	7.1	ND	ND	ND
101	40.95678	-73.0885	27	6.7	ND	ND	ND
102	40.95603	-73.0713	18	6.8	ND	ND	250.8
103	40.95469	-73.0708	21.7	6.9	ND	ND	ND

Figure 33 Study area of Port Jefferson Harbor (bottom). Location of New York state (top left) and Long Island (top right) given for reference.

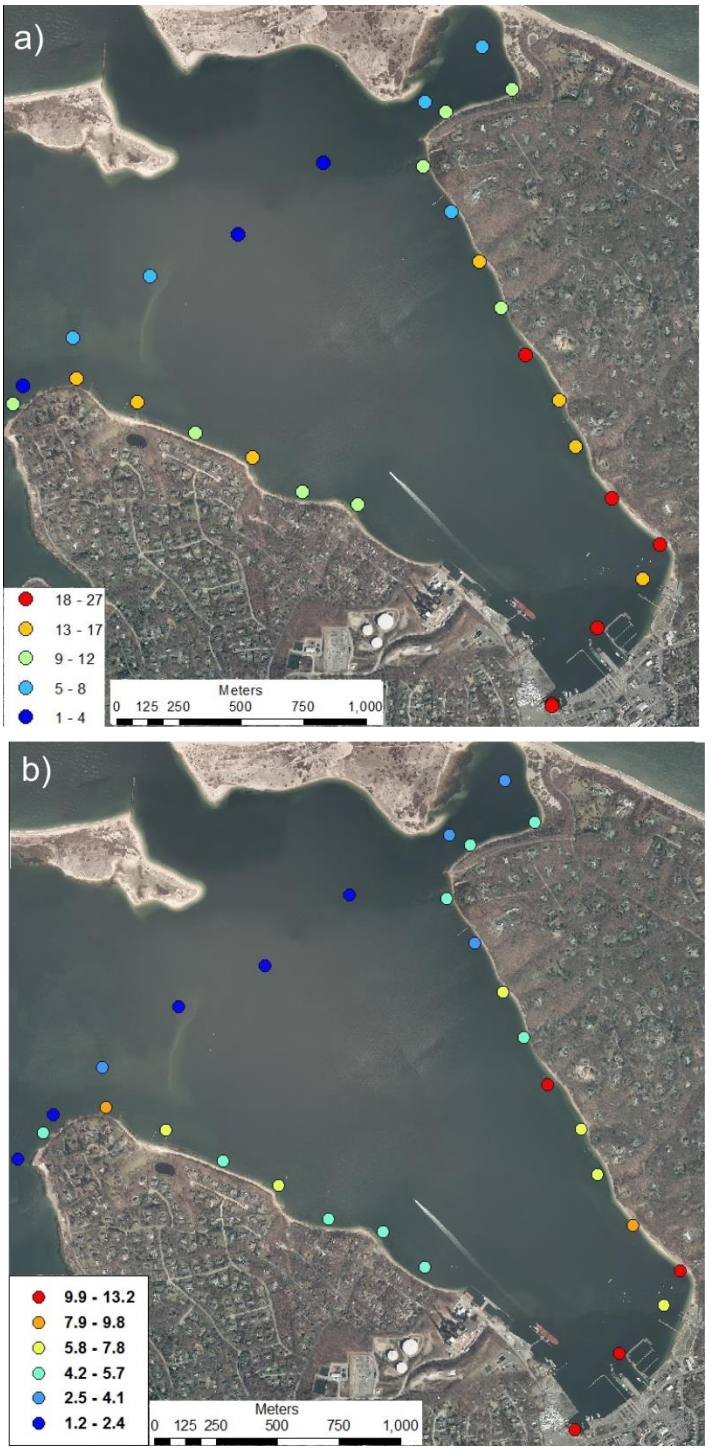

Figure 34 Spatial distribution of a) excess ^{222}Rn (dpm L^{-1}) and b) $SGD_{discrete}$ as calculated using equations 2-6.

Figure 35 SGD_{total} for harbor shoreline. Each polygon represents the half-way point between radon measurements, and is comprised of 11m of intertidal area plus 9m of sub-tidal area.

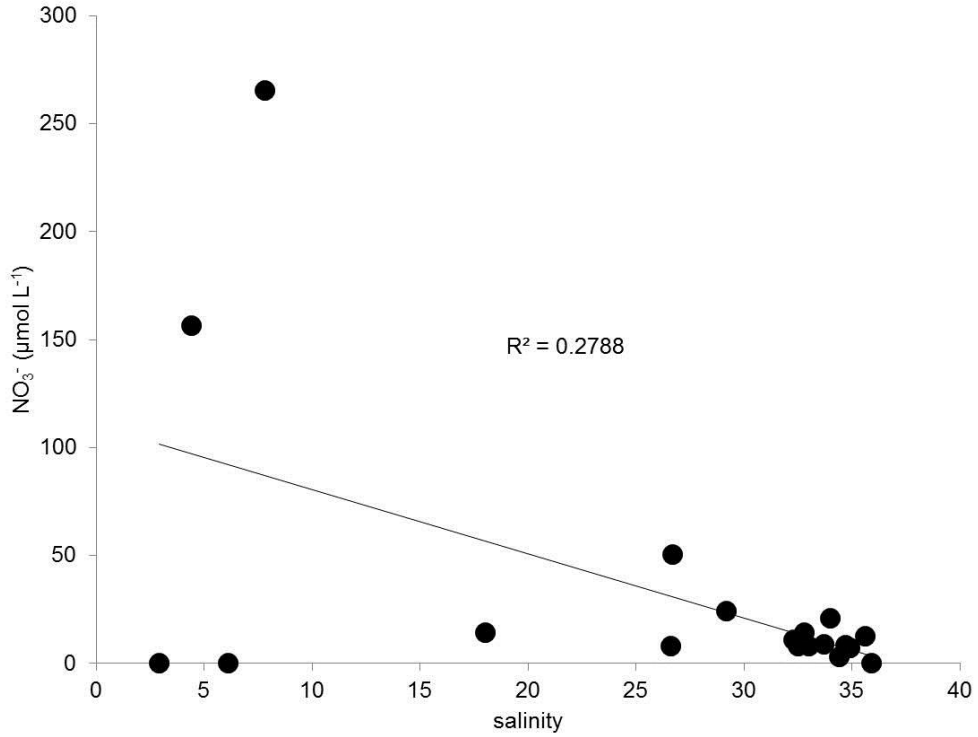

Figure 36 Relationship between porewater salinity and nitrate concentrations. All samples taken from 60cm beneath the sediment water interface

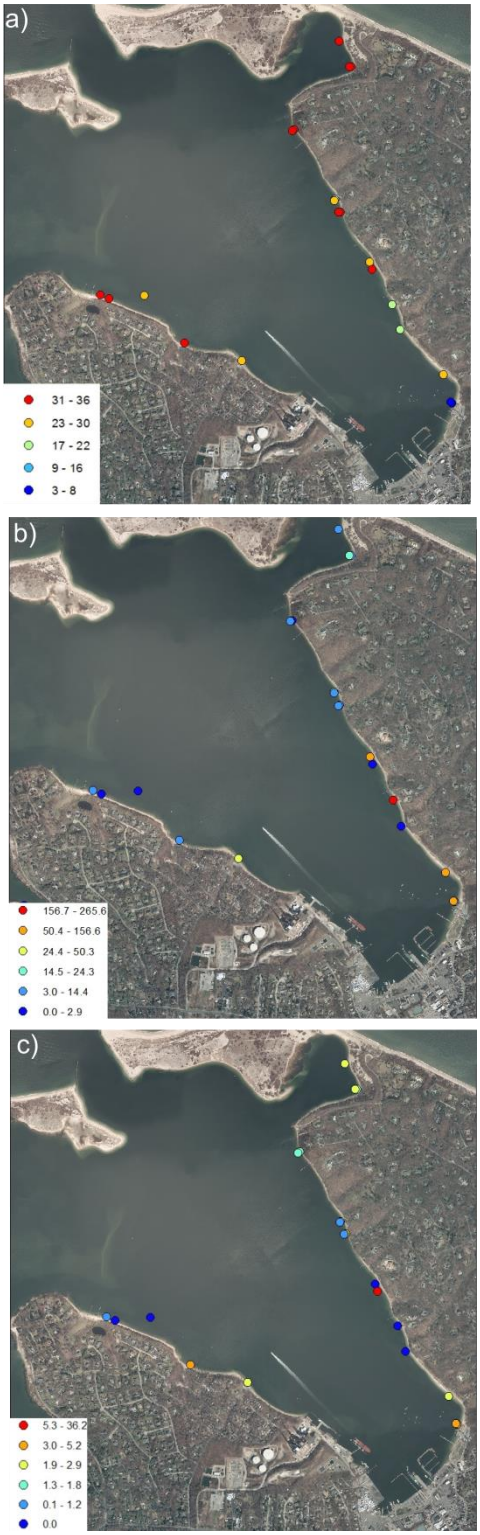

Figure 37 Spatial distribution of porewater salinity (a, ppt), nitrate (b, µmol L^{-1}) and phosphate (c, µmol L^{-1}).

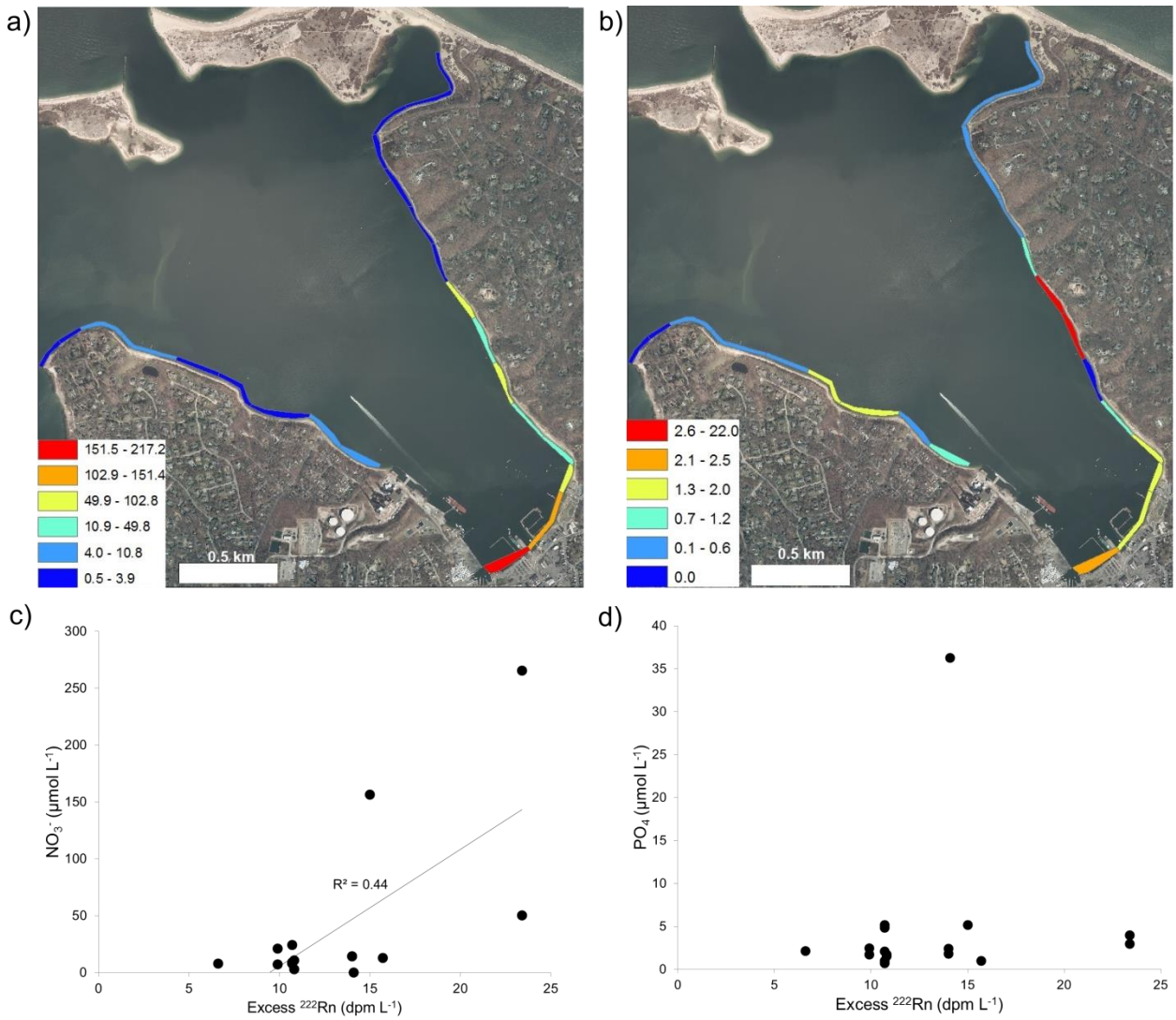

Figure 38 Total discharge of nitrate (a) and phosphate (b) for shoreline segments, as shown in Figure 35. Relationship between excess ^{222}Rn and nitrate (c) and phosphate (d) indicate nitrate is correlated with SGD while no direct links exist between phosphate and excess ^{222}Rn .

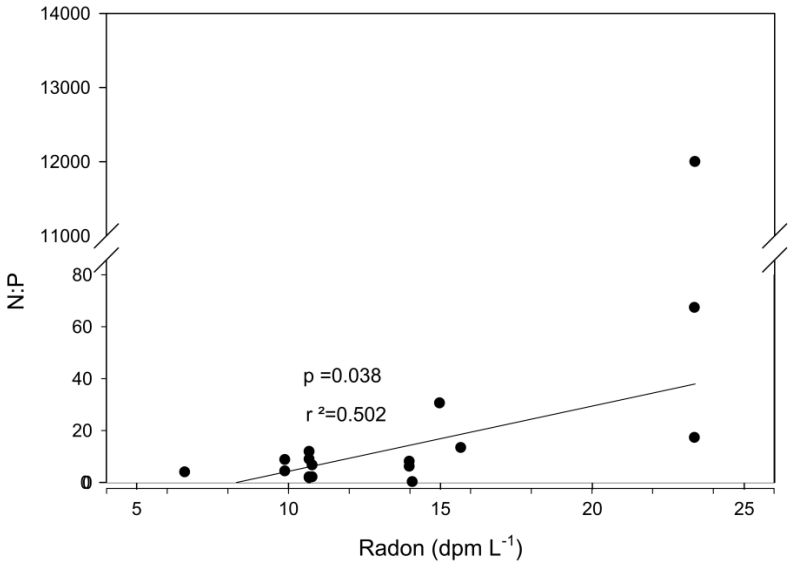

Figure 39 Radon vs nutrient ratio (N:P) for the entire study. N:P is positively correlated with excess ^{222}Rn which indicates porewater nutrient concentrations are controlled by the presence of SGD in the near shore environment.

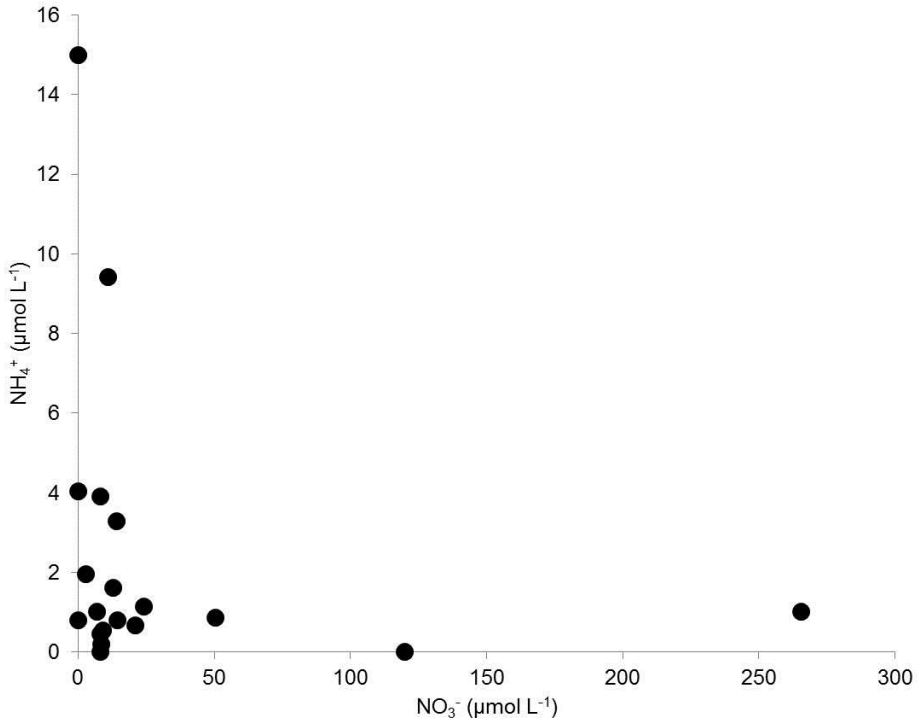

Figure 40 Relationship between porewater nitrate and ammonium concentrations in samples taken from 60cm beneath the sediment water interface. Approximately 90% of samples contain both nitrate and ammonium.

CHAPTER VI: SECONDARY AMMONIUM PRODUCTION FROM MICRO-SCALE ZERO VALENT IRON (FE^0)

Abstract

Zero valent iron (Fe^0) is an effective and inexpensive tool increasingly used to remediate abiotic and biotic groundwater contamination worldwide. This study reveals that internal nitridation of Fe^0 can produce secondary ammonium contamination during groundwater remediation efforts. Three commercially available Fe^0 powders were tested using Fe^0-H_2O elution columns run under anoxic and oxic conditions. Two of three Fe^0 powders tested in this work released ammonium into solution during corrosion of Fe^0 particles. Fe^0 powders were also used in nitrate reduction experiments to mimic groundwater remediation scenarios. One Fe^0 powder produced ammonium in significantly stoichiometric excess of nitrate inputs, indicating that the corrosion of Fe^0 powder associated internal nitride can produce substantial amounts of secondary ammonium in the environment. Release of ammonium from Fe^0 powders with internal nitride varies depending on Fe^0 particle surface area, total nitrogen content (percent weight) and redox conditions of the groundwater system. Excess ammonium produced due to internal nitridation of Fe^0 may potentially offset positive effects of groundwater nitrate remediation and have negative consequences in ecologically sensitive settings.

Introduction

Zero valent iron (Fe^0) is commonly used as a remediation product for contaminated groundwater. Numerous investigations have found Fe^0 an effective product for removal of nitrate (Xiong et al., 2009, Choi et al., 2009, Yang and Lee, 2005, Auffan et al., 2008), heavy metals (Ramos et al., 2009, Gheju, 2011, Dries et al., 2005), volatile organic compounds (Dries et al., 2005, Quinn et al., 2005) and biological contaminants (Auffan et al., 2008). While much attention is paid to the pathway of remediation, the final product of remediation is at times overlooked. For instance, nitrate remediation via Fe^0 results in conversion of up to 90% of nitrogen to ammonium or ammonia gas, yet high levels of ammonium are equally undesirable in drinking water (Huang and Zhang, 2004, Hwang et al., 2010). With the expansion of Fe^0 remediation it is crucial that studies focus on contaminant removal from the system, not just contaminant chemical transformation (Noubactep, 2011).

Micro-scale Fe^0 is principally produced for the commercial market by chemical and construction companies that have pre-existing iron and steel manufacturing capacity. The emerging Fe^0 market for groundwater remediation usage is currently (to the authors knowledge) without regulation. Government agencies and environmental remediation firms make Fe^0 purchasing decisions based on both cost and particle size requirements. Commercial suppliers regularly list surface area and Fe percentage but information regarding exact production methods is unavailable to the purchasers. Atomization, the production process of micro-scale Fe^0 powder, can be done using either water or gas. During atomization pure or scrap iron is melted at a high temperature then sprayed into a chamber where either water or gas is used to break up the molten metal stream into uniform particles prior to cooling and solidification (German, 1994).

The gas composition of the atomization chamber will dictate which light elements, such as hydrogen, argon and nitrogen, will be included in the solid Fe^0 (Shreir et al., 1994). Inert gases, such as nitrogen, are preferred by manufacturers to avoid instantaneous corrosion of Fe^0 by oxygen. These gases are incorporated in to the Fe^0 structure according to Sieverts law:

$$p_{A_2} = kx_A^2 \quad (1)$$

where x_A is the mole fraction of diatomic gas A in solution, p_{A2} is the partial pressure of A and k is the rate constant. Atomization chamber gases are therefore an important, but often neglected, factor in determining the total composition of Fe^0.

Diatomic nitrogen gas is inexpensive and abundant, making it an excellent choice for atomization gas during microscale Fe^0 production. Incorporation of nitrogen into iron structure, or nitridation, is favorable for many applications as it modifies metal hardness, fracture, roughness and corrosion properties (Schaaf et al., 1998, Sun et al., 2005). Problems arise when Fe^0 produced in a N_2 environment is used for groundwater remediation projects. Upon immersion in water Fe^0 immediately begins to corrode due to differences in electrical potential between the metal and water (Noubactep, 2010). We found that corrosion reactions release nitrogen (iron nitride), incorporated in the Fe^0 structure during production. The iron nitride reacts with water to produce ammonium, causing secondary contamination of groundwater.

Excess nitrogen in groundwater and surface waters is recognized as an environmental and health threat worldwide (Alvarez-Cobelas et al., 2008, Howarth, 2008, Hua et al., 2009). Much attention is given to Fe^0 as a nitrate remediation tool but there is no literature concerning possible secondary pollution from the nitridation of commercially produced Fe^0. The purpose of this paper is to shed light on secondary nitrogen pollution from Fe^0 corrosion in water. We present evidence that during hydrogen (anoxic) and oxygen (oxic) driven Fe^0 corrosion, incorporated nitride in Fe^0 is released into the surrounding water as ammonium. When Fe^0 is added to NO_3^- contaminated water, primary NH_4^+ is produced from NO_3^- reduction. Our results indicate that corrosion of some Fe^0 micro-particles can produce substantial amounts of additional secondary ammonium in the environment which has potentially negative consequences in ecologically sensitive settings such as riparian and coastal zones. Secondary ammonium also diminishes the positive effects of Fe^0 driven remediation of drinking water because it adds to the total nitrogen concentration of the water.

Experimental

Materials and Reagents

Micro scale Fe^0 powders were obtained from three suppliers; BASF, Quebec Metals (H²Omet™Granular Iron Powder), and Sigma-Aldrich. Of these, Sigma Aldrich was reagent grade, BASF and Quebec Metals were commercial grade. Indophenol blue, NH_4Cl, $NaNO_3$ and hydrochloric acid were obtained from Fisher Scientific. Quartz sand (50-70 mesh) was purchased from Sigma-Aldrich. Ferrozine (3-(2-Pyridyl)-5, 6-diphenyl-1, 2, 4-triazine-*p*, *p′*-disulfonic acid monosodium salt hydrate) was obtained from J.T. Baker Inc. (Philipsburg, NJ). All reagents were

of analytical reagent grade, and Milli-Q ultrapure water (18.2MΩ) were used throughout unless stated otherwise.

Anoxic and Oxic Column Experiments

Three microscale Fe^0 powders from BASF, Sigma-Aldrich and Quebec Metals were tested for ammonium production due to incorporated nitridation. For each Fe^0 powder four sets of experiments were performed in triplicate to mimic anoxic and oxic aquifer environments and to test the effect of acid pre-treatment on Fe^0 in each environment (Figure 1). All experiments were carried out using Kimble Chase Flex columns, maximum volume 24 ml, with a flow adapter to enhance bed stabilization. In anoxic experiments DW was deoxygenated by bubbling with Argon gas for 60 minutes prior to experiment to produce O_2-free deionized water (DDW). Fe^0 powder and clean quartz sand were weighed and placed into an anoxic chamber containing 90% N_2 and 10%H_2. For acid washed experiments, 0.1 M HCl solution was prepared by diluting concentrated HCl with O_2-free deionized water (DDW). A Fe^0 sample was acid washed using 15 ml of 0.1 M HCl in a vial and rotated end over end for 5 minutes to provide a fresh Fe surface for elution experiments. Vials were then removed from the anoxic chamber, centrifuged and returned to the anoxic chamber where HCl was decanted. Oxic experiments were prepared in the same manner, including acid washing of Fe^0, but without deoxygenation of deionized water or pre-treatment acid. Oxic experiments were carried out under atmospheric conditions, at 22^0C.

Anoxic column experiment was performed in an anoxic chamber. Fe^0 columns were assembled by loading 30 g quartz sand into each column and rinsing the sand with DDW prior to addition of 2.0 g Fe^0. Acidified Fe^0 was mixed with 2 ml DDW and injected into the top of the wet sand column. The elution solution, DDW, was run through the column at a rate of 1.1-1.4 ml/min. BASF powder required a slightly slower (1.1 ml/min) flow rate due to smaller particle size, which can clog the pores in the underlying quartz. Elution samples were collected at predefined intervals. Samples were collected into a syringe over a period of 3 minutes and filtered into pre-cleaned (10% HCl rinse) sample vials through Whatman Puradisc 0.2 µm PES filters. Eluate samples from anoxic experiments remained in the anoxic chamber until analysis.

Nitrate Reduction Experiments

Nitrate reduction experiments using BASF and Sigma-Aldrich Fe^0 were performed to mimic addition of Fe^0 to a nitrate contaminated aquifer. A blank control column packed with quartz sand with no Fe^0 was run simultaneously with each experiment set to establish a baseline analyte concentration in column eluate. Experiments were performed in triplicate, under anoxic conditions using the same procedure as above but with the following modifications. Experiment columns were assembled using clean quartz sand and wet with a solution of 1.75 mM $NaNO_3$. Fe^0 powder was acidified (as above) then injected into the top of the column. O_2-free solution of 1.75 mM $NaNO_3$ was run through the experiment and control columns at a rate of 1.1-1.4 ml/min. The resulting eluent filtered through Whatman Puradisc 0.2 µm PES filters and collected into pre-cleaned vials at timed intervals for 4 hours.

Fe0 Characterization

Each of the three micro-scale Fe^0 powders was analyzed for surface area and total nitrogen (% weight). All products were used as received without sorting or treatment. Surface area (A, m^2g^{-1}) was analyzed by BET gas adsorption using a Micromeritics ASAP 2010 analyzer with a 10-mm Hg transducer using UHP N_2 gas. Total nitrogen % weight was determined on a separate set of samples by inert gas fusion-thermal conductivity, performed by IMR Test Labs, Lansing NY.

Fe^0 surface evolution during timed experiments using BASF Fe^0 powder was examined using Scanning Electron Microscope (SEM). Anoxic acidified Fe^0 column experiments were run for 0, 1, 3, 6, 12 and 24 hours. After each experiment terminated, the corroded Fe^0 was collected by carefully removing the upper portion of the column and allowing it to dry in an anoxic chamber. The dry Fe^0 was then separated from bed quartz by magnet. Samples were removed from the chamber and mounted onto standard SEM mounts. Scanning Electron Analysis (SEM) was performed on a LEO 1550 SFEG scanning electron microscope equipped with an EDAX energy dispersive X-ray spectrometer (EDS).

Chemical Analysis

Eluate samples were analyzed for NH_4^+ by indophenol blue method (Solorzano, 1969) and Fe_{total} by Ferrizone method (Stookey, 1970). NO_3^-/NO_2^- were analyzed using a Dionex DX-500 ion chromatograph (IC) with 4 mm Dionex IonPac® AS4A-SC (22°C, Sodium Carbonate/ Bicarbonate eluent concentrate). Concentrations were calculated from a 6 point calibration curve with R^2 values above 0.99.

Results and Discussion

Iron nitride in Fe^0

Micro-scale Fe^0 is produced commercially by thermal spraying of molten iron into an anoxic chamber at temperatures in excess of 1200°C. During thermal spraying Fe^0 undergoes internal nitridation whereby gaseous diatomic nitrogen in the anoxic chamber forms a solution in liquid iron according to Sieverts law:

$$N_{2(gas)} \Leftrightarrow 2N \tag{2}$$

A linear relationship exists between the solubility of nitrogen in liquid iron and the square root of the partial pressure of nitrogen in contact with the iron as shown in Equation (2) (Shreir et al., 1994).

$$N_{eq} = K_{eq}\sqrt{P_{N_2}} \tag{3}$$

Where N_{eq} is the nitrogen concentration in the liquid iron, K_{eq} is the equilibrium constant and P_{N2} is the partial pressure of nitrogen in contact with liquid iron (Coudurier et al., 1985). Nitridation, the method by which nitrogen enters molten iron, is well documented in literature (Shreir et al., 1994, Talbot and Talbot, 1998). In this study all three iron powders exhibit nitridation as evidenced by per cent weight nitrogen concentrations. Total weight percent nitrogen was analyzed to determine the extent of internal nitridation using inert gas fusion-

thermal conductivity. Results in Table 13 show that powder BASF contains 0.74% N, powder QB contains 0.005% N and powder SA contains 0.001% N. Surface area, as measured by BET, is 0.242, 0.308 and 0.138 m^2g^{-1} for BASF, QB and SA, respectively (Table 13)

Internal nitridation of Fe^0 powder provides nitrogen source for the production of secondary ammonium during corrosion by H_2O. The released iron nitride reacts with surrounding water to produce ammonium. During oxic corrosion oxygen is reduced as Fe^0 is oxidized, producing Fe^{2+} and/or Fe^{3+} ions that combine with OH^- form an oxide film on the surface of the Fe^0 (Stratmann, 1990). The corrosion reaction, and consequently NH_4^+ release, occurs to different extents depending on the oxygen conditions surrounding the Fe^0.

None of the 3 Fe^0 powders tested produced NH_4^+ under either oxic or anoxic conditions without acid washing. This indicates microscale Fe^0 particles undergo surface oxidation during storage and require acid washing to remove Fe-oxide corrosion shell that inhibits reduction reactions. Nitrate/nitrite was not detected in eluate from any Fe^0 column experiments run with DDW as the eluent.

Anoxic experiments were placed in a chamber containing 90% nitrogen and 10% hydrogen, limiting available oxygen for Fe^0 corrosion processes. Because the redox potential of Fe^{2+} is less than that of H^+, Fe^0 can be oxidized to Fe^{2+} by production of H^+ ions from H_2O under anoxic conditions. Anoxic conditions promote slow oxide scale growth which allows for continual release of N^{-3} from iron particles over the course of hours to days (Figure 42a,c). In contrast, oxic experiments were performed at atmospheric conditions which allows for rapid reaction of Fe^0 with dissolved and atmospheric O_2 , thereby releasing peak NH_4^+ concentration during the initial phase of the experiment, followed by rapid iron oxide precipitation on Fe^0 core that prevents further NH_4^+ release (Figure 41 b,d). These two scenarios provide insights into how nitridation of Fe^0 will release NH_4^+ in different groundwater settings.

Anoxic Fe^0 Corrosion

Anoxic acid washed column experiments were run for 1, 3, 6, 12 and 24 hours and 7 days under anoxic conditions using DDW as the eluent. Powder BASF eluate contained NH_4^+ at all times for up to 7 days, eluate from powder QB did not contain NH_4^+ after 6 hours. No ammonium was detected in powder SA eluate during the whole experiment (Figure 1). The dynamic concentrations of ammonium and Fe_{total} eluted from the powder BASF, QB and SA under anoxic and oxic conditions are shown in Figure 41. Each data point represents average with standard error of the mean for three replicate trials.

In anoxic acid washed experiments, the initially eluted average ammonium and total iron from powder BASF were 9.6 µmol L^{-1} and 9.1 µmol L^{-1}, respectively. Fe_{total} concentrations decreased as NH_4^+ concentrations increased along with elution time reaching Fe minimum concentrations of 0.4 µmol L^{-1} and NH_4^+ maximum 318 µmol L^{-1} at 180 min, respectively. Then eluted NH_4^+ gradually decreased to 14.6 µmol L^{-1} at 460 min with an inverse correlation of Fe elution (Figure 41a). Significantly less NH_4^+ but higher concentrations of Fe_{total} were observed in eluate from powder QB when compared to powder BASF. The average QB eluate maximum NH_4^+ and Fe_{total} were 4.5 and 76.1 µmol L^{-1}, respectively. The correlation between eluted NH_4^+

and Fe_{total} in powder QB showed positive correlation for both anoxic and oxic elution (**Figure 41**c, d). Powder SA produced no NH_4^+ in acid washed experiments under anoxic experiments (Figure 41e), but produced an average maximum Fe_{total} of 1.8 µmol L^{-1}. The presence of Fe_{total} in SA eluate indicates Fe^0 corrosion processes occur but secondary ammonium is not produced due to very low internal nitrogen, 0.001% and decreased surface area of 0.138 m^2g^{-1} (Table 13) as compared to powders BASF and QB.

The pathway for Fe^0-H_2O corrosion in anoxic regime can be described by the following reaction:

$$Fe^0(s) + 2H_2O \rightarrow Fe^{2+} + 2OH^- + H_2(g) \quad (4)$$

$$Fe^{2+} + 2OH^- = Fe(OH)_2\ (s) \quad (5)$$

This redox reaction is unsustainable under pH neutral groundwater conditions. The pH can rapidly increase from initial neutral value to greater than 9 within 4 hours, at which point the basic solution would dramatically slow the Fe redox reaction (Choe et al., 2004). In this work, pH of the eluate ranged 5.5-7.5 throughout the experiment. Fresh deoxygened MQ water was continuously run through each Fe^0 column, thereby preventing pH increase.

During anoxic Fe^0 corrosion, we hypothesize that iron nitride Fe_xN is exposed to surrounding water and released along with Fe^{2+}, as shown in Figure 42. Corrosion reactions can release Fe^{2+} and Fe^{3+} ions into solution according to

$$Fe^0 \leftrightarrow Fe^{2+} + 2e^- \quad (6)$$

$$Fe^{2+} \leftrightarrow Fe^{3+} + e^- \quad (7)$$

$$Fe^0 + 2Fe^{3+} \leftrightarrow 3Fe^{2+} \quad (8)$$

Additionally, there may be loosely bound Fe on the surface of acid washed anoxic particles, as evidenced by powder BASF elution Fe_{total} concentration of 9.1µmol L^{-1} at 10 minutes (Figure 41a). It is unclear why anoxic powder QB elutions (Figure 41c) did not exhibit the same initial Fe_{total} spike.

In pH 5.5-7.5 H_2O system, the exposed Fe_xN along with Fe^0 corrosion may react with protons (H^+) in DDW^+ to generate NH_4^+ and released into the surrounding eluate solution according to

$$Fe_xN + 4H^+ \leftrightarrow xFe^{2+} + NH_4^+ \quad (9)$$

Lack of available oxygen slows the transformation of $Fe(OH)_2$ to Fe_3O_4, which prolongs the stage where Fe_xN is exposed from Fe^0 and can interact with proton diffused through the thin surface layer of $Fe(OH)_2$ and $Fe(OH)_3$, as shown in Figure 42c. The $Fe(OH)_2$ scale is metastable

at low temperatures but will eventually be converted to to magnetite via the Schikorr reaction (Figure 42d):

$$3Fe(OH)_2\ (s) \rightarrow Fe_3O_4\ (s) + H_2(g) + 2H_2O \quad (10)$$

It is possible that this transformation causes the cessation of ammonium release as the structural change reduces oxides scale porosity. Therefore, we hypothesize that as Fe^0 outer layers convert from amorphous to crystalline iron oxides the reaction rate slowly decreases to 0, as demonstrated in Figure 42. SEM images of anoxic powder BASF Fe^0 corrosion in Figure 43b show that within 3 hours secondary mineral precipitation is present around Fe^0 particles. Within 24 hours thin platy scales cover the outside of column quartz particles, (Figure 43c,d). Experiments lasting 7 days show continual release of NH_4^+ at low concentrations, therefore the kinetics of Fe-oxide scale growth and/or particle cementation is unknown and requires further investigation.

Anoxic groundwater systems receiving Fe^0 treatment are likely to experience greater secondary ammonium pollution during application of Fe^0 with internal nitridation due to longer elution times resulting from slow Fe-oxide scale growth. Cation exchange onto sediments could offset secondary production of ammonium by addition of ZVI in sediments with high cation exchange capacity (CEC) (Appelo and Postma, 1999)

Oxic Fe^0 Corrosion

Oxic acid washed experiments of powder BASF column show an inverse correlation between ammonium and Fe_{total} elution, with an initial elution of 125.1 µmol L^{-1} NH_4^+ corresponding to 0.0 µmol L^{-1} Fe_{total}. Ammonium concentration in eluate decreased from the maximum 128 µmol L^{-1} at 25 minutes to 19 µmol L^{-1} after 81 minutes, correlating with a Fe_{total} maximum of 1.4 µmol L^{-1} after 81 minutes (Figure 41b). It is notable that maximum concentrations of both ammonium and Fe_{total} are less than half of values observed in anoxic experiments (Figure 41a). This indicates rapid corrosion, driven by dissolved oxygen in the elution distilled water and atmospheric O_2, likely occurred during injection of Fe^0 into column. Acid washed QB did not show the same inverse correlation between released ammonium and Fe_{total}. From experiment time 10 to 48 minutes, QB eluate concentrations of ammonium rose from 0.0 to 1.9 µmol L^{-1} and Fe_{total} rose from 0.0to 145.1 µmol L^{-1}, concentrations of ammonium and Fe_{total} then drop concurrently reaching levels of 0.0 µmol L^{-1} and 1.7 µmol L^{-1} respectively after 240 minutes (Figure 41d). Powder SA produced no ammonium in acid washed experiments under oxic conditions (Figure 41f). Maximum Fe_{total} eluted from SA powder occurred after 5 minutes, with an average concentration of 6.4 µmol L^{-1}, Fe_{total} concentration then dropped below 2.5 µmol L^{-1} for the remainder of the experiment. These results indicate rapid release of Fe_{total} after acid washing and oxide scale formation within 15 minutes of corrosion initiation.

When bare Fe^0 is exposed to oxic DW and atmospheric oxygen levels, Fe^0 corrosion and O_2 reduction may occur according to

$$2Fe^0 + O_2 + 2H_2O \rightarrow 2Fe^{2+} + 4OH^- \quad (11)$$

$2Fe^{2+} + O_2 + 2OH^- \rightarrow 2FeOOH\ (s)$ (12)

Under conditions where Fe(III)- oxihydroxide is not stable it can undergo reduction due to partial pressure of oxygen changes (Stratmann and Muller, 1994). Previous work investigating FeO films plated on Pt(III) indicate the presence of both oxygen and water create a trilayer structure with terminal OH groups (Ringleb et al., 2011). Ringleb et al [27] (2011) point out that this structural motif is a precursor of goethite (FeOOH), which is known to rapidly oxidize to Fe_3O_4 in low temperature systems (Talbot and Talbot, 1998). These structural differences facilitate electron transfer and set up differing redox potential within the oxide coating. We hypothesize an oxide coating with a layered structure where redox conditions vary within the shell, as seen in studies investigating the reduction of Arsenic using nanoscale Fe^0 (Yan et al., 2010, Ramos et al., 2009). The iron oxide shell structure leads to rapid corrosion of Fe^0 and elution of internal nitridation, which reacts with H^+ in the system and produces NH_4^+ in eluate (Figure 42). Peak NH_4^+ concentration for oxic experiments occurs ~ 50 minutes (Fig 1 B&D) whereas in anoxic experiments NH_4^+ peaks between ~100-200 minutes (Fig 1. A&C).

Stratmann and Muller found that inner portions of an iron electrode are less accessible as oxide scale thickness increases, therefore further corrosion is inhibited by the formation of a dense rust layer (Stratmann and Muller, 1994). While their study was done on Fe^0 with lower surface area per mass, with consequently longer diffusion path lengths, our results working with micro-scale Fe^0 reach the same conclusion; the shift in corrosion reaction site to outer layers of the oxide scale results in the cessation of NH_4^+ elution, either by preventing further corrosion of the inner layers which inhibits inward H^+ and/or H_2O diffusion or movement of the active oxidation sites to outer layers, where nitrogen is already stripped (Figure 43c,d). The complete transformation of the outer Fe-oxide shell, and cessation of NH_4^+ production, occurs within hours of initiating the corrosion reaction in oxic conditions, as compared to days under anoxic conditions.

During groundwater remediation in oxic regimes, nitrate is often the target of Fe^0 applications. In these setting the final product of NO_3^- reduction can be either N_2 gas or NH_4^+. Studies of the final product conclude NH_4^+ represents at least 50-90% of the final nitrogen speciation (Hwang et al., 2010, Hwang et al., 2011, Choe et al., 2004). Ammonium produced by nitrate reduction and internal nitridation of Fe^0 enters a groundwater system as a plume. In oxic groundwater setting, plumes of ammonium will have oxic edges where ammonium is nitrified, similar to septic tank/cesspool plume reactions. Nitrification of secondary ammonium production from Fe^0 nitridation has the potential to offset intended nitrate losses in oxic groundwater systems.

Iron Characterization

Corrosion of Fe^0 by H_2O produces iron-oxide surface coatings which thicken and undergo structural changes with increased corrosion time. To examine surface changes during corrosion, powder BASF was allowed to corrode in DDW under anoxic conditions for 0, 3, 6, 12, 24 hours and the spent Fe^0 was examined using SEM. Figure 43 shows the progression of Fe^0 corrosion; beginning with unwashed Fe^0 (Figure 3A), which is subsequently acid washed. After 3 hour anoxic water corrosion, the formation of initial corrosion products is observed on acid

washed Fe^0 (Figure 43b), increased corrosion product precipitation occurs after 12 hours (Figure 43c) and finally intergrowth of corrosion product and remaining Fe^0 after 24 hours (Figure 43d). After 12 hours SEM shows evidence of a platy crystal growth on the column bed quartz (Figure 44a) which increases in size and thickness after 24 hours (Figure 44b). We hypothesize these crystals are the result of iron oxide precipitation in the column quartz, but structural composition could not be determined using SEM and EDS.

Nitrate Reduction via Fe^0

Fe^0 is widely cited as an effective nitrate reductant in contaminated groundwater. The nitrate reduction can be expressed as:

$$4Fe^0 + NO_3^- + 7H_2O \rightarrow 4Fe^{2+} + NH_4^+ + 10OH^- \quad (13)$$

The produced ammonium concentration in the eluate solution should be stoichiometrically equal to the nitrate concentration which was initially added. However, production of NH_4^+ from corrosion of Fe^0 with internal nitridation will produce concentrations of NH_4^+ in stoichiometric excess of initial nitrate additions. To test this hypothesis, Fe^0 mediated NO_3^- reduction column experiments were performed with a 1750μmol L^{-1} nitrate solution as the eluent under anoxic conditions. Results in Figure 45a show that after passing through powder BASF column, nitrate concentration rapidly decreased from 1750μmol L^{-1} to 400μmol L^{-1} within 10 min, and averaged 480μmol L^{-1} ± 12% for the remainder of the experiment duration. NH_4^+ was produced in the eluate and reached maximum 2200μmol L^{-1} at 45 min, and then slightly decreased to the average of 1500±10% μmol $L^{-1}$for the remainder of the experiment (Figure 45a). Ammonium production exceeds nitrate inputs by a maximum of 75 % at 45 min, demonstrating secondary ammonium release from particles during Fe^0 corrosion.

Because powder SA does not produce excess NH_4^+ in anoxic or oxic column trials using deoxygenized Milli-Q water as the elute (Fig. 1E), the production of NH_4^+ in powder SA column is completely attributable to NO_3^- reduction (Figure 45b). The concentrations of NO_3^- in eluate decreased from 1750 μM to 1586 μM when the experiment was run for 3 hours. During this time NH_4^+ concentration increased from 0 to 25.8μM, indicating a maximum of 9.37% conversion of initial nitrate concentration to ammonium. Figure 45b indicates that the nitrogen reduction using Powder SA is much slower than when using Powder BSAF. The differences in denitrification capacity for powders BASF and SA are likely due to differences in surface area (Table 13), as powder BASF has a larger surface area, allowing greater contact with NO_3^- solution. No nitrate reduction was observed in the control column packed with quartz sand (Figure 45c), further demonstrating that the ammonium in eluate from powder BASF resulted from nitrate reduction and release of Fe^0 internal nitridation.

Conclusions

Fe^0 is an important groundwater remediation tool for removal of contaminants such as nitrate, heavy metals and oil byproducts. Our results confirm the existence of excess nitrogen elution by Fe^0 micro-scale particles due to internal nitridation. The amount of excess NH_4^+ production is dependent on total nitrogen percent weight of Fe^0 micro particles, particle surface

area and redox conditions during corrosion. Where Fe^0 is used to remediate nitrate or other contaminants, internal nitridation can cause unintentional ammonium pollution in groundwater.

References

ADDY, K., GOLD, A., NOWICKI, B., MCKENNA, J., STOLT, M. & GROFFMAN, P. 2005. Denitrification capacity in a subterranean estuary below a Rhode Island fringing salt marsh. *Estuaries,* 28**,** 896-908.

AESCHBACH-HERTIG, W., PEETERS, F., BEYERLE, U. & KIPFER, R. 1999. Interpretation of dissolved atmospheric noble gases in natural waters. *Water Resources Research,* 35**,** 2779-2792.

ALVAREZ-COBELAS, M., ANGELER, D. G. & SANCHEZ-CARRILLO, S. 2008. Export of nitrogen from catchments: A worldwide analysis. *Environmental Pollution,* 156**,** 261-269.

AN, S. M. & GARDNER, W. S. 2002. Dissimilatory nitrate reduction to ammonium (DNRA) as a nitrogen link, versus denitrification as a sink in a shallow estuary (Laguna Madre/Baffin Bay, Texas). *Marine Ecology-Progress Series,* 237**,** 41-50.

ANDERSEN, M. S., BARON, L., GUDBJERG, J., GREGERSEN, J., CHAPELLIER, D., JAKOBSEN, R. & POSTMA, D. 2007. Discharge of nitrate-containing groundwater into a coastal marine environment. *Journal of Hydrology,* 336**,** 98-114.

ANISFELD, S. C. & HILL, T. D. 2012. Fertilization Effects on Elevation Change and Belowground Carbon Balance in a Long Island Sound Tidal Marsh. *Estuaries and Coasts,* 35**,** 201-211.

ANSCHUTZ, P., SMITH, T., MOURET, A., DEBORDE, J., BUJAN, S., POIRIER, D. & LECROART, P. 2009. Tidal sands as biogeochemical reactors. *Estuarine Coastal and Shelf Science,* 84**,** 84-90.

APPELO, C. A. J. & POSTMA, D. 1999. *Geochemistry, groundwater and pollution,* Rotterdam, A.A. Balkema.

AUFFAN, M., ACHOUAK, W., ROSE, J., RONCATO, M. A., CHANEAC, C., WAITE, D. T., MASION, A., WOICIK, J. C., WIESNER, M. R. & BOTTERO, J. Y. 2008. Relation between the redox state of iron-based nanoparticles and their cytotoxicity toward Escherichia coli. *Environmental Science & Technology,* 42**,** 6730-6735.

AVERY, G. B., KIEBER, R. J., TAYLOR, K. J. & DIXON, J. L. 2012. Dissolved organic carbon release from surface sand of a high energy beach along the Southeastern Coast of North Carolina, USA. *Marine Chemistry,* 132**,** 23-27.

BARROW, N. J., BOWDEN, J. W., POSNER, A. M. & QUIRK, J. P. 1980. DESCRIBING THE EFFECTS OF ELECTROLYTE ON ADSORPTION OF PHOSPHATE BY A VARIABLE CHARGE SURFACE. *Australian Journal of Soil Research,* 18.

BAUER, C. 2012. ***Physical Processes Contributing to Localized, Seasonal Hypoxic Conditions in the Bottom Waters of Smithtown Bay, Long Island Sound, New York***. MS, Stony Brook University.

BECK, A. 2007. *SUBMARINE GROUNDWATER DISCHARGE (SGD) AND DISSOLVED TRACE METAL CYCLING IN THE SUBTERRANEAN ESTUARY AND COASTAL OCEAN.* Ph.D, Stony Brook University.

BECK, A. J., COCHRAN, J. K. & SANUDO-WILHELMY, S. A. 2010. The distribution and speciation of dissolved trace metals in a shallow subterranean estuary. *Marine Chemistry,* 121**,** 145-156.

BECK, A. J., RAPAGLIA, J. P., COCHRAN, J. K., BOKUNIEWICZ, H. J. & YANG, S. 2008. Submarine groundwater discharge to Great South Bay, NY, estimated using Ra isotopes. *Marine Chemistry,* 109**,** 279-291.

BENNINGTON, B. 2003. NEW OBSERVATIONS ON THE GLACIAL GEOMORPHOLOGY OF LONG ISLANDFROM A DIGITAL ELEVATION MODEL (DEM). *Long Island Geologists Conference.* Stony Brook, NY.

BERNOT, M. J., DODDS, W. K., GARDNER, W. S., MCCARTHY, M. J., SOBOLEV, D. & TANK, J. L. 2003. Comparing denitrification estimates for a texas estuary by using acetylene inhibition and membrane inlet mass spectrometry. *Applied and Environmental Microbiology,* 69**,** 5950-5956.

BILLERBECK, M., WERNER, U., BOSSELMANN, K., WALPERSDORF, E. & HUETTEL, M. 2006. Nutrient release from an exposed intertidal sand flat. *Marine Ecology Progress Series,* 316**,** 35-51.

BITTNER, H. 1997. *Characterization of Port Jefferson Harbor Sediments using a recoverable bottom penetrometer.* Ph.D, Stony Brook University, School of Atmospheric and Marine Sciences.

BLICHER-MATHIESEN, G. & HOFFMANN, C. C. 1999. Denitrification as a sink for dissolved nitrous oxide in a freshwater riparian fen. *Journal of Environmental Quality,* 28**,** 257-262.

BLICHER-MATHIESEN, G., MCCARTY, G. W., NIELSEN, L. P. & TZ 1998. Denitrification and degassing in groundwater estimated from dissolved dinitrogen and argon. *Journal of Hydrology,* 208**,** 16-24.

BOEHM, A. B., SHELLENBARGER, G. G. & PAYTAN, A. 2004. Groundwater discharge: Potential association with fecal indicator bacteria in the surf zone. *Environmental Science & Technology,* 38.

BOGUSLAVSKY, S. 2000. *Organic Sorption and Cation Exchange Capacity of Glacial Sand, Long Island.* Masters, SUNY Stony Brook.

BOHLKE, J. K. & DENVER, J. M. 1995. COMBINED USE OF GROUNDWATER DATING, CHEMICAL, AND ISOTOPIC ANALYSES TO RESOLVE THE HISTORY AND FATE OF NITRATE CONTAMINATION IN 2 AGRICULTURAL WATERSHEDS, ATLANTIC COASTAL-PLAIN, MARYLAND. *Water Resources Research,* 31**,** 2319-2339.

BOHLKE, J. K., HATZINGER, P. B., STURCHIO, N. C., GU, B. H., ABBENE, I. & MROCZKOWSKI, S. J. 2009. Atacama Perchlorate as an Agricultural Contaminant in Groundwater: Isotopic and Chronologic Evidence from Long Island, New York. *Environmental Science & Technology,* 43**,** 5619-5625.

BOHLKE, J. K., WANTY, R., TUTTLE, M., DELIN, G. & LANDON, M. 2002. Denitrification in the recharge area and discharge area of a transient agricultural nitrate plume in a glacial outwash sand aquifer, Minnesota. *Water Resources Research,* 38**,** 26.

BOKUNIEWICZ, H. 1980. Groundwater Seepage Into Great South Bay, New-York. *Estuarine and Coastal Marine Science,* 10**,** 437-444.

BOKUNIEWICZ, H., POLLOCK, M., BLUM, J. & WILSON, R. 2004. Submarine Ground Water Discharge and Salt Penetration Across the Sea Floor. *Ground Water,* 42**,** 983-989.

BOUDREAU, B. P. 1996. The diffusive tortuosity of fine-grained unlithified sediments. *Geochimica Et Cosmochimica Acta,* 60**,** 3139-3142.

BOWEN, J. L., KROEGER, K. D., TOMASKY, G., PABICH, W. J., COLE, M. L., CARMICHAEL, R. H. & VALIELA, I. 2007. A review of land-sea coupling by groundwater discharge of nitrogen to New England estuaries: Mechanisms and effects. *Applied Geochemistry,* 22**,** 175-191.

BOWEN, J. L. & VALIELA, I. 2001. Historical changes in atmospheric nitrogen deposition to Cape Cod, Massachusetts, USA. *Atmospheric Environment,* 35**,** 1039-1051.

BRATTON, J. F. 2010. The Three Scales of Submarine Groundwater Flow and Discharge across Passive Continental Margins. *Journal of Geology,* 118**,** 565-575.

BRATTON, J. F., BOHLKE, J. K., KRANTZ, D. E. & TOBIAS, C. R. 2009. Flow and geochemistry of groundwater beneath a back-barrier lagoon: The subterranean estuary at Chincoteague Bay, Maryland, USA. *Marine Chemistry,* 113**,** 78-92.

BRESLIN, V. T. & SANUDO-WILHELMY, S. A. 1999. High spatial resolution sampling of metals in the sediment and water column in Port Jefferson Harbor, New York. *Estuaries,* 22**,** 669-680.

BRICKER, S., LONGSTAFF, B., DENNISON, W., JONES, A., BOICOURT, K., WICKS, C. & WOERNER, J. 2007. Effects of Nutrient Enrichment In the Nation's Estuaries: A Decade of Change. *In:* NOAA (ed.). Silver Spring, Maryland: National Centers for Coastal Ocean Science.

BURDIGE, D. 2002. Sediment Pore Waters. *In:* DENNIS, H. & CARLSON, C. (eds.) *Biogeochemistry of Marine Dissolved Organic Matter* Elsevier Science.

BURGIN, A. J. & HAMILTON, S. K. 2007. Have we overemphasized the role of denitrification in aquatic ecosystems? A review of nitrate removal pathways. *Frontiers in Ecology and the Environment,* 5**,** 89-96.

BURNETT, W. C., AGGARWAL, P. K., AURELI, A., BOKUNIEWICZ, H., CABLE, J. E., CHARETTE, M. A., KONTAR, E., KRUPA, S., KULKARNI, K. M., LOVELESS, A., MOORE, W. S., OBERDORFER, J. A., OLIVEIRA, J., OZYURT, N., POVINEC, P., PRIVITERA, A. M. G., RAJAR, R., RAMASSUR, R. T., SCHOLTEN, J., STIEGLITZ, T., TANIGUCHI, M. & TURNER, J. V. 2006. Quantifying submarine groundwater discharge in the coastal zone via multiple methods. *Science of the Total Environment,* 367**,** 498-543.

BURNETT, W. C., BOKUNIEWICZ, H., HUETTEL, M., MOORE, W. S. & TANIGUCHI, M. 2003. Groundwater and pore water inputs to the coastal zone. *Biogeochemistry,* 66**,** 3-33.

BURNETT, W. C. & DULAIOVA, H. 2003. Estimating the dynamics of groundwater input into the coastal zone via continuous radon-222 measurements. *Journal of Environmental Radioactivity,* 69**,** 21-35.

BUXTON, H. T. & MODICA, E. 1992. PATTERNS AND RATES OF GROUNDWATER-FLOW ON LONG-ISLAND, NEW-YORK. *Ground Water,* 30**,** 857-866.

CABLE, J. E., BURNETT, W. C., CHANTON, J. P. & WEATHERLY, G. 1996. Modeling groundwater flow into the ocean based on ^{222}Rn. *Earth and Planetary Science Letters,* 144**,** 591-604.

CABRITA, M. T. & BROTAS, V. 2000. Seasonal variation in denitrification and dissolved nitrogen fluxes in intertidal sediments of the Tagus estuary, Portugal. *Marine Ecology Progress Series,* 202**,** 51-65.

CADEMARTORI, E. 2000. *An assessment of salt marsh vegetation changes in southern Stony Brook Harbor: Implications for future management* M.S, Stony Brook University.

CAMBARERI, T. C. & EICHNER, E. M. 1998. Watershed delineation and ground water discharge to a coastal embayment. *Ground Water,* 36**,** 626-634.

CHARETTE, M., BREIER, C., DULAIOVA, H., GONNEEA, M., HENDERSON, P., KROEGER, K., MULLIGAN, A., RAO, A. & SLOMP, C. 2010. Nutrient

biogeochemistry in permeable sediments impacted by submarine groundwater discharge. *Geochimica Et Cosmochimica Acta,* 74.

CHARETTE, M. A. 2007. Hydrologic forcing of submarine groundwater discharge: Insight from a seasonal study of radium isotopes in a groundwater-dominated salt marsh estuary. *Limnology and Oceanography,* 52**,** 230-239.

CHARETTE, M. A. & ALLEN, M. C. 2006. Precision ground water sampling in coastal aquifers using a direct-push, shielded-screen well-point system. *Ground Water Monitoring and Remediation,* 26**,** 87-93.

CHARETTE, M. A., BUESSELER, K. O. & ANDREWS, J. E. 2001. Utility of radium isotopes for evaluating the input and transport of groundwater-derived nitrogen to a Cape Cod estuary. *Limnology and Oceanography,* 46**,** 465-470.

CHARETTE, M. A. & SHOLKOVITZ, E. R. 2002. Oxidative precipitation of groundwater-derived ferrous iron in the subterranean estuary of a coastal bay. *Geophysical Research Letters,* 29.

CHARETTE, M. A. & SHOLKOVITZ, E. R. 2006. Trace element cycling in a subterranean estuary: Part 2. Geochemistry of the pore water. *Geochimica Et Cosmochimica Acta,* 70.

CHARETTE, M. A., SHOLKOVITZ, E. R. & HANSEL, C. M. 2005. Trace element cycling in a subterranean estuary: Part 1. Geochemistry of the permeable sediments. *Geochimica Et Cosmochimica Acta,* 69**,** 2095-2109.

CHOE, S. H., LJESTRAND, H. M. & KHIM, J. 2004. Nitrate reduction by zero-valent iron under different pH regimes. *Applied Geochemistry,* 19**,** 335-342.

CHOI, J. H., SHIN, W. S., CHOI, S. J. & KIM, Y. H. 2009. Reductive denitrification using zero-valent iron and bimetallic iron. *Environmental Technology,* 30**,** 939-946.

CONLEY, D. J., CARSTENSEN, J., AERTEBJERG, G., CHRISTENSEN, P. B., DALSGAARD, T., HANSEN, J. L. S. & JOSEFSON, A. B. 2007. Long-term changes and impacts of hypoxia in Danish coastal waters. *Ecological Applications,* 17**,** S165-S184.

CONLEY, D. J., PAERL, H. W., HOWARTH, R. W., BOESCH, D. F., SEITZINGER, S. P., HAVENS, K. E., LANCELOT, C. & LIKENS, G. E. 2009. ECOLOGY Controlling Eutrophication: Nitrogen and Phosphorus. *Science,* 323**,** 1014-1015.

COUDURIER, L., HOPKINS, D. & WILKOMIRSKY, I. 1985. *Fundamentals of Metallurgical Processes,* Oxford, Pergamon Press.

CRUSIUS, J., KOOPMANS, D., BRATTON, J. F., CHARETTE, M. A., KROEGER, K., HENDERSON, P., RYCKMAN, L., HALLORAN, K. & COLMAN, J. A. 2005. Submarine groundwater discharge to a small estuary estimated from radon and salinity measurements and a box model. *Biogeosciences,* 2**,** 141-157.

DACEY, J. W. H. & HOWES, B. L. 1984. WATER-UPTAKE BY ROOTS CONTROLS WATER-TABLE MOVEMENT AND SEDIMENT OXIDATION IN SHORT SPARTINA MARSH. *Science,* 224**,** 487-489.

DAVIS, J. L., NOWICKI, B. & WIGAND, C. 2004. Denitrification in fringing salt marshes of Narragansett Bay, Rhode Island, USA. *Wetlands,* 24**,** 870-878.

DE SIEYES, N. R., YAMAHARA, K. M., LAYTON, B. A., JOYCE, E. H. & BOEHM, A. B. 2008. Submarine discharge of nutrient-enriched fresh groundwater at Stinson Beach, California is enhanced during neap tides. *Limnology and Oceanography,* 53.

DEBORDE, J., ANSCHUTZ, P., AUBY, I., GLE, C., COMMARIEU, M. V., MAURER, D., LECROART, P. & ABRIL, G. 2008. Role of tidal pumping on nutrient cycling in a temperate lagoon (Arcachon Bay, France). *Marine Chemistry,* 109**,** 98-114.

DESBARATS, A. J., LOGAN, C. E., HINTON, M. J. & SHARPE, D. R. 2002. On the kriging of water table elevations using collateral information from a digital elevation model. *Journal of Hydrology,* 255**,** 25-38.

DEUTSCH, B., FORSTER, S., WILHELM, M., DIPPNER, J. W. & VOSS, M. 2010. Denitrification in sediments as a major nitrogen sink in the Baltic Sea: an extrapolation using sediment characteristics. *Biogeosciences,* 7**,** 3259-3271.

DILLON, K. S., CHANTON, J. P. & SMITH, L. K. 2007. Nitrogen sources and sinks in a wastewater impacted saline aquifer beneath the Florida Keys, USA. *Estuarine Coastal and Shelf Science,* 73**,** 148-164.

DORSETT, A., CHERRIER, J., MARTIN, J. B. & CABLE, J. E. 2011. Assessing hydrologic and biogeochemical controls on pore-water dissolved inorganic carbon cycling in a subterranean estuary: A C-14 and C-13 mass balance approach. *Marine Chemistry,* 127**,** 76-89.

DRIES, J., BASTIAENS, L., SPRINGAEL, D., AGATHOS, S. N. & DIELS, L. 2005. Combined removal of chlorinated ethenes and heavy metals by zerovalent iron in batch and continuous flow column systems. *Environmental Science & Technology,* 39**,** 8460-8465.

DUGAN, J. E., HUBBARD, D. M., PAGE, H. M. & SCHIMEL, J. P. 2011. Marine Macrophyte Wrack Inputs and Dissolved Nutrients in Beach Sands. *Estuaries and Coasts,* 34**,** 839-850.

DULAIOVA, H., CAMILLI, R., HENDERSON, P. B. & CHARETTE, M. A. 2010. Coupled radon, methane and nitrate sensors for large-scale assessment of groundwater discharge and non-point source pollution to coastal waters. *Journal of Environmental Radioactivity,* 101**,** 553-563.

DULAIOVA, H., GONNEEA, M. E., HENDERSON, P. B. & CHARETTE, M. A. 2008. Geochemical and physical sources of radon variation in a subterranean estuary - Implications for groundwater radon activities in submarine groundwater discharge studies. *Marine Chemistry,* 110**,** 120-127.

DULAIOVA, H., PETERSON, R., BURNETT, W. C. & LANE-SMITH, D. 2005. A multi-detector continuous monitor for assessment of Rn-222 in the coastal ocean. *Journal of Radioanalytical and Nuclear Chemistry,* 263**,** 361-365.

EMERSON, S., JAHNKE, R. & HEGGIE, D. 1984. SEDIMENT-WATER EXCHANGE IN SHALLOW-WATER ESTUARINE SEDIMENTS. *Journal of Marine Research,* 42**,** 709-730.

EYRE, B. D., RYSGAARD, S., DALSGAARD, T. & CHRISTENSEN, P. B. 2002. Comparison of isotope pairing and N-2 : Ar methods for measuring sediment-denitrification-assumptions, modifications, and implications. *Estuaries,* 25**,** 1077-1087.

FORBES, V. E. & LOPEZ, G. R. 1990. THE ROLE OF SEDIMENT TYPE IN GROWTH AND FECUNDITY OF MUD SNAILS (HYDROBIIDAE). *Oecologia,* 83**,** 53-61.

FREEZE, R. & CHERRY, J. 1979. *Groundwater,* Englewood Cliffs, NJ, Prentice Hall.

FROELICH, P. N. 1988. KINETIC CONTROL OF DISSOLVED PHOSPHATE IN NATURAL RIVERS AND ESTUARIES - A PRIMER ON THE PHOSPHATE BUFFER MECHANISM. *Limnology and Oceanography,* 33**,** 649-668.

GARCIA-ORELLANA, J., COCHRAN, J. K., BOKUNIEWICZ, H., YANG, S. & BECK, A. J. 2010. Time-series sampling of Ra-223 and Ra-224 at the inlet to Great South Bay (New

York): a strategy for characterizing the dominant terms in the Ra budget of the bay. *Journal of Environmental Radioactivity,* 101**,** 582-588.

GEORGAS, N. 2001. *Tidal Hydrodynamics and Bedload Transport in a Shallow, Vegetated Harbor (Stony Brook Harbor, Long Island, New York): A Modeling Approach with Management Implications* Masters of Science, State University of New York at Stony Brook.

GERMAN, R. 1994. *Powder Metallurgy Science,* Princeton, N.J., Metal Powder Industries Federation.

GHEJU, M. 2011. Hexavalent Chromium Reduction with Zero-Valent Iron (ZVI) in Aquatic Systems. *Water Air and Soil Pollution,* 222**,** 103-148.

GIBLIN, A. E., TOBIAS, C. R., SONG, B., WESTON, N., BANTA, G. T. & RIVERA-MONROY, V. H. 2013. The Importance of Dissimilatory Nitrate Reduction to Ammonium (DNRA) in the Nitrogen Cycle of Coastal Ecosystems. *Oceanography,* 26**,** 124-131.

GONNEEA, M. E., MORRIS, P. J., DULAIOVA, H. & CHARETTE, M. A. 2008. New perspectives on radium behavior within a subterranean estuary. *Marine Chemistry,* 109**,** 250-267.

GREEN, C. T., PUCKETT, L. J., BOHLKE, J. K., BEKINS, B. A., PHILLIPS, S. P., KAUFFMAN, L. J., DENVER, J. M. & JOHNSON, H. M. 2008. Limited occurrence of denitrification in four shallow aquifers in agricultural areas of the United States. *Journal of Environmental Quality,* 37**,** 994-1009.

GREGORCYK, K. & HILL, J. C. 2013. Benthic habitat mapping of Port Jefferson Harbor in Long Island Sound, NY. *American Society of Limnology and Oceanography*. New Orleans, LA.

GROFFMAN, P. M., ALTABET, M. A., BOHLKE, J. K., BUTTERBACH-BAHL, K., DAVID, M. B., FIRESTONE, M. K., GIBLIN, A. E., KANA, T. M., NIELSEN, L. P., VOYTEK, M. A. & CC 2006. Methods for measuring denitrification: Diverse approaches to a difficult problem. *Ecological Applications,* 16**,** 2091-2122.

GROFFMAN, P. M., BUTTERBACH-BAHL, K., FULWEILER, R. W., GOLD, A. J., MORSE, J. L., STANDER, E. K., TAGUE, C., TONITTO, C. & VIDON, P. 2009. Challenges to incorporating spatially and temporally explicit phenomena (hotspots and hot moments) in denitrification models. *Biogeochemistry,* 93**,** 49-77.

GROSS, W., GRANT, M., DAVIES, D. & LIN, P. 1972. **Characteristics and Environmental Quality of Six North Shore Bays, Nassau and Suffolk Counties, Long Island, New York**. *In:* CENTER, M. S. R. (ed.) *Technical Report.* Stony Brook, NY: State University of New York.

HARTNETT, H. E., SEITZINGER, S. P. & RZ 2003. High-resolution nitrogen gas profiles in sediment porewaters using a new membrane probe for membrane-inlet mass spectrometry. *Marine Chemistry,* 83**,** 23-30.

HAYS, R. L. & ULLMAN, W. J. 2007. Dissolved nutrient fluxes through a sandy estuarine beachface (Cape Henlopen, Delaware, USA): Contributions from fresh groundwater discharge, Seawater recycling, and diagenesis. *Estuaries and Coasts,* 30**,** 710-724.

HEATON, T. H. E. & VOGEL, J. C. 1981. EXCESS AIR IN GROUNDWATER. *Journal of Hydrology,* 50**,** 201-216.

HOPFENSPERGER, K. N., KAUSHAL, S. S., FINDLAY, S. E. G. & CORNWELL, J. C. 2009. Influence of Plant Communities on Denitrification in a Tidal Freshwater Marsh of the Potomac River, United States. *Journal of Environmental Quality,* 38**,** 618-626.

HOSONO, T., ONO, M., BURNETT, W. C., TOKUNAGA, T., TANIGUCHI, M. & AKIMICHI, T. 2012. Spatial Distribution of Submarine Groundwater Discharge and Associated Nutrients within a Local Coastal Area. *Environmental Science & Technology,* 46**,** 5319-5326.

HOWARTH, R., CHAN, F., CONLEY, D. J., GARNIER, J., DONEY, S. C., MARINO, R. & BILLEN, G. 2011. Coupled biogeochemical cycles: eutrophication and hypoxia in temperate estuaries and coastal marine ecosystems. *Frontiers in Ecology and the Environment,* 9**,** 18-26.

HOWARTH, R., SWANEY, D., BILLEN, G., GARNIER, J., HONG, B. G., HUMBORG, C., JOHNES, P., MORTH, C. M. & MARINO, R. 2012. Nitrogen fluxes from the landscape are controlled by net anthropogenic nitrogen inputs and by climate. *Frontiers in Ecology and the Environment,* 10**,** 37-43.

HOWARTH, R. W. 2008. Coastal nitrogen pollution: A review of sources and trends globally and regionally. *Harmful Algae,* 8**,** 14-20.

HOWARTH, R. W., BOYER, E. W., PABICH, W. J. & GALLOWAY, J. N. 2002. Nitrogen use in the United States from 1961-2000 and potential future trends. *Ambio,* 31**,** 88-96.

HUA, B., YANG, J. & DENG, B. L. 2009. Groundwater Quality. *Water Environment Research,* 81**,** 1975-1995.

HUANG, Y. H. & ZHANG, T. C. 2004. Effects of low pH on nitrate reduction by iron powder. *Water Research,* 38**,** 2631-2642.

HULTH, S., ALLER, R. C., CANFIELD, D. E., DALSGAARD, T., ENGSTROM, P., GILBERT, F., SUNDBACK, K. & THAMDRUP, B. 2005. Nitrogen removal in marine environments: recent findings and future research challenges. *Marine Chemistry,* 94**,** 125-145.

HWANG, Y. H., KIM, D. G., AHN, Y. T., MOON, C. M. & SHIN, H. S. 2010. Fate of nitrogen species in nitrate reduction by nanoscale zero valent iron and characterization of the reaction kinetics. *Water Science and Technology,* 61**,** 705-712.

HWANG, Y. H., KIM, D. G. & SHIN, H. S. 2011. Mechanism study of nitrate reduction by nano zero valent iron. *Journal of Hazardous Materials,* 185**,** 1513-1521.

HYUN, J. H., MOK, J. S., CHO, H. Y., KIM, S. H., LEE, K. S. & KOSTKA, J. E. 2009. Rapid organic matter mineralization coupled to iron cycling in intertidal mud flats of the Han River estuary, Yellow Sea. *Biogeochemistry,* 92**,** 231-245.

IBANHEZ, J. S. P., LEOTE, C. & ROCHA, C. 2011. Porewater nitrate profiles in sandy sediments hosting submarine groundwater discharge described by an advection-dispersion-reaction model. *Biogeochemistry,* 103**,** 159-180.

JENG, D. S., MAO, X., ENOT, P., BARRY, D. A. & LI, L. 2005. Spring-neap tide-induced beach water table fluctuations in a sloping coastal aquifer. *Water Resources Research,* 41.

JOHANNES, R. E. 1980. THE ECOLOGICAL SIGNIFICANCE OF THE SUBMARINE DISCHARGE OF GROUNDWATER. *Marine Ecology Progress Series,* 3**,** 365-373.

JOHANNESSON, K. H., CHEVIS, D. A., BURDIGE, D. J., CABLE, J. E., MARTIN, J. B. & ROY, M. 2011. Submarine groundwater discharge is an important net source of light and middle REEs to coastal waters of the Indian River Lagoon, Florida, USA. *Geochimica Et Cosmochimica Acta,* 75**,** 825-843.

JOHNSON, K. S. & PETTY, R. L. 1982. Determination of Phosphate in Sea-Water by Flow Injection Analysis with Injection of Reagent. *Analytical Chemistry,* 54**,** 1185-1187.

JØRGENSEN, B. 2006. Bacteria and Marine Biogeochemistry. *Marine Geochemistry*. Berlin: Springer.

KANA, T. M., DARKANGELO, C., HUNT, M. D., OLDHAM, J. B., BENNETT, G. E., CORNWELL, J. C. & PU 1994. Membrane inlet mass-spectrometer for rapid high-precision determination of N2, O2 and Ar in environmental water samples. *Analytical Chemistry,* 66**,** 4166-4170.

KAUL, L. W. & FROELICH, P. N. 1984. MODELING ESTUARINE NUTRIENT GEOCHEMISTRY IN A SIMPLE SYSTEM. *Geochimica Et Cosmochimica Acta,* 48**,** 1417-1433.

KELLY, J. L., GLENN, C. R. & LUCEY, P. G. 2013. High-resolution aerial infrared mapping of groundwater discharge to the coastal ocean. *Limnology and Oceanography-Methods,* 11**,** 262-277.

KELSO, B. H. L., SMITH, R. V., LAUGHLIN, R. J. & LENNOX, S. D. 1997. Dissimilatory nitrate reduction in anaerobic sediments leading to river nitrite accumulation. *Applied and Environmental Microbiology,* 63**,** 4679-4685.

KIM, T. H., WASKA, H., KWON, E., SURYAPUTRA, I. G. N. & KIM, G. 2012. Production, degradation, and flux of dissolved organic matter in the subterranean estuary of a large tidal flat. *Marine Chemistry,* 142**,** 1-10.

KINNEY, E. L. & VALIELA, I. 2011. Nitrogen Loading to Great South Bay: Land Use, Sources, Retention, and Transport from Land to Bay. *Journal of Coastal Research,* 27.

KNEE, K. L., STREET, J. H., GROSSMAN, E. E., BOEHM, A. B. & PAYTAN, A. 2010. Nutrient inputs to the coastal ocean from submarine groundwater discharge in a groundwater-dominated system: Relation to land use (Kona coast, Hawaii, USA). *Limnology and Oceanography,* 55**,** 1105-1122.

KOOP-JAKOBSEN, K. & GIBLIN, A. E. 2010. The effect of increased nitrate loading on nitrate reduction via denitrification and DNRA in salt marsh sediments. *Limnology and Oceanography,* 55**,** 789-802.

KOPPELMAN, L. 1976. ***The Urban sea: Long Island Sound***, New York, Praeger.

KOPPELMAN, L. 1978. The Long Island comprehensive waste treatment management plan: Hauppauge, Long Island Regional Planning Board.

KOROM, S. F. 1992. NATURAL DENITRIFICATION IN THE SATURATED ZONE - A REVIEW. *Water Resources Research,* 28**,** 1657-1668.

KROEGER, K. D. & CHARETTE, M. A. 2008. Nitrogen biogeochemistry of submarine groundwater discharge. *Limnology and Oceanography,* 53**,** 1025-1039.

KUMAR, P., TSUJIMURA, M., NAKANO, T. & MINORU, T. 2013. Time series analysis for the estimation of tidal fluctuation effect on different aquifers in a small coastal area of Saijo plain, Ehime prefecture, Japan. *Environmental geochemistry and health,* 35**,** 239-50.

LAMONTAGNE, M., ASTORGA, V., GIBLIN, A. E. & VALIELA, I. 2002. Denitrification and the stoichiometry of nutrient regeneration in Waquoit Bay, Massachusetts. *Estuaries,* 25**,** 272-281.

LANGMUIR, C. H., VOCKE, R. D., HANSON, G. N. & HART, S. R. 1978. General Mixing Equation with Applications to Icelandic Basalts. *Earth and Planetary Science Letters,* 37**,** 380-392.

LAPOINTE, B. E. 1997. Nutrient thresholds for bottom-up control of macroalgal blooms on coral reefs in Jamaica and southeast Florida. *Limnology and Oceanography,* 42**,** 1119-1131.

LEE, D. R. 1977. DEVICE FOR MEASURING SEEPAGE FLUX IN LAKES AND ESTUARIES. *Limnology and Oceanography,* 22**,** 140-147.

LEENHER, J., MALCOLM, R., MCKINLEY, P. & ECCLES, L. (1974). Occurrence of dissolved organic carbon in selected ground-water samples in the United States. Journal of Research: U.S Geological Survey.

LEVY, S. 2011. Suffolk County Comprehensive Plan 2035. *In:* PLANNING (ed.). Hauppauge NY.

LEWIS, E. L. & PERKIN, R. G. 1981. THE PRACTICAL SALINITY SCALE 1978 - CONVERSION OF EXISTING DATA. *Deep-Sea Research Part a-Oceanographic Research Papers,* 28.

LI, L., BARRY, D. A., CUNNINGHAM, C., STAGNITTI, F. & PARLANGE, J. Y. 2000. A two-dimensional analytical solution of groundwater responses to tidal loading in an estuary and ocean. *Advances in Water Resources,* 23**,** 825-833.

LI, L., BARRY, D. A., PARLANGE, J. Y. & PATTIARATCHI, C. B. 1997. Beach water table fluctuations due to wave run-up: Capillarity effects. *Water Resources Research,* 33**,** 935-945.

LI, L., BARRY, D. A., STAGNITTI, F. & PARLANGE, J. Y. 1999. Submarine groundwater discharge and associated chemical input to a coastal sea. *Water Resources Research,* 35**,** 3253-3259.

LI, Y. H. & GREGORY, S. 1974. DIFFUSION OF IONS IN SEA-WATER AND IN DEEP-SEA SEDIMENTS. *Geochimica Et Cosmochimica Acta,* 38**,** 703-714.

LONGUETHIGGINS, M. S. 1983. WAVE SET-UP, PERCOLATION AND UNDERTOW IN THE SURF ZONE. *Proceedings of the Royal Society of London Series a-Mathematical Physical and Engineering Sciences,* 390**,** 283-&.

LOVELESS, A. M. & OLDHAM, C. E. 2010. Natural attenuation of nitrogen in groundwater discharging through a sandy beach. *Biogeochemistry,* 98**,** 75-87.

LU, Y., TANG, C., CHEN, J. & SAKURA, Y. 2008. Impact of septic tank systems on local groundwater quality and water supply in the Pearl River Delta, China: case study. *Hydrological Processes,* 22**,** 443-450.

MACINTYRE, S., WANNINKHOF, R. & J.P, C. 1995. **Trace gas exchange across the air-sea interface in freshwater and coastal marine environments**. *In:* MATSON, P. A. & R.C, H. (eds.) *Biogenic Trace Gases: Measuring Emissions from Soil and Water.* Blackwell Science Ltd.

MAGALHAES, C. M., BORDALO, A. A. & WIEBE, W. J. 2002. Temporal and spatial patterns of intertidal sediment-water nutrient and oxygen fluxes in the Douro River estuary, Portugal. *Marine Ecology Progress Series,* 233**,** 55-71.

MAJI, R. & SMITH, L. 2009. Quantitative analysis of seabed mixing and intertidal zone discharge in coastal aquifers. *Water Resources Research,* 45.

MARTIN, J. B., CABLE, J. E., SMITH, C., ROY, M. & CHERRIER, J. 2007. Magnitudes of submarine groundwater discharge from marine and terrestrial sources: Indian River Lagoon, Florida. *Water Resources Research,* 43.

MARTIN, J. B., CABLE, J. E., SWARZENSKI, P. W. & LINDENBERG, M. K. 2004. Enhanced Submarine Ground Water Discharge from Mixing of Pore Water and Estuarine Water. *Ground Water,* 42**,** 1000-1010.

MEILE, C., PORUBSKY, W. P., WALKER, R. L. & PAYNE, K. 2010. Natural attenuation of nitrogen loading from septic effluents: Spatial and environmental controls. *Water Research,* 44**,** 1399-1408.

MEYSMAN, F. J. R., GALAKTIONOV, E. S., GRIBSHOLT, B. & MIDDELBURG, J. J. 2006. Bioirrigation in permeable sediments: Advective pore-water transport induced by burrow ventilation. *Limnology and Oceanography,* 51**,** 142-156.

MICHAEL, H. A., MULLIGAN, A. E. & HARVEY, C. F. 2005. Seasonal oscillations in water exchange between aquifers and the coastal ocean. *Nature,* 436**,** 1145-1148.

MOOKHERJI, S., MCCARTY, G. W., ANGIER, J. T. & BR 2003. Dissolved gas analysis for assessing the fate of nitrate in wetlands. *Journal of the American Water Resources Association,* 39**,** 381-387.

MOORE, W. S. 1996. Large groundwater inputs to coastal waters revealed by Ra-226 enrichments. *Nature,* 380**,** 612-614.

MOORE, W. S. 1999. The subterranean estuary: a reaction zone of ground water and sea water. *Marine Chemistry,* 65**,** 111-125.

MOSIER, A. C. & FRANCIS, C. A. 2010. Denitrifier abundance and activity across the San Francisco Bay estuary. *Environmental Microbiology Reports,* 2**,** 667-676.

MULCH, D. & HANSON, G. 2010. Port Jefferson Geomorphology *Geology of Long Island and Metropolitan New York.* Stony Brook University.

MULLIGAN, A. E. & CHARETTE, M. A. 2006. Intercomparison of submarine groundwater discharge estimates from a sandy unconfined aquifer. *Journal of Hydrology,* 327.

MUNSTER, J. 2004. *Evaluating Nitrate Sources in Suffolk County groundwater, Long Island, New York.* M.S., SUNY Stony Brook.

MUNSTER, J. 2008a. *Non-point sources of nitrate and perchlorate in urban land use to groundwater, Suffolk County, NY.* Ph.D, Stony Brook University, Stony Brook, NY.

MUNSTER, J. 2008b. Non-point sources of nitrate and perchlorate in urban land use to groundwater, Suffolk County, NY. http://www.geo.sunysb.edu/reports/.

MWASHOTE, B. M., MURRAY, M., BURNETT, W. C., CHANTON, J., KRUSE, S. & FORDE, A. 2013. Submarine groundwater discharge in the Sarasota Bay system: Its assessment and implications for the nearshore coastal environment. *Continental Shelf Research,* 53**,** 63-76.

NIELSEN, P. 1990. Tidal Dynamics of the Water-Table in Beaches. *Water Resources Research,* 26**,** 2127-2134.

NOAA. 2011. *Climatological Report (Annual)* [Online]. http://www.crh.noaa.gov/product.php?site=NWS&issuedby=ISP&product=CLA&format=CI&version=1&glossary=1&highlight=off. [Accessed 4-10-2012 2012].

NOUBACTEP, C. 2010. Metallic iron for safe drinking water worldwide. *Chemical Engineering Journal,* 165**,** 740-749.

NOUBACTEP, C. 2011. Comments on "Mechanism study of nitrate reduction by nano zero valent iron" by Hwang et al. J. Hazard. Mater. (2010), doi:10.1016/j.jhazmat.2010.10.078. *Journal of Hazardous Materials,* 186**,** 946-947.

NOWICKI, B. L., REQUINTINA, E., VANKEUREN, D. & KELLY, J. R. 1997. Nitrogen losses through sediment denitrification in Boston Harbor and Massachusetts Bay. *Estuaries,* 20**,** 626-639.

NULL, K. A., CORBETT, D. R., DEMASTER, D. J., BURKHOLDER, J. M., THOMAS, C. J. & REED, R. E. 2011. Porewater advection of ammonium into the Neuse River Estuary, North Carolina, USA. *Estuarine Coastal and Shelf Science,* 95**,** 314-325.

OLANREWAJU, J. & WONG, T.-F. 2010. Hydraulic Conductivity, Porosity and Particle-Size Distribution of Core Samples of the Upper Glacial Aquifer: Laboratory Observations. Department of Earth and Space Sciences: Stony Brook University.

PABICH, W. J., VALIELA, I. & HEMOND, H. F. 2001. Relationship between DOC concentration and vadose zone thickness and depth below water table in groundwater of Cape Cod, USA. *Biogeochemistry,* 55**,** 247-268.

PAULSEN, R. J., SMITH, C. F., O'ROURKE, D. & WONG, T. F. 2001. Development and evaluation of an ultrasonic ground water seepage meter. *Ground Water,* 39**,** 904-911.

PETERSON, R. N., BURNETT, W. C., GLENN, C. R. & JOHNSON, A. G. 2009. Quantification of point-source groundwater discharges to the ocean from the shoreline of the Big Island, Hawaii. *Limnology and Oceanography,* 54**,** 890-904.

POISSON, A. 1980a. CONDUCTIVITY-SALINITY-TEMPERATURE RELATIONSHIP OF DILUTED AND CONCENTRATED STANDARD SEAWATER. *Ieee Journal of Oceanic Engineering,* 5.

POISSON, A. 1980b. Conductivity/salinity/temperature relationship of diluted and concentrated standard seawater. *Oceanic Engineering, IEEE Journal of,* 5**,** 41-50.

PORTER, K. S. 1980. AN EVALUATION OF SOURCES OF NITROGEN AS CAUSES OF GROUNDWATER CONTAMINATION IN NASSAU-COUNTY, LONG-ISLAND. *Ground Water,* 18**,** 617-625.

POSTMA, D., BOESEN, C., KRISTIANSEN, H. & LARSEN, F. 1991. NITRATE REDUCTION IN AN UNCONFINED SANDY AQUIFER - WATER CHEMISTRY, REDUCTION PROCESSES, AND GEOCHEMICAL MODELING. *Water Resources Research,* 27**,** 2027-2045.

POVINEC, P. P., BOKUNIEWICZ, H., BURNETT, W. C., CABLE, J., CHARETTE, M., COMANDUCCI, J. F., KONTAR, E. A., MOORE, W. S., OBERDORFER, J. A., DE OLIVEIRA, J., PETERSON, R., STIEGLITZ, T. & TANIGUCHI, M. 2008. Isotope tracing of submarine groundwater discharge offshore Ubatuba, Brazil: results of the IAEA-UNESCO SGD project. *Journal of Environmental Radioactivity,* 99**,** 1596-1610.

QUINN, J., GEIGER, C., CLAUSEN, C., BROOKS, K., COON, C., O'HARA, S., KRUG, T., MAJOR, D., YOON, W. S., GAVASKAR, A. & HOLDSWORTH, T. 2005. Field demonstration of DNAPL dehalogenation using emulsified zero-valent iron. *Environmental Science & Technology,* 39**,** 1309-1318.

RAMOS, M. A. V., YAN, W., LI, X.-Q., KOEL, B. E. & ZHANG, W.-X. 2009. Simultaneous Oxidation and Reduction of Arsenic by Zero-Valent Iron Nanoparticles: Understanding the Significance of the Core-Shell Structure. *Journal of Physical Chemistry C,* 113**,** 14591-14594.

RAO, A. M. F. & CHARETTE, M. A. 2012. Benthic Nitrogen Fixation in an Eutrophic Estuary Affected by Groundwater Discharge. *Journal of Coastal Research,* 28**,** 477-485.

RAPAGLIA, J. P. & BOKUNIEWICZ, H. J. 2009. The effect of groundwater advection on salinity in pore waters of permeable sediments. *Limnology and Oceanography,* 54**,** 630-643.

REDFIELD, A. C. 1963. The influence of organisms on the composition of sea-water. *The Sea***,** 26-77.

RIEDEL, T., LETTMANN, K., SCHNETGER, B., BECK, M. & BRUMSACK, H. J. 2011. Rates of trace metal and nutrient diagenesis in an intertidal creek bank. *Geochimica Et Cosmochimica Acta,* 75**,** 134-147.

RIEXINGER, P. 2005. *COASTAL FISH & WILDLIFE HABITAT ASSESSMENT FORM* [Online]. New York: NYS Department of State. [Accessed July 18 2013].

RINGLEB, F., FUJIMORI, Y., WANG, H.-F., ARIGA, H., CARRASCO, E., STERRER, M., FREUND, H.-J., GIORDANO, L., PACCHIONI, G. & GONIAKOWSKI, J. 2011. Interaction of Water with FeO(111)/Pt(111): Environmental Effects and Influence of Oxygen. *Journal of Physical Chemistry C,* 115**,** 19328-19335.

RIVETT, M. O., SMITH, J. W. N., BUSS, S. R. & MORGAN, P. 2007. Nitrate occurrence and attenuation in the major aquifers of England and Wales. *Quarterly Journal of Engineering Geology and Hydrogeology,* 40**,** 335-352.

ROBINSON, C., GIBBES, B., CAREY, H. & LI, L. 2007a. Salt-freshwater dynamics in a subterranean estuary over a spring-neap tidal cycle. *Journal of Geophysical Research-Oceans,* 112.

ROBINSON, C., LI, L. & BARRY, D. A. 2007b. Effect of tidal forcing on a subterranean estuary. *Advances in Water Resources,* 30.

ROBINSON, C., LI, L. & PROMMER, H. 2007c. Tide-induced recirculation across the aquifer-ocean interface. *Water Resources Research,* 43.

ROSE, P. 2011. *Medically-derived ^{131}I as a tracer in aquatic environments.* Ph.D, Stony Brook University.

ROTZOLL, K. & EL-KADI, A. I. 2008. Estimating hydraulic properties of coastal aquifers using wave setup. *Journal of Hydrology,* 353**,** 201-213.

ROY, M., MARTIN, J. B., CABLE, J. E. & SMITH, C. G. 2013. Variations of iron flux and organic carbon remineralization in a subterranean estuary caused by inter-annual variations in recharge. *Geochimica Et Cosmochimica Acta,* 103**,** 301-315.

ROY, M., MARTIN, J. B., SMITH, C. G. & CABLE, J. E. 2011. Reactive-transport modeling of iron diagenesis and associated organic carbon remineralization in a Florida (USA) subterranean estuary. *Earth and Planetary Science Letters,* 304.

SAAD, D. A. 2008. Agriculture-related trends in groundwater quality of the glacial deposits aquifer, central Wisconsin. *Journal of Environmental Quality,* 37**,** S209-S225.

SAKAMAKI, T., NISHIMURA, O. & SUDO, R. 2006. Tidal time-scale variation in nutrient flux across the sediment-water interface of an estuarine tidal flat. *Estuarine Coastal and Shelf Science,* 67**,** 653-663.

SANTORO, A. E., BOEHM, A. B. & FRANCIS, C. A. 2006. Denitrifier community composition along a nitrate and salinity gradient in a coastal aquifer. *Applied and Environmental Microbiology,* 72**,** 2102-2109.

SANTOS, I. R., BURNETT, W. C., CHANTON, J., MWASHOTE, B., SURYAPUTRA, I. G. N. A. & DITTMAR, T. 2008a. Nutrient biogeochemistry in a Gulf of Mexico subterranean estuary and groundwater-derived fluxes to the coastal ocean. *Limnology and Oceanography,* 53.

SANTOS, I. R., BURNETT, W. C., DITTMAR, T., SURYAPUTRA, I. & CHANTON, J. 2009. Tidal pumping drives nutrient and dissolved organic matter dynamics in a Gulf of Mexico subterranean estuary. *Geochimica Et Cosmochimica Acta,* 73**,** 1325-1339.

SANTOS, I. R., BURNETT, W. C., MISRA, S., SURYAPUTRA, I. G. N. A., CHANTON, J. P., DITTMAR, T., PETERSON, R. N. & SWARZENSKI, P. W. 2011. Uranium and barium cycling in a salt wedge subterranean estuary: The influence of tidal pumping. *Chemical Geology,* 287.

SANTOS, I. R., COOK, P. L. M., ROGERS, L., DE WEYS, J. & EYRE, B. D. 2012. The "salt wedge pump": Convection-driven pore-water exchange as a source of dissolved organic and inorganic carbon and nitrogen to an estuary. *Limnology and Oceanography,* 57**,** 1415-1426.

SANTOS, I. R., MACHADO, M. I., NIENCHESKI, L. F., BURNETT, W., MILANI, I. B., ANDRADE, C. F. F., PETERSON, R. N., CHANTON, J. & BAISCH, P. 2008b. Major ion chemistry in a freshwater coastal lagoon from southern Brazil (Mangueira Lagoon): Influence of groundwater inputs. *Aquatic Geochemistry,* 14**,** 133-146.

SCHAAF, P., ILLGNER, C., LANDRY, F. & LIEB, K. P. 1998. Correlation of the microhardness with the nitrogen profiles and the phase composition in the surface of laser-nitrided steel. *Surface & Coatings Technology,* 100**,** 404-407.

SCHLUTER, M., SAUTER, E. J., ANDERSEN, C. E., DAHLGAARD, H. & DANDO, P. R. 2004. Spatial distribution and budget for submarine groundwater discharge in Eckernforde Bay (Western Baltic Sea). *Limnology and Oceanography,* 49**,** 157-167.

SCHMIDT, C., HANFLAND, C., REGNIER, P., VAN CAPPELLEN, P., SCHLUTER, M., KNAUTHE, U., STIMAC, I. & GEIBERT, W. 2011. Ra-228, Ra-226, Ra-224 and Ra-223 in potential sources and sinks of land-derived material in the German Bight of the North Sea: implications for the use of radium as a tracer. *Geo-Marine Letters,* 31**,** 259-269.

SCORCA, M. & MONTI, J. 2001. Estimates of Nitrogen Loads Entering Long Island Sound from Ground Water and Streams on Long Island, New York, 1985-96. *In:* INVESTIGATION, W. R. (ed.). Troy, NY: U.S Geological Survey.

SHREIR, L., BURSTEIN, G. & JARMAN, R. 1994. *Corrosion,* Boston, Butterworth-Heinemann.

SIMMONS, G. M. 1992. Importance of Submarine Groundwater Discharge (SGWD) and Seawater cycling to Material Flux Across Sediment Water Interfaces in Marine Environments. *Marine Ecology-Progress Series,* 84**,** 173-184.

SLOMP, C. P. & VAN CAPPELLEN, P. 2004. Nutrient inputs to the coastal ocean through submarine groundwater discharge: controls and potential impact. *Journal of Hydrology,* 295**,** 64-86.

SMITH, C. G. & SWARZENSKI, P. W. 2012. An investigation of submarine groundwater-borne nutrient fluxes to the west Florida shelf and recurrent harmful algal blooms. *Limnology and Oceanography,* 57**,** 471-485.

SMITH, J. K., LONSDALE, D. J., GOBLER, C. J. & CARON, D. A. 2008. Feeding behavior and development of Acartia tonsa nauplii on the brown tide alga Aureococcus anophagefferens. *Journal of Plankton Research,* 30**,** 937-950.

SMITH, L. K., VOYTEK, M. A., BOHLKE, J. K. & HARVEY, J. W. 2006. Denitrification in nitrate-rich streams: Application of N-2 : Ar and N-15-tracer methods in intact cores. *Ecological Applications,* 16**,** 2191-2207.

SOLORZANO, L. 1969. Determination of Ammonia in Natural Waters by Phenolhypochlorite Method. *Limnology and Oceanography,* 14**,** 799-&.

SONG, Z. Y., LI, L., NIELSEN, P. & LOCKINGTON, D. 2006. Quantification of tidal watertable overheight in a coastal unconfined aquifer. *Journal of Engineering Mathematics,* 56**,** 437-444.

SPITERI, C., REGNIER, P., SLOMP, C. P. & CHARETTE, M. A. 2006. pH-Dependent iron oxide precipitation in a subterranean estuary. *Journal of Geochemical Exploration,* 88**,** 399-403.

SPITERI, C., VAN CAPPELLEN, P. & REGNIER, P. 2008. Surface complexation effects on phosphate adsorption to ferric iron oxyhydroxides along pH and salinity gradients in estuaries and coastal aquifers. *Geochimica Et Cosmochimica Acta,* 72.

STEENHUIS, T. S., JACKSON, C. D., KUNG, S. K. J. & BRUTSAERT, W. 1985. MEASUREMENT OF GROUNDWATER RECHARGE ON EASTERN LONG-ISLAND, NEW-YORK, USA. *Journal of Hydrology,* 79**,** 145-169.

STIEGLITZ, T. C., COOK, P. G. & BURNETT, W. C. 2010. Inferring coastal processes from regional-scale mapping of (222)Radon and salinity: examples from the Great Barrier Reef, Australia. *Journal of Environmental Radioactivity,* 101**,** 544-552.

STOOKEY, L. L. 1970. Ferrozine- A New Spectrophotometric Reagent for Iron. *Analytical Chemistry,* 42**,** 779-&.

STRATMANN, M. 1990. THE ATMOSPHERIC CORROSION OF IRON - A DISCUSSION OF THE PHYSICOCHEMICAL FUNDAMENTALS OF THIS OMNIPRESENT CORROSION PROCESS - INVITED REVIEW. *Berichte Der Bunsen-Gesellschaft-Physical Chemistry Chemical Physics,* 94**,** 626-639.

STRATMANN, M. & MULLER, J. 1994. THE MECHANISM OF THE OXYGEN REDUCTION ON RUST-COVERED METAL SUBSTRATES. *Corrosion Science,* 36**,** 327-359.

STRICKLAND, J. & PARSONS, T. 1978. *A practical handbook of seawater analysis,* Ottowa, Fisheries Research Board of Canada.

STUMM, W. & MORGAN, J. 1996. *Aquatic Chemistry: Chemical Equilibria and Rates in Natural Waters,* New York, Wiley.

SUN, F. J., LIU, J. Y., YANG, Y. L. & YU, H. J. 2005. Nitridation of iron by CW-CO2 laser nitriding technologies. *Materials Science and Engineering B-Solid State Materials for Advanced Technology,* 122**,** 29-33.

TALBOT, D. & TALBOT, J. 1998. *Corrosion Science and Technology,* Boca Raton, CRC Press.

TANIGUCHI, M. 2002. Tidal effects on submarine groundwater discharge into the ocean. *Geophysical Research Letters,* 29.

TANIGUCHI, M., BURNETT, W. C., CABLE, J. E. & TURNER, J. V. 2002. Investigation of submarine groundwater discharge. *Hydrological Processes,* 16**,** 2115-2129.

TEIXEIRA, C., MAGALHAES, C., JOYE, S. B. & BORDALO, A. A. 2013. The role of salinity in shaping dissolved inorganic nitrogen and N2O dynamics in estuarine sediment-water interface. *Marine Pollution Bulletin,* 66**,** 225-229.

TESORIERO, A. J. & PUCKETT, L. J. 2011. O-2 reduction and denitrification rates in shallow aquifers. *Water Resources Research,* 47.

THORN, P. & URISH, D. 2012. Preliminary Observation of Complex Salt-FreshWater Mixing in a Beach Aquifer. *Ground Water.*

TOBIAS, C. R., ANDERSON, I. C., CANUEL, E. A. & MACKO, S. A. 2001a. Nitrogen cycling through a fringing marsh-aquifer ecotone. *Marine Ecology-Progress Series,* 210**,** 25-39.

TOBIAS, C. R., MACKO, S. A., ANDERSON, I. C., CANUEL, E. A. & HARVEY, J. W. 2001b. Tracking the fate of a high concentration groundwater nitrate plume through a fringing marsh: A combined groundwater tracer and in situ isotope enrichment study. *Limnology and Oceanography,* 46**,** 1977-1989.

TORTELL, P. D. 2005. Dissolved gas measurements in oceanic waters made by membrane inlet mass spectrometry. *Limnology and Oceanography-Methods,* 3**,** 24-37.

ULLMAN, W. J., CHANG, B., MILLER, D. C. & MADSEN, J. A. 2003. Groundwater mixing, nutrient diagenesis, and discharges across a sandy beachface, Cape Henlopen, Delaware (USA). *Estuarine Coastal and Shelf Science,* 57**,** 539-552.

VALIELA, I., GEIST, M., MCCLELLAND, J. & TOMASKY, G. 2000. Nitrogen loading from watersheds to estuaries: Verification of the Waquoit Bay Nitrogen Loading Model. *Biogeochemistry,* 49**,** 277-293.

VAN BREEMEN, N., BOYER, E. W., GOODALE, C. L., JAWORSKI, N. A., PAUSTIAN, K., SEITZINGER, S. P., LAJTHA, K., MAYER, B., VAN DAM, D., HOWARTH, R. W., NADELHOFFER, K. J., EVE, M. & BILLEN, G. 2002. Where did all the nitrogen go? Fate of nitrogen inputs to large watersheds in the northeastern USA. *Biogeochemistry,* 57**,** 267-293.

VARMA, S., TURNER, J. & UNDERSCHULTZ, J. 2010. Estimation of submarine groundwater discharge into Geographe Bay, Bunbury, Western Australia. *Journal of Geochemical Exploration,* 106**,** 197-210.

VOLKENBORN, N., HEDTKAMP, S. I. C., VAN BEUSEKOM, J. E. E. & REISE, K. 2007. Effects of bioturbation and bioirrigation by lugworms (Arenicola marina) on physical and chemical sediment properties and implications for intertidal habitat succession. *Estuarine Coastal and Shelf Science,* 74**,** 331-343.

WAKIDA, F. T. & LERNER, D. N. 2005. Non-agricultural sources of groundwater nitrate: a review and case study. *Water Research,* 39**,** 3-16.

WANG, W. W., LI, D. J., ZHOU, J. L. & GAO, L. 2011. Nutrient dynamics in pore water of tidal marshes near the Yangtze Estuary and Hangzhou Bay, China. *Environmental Earth Sciences,* 63**,** 1067-1077.

WASKA, H. & KIM, G. 2011. Submarine groundwater discharge (SGD) as a main nutrient source for benthic and water-column primary production in a large intertidal environment of the Yellow Sea. *Journal of Sea Research,* 65**,** 103-113.

WEIGEL, V. F. 1978. Radon. *Chemiker Zeitung,* 102**,** 287-299.

WEINSTEIN, Y., YECHIELI, Y., SHALEM, Y., BURNETT, W. C., SWARZENSKI, P. W. & HERUT, B. 2011. What Is the Role of Fresh Groundwater and Recirculated Seawater in Conveying Nutrients to the Coastal Ocean? *Environmental Science & Technology,* 45**,** 5195-5200.

WEISS, R. F. 1970. Solubility of Nitrogen, Oxygen and Argon in Water and Seawater. *Deep-Sea Research,* 17**,** 721-&.

WILSON, G. B. & MCNEILL, G. W. 1997. Noble gas recharge temperatures and the excess air component. *Applied Geochemistry,* 12**,** 747-762.

WILSON, J. & ROCHA, C. 2012. Regional scale assessment of Submarine Groundwater Discharge in Ireland combining medium resolution satellite imagery and geochemical tracing techniques. *Remote Sensing of Environment,* 119**,** 21-34.

XIA, Y. Q. & LI, H. L. 2012. A combined field and modeling study of groundwater flow in a tidal marsh. *Hydrology and Earth System Sciences,* 16.

XIN, P., KONG, J., LI, L. & BARRY, D. A. 2012. Effects of soil stratigraphy on pore-water flow in a creek-marsh system. *Journal of Hydrology,* 475**,** 175-187.

XIN, P., ROBINSON, C., LI, L., BARRY, D. A. & BAKHTYAR, R. 2010. Effects of wave forcing on a subterranean estuary. *Water Resources Research,* 46.

XIN, P., YUAN, L. R., LI, L. & BARRY, D. A. 2011. Tidally driven multiscale pore water flow in a creek-marsh system. *Water Resources Research,* 47.

XIONG, Z., ZHAO, D. Y. & PAN, G. 2009. Rapid and controlled transformation of nitrate in water and brine by stabilized iron nanoparticles. *Journal of Nanoparticle Research,* 11**,** 807-819.

YAN, W., RAMOS, M. A. V., KOEL, B. E. & ZHANG, W.-X. 2010. Multi-tiered distributions of arsenic in iron nanoparticles: Observation of dual redox functionality enabled by a core-shell structure. *Chemical Communications,* 46**,** 6995-6997.

YANG, G. C. C. & LEE, H. L. 2005. Chemical reduction of nitrate by nanosized iron: Kinetics and pathways. *Water Research,* 39**,** 884-894.

YELVERTON, G. F. & HACKNEY, C. T. 1986. FLUX OF DISSOLVED ORGANIC-CARBON AND PORE WATER THROUGH THE SUBSTRATE OF A SPARTINA-ALTERNIFLORA MARSH IN NORTH-CAROLINA. *Estuarine Coastal and Shelf Science,* 22**,** 255-267.

YOUNG, C. 2010. *Extent of Denitrification in Northport Groundwater.* M.S. Geosciences, SUNY Stony Brook.

YOUNG, C., KROEGER, K. & HANSON, G. 2013. Limited denitrification in glacial deposit aquifers having thick unsaturated zones (Long Island, USA). *Hydrogeology Journal*.

ZEHR, J. & PAERL, H. 2008. *Microbial Ecology of the Oceans,* New York, Wiley.

ZHAO, S., ZHANG, P., CRUSIUS, J., KROEGER, K. D. & BRATTON, J. F. 2011. Use of pharmaceuticals and pesticides to constrain nutrient sources in coastal groundwater of northwestern Long Island, New York, USA. *Journal of Environmental Monitoring,* 13.

ZHOU, L. 2008. *Annual precipitation pattern over Long Island Based on Radar Data* M.S, Stony Brook University.

Tables and Figures

Table 13 Micro-scale Fe^0 surface area and total nitrogen content of three Fe^0 powders

Fe^0 Powder	Surface Area (m^2g^{-1})	Total Nitrogen (%wt)
BASF	0.242	0.74
QB	0.308	0.005
SA	0.138	0.001

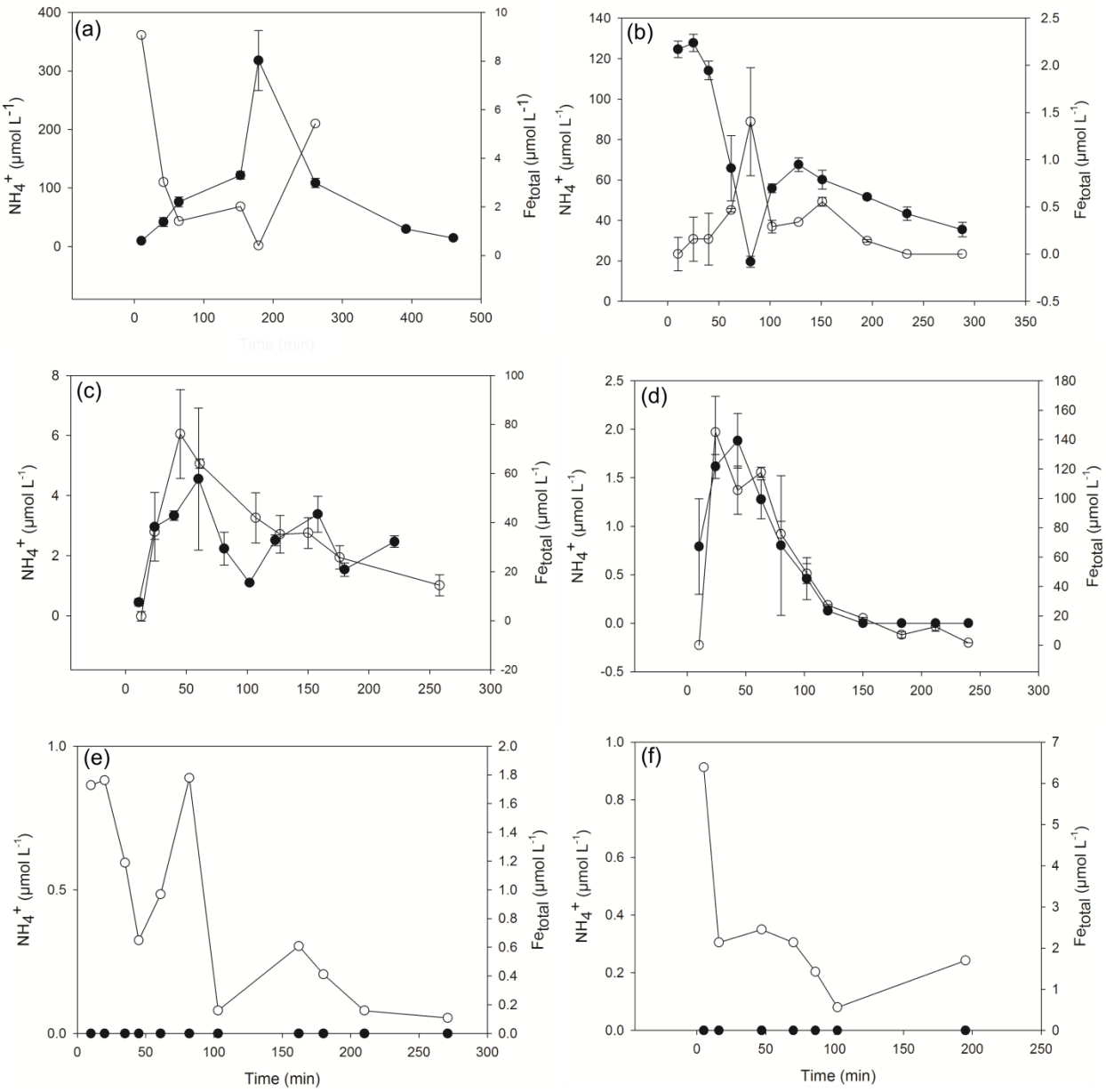

Figure 41 Ammonium (●) and total iron (○) elution's from anoxic (A,C,E) and oxic (B,D,F) experiments. Fe^0 from BASF is shown in A (anoxic) and B (oxic). Fe^0 from Quebec Metals is shown in C (anoxic) and D (oxic). Fe^0 from Sigma Aldrich is shown in E (anoxic) and F (oxic). All powders underwent acid pretreatment. Average and standard error of mean is given for three replicate column experiments. All concentrations are normalized Fe^0 g^{-1}.

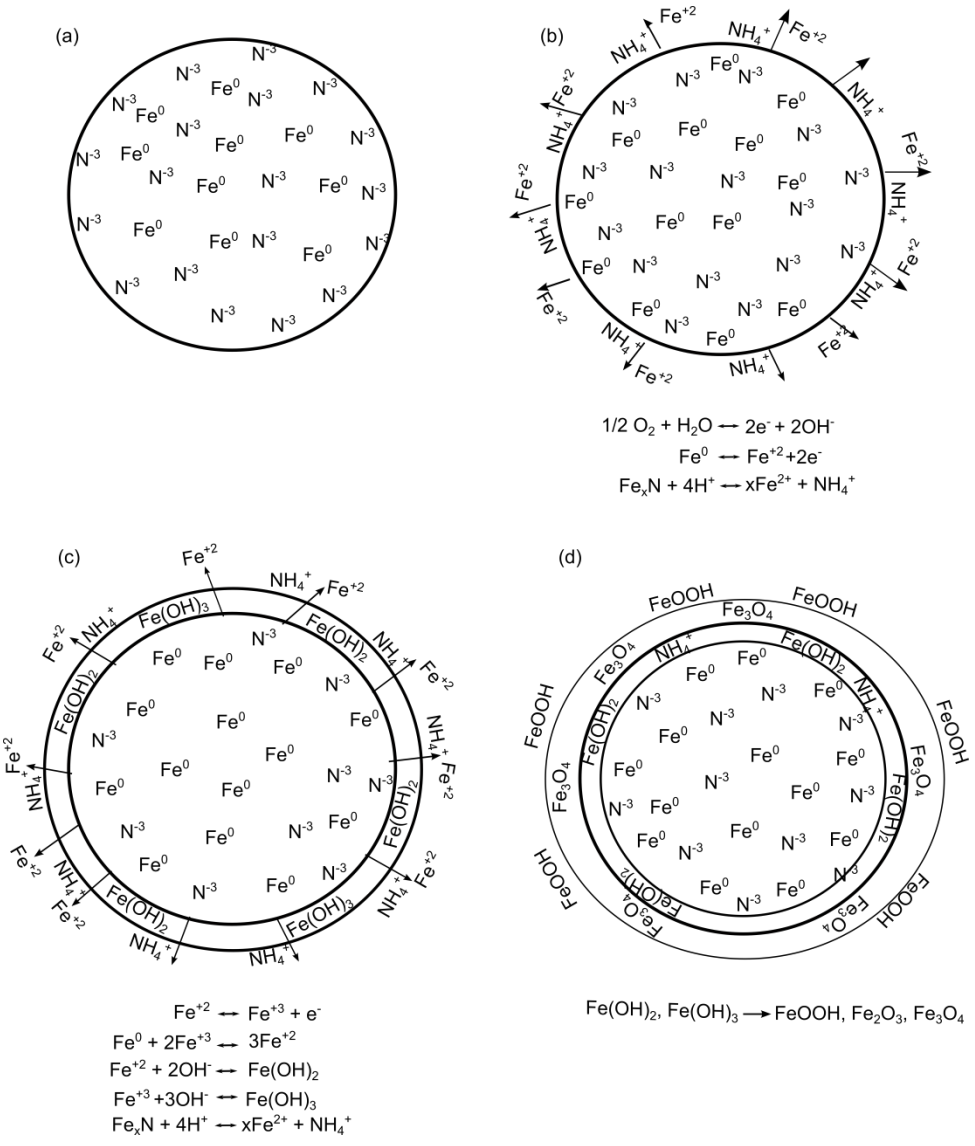

Figure 42 Conceptual model of Fe-H_2O corrosion and NH_4^+ release. Raw Fe^0 with internal nitridation (a) is acid washed and immersed in H_2O where corrosion begins the process of NH_4^+ release (b). Oxygen forms an amorphous scale that thinly coats the surface of Fe^0, during which NH_4^+ is continually released (c). Finally, the amorphous Fe-oxides build a sufficiently thick barrier and transform to more stable Fe_3O_4 which prevents further NH_4^+ elution (d). Primary reactions for each stage are given below diagram.

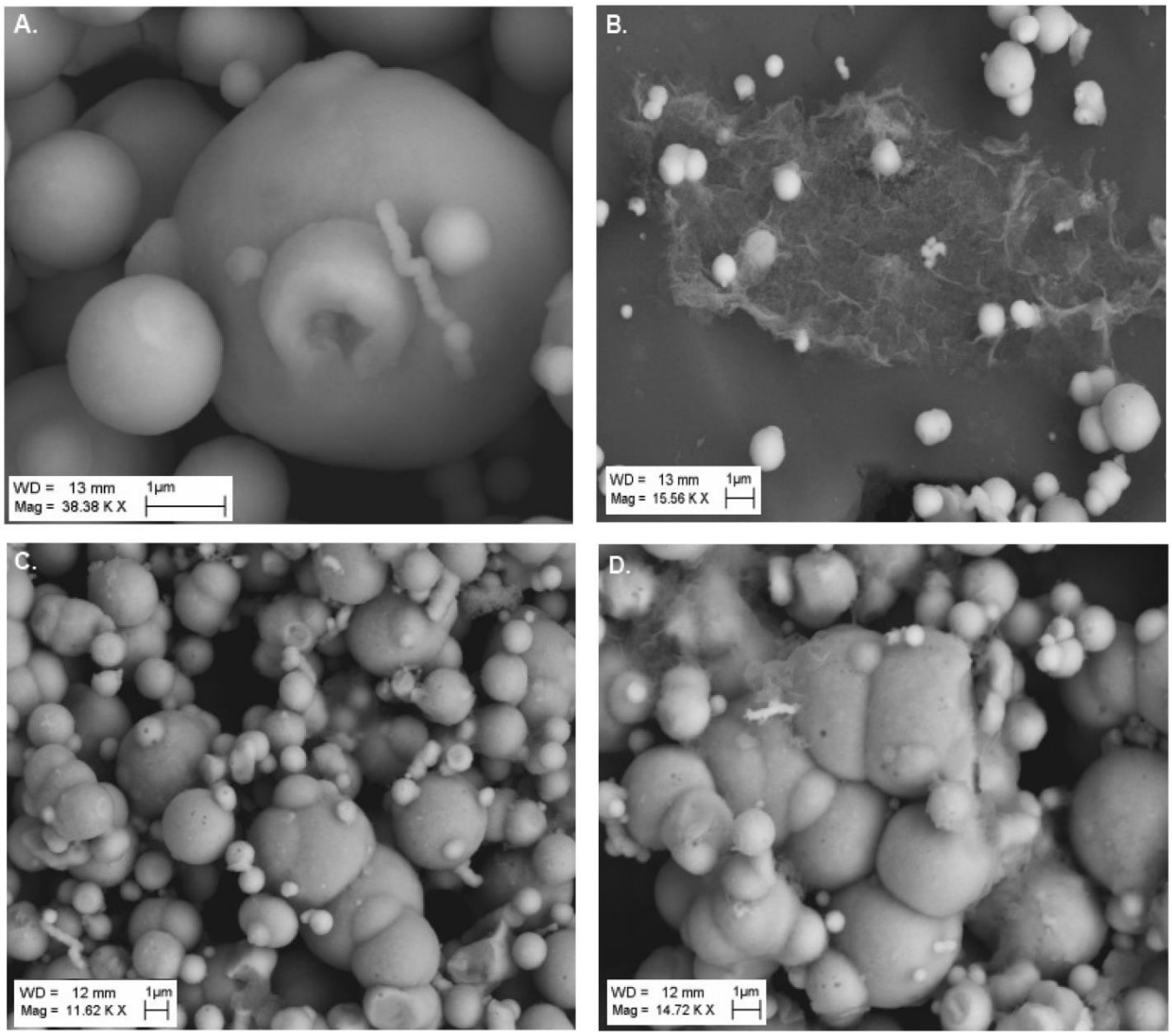

Figure 43 SEM images of powder BASF Fe^0 anoxic corrosion. Raw Fe^0 (a) prior to acid washing rapidly begins to precipitate amorphous iron oxides after 3 hours (b). Development of precipitate causes cementation of micro-scale Fe^0 after 12 hours (c) and shows significant agglomeration of Fe^0 particles after 24 hours (d).

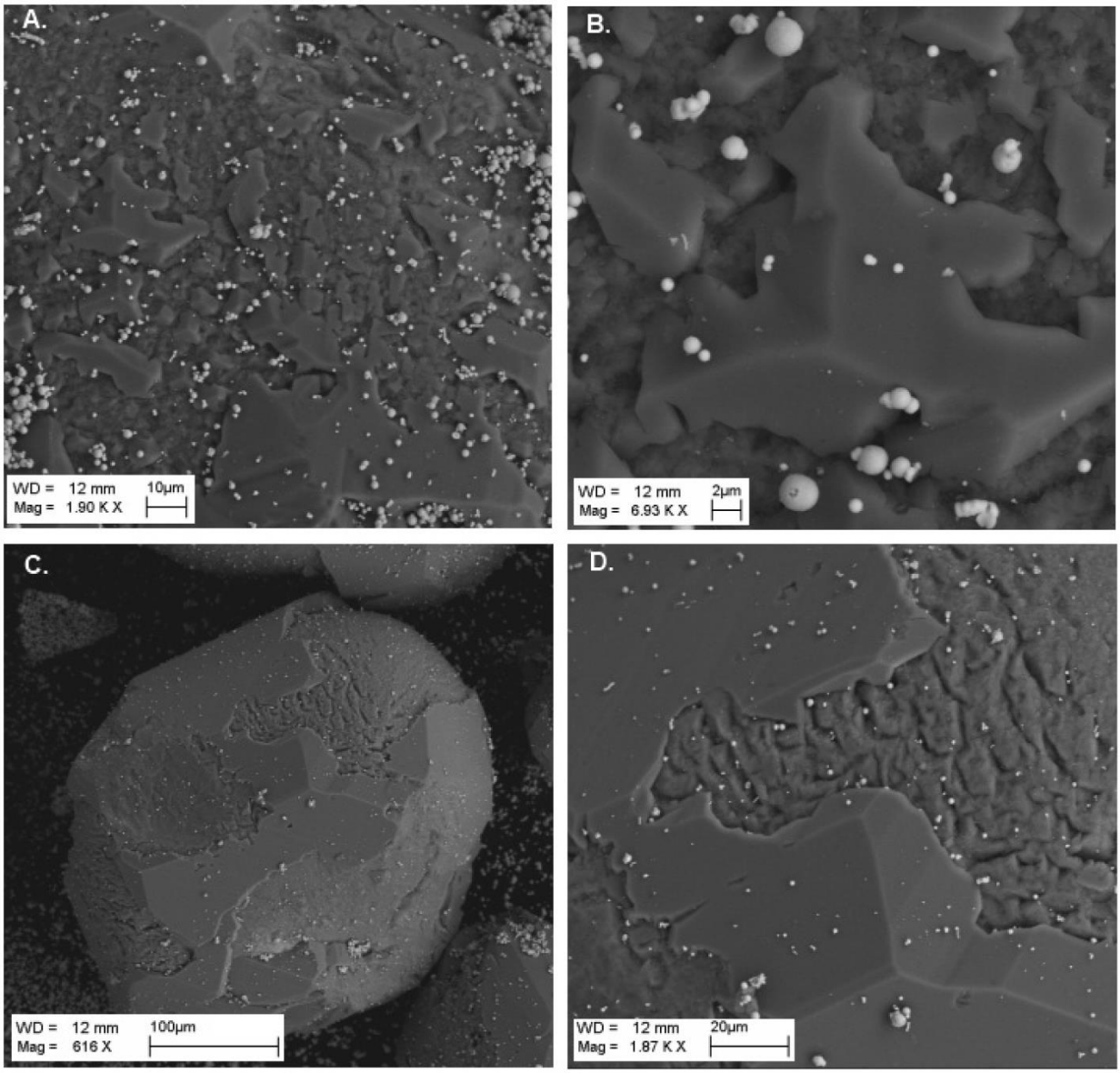

Figure 44 SEM images of iron oxide precipitation onto column quartz during powder BASF Fe^0 anoxic corrosion. After 12 hours platy crystals have formed on the quartz surface (A and B). After 24 hours quartz grains are covered in thin platy crystals (C) with well-formed crystal structures (D).

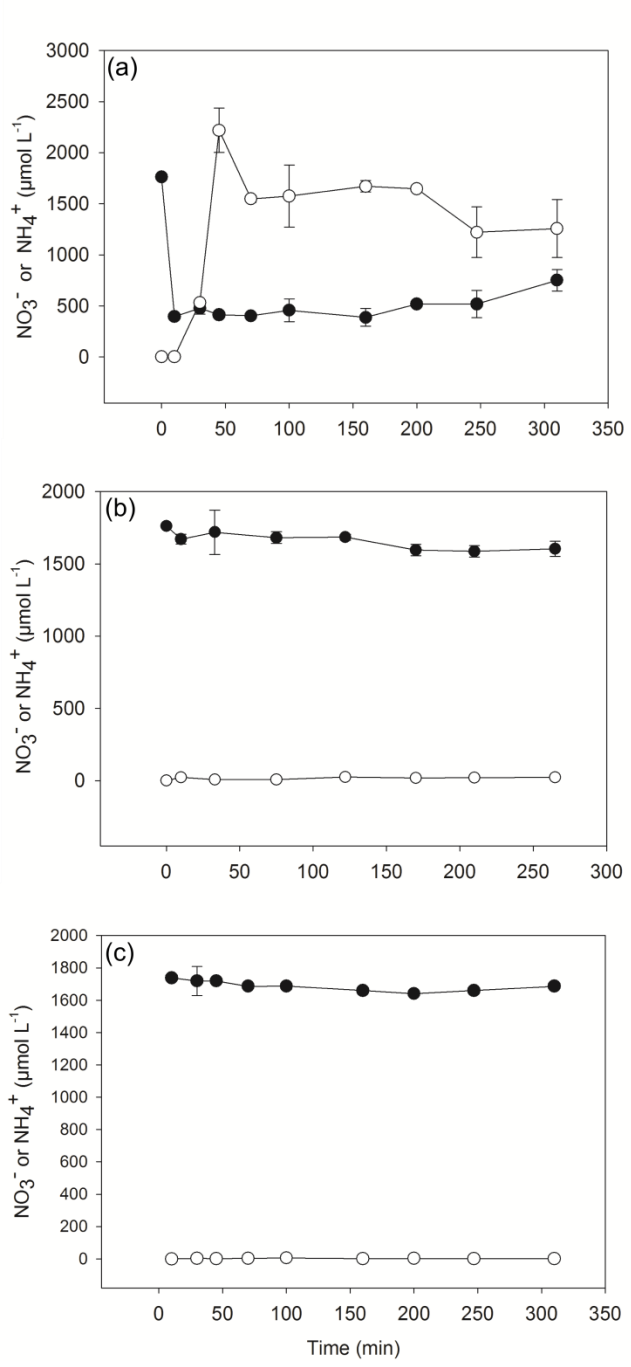

Figure 45 Nitrate (●) and ammonium (○) in nitrate reduction columns. Powder BASF (a) rapidly reduces nitrate while producing excess ammonium in concentrations greater than initial nitrate inputs. Powder SA does not rapidly reduce nitrate and equivalent ammonium is produced (b). Control column (c) shows no ammonium accumulation.